CHAPTER 4

TABLE OF CONTENTS

TABLE OF CONTENTS (Cont)

LIST OF TABLES

LIST OF FIGURES (Cont)

LIST OF FIGURES (Cont)

CHAPTER 4

REACTOR

4.1 SUMMARY DESCRIPTION

4.1.1 General

This chapter describes: 1) the mechanical components of the reactor core including the fuel rods, fuel assemblies, and control rods; 2) the nuclear design; and 3) the thermal-hydraulic design.

The reactor core is composed of an array of one type or a combination of 17 x 17 (STD), VANTAGE 5H (V5H), VANTAGE+, and/or Robust Fuel Assembly (RFA/RFA-2) fuel assemblies. The significant new mechanical design features of the VANTAGE 5H fuel assembly design are described in (Davidson, 1985) and (Davidson 1989). These features include the following:

1. Integral Fuel Burnable Absorbers (IFBAs)

2. Axial Blankets (six inches of natural or slightly enriched uranium dioxide pellets at both ends of the fuel stack)

3. Replacement of six intermediate Inconel grids with Zircaloy grids

4. Slightly longer fuel rods and thinner top and bottom nozzle end plates to accommodate extended burnup

5. Reconstitutable Top Nozzles (RTNs)

6. Redesigned fuel rod bottom end plug to facilitate reconstitution capability

7. Reduction in guide thimble and instrumentation tube diameter

Commencing with Beaver Valley Unit 2 Cycle 7, features of the VANTAGE+ fuel assembly design were incorporated into the fresh fuel feed regions. The VANTAGE+ fuel assembly design (Davidson/Nuhfer 1995) included the following features: ZIRLO^{TM} clad fuel rods, thimble tubes, and instrumentation tubes$_{TM}$ The intermediate grid strap material was also changed to ZIRLO^{TM}. As an added debris mitigation feature, a protective bottom grid was incorporated.

Commencing with Beaver Valley Unit 2 Cycle 9, features of the ZIRLO+2 fuel assembly design (incorporating Low Pressure Rod Design Phase I) were incorporated into the fresh fuel feed regions. The ZIRLO+2 fuel assembly design includes the following additional features to the VANTAGE+ fuel assembly design: the fuel tube length has been increased by 0.32 inches, the external gripper top end plug of the VANTAGE+ design has been replaced with a shorter end plug without a gripper (by 0.12 inches) to limit the overall fuel rod length increase to 0.2 inches, a longer free length plenum spring due to the longer fuel tube, longer guide thimbles and instrumentation thimble (by 0.2 inches), and a redesigned top nozzle spring pack to maintain the overall fuel assembly length. These changes were implemented to accommodate additional fission gas release from increased fuel burnup operation.

Beginning with Beaver Valley Unit 2 Cycle 10, the Robust Fuel Assembly (RFA) design was incorporated into the fresh fuel regions. The significant new mechanical design features relative to the V5H and VANTAGE+ designs are:

- Modified Low Pressure Drop (LPD) mid-grids. This will provide increased DNB margin and increased resistance to fuel rod wear.

- The addition of three Intermediate Flow Mixer (IFM) grids between the top three mid-grid spans (grids 4 through 7). This will provide increased DNB margin.

- Increased guide and instrument thimble wall thickness by approximately 25% with no change to the inside diameters. This improves the stiffness of the tubes and addresses incomplete rod insertion considerations.

Beginning with Cycle 11, the RFA-2 design was incorporated into the fresh fuel regions. The RFA-2 design is the same as the RFA with the exception that the mid-grids of the RFA-2 have increased contact area between the dimples/springs and the fuel rods.

In Cycle 17, the RFA-2 fuel assemblies integrated the following design features:

- Standardized Debris Filter Bottom Nozzle (SDFBN) to improve the debris mitigation performance of the bottom nozzle.

- Robust Protective Grid (RPG) to help address the issues of fatigue failures and failures due to stress corrosion cracking within the rod support dimples.

- Low Strain Radius mid-grids and IFM grids to lower the strain imposed on the formed features and improve the manufacturability.

The core is cooled and moderated by light water at a normal operating pressure of 2,250 psia in the reactor coolant system (RCS). The reactor coolant contains soluble boron as a neutron absorber. The concentration of boron in the reactor coolant is varied as required to control relatively slow reactivity changes including the effects of fuel burnup. Additional boron, in the form of integral burnable absorbers (IFBA) or discrete burnable absorber rods, may be employed to limit the moderator temperature coefficient (MTC) and the total power peaking that can be achieved.

Two hundred and sixty-four fuel rods are mechanically joined in a square 17 by 17 array to form a fuel assembly. The fuel rods are supported in intervals along their length by grid assemblies (and IFMs for the RFA) which maintain the lateral spacing between the rods throughout the design life of the assembly. The grid assembly consists of an "egg-crate" arrangement of interlocked straps. The straps contain spring fingers and dimples for fuel rod support as well as reactor coolant mixing vanes. The fuel rods consist of slightly enriched uranium dioxide ceramic cylindrical pellets contained in Zircaloy-4 or ZIRLO^{TM} tubing which is plugged and seal welded at the

ends to encapsulate the fuel. All fuel rods are pressurized with helium during fabrication to reduce stresses and strains in order to increase fatigue life. A protective bottom grid has been added located just above the bottom nozzle. The grid straps intersect the nozzle flow holes, thus, further reducing the possibility of fuel rod damage due to debris induced fuel rod fretting. In addition, the ZIRLO^{TM} fuel rods will be oxide coated at the lower end for additional protection against fretting.

Fuel assemblies may also contain non-fueled rods (stainless steel Zircaloy-4 or ZIRLO^{TM} filler rods). Non-fueled rods may be used in core locations where fuel damage has occurred or may occur. The use of non-fueled rods began when fuel inspections performed during the third refueling outage identified leaking fuel rods. The solution to this problem, recommended by Westinghouse and used by other utilities, involves fuel assembly reconstitution as a means to allow the insertion of non-fueled rods into a fuel assembly. In the reconstitution process, the fuel rods in positions subject to problem conditions would be removed and replaced with non-fueled rods. The

reconstituted fuel assemblies meet essentially the same design requirement as the original fuel assembly, and the use of reconstituted assemblies will not result in a change to existing safety criteria and design limits. The effects of fuel assembly reconstitution are evaluated in accordance with the methods described by Slagle 1993.

The center array position in each assembly is reserved for the incore instrumentation, 24 additional positions in the array are equipped with guide thimbles joined to the grids and the top and bottom nozzles. Depending upon the position of the assembly in the core, the guide thimbles are used as core locations for rod cluster control assemblies (RCCAs), neutron source assemblies, and burnable absorber rods.

The bottom nozzle is a box-like structure which serves as a bottom structural support element of the fuel assembly and directs the reactor coolant into the flow channels of the assembly. The top nozzle assembly serves as the upper structural support element of the fuel assembly and provides a partial protective housing for the RCCA or other components. The Reconstitutible Top Nozzle (RTN) may be removed between operating cycles to provide access for fuel rod examination or reconstitution of damaged fuel.

The RCCAs each consist of a group of individual absorber rods fastened at the top end to a structure called a spider assembly. These absorber rods contain absorber material to control the reactivity of the core under operating conditions. The nuclear design analyses and evaluation establish physical locations for control rods, burnable absorber assemblies, and physical parameters such as fuel enrichments and boron concentration in the reactor coolant. The nuclear design analyses establish that the reactor core and the reactor control system satisfy all design criteria, even if the highest reactivity worth RCCA is stuck in the fully withdrawn position. The core has inherent stability against diametral and azimuthal power oscillations. Axial power oscillations which may be induced by load changes and resultant transient xenon may be suppressed by the use of RCCAs.

The thermal-hydraulic design analyses establish reactor coolant flow parameters which assure that adequate heat transfer is provided between the fuel clad and the reactor coolant. The thermal design takes into account local variations in dimensions, power generation, flow distribution, and mixing. The mixing vanes incorporated in the fuel assembly spacer grid design induce additional flow-mixing between the various flow channels within a fuel assembly as well as between adjacent assemblies.

The performance of the core is monitored by excore neutron detectors, movable incore neutron detectors, and thermocouples at the outlet of selected fuel assemblies.

Table 4.1-1 presents a listing of the principal nuclear, thermal-hydraulic, and mechanical design parameters for Beaver Valley Power Station-Unit 2 (BVPS-2).

The BVPS-2 position with respect to Regulatory Guide 1.126 is given in Section 1.8.

The analytical techniques employed in the core design are tabulated in Table 4.1-2.

4.1.2 Reference for Section 4.1

Davidson, S.L. (Ed.), et al, "VANTAGE 5H Fuel Assembly," WCAP-10444-P-A, Addendum 2-A, February 1989.

Davidson, S.L. (Ed.), et al, "VANTAGE 5H Fuel Assembly Reference Core Report," WCAP-10444, September 1985.

Davidson, S.L., Nuhfer, D.L. (Ed.), "VANTAGE+ Fuel Assembly Reference Core Report," WCAP-12610-P-A and Appendices A through D, April 1995.

Slagle, W. H. (Ed.), 1991. "Westinghouse Fuel Assembly Reconstitution Evaluation Methodology" WCAP-13060-P-A, July 1993.

Tables for Section 4.1

TABLE 4.1-1

REACTOR DESIGN PARAMETERS

Thermal and Hydraulic Design Parameters	Design Value
Reactor core heat output (Mwt)	2,900
Reactor core heat output (10^6 Btu/hr)	9,895
Heat generated in fuel (percent)	97.4
System pressure, nominal (psia)	2,250
Minimum departure from nucleate boiling ratio for design transients, typical/thimble	1.22/1.22(RFA/RFA-2)[Note 1] 1.23/1.22(V5H)

Coolant Flow

Total thermal flow rate (10^6 lbm/hr)	99.3
Effective flow rate for heat transfer (10^6 lb/hr)	92.8[Note 5]
Effective flow area for heat transfer (ft^2)	41.5 (STD/RFA/RFA-2) 41.7 (V5H)
Average velocity along fuel rods (ft/sec)	14.0(RFA/RFA-2) 13.9(V5H)
Average mass velocity (10^6 lbm/hr-ft^2)	2.10(RFA/RFA-2) 2.09(V5H)

Coolant Temperature (°F)

Nominal inlet	543.1[Note 6]
Average rise in vessel	73.9[Note 6]
Average rise in core	78.3[Note 6]

TABLE 4.1-1 (Cont)

Thermal and Hydraulic Design Parameters	Design Value
Average in core	584.6[Note 6]
Average in vessel	580.0[Note 6]
Heat Transfer	
Active heat transfer, surface area (ft^2)	48,600
Average heat flux ($Btu/hr\text{-}ft^2$)	198,300
Maximum heat flux for normal operation ($Btu/hr\text{-}ft^2$)	499,700[Note 3]
Average thermal output (kW/ft)	5.69
Maximum thermal output for normal operation (kW/ft)	14.3[Note 3]
Peak linear power resulting from overpower transients, operator errors, assuming a maximum overpower of 118 percent kW/ft	22.4[Note 2]
Heat flux hot channel factor (F_Q)	2.40[Note 7]
Peak fuel central temperature at maximum thermal output for maximum overpower trip point (°F)	<4,700

Core Mechanical Design Parameters

Fuel Assemblies

Design	RCC canless
Number of fuel assemblies	157
UO_2 rods per assembly	264

TABLE 4.1-1 (Cont)

Thermal and Hydraulic Design Parameters	Design Value
Rod pitch (in)	0.496
Overall dimensions (in)	8.426 x 8.426
Fuel weight (as UO_2) (lb)	181,200
Zircaloy/ZIRLO^{TM} weight (lb)	41,400
Number of Grids per Assembly (17 x 17 STD, V5H, VANTAGE+)	2 - non-Mixing Vane 6 - Type R Mixing Vane 1 - Protective Bottom Grid (VANTAGE+ only)
Number of Grids per Assembly (Robust Fuel Assembly - RFA/RFA-2)	2 - non-Mixing Vane 6 - LPD Mixing Vane 3 - IFM 1 - Protective Bottom Grid
Loading technique	multi-region nonuniform

Fuel Rods

Number	41,448
Outside diameter (in)	0.374
Diametral gap (in)	0.0065
Clad thickness (in)	0.0225
Clad material	Zircaloy-4/ ZIRLO^{TM}

Fuel Pellets

Material	UO_2 sintered
Density (percent of theoretical)	95
Diameter (in)	0.3225
Enriched - Solid Length (in)	0.387
Solid Axial Blanket Length (in)	0.462, 0.500[Note 4]
Annular Axial Blanket Length (in)	0.462, 0.500[Note 4]
Diameter of annulus (in)	0.155

Rod Cluster Control Assemblies

Neutron absorber	Ag-In-Cd
Cladding material	Type 304 SS- cold worked
Clad thickness (in)	0.0185
Optional chrome plating (in)	0.0005
Number of clusters	48

TABLE 4.1-1 (Cont)

Thermal and Hydraulic Design Parameters	Design Value
Number of absorber rods per cluster	24
Core Structure	
Core barrel, I.D./O.D. (in)	133.85/137.875
Core barrel design	Neutron pad design
Structure Characteristics	
Core equivalent diameter (in)	119.7
Core active fuel height (in)	144
Reflector Thickness and Composition	
Top - water plus steel (in)	~10
Bottom - water plus steel (in)	~10
Side - water plus steel (in)	~15
H_2O/U molecular ratio core, lattice (cold)	2.42
First Core Fuel enrichment, weight percent	
Region 1	2.10
Region 2	2.60
Region 3	3.10

NOTES:

1. Revised Thermal Design Procedure DNBR design limits
2. Refer to Section 4.3.2.2.6.
3. This limit is associated with the value of F_Q = 2.52.
4. Length increases starting with Region 12 (Cycle 10).
5. Based on 6.5% core bypass flow.
6. Based on high Tavg at 580.0°F
7. Limiting F_Q based on small break LOCA. Other DBA analyses use F_Q of 2.52.

TABLE 4.1-2

ANALYTIC TECHNIQUES IN CORE DESIGN

Analysis	Technique	Computer Code	Section Reference
Fuel rod design			
1. Fuel performance characteristics (temperature, internal pressure clad stress, etc)	Semi-empirical thermal model of fuel rod consideration of fuel density changes, heat transfer, fission gas release, etc.	Westinghouse fuel rod design model	4.2.1.3.1 4.3.3.1 4.4.2.2
Nuclear design			
1. Cross sections and group constants	Microscopic data; Macroscopic constants for homogenized core regions	Modified ENDF/B library LEOPARD/CINDER type and PHOENIX-P and NEXUS/PARAGON	4.3.3.2 4.3.3.2
	Group constants for control rods with self-shielding	HAMMER-AIM and NEXUS/PARAGON	4.3.3.2
2. X-Y Power distributions, fuel depletion, critical boron concentrations, X-Y xenon distributions, reactivity coefficients	2-D 2-group diffusion theory	ANC	4.3.3.3
3. X-Y-Z Power Distributions, Fuel Depletion, Critical Boron Concentrations, X-Y-Z Xenon Distributions, Reactivity Coefficients and Control Rod Worths	3-D 2-group diffusion theory	3D ANC	4.3.3.3
4. Axial power distributions, control rod worths, and axial xenon distribution	1-D, 2-group diffusion theory	APOLLO	4.3.3.3
5. Fuel rod power	Integral transport theory	LASER	4.3.3.1
Effective resonance temperature	Monte Carlo weighting function	REPAD	

TABLE 4.1-2 (Cont)

Analysis	Technique	Computer Code	Section Reference	
Thermal-hydraulic design				
1. Steady-state	Subchannel analysis of local fluid conditions in rod bundles, including inertial and crossflow resistance terms, solution progresses from core-wide to hot assembly to hot channel	VIPRE-01	4.4.4.5		
2. Transient departure from nucleate boiling analysis	Subchannel analysis of local fluid conditions in rod bundles during transients by including accumulation terms in conservation equations; solution progresses from core-wide to hot assembly to hot channel	VIPRE-01	4.4.4.5		

4.2 FUEL SYSTEM DESIGN

Beaver Valley Power Station - Unit 2 (BVPS-2) design conditions are divided into four categories in accordance with their anticipated frequency of occurrence and risk to the public: American Nuclear Standards (ANS) Condition I - Normal Operation; ANS Condition II - Incidents of Moderate Frequency; ANS Condition III - Infrequent Incidents; and ANS Condition IV - Limiting Faults. Chapter 15 describes the bases, BVPS-2 operational conditions, and events involving each ANS Condition.

The reactor is designed so that its components meet the following performance and safety criteria:

1.   The mechanical design of the reactor core components and their physical arrangement, together with corrective actions of the reactor control, protection, and emergency cooling systems (when applicable) ensure that:

   a.   Fuel damage is not expected during ANS Condition I and ANS Condition II events. Fuel damage as used here is defined as penetration of the fission product barrier (that is, the fuel rod clad). It is not possible, however, to preclude a very small number of rod failures resulting in the release of fission products. The chemical and volume control system (CVCS) is designed to remove these fission products from the reactor coolant, keeping the reactor coolant activity within BVPS-2 design basis limits.

   b.   The reactor can be brought to a safe state following an ANS Condition III event with only a small fraction of fuel rods damaged although sufficient fuel damage might occur to preclude immediate resumption of operation. In any case, the fraction of fuel rods damaged must be limited to meet regulatory dose guidelines.

   c.   The reactor can be brought to a safe state and the core can be kept subcritical with acceptable heat transfer geometry following transients arising from ANS Condition IV events.

2.   The fuel assemblies are designed to withstand loads induced during shipping, handling, and core loading without exceeding the criteria of Section 4.2.1.5.

3.   The fuel assemblies are designed to accept control rod insertions in order to provide the required reactivity control for power operations and reactivity shutdown conditions.

4.   All fuel assemblies have provisions for the insertion of incore instrumentation necessary for BVPS-2 operation.

5.   The reactor internals in conjunction with the fuel assemblies and incore control components direct reactor coolant through the core. This achieves acceptable flow distribution and restricts bypass

flow so that the heat transfer performance requirements can be met for all modes of operation.

The following section provides the fuel system design bases and design limits. This information, augmented by the clarifying information submitted to the USNRC during their review of Westinghouse Topical Report, WCAP-10444-A, Addendum 2-A, "VANTAGE 5H Fuel Assembly" (W. J. Johnson (Westinghouse) to M. W. Hodges (NRC), Letter No. NS-NRC-88-3319, dated April 15, 1988. W. J. Johnson (Westinghouse) to M. W. Hodges (NRC), Letter No. NS-NRC-88-3363, dated July 29, 1988.) provide information consistent with the acceptance criteria of the Standard Review Plan (SRP) 4.2.

Design values in Section 4.2.1 for the properties of the materials which comprise the fuel rod, fuel assembly and the incore control components are given in Beaumont 1978, Rev. 1, 1980 for Zircaloy-4 and Davidson et al (1990) for ZIRLO^{TM}. Other supplementary fuel design criteria/ acceptance limits are given in Davidson 1994.

4.2.1 Design Bases

The fuel rod and fuel assembly design bases are established for the 17 x 17 STD, V5H, VANTAGE+, and the RFA/RFA-2 fuel assemblies to satisfy the general performance and safety criteria presented in Section 4.2. Fuel rods may be replaced by non-fueled rods during reconstitution. For a description of the use of non-fueled rods in the reconstitution process, see Section 4.1.

The detailed fuel rod design established such parameters as pellet size and density, clad/pellet diametral gap, gas plenum size, and helium prepressurization level. The design also considers effects such as fuel density changes, fission gas release, clad creep, and other physical properties which vary with burnup. The integrity of the fuel rods is ensured by designing to prevent excessive fuel temperatures, excessive internal rod gas pressures due to fission gas releases, and excessive cladding stresses and strains. This is achieved by designing the fuel rods so that the conservative design bases in the following subsections are satisfied during ANS Condition I and ANS Condition II events over the fuel lifetime. For each design basis, the performance of the limiting fuel rod must not exceed the limits specified by the design basis. Refer to design bases and acceptance limits provided in Davidson 1994.

Integrity of the fuel assembly structure is ensured by setting limits on stresses and deformations due to various loads and by preventing the assembly structure from interfering with the function of other components. Three types of loads are considered.

1.   Nonoperational loads such as those due to shipping and handling.

2.   Normal and abnormal loads which are defined for ANS Conditions I and II.

3.   Abnormal loads which are defined for ANS Conditions III and
      IV.

The design bases for the incore control components are described in
Section 4.2.1.6.

4.2.1.1 Cladding

1.   Material and Mechanical Properties

      Zircaloy-4 and ZIRLO^{TM} combine low absorption cross
      sections, high corrosion resistance to coolant, fuel and
      fission products, high strength and ductility at operating
      temperatures and high reliability. Slagle WCAP-8183 (1996)
      documents the operating experience with Zircaloy-4 and
      ZIRLO^{TM} fuel rod clad material. Beaumont (1978 and 1980)
      and Davidson et al (1990) provide the mechanical properties
      and due consideration of their temperature and irradiation
      effects.

2.   Stress-Strain Limits

   a.   Clad stress - The clad stresses under ANS Conditions I and II are less than the Zircaloy or the ZIRLO^{TM} 0.2 percent offset yield stress, with due consideration of temperature and irradiation effects. While the clad has some capability for accommodating plastic strain, the yield stress has been accepted as a conservative design basis.

   b.   Clad tensile strain - The total tensile creep strain is less than one percent from the unirradiated condition. The elastic tensile strain during a transient is less than one percent from the pretransient value. This limit is consistent with proven practice (Beaumont et al 1978).

3.   Vibration and Fatigue

   a.   Strain fatigue - The cumulative strain fatigue cycles are less than the design strain fatigue life. This basis is consistent with proven practice (Section 4.2.3.3) (Christensen; Allio; and Biancheria 1965).

   b.   Vibration - Potential fretting wear due to vibration is limited, ensuring that the stress limits are not exceeded during design life. Fretting of the clad surface can occur due to flow-induced vibration between the fuel rods and fuel assembly grid springs. Vibration and fretting forces vary during the fuel life due to clad diameter creepdown combined with grid spring relaxation.

4.   Chemical properties of the Zircaloy-4 cladding are discussed by Beaumont et al (1978) and for ZIRLO^{TM} cladding by Davidson et al (1990).

4.2.1.2 Fuel Material

1.   Thermal-physical properties - fuel pellet temperature. The center temperature of the hottest pellet is to be below the melting temperature of the unirradiated UO_2 melting point of 5,080°F (Christensen, Allio, and Biancheria 1965) and decreasing by 58°F per 10,000 MWD/MTU). While a limited amount of center melting can be tolerated, the design conservatively precludes center melting. A calculated fuel centerline temperature of 4,700°F has been selected as an overpower limit to assure no fuel melting. This provides sufficient margin for uncertainties as described in Section 4.4.2.9.

The normal design density of the fuel is 95 percent of theoretical. Additional information on fuel properties is given by Beaumont (1978) for Zircaloy-4 and by Davidson et al (1990) for ZIRLO[TM].

2. Fuel densification and fission product swelling - The design bases and models used for fuel densification and swelling are provided by Hellman (1975), Miller (1976), Weiner (1988), and Foster (2000).

3. Chemical properties - for Zircaloy-4 Beaumont (et al 1978) and Davidson et al (1990) for ZIRLO[TM] provides the basis for justifying that no adverse chemical interactions occur between the fuel and its adjacent material.

4.2.1.3 Fuel Rod Performance

1. Fuel rod models - The basic fuel rod models and the ability to predict operating characteristics are given by Davidson (1985), Miller (1976), Weiner (1988), and Foster (2000) (Section 4.2.3).

2. Mechanical design limits - Fuel rod design methodology has been introduced that reduces the densification power spike factor to 1.0 and demonstrates that clad flattening will not occur in Westinghouse fuel designs (Kersting).

    The rod internal gas pressure remains below the value which causes the fuel/clad diametral gap to increase due to outward cladding creep during steady state operation.

    Rod pressure is also limited such that extensive departure from nucleate boiling (DNB) propagation shall not occur during normal operation and any accident event.

4.2.1.4 Spacer Grids

Mechanical limits and materials properties - The grid component strength criteria are based on experimental tests. The grid strength was based on the 95 percent confidence level on the true mean as taken from the distribution of measurements. This limit is sufficient to assure that under worst-case combined seismic and blowdown loads from an ANS Condition IV, loss-of-coolant accident (LOCA), the core will maintain a geometry amenable to cooling. As an integral part of the fuel assembly structure, the grids must satisfy the applicable fuel assembly design bases and limits defined in Section 4.2.1.5.

The grid material and chemical properties are given by Beaumont et al (1978) for Zircaloy-4 and by Davidson et al (1990) for ZIRLO[TM].

4.2.1.5 Fuel Assembly

Structural design - As discussed in Section 4.2.1, the structural integrity of the fuel assembly is ensured by setting design limits on stresses and deformations due to various nonoperational, operational,

and accident loads.   These limits are applied to the design and evaluation of the top and bottom nozzles, guide thimbles, grids, and thimble joints.

The design bases for evaluating the structural integrity of the fuel assemblies are:

1.   Nonoperation - 6 g lateral and 4 g axial loading with dimensional stability.

2.   For the normal operating and upset conditions, the fuel assembly component structural design criteria are established for the two primary material categories, namely austenitic steels and Zirconium alloys.   The stress categories and strength theory presented in the ASME Boiler and Pressure Vessel Code, Section III, are used as a general guide. The maximum shear-theory (Tresca criterion) for combined stresses is used to determine the stress intensities for the austenitic steel components.   The stress intensity is defined as the numerically largest difference between the various principal stresses in a three-dimensional field.   The allowable stress intensity value for austenitic steels, such as nickel-chromium-iron alloys, is given by the lowest of the following:

   a.   One-third of the specified minimum tensile strength or 2/3 of the specified minimum yield strength at room temperature.

   b.   One-third of the tensile strength or 90 percent of the yield strength at temperature, but not to exceed 2/3 of the specified minimum yield strength at room temperature.

      The stress limits for the austenitic steel components are given below (All stress nomenclature is per the ASME Code, Section III):

               Stress Intensity Limits

         Categories   Limits

         Local primary membrane   1.5 Sm
         stress intensity

         Primary membrane plus bending   1.5 Sm
         stress intensity

         Total primary plus secondary   3.0 Sm
         stress intensity

         where:

         Sm is the general primary membrane stress intensity

         The Zircaloy or ZIRLO^{TM} structural components which consist of guide thimbles and fuel tubes are in turn subdivided into two categories because of material differences and functional requirements.

The fuel cladding design criteria is covered separately in Section 4.2.1.1. The maximum shear theory is used to evaluate the guide thimble design. For conservative purposes, the Zircaloy and the ZIRLO^{TM} unirradiated properties are used to define the stress limits.

c. Abnormal loads during ANS Conditions III and IV - worst cases represented by combined seismic and blowdown loads.

   1) Deflections or failures of components cannot interfere with the reactor shutdown or emergency cooling of the fuel rods.

   2) The fuel assembly structural component stresses under faulted conditions are evaluated using primarily the methods outlined in Appendix F of the ASME Code, Section III. Because the current analytical methods utilize elastic analysis, the stress allowables are defined as the small value of 2.4 Sm or 0.70 Su for primary membrane and 3.6 Sm or 1.05 Su for primary membrane plus primary bending. For the austenitic steel fuel assembly components, the stress intensity is defined in accordance with the rules described in Section 4.2.1.4 for normal operating conditions. For the Zircaloy and ZIRLO^{TM} components the stress intensity limits are set at 2/3 of the material yield strength, Sy, at reactor operating temperature. This results in Zircaloy and ZIRLO^{TM} stress limits being the smaller of 1.6 Sy or 0.70 Su for primary membrane and 2.4 Sy or 1.05 Su for primary membrane plus bending. For conservative purposes, the Zircaloy and ZIRLO^{TM} unirradiated properties are used to define the stress limits.

       The material and chemical properties of the fuel assembly components are given in Beaumont et al (1978) for Zircaloy-4 and in Davidson et al (1990) for ZIRLO^{TM}.

   3) Thermal-hydraulic design - This topic is discussed in Section 4.4.

4.2.1.6 Reactivity Control Assembly; Burnable Absorber Rods and Source Rods

The core components are subdivided into permanent and temporary devices. The permanent type components are the rod cluster control assemblies (RCCAs) and secondary neutron source assemblies. The temporary components are the burnable absorber assemblies, thimble plug assemblies, and the primary neutron source assemblies; the primary neutron source assemblies are normally used only in the initial core. A description of these components is provided in Section 4.2.2.

Materials are selected for compatibility in a pressurized water reactor (PWR) environment, for adequate mechanical properties at room and operating temperatures, for resistance to adverse property changes in a radioactive environment, and for compatibility with interfacing components. Material properties are given by Beaumont et al (1978) for Zircaloy-4 and by Davidson et al (1990) for ZIRLO^{TM}.

For ANS Conditions I and II, the stress categories and strength theory presented in the ASME Boiler and Pressure Vessel Code, Section III, Subsection NB and NG are used as a general guide to establish core component rod cladding stress/strain limits. The code methodology is applied, as with fuel assembly structural design where possible. For ANS Conditions III and IV, code stresses are not limiting.

Additional design bases for each of the mentioned components are given in the following subsections.

A.   Mechanical Design Bases

  1.   Rod Cluster Control Assemblies

        Design conditions which are considered under Subsections NB and NG of the ASME Code, Section III are as follows:

        a.   External pressure equal to the reactor coolant system (RCS) operating pressure with appropriate allowance for overpressure transients.

        b.   Wear allowance for continuous load follow operation during control rod assembly lifetime.

        c.   Bending of the rod due to a misalignment in the guide tube.

        d.   Forces imposed on the rods during rod drop.

        e.   Loads imposed by the accelerations of the control rod drive mechanism (CRDM).

      f.   Radiation exposure during maximum core life.

      g.   Temperature effects at operating conditions.

2.   Burnable Absorber, Thimble Plug and Source Rod Assemblies

The burnable absorber assemblies, thimble plug assemblies and source assemblies are static core components. The mechanical design of these components satisfies the following:

      a.   Accommodate the differential thermal expansion between the fuel assembly and the core internals.

      b.   Maintain positive contact with the fuel assembly and the core internals.

B.   Thermal-Physical Properties of the Absorber Material

The absorber material for the RCCA is Ag-In-Cd. The thermal-physical properties of Ag-In-Cd are described in Cohen (1959). The absorber material temperature shall not exceed its melting temperature (1,454°F for Ag-In-Cd).

The burnable absorber material is B_4C contained in an alumina matrix.

Thermal-physical and gas release properties of AL_2O_3-B_4C are described in Beaumont (et al 1978) and Skaritka (et al 1983). Westinghouse wet annular burnable absorber (WABA) rods are designed so that the absorber temperature does not exceed 1,200°F during normal operation or during an overpower transient. The 1,200°F maximum assures that the total maximum He gas release in a WABA rod will not exceed 30 percent (Skaritka et al 1983).

C.   Compatibility of the Absorber and Cladding Materials

The control rod cladding is cold drawn type 304 stainless steel tubing. Extensive in-reactor experience and available quantitative information show that reaction rates between 304 stainless steel and water and other contacting metals are negligible at operational temperatures (Beaumont et al 1978).

The WABA rod cladding is Zircaloy-4. Due to the relatively low pellet design temperature, no appreciable reaction will occur between the absorber materials and the cladding. Diffusion rates are slow at the temperatures; Al_2O_3-B_4C remains at temperatures less than 1,200°F.

Compatibility of Al_2O_3-B_4C with a similar alloy, Zircaloy-2, has been demonstrated in irradiation tests at BMI (Burian, Fromui, and Gates 1963).

D.   Cladding Stress-Strain Limits

1.   Control Rod and Source Rod Cladding

For Conditions I and II, the stress categories and strength theory presented in the ASME Boiler and Pressure Vessel Code, Section III, subsection NG-3000, are used as a general guide. The Code methodology is applied, as with fuel assembly structural design, where possible. For Conditions III and IV code stresses are not limiting.

The deformation or failure of the control rod cladding must not prevent reactor shutdown or cooling of the fuel rods. A breach in the cladding does not result in serious consequences because the Ag-In-Cd material is relatively inert (Cohen 1939).

2.   Burnable Absorber Rod Cladding

For Conditions I and II loading conditions occurring during the design life, all structural parts account for external pressure, differential expansion of pellets and clad, pellet swelling, clad creep, helium gas release, initial internal helium pressure, thermal stress, and flow-induced vibrations. The structural criteria for normal operating and upset conditions, Conditions I and II are satisfied since the maximum primary tensile stress in the Zircaloy clad does not exceed the unirradiated yield strength, and the burnable absorber cladding uses a total strain limit of 3 percent at strain rates of less than 10^{-4}/hr and temperatures below 720°F. For strain rates greater than 10^{-4}/hr, the fuel rod ductility limit of 1 percent is imposed. For normal occurrence, Conditions III and IV, stress limits are not considered applicable (Skaritka et al 1983).

The design evaluation of the core components is discussed in Section 4.2.3.6.

E.   Irradiated Behavior of Absorber Material

Operating experience and testing evaluation of the effects of irradiation upon the properties of Ag-In-Cd have shown that in-pile corrosion behavior is similar to out-of-pile behavior and that, for low oxygen content water, corrosion rates are low (Beaumont et al 1978).

The microstructure and density of the burnable absorber $AL_2O_3-B_4C$ pellet achieves an acceptable combination of gas release and pellet swelling to maintain integrity under irradiation. Material evaluation and the good performance of WABA demonstration rods are presented in Skaritka (et al 1983).

4.2.1.7 Surveillance Program

Sections 8 and 23 of Eggleston (1978) and Section 4.2.4.5 discuss the testing and fuel surveillance operational experience program which is being conducted to verify the adequacy of the fuel performance and design bases. Fuel surveillance and testing results, as they become available, are used to improve fuel rod design and manufacturing processes and ensure that the

design bases and safety criteria are satisfied. Slagle (1996)
provides results of fuel operating experience, which includes a
substantial amount of 17 by 17 fuel assembly irradiation. The
improved corrosion resistance of ZIRLO cladding has been demonstrated
to high burnups in the BR-3, North Anna and V. C. Summer demonstration
assemblies. Cladding corrosion measurement showed that the reduced
corrosion exhibited by the ZIRLO^{TM} clad rods was better than
anticipated.

4.2.2 Design Description

The fuel assembly, fuel rod, and incore control component design are
given in Table 4.3-1.

Each 17 by 17 fuel assembly consists of 264 fuel rods, 24 guide
thimble tubes, and one instrumentation thimble tube arranged within a
supporting structure. The instrumentation thimble is located in the
center position and provides a channel for insertion of an incore
neutron detector, if the fuel assembly is located in an instrumented
core position. The guide thimbles provide channels for insertion of
either an RCCA, a neutron source assembly, a burnable absorber
assembly, or a thimble plug assembly, depending on the position of the
particular fuel assembly in the core. Figure 4.2-1 shows a cross
section of the fuel assembly array. A fuel assembly full-length view
is shown in Figure 4.2-2 for the V5H fuel assembly, Figure 4.2-2a for
the V5H + ZIRLO (VANTAGE+) fuel assembly, Figure 4.2-2b for the Robust
Fuel Assembly (RFA/RFA-2) and Figure 4.2-2c for the robust fuel
assembly with Standardized Debris Filter Bottom Nozzle and Robust
Protective Grid. The fuel rods are loaded in the fuel assembly
structure so that there is clearance between the fuel rod ends and the
top and bottom nozzles. Fuel assemblies are installed vertically in
the reactor vessel and stand upright on the lower core plate which is
fitted with alignment pins to locate and orient each assembly. After
all fuel assemblies are set in place, the upper support structure is
installed. Alignment pins, built into the upper core plate, engage
and locate the upper ends of the fuel assemblies. The upper core
plate then bears downward against the hold-down springs on the top
nozzle of each fuel assembly to hold the fuel assemblies in place.
The fuel rod also has an oxide coating on the bottom of the fuel rod
to provide additional rod fretting wear protection.

The VANTAGE+ assembly skeleton is identical to that previously
described for VANTAGE 5H except for those modifications necessary to
accommodate the intended fuel operation to higher burnups. The
modifications consist of the use of ZIRLO^{TM} guide thimbles and small
skeleton dimensional alterations to provide additional fuel assembly
and rod growth space at the extended burnup levels. The VANTAGE+ fuel
assembly is shorter than the VANTAGE 5H fuel assembly. The grid
centerline elevations of the VANTAGE+ are identical to those of the
VANTAGE 5H fuel assembly, except that the top grid has been lowered
and, to accommodate the bottom protective grid, the first grid has
been raised slightly and the second grid has been lowered slightly to
maintain an equivalent pressure drop. However, since the VANTAGE+
fuel is intended to replace the VANTAGE 5H fuel, the VANTAGE+ exterior
assembly envelope is equivalent in design dimensions, and the
functional interface with the reactor internals is also equivalent to

those of previous Westinghouse fuel designs. Also the VANTAGE+ fuel
assembly is designed to be mechanically and hydraulically compatible
with the VANTAGE 5H fuel assembly. The same functional requirements
and design criteria as previously established for the Westinghouse
VANTAGE 5H fuel assembly remains valid for the VANTAGE+ fuel assembly.
The VANTAGE+ fuel assembly design and a comparison to the VANTAGE 5H
design is provided in Figures 4.2-2 and 4.2-2a.

The Robust Fuel Assembly (RFA/RFA-2) design is shown in Figure 4.2-2b.
The design changes from the VANTAGE+ to the RFA/RFA-2 design includes:
modified low pressure drop (LPD) mid-grids, the inclusion of three
intermediate flow mixer (IFM) grids, and thicker guide thimbles and
instrument tube. Based on post irradiation examinations (PIE) data on
fuel assembly growth with ZIRLO^{TM} guide thimbles, the fuel assembly
and fuel rod lengths were increased by 0.200 inch relative to the
VANTAGE+ design.   The mid-grid centerlines are identical to the
VANTAGE+ design with the exception of the top grid, which was raised
0.200 inch along with the increase in fuel assembly length of the
RFA/RFA-2 design.   The RFA/RFA-2 design continues to utilize the
protective bottom grid and ZIRLO^{TM} fuel rods and skeleton.   The
VANTAGE+ and RFA/RFA-2 assembly exterior envelope is equivalent in
design dimensions to the STD and VANTAGE 5H assembly. The functional
interface with the reactor internals is also equivalent to those of
the STD and VANTAGE 5H fuel assembly designs.   The VANTAGE+ and
RFA/RFA-2 are designed to be mechanically and hydraulically compatible
with the STD and VANTAGE 5H, and the same functional requirements and
design criteria as previously established for the Westinghouse VANTAGE
5H fuel assembly remain valid for the VANTAGE+ and RFA/RFA-2.   The
RFA-2 design has an increased contact area between the mid-grid
dimples/springs and the fuel rods relative to the RFA design.   The
increased contact area is intended to reduce fretting wear.

In Cycle 17, the RFA-2 design incorporated the Robust Protective Grid
(RPG) to reduce the probability of cracking and dimple/ligament
separation.   The RPG design increases the height of the grid,
increases the ligament length and radii of the ligament cutouts, and
increases the number of insert welds from four to eight to help
support the grid.   These modifications are designed to reduce the
fatigue failures due to stress corrosion cracking within the rod
support dimples of the protective grid.   An additional feature
incorporated to the RFA-2 design in Cycle 17 is the Low Strain Radius
mid grid and IFM grid design, which is designed to lower the strain
imposed on the formed features of the grids and improve their
manufacturability.

Improper orientation of fuel assemblies within the core is prevented
by the use of an indexing hole in one corner of the top nozzle top
plate. The assembly is oriented with respect to the handling tool and
the core by means of a pin which is inserted into this indexing hole.
Visual confirmation of proper orientation is also provided by an
engraved identification number on the opposite corner clamp.

4.2.2.1 Fuel Rods

The fuel rods consist of uranium dioxide ceramic pellets contained in
slightly cold worked Zircaloy-4 or ZIRLO^{TM} tubing which is plugged and
seal welded at the ends to encapsulate the fuel. A schematic of the

fuel rod is shown on Figures 4.2-3, 4.2-3a, and 4.2-3b. The fuel pellets are right circular cylinders consisting of slightly enriched uranium dioxide powder which has been compacted by cold pressing and then sintered to the required density. The ends of each pellet are dished slightly to allow greater axial expansion at the center of the pellets. The fuel rods may also contain annular pellets in the upper and lower six inch axial blanket regions which have no dish on the pellet ends, but are hollow for additional gas volume.

The VANTAGE+ fuel rod represents a modification to the VANTAGE 5H fuel rod intended to support operation for fuel clad in place of Zircaloy-4 clad. The ZIRLO^{TM} alloy is a zirconium alloy similar to Zircaloy-4, which has been specifically developed to enhance corrosion resistance.

The VANTAGE+ fuel rods will contain, as in VANTAGE 5H enriched uranium dioxide fuel pellets, and an Integral Fuel Burnable Absorber (IFBA) coating on some of the enriched fuel pellets. Schematics of the fuel rods are shown in Figure 4.2-3A.

The VANTAGE+ fuel rod has the same clad wall thickness as the VANTAGE 5H design. The VANTAGE+ fuel tube is shorter to provide room for the required fuel rod growth. To offset the reduction in the plenum length, the VANTAGE+ fuel rod has a variable pitch plenum spring. This spring has a smaller wire diameter and coil diameter and a shorter coil length. The variable pitch plenum spring provides the same support as the regular VANTAGE+ plenum spring but with fewer spring turns which translates to less spring volume. The bottom end plug has an internal grip feature to facilitate fuel rod loading on both designs (VANTAGE+ and VANTAGE 5) and provides appropriate lead-in for the removable top nozzle reconstitution feature. The VANTAGE+ fuel rod also has an oxide coating at the bottom end of the fuel rod. The extra layer of oxide coating provides additional debris induced rod fretting wear protection.

The RFA fuel rod utilizes the same ZIRLO^{TM} cladding material and clad wall thickness as the VANTAGE+ design. The RFA fuel rod is longer than the VANTAGE 5H and VANTAGE+ designs but maintains sufficient margin for fuel rod growth. This provides additional plenum length to accommodate fission gas release associated with high burnup. The remaining fuel rod features of the RFA fuel rod are the same as the VANTAGE+ design with the exception of the external gripper feature of the VANTAGE+ top end plug which has been eliminated for the RFA design to also afford additional plenum volume. A schematic of the RFA fuel rods is shown in Figure 4.2-3b. The RFA and RFA-2 fuel rod designs are identical.

Void volume and clearances are provided within the rods to accommodate fission gases released from the fuel, differential thermal expansion between the clad and the fuel, and fuel density changes during irradiation. Shifting of the fuel within the clad during handling or shipping prior to core loading is prevented by a stainless steel helical spring which bears on top of the fuel. During assembly, the pellets are stacked in the clad to the required fuel height. The spring (VANTAGE+ and RFA/RFA-2 have a variable pitch) is then inserted into the top end of the fuel tube and the end plugs pressed into the ends of the tube and welded. All fuel rods are internally pressurized with helium during the welding process in order to minimize compressive clad stresses and prevent clad flattening due to reactor coolant operating pressures.

The axial blankets are a nominal 6 inches of either unenriched or slightly enriched fuel pellets at each end of the fuel rod pellet stack. Axial blankets reduce neutron leakage and improve fuel utilization. The axial blankets utilize chamfered pellets which are physically different (length) than the enriched pellets to help prevent accidental mixing during manufacturing. Annular pellets may be utilized in the axial blanket region to allow for additional gas volume.

The IFBA coated fuel pellets are identical to the enriched uranium dioxide pellets except for the addition of a thin zirconium diboride

(ZrB_2) coating on the pellet cylindrical surface. Coated pellets occupy the central portion of the fuel column (up to 132 inches). The number and pattern of IFBA rods within an assembly may vary depending on the specific application. The ends of the IFBA enriched coated pellets, like the enriched uncoated pellets, are also dished to allow for greater axial expansion at the pellet centerline and void volume for fission gas release. An evaluation and test program for the IFBA design features is given in Section 2.5 of Davidson (1985). Standard IFBA patterns have been introduced in Beaver Valley Unit 2.

The fuel rods are prepressurized and designed so that: 1) the internal gas pressure mechanical design limit discussed in Section 4.2.1.3 is not exceeded, 2) the cladding stress-strain limits (Section 4.2.1.1) are not exceeded for ANS Condition I and II events, and 3) clad flattening will not occur during the fuel core life.

4.2.2.2 Fuel Assembly Structure

The fuel assembly structure consists of a bottom nozzle, top nozzle, guide thimbles, and grids, as shown on Figures 4.2-2, 4.2-2a, and 4.2-2b.

4.2.2.2.1 Bottom Nozzle

The bottom nozzle serves as bottom structural element of the fuel assembly and directs the reactor coolant flow distribution to the assembly. The nozzle is fabricated from Type 304 stainless steel and consists of a perforated plate skirt, and four angle legs with bearing plates as shown on Figures 4.2-2, 4.2-2a, 4.2-2b and 4.2-2c. The legs and skirt form a plenum for the inlet coolant flow to the fuel assembly. The plate also prevents accidental downward ejection of the fuel rods from the fuel assembly. The bottom nozzle is fastened to the fuel assembly guide tubes by screws which penetrate through the nozzle and mate with a threaded plug in each guide tube. The screw is prevented from loosening by a stainless steel thimble screw with integral locking cap.

The VANTAGE 5H, VANTAGE+, and RFA/RFA-2 designs will include use of the Debris Filter Bottom Nozzle (DFBN) to reduce the possibility of fuel rod damage due to debris-induced fretting. The relatively large flow holes in a conventional nozzle are replaced with a new pattern of smaller flow holes. The holes are sized to minimize passage of debris particles large enough to cause damage while providing sufficient flow area, comparable pressure drop, and continued structural integrity of the nozzle. In Cycle 17 the RFA-2 fuel design incorporated the Standardized Debris Filter Bottom Nozzle (SDFBN) which is designed to have a loss coefficient that is independent of nozzle sub-supplier and varies less from nozzle to nozzle within each sub-supplier. The SDFBN has the same nominal loss coefficient as the DFBN. The SDFBN has eliminated the side skirt communication flow holes as a means of improving the debris mitigation performance of the bottom nozzle. This nozzle has been extensively evaluated and analyzed and it was demonstrated that it meets all of the applicable mechanical design criteria. Further, specific testing was performed to demonstrate that there is no adverse effect on the thermal hydraulic performance of the SDFBN either with respect to the pressure drop or with respect to DNB.

Reactor coolant flows from the plenum in the bottom nozzle upward through the penetration in the plate to the channels between the fuel rods. The penetrations in the plate are positioned between the rows of fuel rods.

Axial loads (holddown) imposed on the fuel assembly and the weight of the fuel assembly are transmitted through the bottom nozzle to the lower core plate. Indexing and positioning of the fuel assembly are provided by alignment holes in two diagonally opposite bearing plates which mate with locating pins in the lower core plate. Lateral loads on the fuel assembly are transmitted to the lower core plate through the locating pins.

4.2.2.2.2 Top Nozzle

<u>Westinghouse Integral Nozzle</u>

Commencing with Beaver Valley Unit 2, Cycle 19, the Westinghouse
Integral Nozzle (WIN) will replace the Reconstitutable Top Nozzle
(RTN) as part of the RFA-2 fuel assembly. The WIN top nozzle
functions as the upper structural element of the fuel assembly in
addition to providing a partial protective housing for the RCCA or
other components. The top nozzle consists of an adapter plate,
enclosure, top plate, and pads. The holddown springs are mounted on
the assembly, with the tail of the spring captured beneath a corner
clamp that is integral to the nozzle body. For the WIN, the springs
are made of Alloy 718 and the main nozzle body and the pins are made
of Type 304 stainless steel.

The WIN design, while similar to the RTN described in the following
section, incorporates design and manufacturing improvements to
eliminate the Alloy 718 spring screw for attachment of the holddown
springs. In the WIN nozzle, the springs are assembled into the nozzle
pad and pinned in place. The WIN design provides a wedged rather than
a clamped (bolted) joint for transfer of the fuel assembly holddown
forces into the top nozzle structure. Integral pads which contain
alignment holes for locating the upper end of the fuel assembly are
positioned on the other two corners of the WIN. The flow plate,
thermal characteristics, and method of attachment of the nozzle are
all unchanged from the RTN top nozzle design, as described in the
following section. The fuel assembly dimensions, shown in
Figure 4.2-2c, are unchanged by the WIN.

<u>Reconstitutable Top Nozzle (RTN)</u>

The VANTAGE 5H, VANTAGE+, and RFA/RFA-2 reconstitutable top nozzle
assembly functions as the upper structural element of the fuel
assembly in addition to providing a partial protective housing for the
RCCA or other components, which are installed in the guide thimble
tubes. It consists of an adapter plate, enclosure, top plate, and
pads. The top nozzle assembly comprises holddown springs, screws, and
clamps mounted on the top plate as shown on Figures 4.2-2, 4.2-2a and
4.2-2b. The springs and spring screws are made of Inconel-718 and –
600, respectively, whereas other components are made of Type 304
stainless steel. Beginning with Beaver Valley Unit 2 Cycle 9, the top
nozzle assembly utilizes a composite (cast) design. The top nozzle
holddown spring screws are made of Inconel-718 and bead-blasted (shot
peened) in the shank-to-thread area of the spring screw to inhibit
initiation and propagation of primary water stress corrosion cracking
(PWSCC). The nozzle adapter plate, thimble holes and flow hole
pattern remain unchanged, thus there is no impact on flow conditions.

The adapter plate is provided with round penetrations and semicircular
ended slots to permit the flow of coolant upward through the top
nozzle. Other round holes are provided to accept inserts which are
locked into internal grooves in the adapter plate at their upper ends
using a lock tube and mechanically attached to the thimble tubes at
the lower end. See Figures 4.2-2, 4.2-2a, and 4.2-2b. The ligaments
in the plate cover the tops of the fuel rods and prevent their upward

ejection from the fuel assembly. The enclosure is a box-like structure which sets the distance between the adapter plate and the top plate. The top plate has a large square hole in the center to permit access for the control rods and the control rod spiders. Holddown springs are mounted on the top plate and are retained by spring screws and clamps located at two diagonally opposite corners. On the other two corners, integral pads are positioned which contain alignment holes for locating the upper end of the fuel assembly.

The reconstitutable top nozzle for the VANTAGE 5H, VANTAGE+, and RFA/RFA-2 fuel assemblies differ from the conventional design in two ways: a groove is provided in each thimble throughhole in the nozzle plate to facilitate attachment and removal; and the nozzle plate thickness is reduced to provide additional axial space for fuel rod growth.

In the VANTAGE 5H, VANTAGE+, and RFA/RFA-2 reconstitutable top nozzle design, a stainless steel nozzle insert is mechanically connected to the top nozzle adapter plate by means of a preformed circumferential bulge near the top of the insert. The insert engages a mating groove in the wall of the adapter plate thimble tube throughhole. The insert has four equally spaced axial slots which allow the insert to deflect inwardly at the elevation of the bulge, thus permitting the installation or removal of the nozzle. The insert bulge is positively held in the adapter plate mating groove by placing a lock tube with a uniform ID identical to that of the thimble tube into the insert. See Figure 4.2-6 for details.

To remove the top nozzle, a tool is first inserted through the lock tube and expanded radially to engage the bottom edge of the tube. An axial force is then exerted on the tool which overrides the local lock tube deformations and withdraws the lock tube from the insert. After the lock tubes have been withdrawn, the nozzle is removed by raising it off the upper slotted ends of the nozzle inserts which deflect inwardly under the axial lift load. With the top nozzle removed, direct access is provided for fuel rod examination or replacement. Reconstitution is completed by the remounting of the nozzle and the insertion of new lock tubes. The design bases and evaluation of the reconstitutable top nozzle are given in Section 2.3.2 of Davidson (1985).

4.2.2.2.3 Guide Thimbles and Instrument Tubes

The guide thimbles are structural members which also provide channels for the neutron absorber rods, burnable absorber rods, neutron source, or thimble plug assemblies. Each thimble is fabricated from Zircaloy-4 or ZIRLO^{TM} tubing having two different diameters. With the exception of a reduction in the guide thimble diameter above the dashpot, the VANTAGE 5H (V5H) and VANTAGE+ guide thimbles are identical to those in the LOPAR design. A 0.008 inch reduction to the guide thimble OD and ID is required due to the thicker grid straps. The guide thimble tube ID provides an adequate nominal diametral clearance of 0.061 inch for the control rods. The reduced thimble tube ID also provides sufficient diametral clearance for burnable absorber rods, source rods, and any dually compatible thimble plugs. The tube diameter at the top section provides the annular area necessary to permit rapid control rod insertion during a reactor trip. The lower portion of the guide thimble is swaged to a smaller diameter to reduce diametral clearances and produce a dashpot action near the end of the control rod travel during normal trip operation. Holes are provided in the thimble tube above the dashpot to reduce the rod drop time. The dashpot is closed at the bottom by means of an end plug which is provided with a small flow port to avoid fluid stagnation in the dashpot volume during normal operation. The top end of the guide thimble is fastened to an insert by three expansion swages. The insert fits into and is locked into the top nozzle adapter plate using a lock tube shown in Figure 4.2-6. The lower end of the guide thimble is fitted with an end plug which is then fastened into the bottom nozzle by an integral locking cup thimble screw.

The RFA/RFA-2 design features include a thicker wall guide thimble tube and thicker wall instrumentation tube relative to the VANTAGE 5H and VANTAGE+ designs. The wall thickness increase was obtained by increasing the outside diameter while maintaining the same inside diameter for control rod insertions. The ZIRLO^{TM} mid and IFM grids had the grid cells with the guide thimble or instrument tube locations embossed (radial) to accommodate the thicker guide thimble and instrument tube. The guide thimble and instrument tube wall thickness is increased by approximately 25% to improve stiffness and mitigate incomplete rod insertion (IRI).

Fuel rod support grids are fastened to the guide thimble assemblies to create an integrated structure. The Inconel and Zircaloy or ZIRLO^{TM} grids are attached to the Zircaloy or ZIRLO^{TM} thimble using the mechanical fastening technique as depicted on Figures 4.2-4 and 4.2-5, except for the bottom grid which is retained by clamping between the thimble end plug and the bottom nozzle.

An expanding tool is inserted into the inner diameter of the Zircaloy or ZIRLO^{TM} thimble tube at the elevation of the grid sleeves which have been previously attached to the Inconel grid top assembly. The four lobed tool forces the thimble and sleeve outward to a predetermined diameter, thus joining the two components.

The top Inconel grid sleeve, top nozzle insert, and thimble tube are joined together using three joint mechanical attachments as shown in Figure 4.2-6. This bulge joint connection was mechanically tested and found to meet all applicable design criteria.

The mixing vane zircaloy or ZIRLO^{TM} grids employ a single bulge connection to the sleeve and thimble as compared to a three bulge connection used in the top inconel grid (Figure 4.2-5). Mechanical testing of this bulge joint connection was also found to be acceptable.

The bottom grid assembly is joined to the assembly as shown on Figure 4.2-7. The stainless steel insert is spot welded to the bottom grid and later captured between the guide thimble and plug and the bottom nozzle by means of a stainless steel integral locking cup thimble screw.

These methods of grid fastening are standard and have, with the exception of the integral locking cup thimble screw, been used successfully since the introduction of Zircaloy guide thimble in 1969.

The central instrumentation tube of each fuel assembly is constrained by seating in a counterbore in the bottom nozzle at its lower end and is expanded at the top and mid grids in the same manner as the previously discussed expansion of the guide thimbles to the grids. This tube is of constant diameter and guides the incore neutron detectors.

The V5H and VANTAGE+ instrumentation tube also has an 0.008 inch diametral decrease compared to the LOPAR assembly instrumentation tube. This decrease still allows sufficient diametral clearance for the incore neutron detector to traverse the tube without binding. The RFA/RFA-2 instrumentation tube has a thicker wall while maintaining the same ID as the V5H and VANTAGE+ designs as described above.

4.2.2.2.4 Grid Assemblies

The fuel rods, as shown on Figures 4.2-2, 4.2-2a, and 4.2-2b, are supported at intervals along their length by grid assemblies which maintain the lateral spacing between the rods. Each fuel rod is supported within each grid by the combination of support dimples and springs. The grid assembly consists of individual slotted straps assembled and interlocked into an "egg-crate" arrangement with the straps permanently joined at their points of intersection.

The magnitude of the grid restraining force on the fuel rod is set high enough to minimize possible fretting, without overstressing the cladding at the points of contact between the grids and fuel rods. The grid assemblies also allow axial thermal expansion of the fuel rods without imposing restraint sufficient to develop buckling or distortion of the fuel rods.

Up to four types of grid types are used in each fuel assembly: mid-grids (structural grids with flow mixing vanes), intermediate flow mixing (IFM) grids (non-structural with flow mixing vanes), top and bottom structural grids without mixing vanes, and the protective grid. The flow mixing vanes project from the edge of the inner grid strap into the coolant stream to promote mixing of the coolant in the high heat flux region of the fuel assembly. The top and bottom structural grids do not contain mixing vanes on the internal straps. The outside straps on all grids contain mixing vanes which, in addition to their mixing function, aid in guiding the grids and fuel assembly past projecting surfaces during fuel handling and loading/unloading the core.

The top and bottom Inconel (non-mixing vane) grids of the STD, V5H, VANTAGE+, and RFA/RFA-2 assemblies are nearly identical in design. The only differences are: 1) V5H, VANTAGE+, and RFA/RFA-2 interactions during core loading/unloading, 2) V5H, VANTAGE+, and RFA/RFA-2 top and bottom grids have dimples which are rotated 90 degrees to minimize fuel rod fretting and dimple cocking, 3) V5H, VANTAGE+, and RFA/RFA-2 top and bottom grid heights have been increased to 1.522 inches, 4) the V5H, VANTAGE+, and RFA/RFA-2 top grid spring force has been reduced to minimize rod bow, and 5) the V5H, VANTAGE+, and RFA/RFA-2 top grid uses 304L stainless steel sleeves.

The six mid-structural (mixing vane) grids are made of zircaloy or ZIRLO™ material rather than Inconel which was used in the STD design. These V5H (known as the VANTAGE 5H zircaloy grids), VANTAGE+, and RFA/RFA-2 grids (known as ZIRLO™ grids) are designed to give the same pressure drop as the Inconel grid. Relative to the Inconel grid, the V5H zircaloy, VANTAGE+ ZIRLO™, and RFA/RFA-2 grid strap thickness and strap height are increased for structural performance. In addition to the snag-resistant design noted above, the upstream strap edges of the V5H zircaloy, VANTAGE+ ZIRLO™, and RFA/RFA-2 grids are chamfered and a diagonal grid spring is employed to reduce pressure drop. The V5H zircaloy grids, VANTAGE+ ZIRLO™, and RFA/RFA-2 grids incorporate the same grid cell support configuration as the Inconel grids (six support locations per cell: four dimples and two springs). The zircaloy and ZIRLO™ grid interlocking strap joints and grid/sleeve joints are fabricated by laser welding, whereas the Inconel grid joints are brazed. The RFA-2 design has an increased contact area between the mid-grid dimples/springs and the fuel rods relative to the RFA design. The increased contact area is intended to further reduce fretting wear.

The V5H zircaloy, VANTAGE+ ZIRLO™ and RFA/RFA-2 mid-structural grids have superior dynamic structural performance relative to the inconel grid.   Structural testing was performed and analyses have shown the V5H zircaloy grid and ZIRLO™ grid seismic/LOCA load margin is superior to that of the Inconel grid.

The RFA/RFA-2 fuel assembly design incorporates three ZIRLO^{TM} intermediate flow mixing (IFM) grids positioned at the mid-spans of the four uppermost mid-grids to further increase the flow turbulence in the axial zone where departure from nucleate boiling (DNB) is limiting. Each IFM grid cell contains four dimples, which are designed to prevent mid-span channel closure in the spans containing IFMs and fuel contact with the mixing vanes. For the RFA/RFA-2 design, the modified low pressure drop mid-grids and IFM grids are embossed to accept the larger diameter guide thimble tubes and instrument tube. Starting in Cycle 17, the RFA-2 design incorporates the Low Strain Radius mid grid and IFM grid design, which is designed to lower the strain imposed on the formed features of the grids and improve their manufacturability.

Commencing with Beaver Valley Unit 2 Cycle 7 the reload fuel assemblies will incorporate a protective bottom grid and modifications to the top and bottom fuel rod end plug. The protective bottom grid illustrated in Figures 4.2-2a and 4.2-2b is a partial height grid similar in configuration to the intermediate flow mixing grid, fabricated of Inconel without mixing vanes and positioned on the top plate of the bottom nozzle. In conjunction with the protective bottom grid, both the bottom and the top fuel rod end plugs were elongated. The protective bottom grid and the elongated bottom end plug together provide a zone below the active fuel in which debris can be trapped.

In Cycle 17, the RFA-2 fuel assemblies incorporated the combination grid which is a combination of the bottom grid and Robust Protective Grid (RPG). The RPG is designed to address the issues of fatigue failures and failures due to stress corrosion cracking within the rod support dimples. The RPG incorporates the following features:

- "Saw Tooth" vibration mitigation feature on both the top and bottom ligament,

- Increased dimple window width and length,

- Increased strap height,

- Increased number of grid inserts welded to the grid from four to eight.

4.2.2.3 Core Components

Reactivity control is provided by neutron absorbing rods and a soluble chemical neutron absorber (boric acid). The boric acid concentration is varied to control long term reactivity changes such as:

    1.   Fuel depletion and fission product buildup.

    2.   Cold to hot, zero power reactivity change.

    3.   Reactivity change produced by intermediate term fission products such as xenon and samarium.

    4.   Burnable absorber depletion.

The Chemical and Volume Control System (CVCS) is discussed in Section 9.3.4.

The RCCAs provide reactivity control for:

    1.   Shutdown,

    2.   Reactivity changes due to reactor coolant temperature changes in the power range,

    3.   Reactivity changes associated with the power coefficient of reactivity, and

    4.   Reactivity changes resulting from void formation.

At hot full power conditions it is necessary to maintain a negative moderator temperature coefficient throughout the entire cycle in order to reduce possible deleterious effects caused by a positive coefficient during LOCA or loss-of-flow accidents. A combination of burnable absorbers, rod withdrawal limits and/or soluble boron is used to ensure a negative moderator temperature coefficient at 100 percent power during all portions of the fuel operating cycle.

The RCCAs and their CRDMs are the only moving parts in the reactor. Figure 4.2-8 illustrates the rod cluster control (RCC) and CRDMs assembly, in addition to the arrangement of these components in the reactor, relative to the interfacing fuel assembly and guide tubes. In the following paragraphs, each reactivity control component is described in detail. The CRDM assembly is described in Section 3.9N.4.

The neutron source assemblies provide a neutron source for monitoring the core during periods of low neutron flux level. The thimble plug assemblies limit bypass flow through those fuel assembly thimbles which do not contain control rods, burnable absorber rods, or neutron source rods.

4.2.2.3.1 Rod Cluster Control Assembly

The RCCAs are divided into two categories: control and shutdown. The control groups compensate for reactivity changes associated with variations in operating conditions of the reactor, that is, power and temperature variations. Two nuclear design criteria have been employed for selection of the control group. First, the total reactivity worth must be adequate to meet the nuclear requirements of the reactor. Second, in view of the fact that these rods may be partially inserted at power operation, the total power peaking factor should be low enough to ensure that the power capability is met. The control and shutdown groups provide adequate shutdown margin.

The RCCA is comprised of 24 neutron absorber rods fastened at the top end to common spider assembly, as illustrated on Figure 4.2-9.

The absorber material used in the control rods is Ag-In-Cd which has a high thermal neutron cross-section and has sufficient additional reasonance absorption to significantly increase their worth. The Ag-In-Cd is in the form of extruded rods which are sealed in cold worked stainless steel tubes to prevent the rods from coming in direct contact with the reactor coolant (Figure 4.2-10). The full length control rod assemblies shall contain a nominal 142 inches of absorber material. The nominal values of absorber material shall be 80 percent silver, 15 percent indium and 5 percent cadmium. All control rods shall be clad with stainless steel tubing. The rodlet tubes may include a hard chrome plating to provide additional wear resistance. Sufficient diametral and end clearance is provided to accommodate relative thermal expansions.

The bottom plugs are made bullet-nosed to reduce the hydraulic drag during reactor trip and to guide the rodlet smoothly into the dashpot section of the fuel assembly guide thimbles.

The absorber rod end plugs are Type 308 stainless steel or equivalent. The design stresses used for the Type 308 material are the same as those defined in the ASME Code, Section III, for Type 304 stainless steel. At room temperature, the yield and ultimate stresses per ASTM-A 580 are the same for the two alloys. In view of the similarity of the alloy composition, the temperature dependence of strength of the two materials is also assumed to be the same.

The allowable stresses used as a function of temperature are listed in Table 1-1.2 of Section III of the ASME Code. The fatigue strength for the Type 308 material is based on the S-N curve for austenitic stainless steels on Figure 1-9.2 or Section III.

The spider assembly is in the form of a central hub with radial vanes containing cylindrical fingers from which the absorber rods are suspended. Handling detents and detents for connection to the drive rod assembly are machined into the upper end of the hub. Coil springs inside the spider body absorb the impact energy at the end of a trip insertion. The radial vanes are joined to the hub by tack welding and brazing, and the fingers are joined to the vanes by brazing. A centerpost which holds the spring and retainer is threaded into the hub within the skirt and welded to prevent loosening in service. All components of the spider assembly are made from Type 304 and 308 stainless steel or equivalent, except for the retainer which is of 17-4 pH material or equivalent and the springs which are Inconel-718 alloy or equivalent.

The absorber rods are fastened to the spider. The rods are first threaded into the spider fingers and then pinned to maintain joint tightness, after which the pins are welded in place. The end plug below the pin position is designed with a reduced section to permit flexing of the rods to correct for small misalignments.

The overall length is such that when the assembly is withdrawn through its full travel, a portion of the absorber rods remain engaged in the guide thimbles so that alignment between rods and thimbles is always maintained. Since the rods are long and slender, they are relatively free to conform to any small misalignments with the guide thimble.

4.2.2.3.2 Burnable Absorber Assembly

Each burnable absorber assembly consists of reduced length wet annular burnable absorber (WABA) rods attached to a hold-down assembly. A burnable absorber assembly is shown in the composite core component figure (Figure 4.2-11). When needed due to nuclear considerations, burnable absorber assemblies are inserted into selected thimbles within fuel assemblies.

A WABA rod consists of annular pellets of alumina-boron carbide (Al_2O_3-B_4C) burnable absorber material contained within two concentric Zircaloy tubes. These Zircaloy tubes, which form the inner and outer clad for the WABA rod, are plugged and seal-welded at each end to encapsulate the annular stack of absorber material. The absorber stack lengths (Figure 4.2-11) are positioned axially within the WABA rods by the use of Zircaloy bottom-end spacers. The spacer in the lower portion of the WABA rod was lengthened to account for the ZIRLO[TM] guide thimbles. The burnable absorber center line is aligned with the fuel center line at Hot Full Power (HFP) conditions at BOL. An annular plenum is provided within the rod to accommodate the helium gas released from the absorber material depletion during irradiation. The reactor coolant flows inside the inner tube and outside the outer tube of the annular rod. Further design details are given in Section 3.0 of Skaritka (et al 1983).

The WABA rods in each fuel assembly are attached by the top end of the rods to a hold-down assembly and flat perforated retaining plate which fits within the fuel assembly top nozzle and rests on the adapter plate.

The retaining plate and the WABA rods are held down and restrained against vertical motion through a spring pack which is attached to the plate and is compressed by the upper core plate when the reactor upper internals assembly is lowered into the reactor. This arrangement ensures that the WABA rods cannot be ejected from the core by flow forces. Each rod is permanently attached to the base plate by a nut which is lock welded into place.

4.2.2.3.3 Neutron Source Assembly

The purpose of the neutron source assembly is to provide a base neutron level to ensure that the detectors are operational and responding to core neutron multiplication. A neutron source may be placed in the reactor to provide a positive neutron emission of at least two counts per second on the source range detectors attributable to core neutrons. The detectors, called source range detectors, are used primarily when the core is subcritical and during special subcritical modes of operations. An irradiated fuel assembly may be used in place of a neutron source assembly to provide the desired base neutron level.

The base neutron level permits detection of changes in the core multiplication factor during core loading, refueling, and approach to criticality. This can be done since the multiplication factor is related to an inverse function of the detector count rate. Changes in the multiplication factor can be detected during addition of fuel assemblies while loading the core, changes in control rod positions, and changes in boron concentration.

Both primary and secondary neutron source assemblies were used in the initial core. The primary source rod, containing a radioactive material, spontaneously emits neutrons during initial core loading, reactor start-up, and initial operation of the first core. After the primary source rod decays beyond the desired neutron flux level, neutrons are then supplied by the secondary source rod. The secondary source rod contains a stable material, which must be activated during reactor operation. The activation results in the subsequent release of neutrons. The primary source assemblies are normally removed after the first cycle of operation.

Four source assemblies were installed in the initial reactor core: two primary source assemblies and two secondary source assemblies. Each primary source assembly contains one primary source rod and a number of burnable absorber rods and thimble plugs. Each secondary source assembly contains a symmetrical grouping of four secondary source rods and thimble plugs in the remaining locations. The source assemblies are shown on Figure 4.2-11.

Neutron source assemblies, when used, are employed at opposite sides of the core (Figure 4.3-5). The assemblies are inserted in the guide thimbles of fuel assemblies at selected unrodded locations.

As shown on Figure 4.2-11, the source assemblies contain a holddown assembly identical to that of the burnable absorber assembly.

The primary and secondary source rods both utilize the same cladding material as the absorber rods. The secondary source rods contain Sb-Be pellets stacked to a height of approximately 88 inches. The primary source rods contain capsules of Californium source material and an alumina spacer to position the source material within the cladding. The rods in each assembly are permanently fastened at the top end to a holddown assembly.

The other structural members are constructed of Type 304 stainless steel except for the springs. The springs exposed to the reactor coolant are Inconel-718.

4.2.2.3.4 Thimble Plug Assembly

Thimble plug assemblies limit bypass flow through the guide thimbles in fuel assemblies which do not contain either control rods, source rods, or burnable absorber rods.

The thimble plug assemblies consist of a hold down assembly with short rods suspended from the base plate and a spring pack assembly, as shown on Figure 4.2-11. The 24 thimble plugs project into the upper ends of the guide thimbles to reduce the bypass flow. Each thimble plug is permanently attached to the base plate by a nut which is crimped to the threaded end of the plug. Similar thimble plugs are also used on the source assemblies and burnable absorber assemblies to plug the ends of all vacant fuel assembly guide thimbles. When in the core, the thimble plug assemblies interface with both the upper core plate and with the fuel assembly top nozzles by resting on the adapter plate. The spring pack is compressed by the upper core plate when the upper internals assembly is lowered into place.

All components in the thimble plug assembly, except for the springs, are constructed from Type 304 stainless steel or equivalent. The springs are Inconel-718 or equivalent.

4.2.3 Design Evaluation

The fuel assemblies, fuel rods, and incore control components are designed to satisfy the performance and safety criteria of the introduction to Section 4.2, the mechanical design bases of Section 4.2.1, and other interfacing nuclear and thermal-hydraulic design bases specified in Sections 4.3 and 4.4.

Effects of ANS Conditions II, III, IV or anticipated transients without trip on fuel integrity are presented in Chapter 15 or supporting topical reports.

The initial step in fuel rod design evaluation for a region of fuel is to determine the limiting rod(s). Limiting rods are defined as those rod(s) whose predicted performance provides the minimum margin to each of the design criteria. For a number of design criteria the limiting rod is the lead burnup rod of a fuel region. In other instances it may be the maximum power or the minimum burnup rod. For the most part, no single rod will be limiting with respect to all design criteria.

After identifying the limiting rod(s), a worst-case performance analysis is performed which considers the limiting rod design basis power history, model uncertainties, and dimensional variations.

Furthermore, to verify adherence to the design criteria, the conservative case evaluation also considers the effects of postulated transient power increases which are achievable during operation consistent with ANS Conditions I and II. These transient power increases can affect both rod average and local power levels. The analytical methods used in the evaluation result in performance parameters which demonstrate the fuel rod behavior. Examples of parameters considered include rod internal pressure, fuel temperature,

clad stress, and clad strain. In fuel rod design analyses these performance parameters provide the basis for comparison between expected fuel rod behavior and the corresponding design criteria limits.

Fuel rod and assembly models used for the various evaluations are documented and maintained under an appropriate control system. Materials properties used in the design evaluation are given by Beaumont (et al 1978).

4.2.3.1 Cladding

    1.   Vibration and wear - fuel rod vibrations are flow induced. The effect of the vibration on the fuel assembly and individual fuel rods is minimal. The cyclic stress range associated with deflections of such small magnitude is insignificant and has no effect on the structural integrity of the fuel rod.

           The reaction force on the grid supports due to rod vibration motions is also small and is much less than the spring preload. Firm fuel clad spring contact is maintained. No significant wear of the clad or grid supports is expected during the life of the fuel assembly based on out-of-pile flow tests (DeMario, 1974), performance of similarly designed fuel in operating reactors (Skaritka 1985), and design analyses.

    2.   Fuel rod internal pressure and cladding stresses - Burnup dependent fission gas release model (Miller 1976, Weiner 1988, and Foster 2000) are used in determining the internal gas pressures as a function of irradiation time. The plenum height of the fuel rod has been designed to ensure that the maximum internal pressure of the fuel rod will not exceed the value which would cause, 1) the fuel/clad diametral gap to increase during steady state operation and, 2) extensive DNB propagation to occur.

           The clad stresses at a constant local fuel rod power are low. Compressive stresses are created by the pressure differential between the reactor coolant pressure and the rod internal gas pressure. Because of the prepressurization with helium, the volume average effective stresses are always less than approximately 13,600 psi at the pressurization level used in this fuel rod design. Stresses due to the temperature gradient are not included in this average effective stress because thermal stresses are, in general, negative at the clad inside diameter and positive at the clad outside diameter and their contributions to the clad volume average stress is small. Furthermore, the thermal stress decreases with time during steady state operation due to stress relaxation. The stress due to pressure differential is highest in the minimum power rod at the beginning-of-life due to low internal gas pressure and the thermal stress is highest in the maximum power rod due to the steep temperature gradient.

The internal gas pressure at beginning-of-life ranges from approximately 100 to 1,000 psia for typical lead power fuel rod. The total tangential stress at the clad inside diameter at beginning-of-life is approximately 19,300 psi compressive (18,100 psi due to ΔP and 1,200 due to ΔT) for an average power rod operating at 5 kW/ft and approximately 20,500 psi compressive (17,200 psi due to ΔP and 3,300 psi due to ΔT) for a high power rod operating at 15 kW/ft. However, the volume average effective stress at beginning-of-life is between approximately 8,000 psi (high power rod) and approximately 13,600 psi (low power rod). These stresses are substantially below even the unirradiated clad strength (55,500 psi) at a typical clad mean operating temperature of 700°F.

Tensile stresses could be created once the clad has come in contact with the pellet. These stresses would be induced by the fuel pellet swelling during irradiation. Fuel swelling can result in small clad strains (<1 percent) for expected discharge burnups, but the associated clad stresses are very low because of clad creep (thermal and irradiation-induced). The one percent strain criterion is extremely conservative for fuel-swelling driven clad strain because the strain rate associated with solid fission products swelling is very slow. A detailed discussion on fuel rod performance is given in Section 4.2.3.3.

3. Materials and chemical evaluation - Zircaloy-4 and ZIRLO[TM] clad have a high corrosion resistance to the reactor coolant, fuel, and fission products. As discussed recently by Slagle (1996), there is considerable PWR operating experience on the capability of Zircaloy and ZIRLO as a clad material. Controls on fuel fabrication specify maximum moisture levels to preclude clad hydriding, that is, less than or equal to 20 ppm hydrogen from all sources.

    Metallographic examination of irradiated commercial fuel rods have shown occurrences of fuel/clad chemical interaction. Reaction layers of <1 mil in thickness have been observed between fuel and clad at limited points around the circumference. Metallographic data indicates that this interface layer remains very thin even at high burnup. Thus, there is no indication of propagation of the layer and eventual clad penetration.

    Stress corrosion cracking is another postulated phenomenon related to fuel/clad chemical interaction. Out-of-pile tests have shown that in the presence of high clad tensile stresses, large concentrations[TM] of iodine can chemically attack the Zircaloy or ZIRLO[TM] tubing and can lead to eventual clad cracking. Extensive post-irradiation examination has produced no inpile evidence that this mechanism is operative in commercial fuel.

4. Rod bowing - Skaritka (1979) presents the U.S. Nuclear
    Regulatory Commission (USNRC) approved model used for the
    evaluation of fuel rod bowing. The effects of rod bowing
    on DNBR are described in Section 4.4.2.2.5.

5. Consequences of power-coolant mismatch - This subject is
    discussed in Chapter 15.

6. Creep collapse and creepdown - This subject and the
    associated irradiation stability of cladding have been
    evaluated using the models described by George (et al
    1974). It has been established that the design basis of no
    clad collapse during planned core life can be satisfied by
    limiting fuel densification and by having a sufficiently
    high initial internal rod pressure.

4.2.3.2 Fuel Materials Considerations

Sintered, high density uranium dioxide fuel reacts only slightly with
the clad at core operating temperatures and pressures. In the event
of clad defects, the high resistance of uranium dioxide to attack by
water protects against fuel deterioration although limited fuel
erosion can occur. As has been shown by operating experience and
extensive experimental work, the thermal design parameters
conservatively account for changes in the thermal performance of the
fuel elements due to pellet fracture which may occur during power
operation. The consequences of defects in the clad are greatly
reduced by the ability of uranium dioxide to retain fission products
including those which are gaseous or highly volatile. Observations at
several operating Westinghouse PWRs have shown that fuel pellets can
densify under irradiation to a density higher than the manufactured
values. Fuel densification and subsequent settling of the fuel
pellets can result in local and distributed gaps in the fuel rods.
Fuel densification has been minimized by improvements in the fuel
manufacturing process and by specifying a nominal 95 percent initial
fuel density.

The evaluation of fuel densification effects and their considerations
in fuel design are described by Hellman (1975), Miller (1976), and
Weiner (1988). The treatment of fuel swelling and fission gas release
is described by Miller (1976), Weiner (1988), and Foster (2000).

The effects of waterlogging on fuel behavior are discussed in Section
4.2.3.3.

4.2.3.3 Fuel Rod Performance

In the calculation of the steady state performance of a nuclear fuel
rod, the following interacting factors must be considered:

1. Clad creep and elastic deflection.

2. Pellet density changes, thermal expansion, gas release, and
    thermal properties as a function of temperature and fuel
    burnup.

3.   Internal pressure as a function of fission gas release, rod
        geometry, and temperature distribution.

These effects are evaluated using fuel rod design models (Miller 1976,
Weiner 1988, and Foster 2000) which include appropriate models for
time-dependent fuel densification. With the above interacting factors
considered, the model determines the fuel rod performance
characteristics for a given rod geometry, power history, and axial
power shape. In particular, internal gas pressure, fuel and clad
temperatures, and clad deflections are calculated. The fuel rod is
divided into several axial sections and radially into a number of
annular zones. Fuel density changes are calculated separately for
each segment. The effects are integrated to obtain the internal rod
pressure.

The initial rod internal pressure is selected to delay fuel/clad
mechanical interaction and to avoid the potential for flattened rod
formation. It is limited, however, by the design criteria for the rod
internal pressure (Section 4.2.1.3).

The gap conductance between the pellet surface and the clad inner
diameter is calculated as a function of the composition, temperature,
and pressure of the gas mixture, and the gap size of contact pressure
between clad and pellet. After computing the fuel temperature for
each pellet annular zone, the fractional fission gas release is
assessed using an empirical model derived from experimental data
(Miller 1976, Weiner 1988, and Foster 2000). The total amount of gas
released is based on the average fractional release within each axial
and radial zone and the gas generation rate which in turn is a
function of burnup. Finally, the gas released is summed over all
zones and the pressure is calculated.

The model shows good agreement in fit for a variety of published and
proprietary data of fission gas release, fuel temperatures, and clad
deflections (Miller 1976, Weiner 1988 and Foster 2000). These data
include variations in power, time, fuel density, and geometry.

Fuel/cladding mechanical interaction - One factor in fuel element duty
is potential mechanical interaction of fuel and clad. This fuel/clad
interaction produces cyclic stresses and strains in the clad, and
these in turn consume clad fatigue life. The reduction of fuel/clad
interaction is therefore a goal of design. The technology of using
prepressurized fuel rods has been developed to further this objective.

The gap between the fuel and clad is initially sufficient to prevent
hard contact between the two. However, during power operation, a
gradual compressive creep of the clad onto the fuel pellet occurs due
to the external pressure exerted on the rod by the reactor coolant.
Clad compressive creep eventually results in the fuel/clad contact.
Once fuel/clad contact occurs, changes in power level result in
changes in clad stresses and strains. By using prepressurized fuel
rods to partially offset the effect of the reactor coolant external
pressure, the rate of clad creep toward the surface of the fuel is
reduced. Fuel rod prepressurization delays the time at which
fuel/clad interaction and contact occurs, and significantly reduces

the number and extent of cyclic stresses and strains experienced by
the clad both before and after fuel/clad contact. These factors
result in an increase in the fatigue life margin of the clad and lead
to greater clad reliability. If gas should form in the fuel stacks,
clad flattening will be prevented by the rod prepressurization so that
the flattening time will be greater than the fuel core life.

A two-dimensional (r,θ) finite element model has been developed to
investigate the effects of radial pellet cracks on stress
concentrations in the clad. Stress concentrations, herein, are
defined as the difference between the maximum clad stress in the θ-
direction and the mean clad stress. The first case has the fuel and
clad in mechanical equilibrium, and, as a result, the stress in the
clad is close to zero. In subsequent cases, the pellet power is
increased in steps and the resultant fuel thermal expansion imposes
tensile stress in the clad. In addition to uniform clad stresses,
stress concentrations develop in the clad adjacent to radial cracks in
the pellet. These radial cracks have a tendency to open during a
power increase, but the frictional forces between fuel and clad oppose
the opening of these cracks and result in localized increases in clad
stress. As the power is further increased, large tensile stresses
exceed the ultimate tensile strength of UO_2 and additional cracks in
the fuel are created which limit the magnitude of the stress
concentration in the clad. As part of the standard fuel rod design
analysis, the maximum stress concentration evaluated from finite
element calculations is added to the volume averaged effective stress
in the clad as determined from one-dimensional stress/strain
calculations. The resultant clad stress is then compared to the
temperature dependent Zircaloy yield stress in order to assure that
the stress/strain criteria are satisfied.

Transient Evaluation Method

Pellet thermal expansion due to power increases is considered the only
mechanism by which significant stresses and strains can be imposed on
the clad. Such increases are a consequence of fuel shuffling (for
example, Region 3 positioned near the center of the core for Cycle 2
operation after operating near the periphery during Cycle 1), reactor
power escalation following extended reduced power operation, and
control rod movement. In the mechanical design model, lead rod burnup
values are obtained using best estimate power histories, as determined
by core physics calculations. During burnup, the amount of diametral
gap closure is evaluated, based upon the pellet expansion cracking
model, clad creep model, and fuel swelling model. At various times
during the depletion, the power is increased locally on the rod to the
burnup-dependent attainable power density, as determined by core
physics calculations. The radial, tangential, and axial clad stresses
resulting from the power increase are combined into a volume average
effective clad stress.

The Von Mises criterion is used to evaluate if the clad yield stress
has been exceeded. The yield stress correlation is that for
irradiated cladding, since fuel/clad interaction occurs at high
burnup. Furthermore, the effective stress is increased by an
allowance, which accounts for stress concentrations in the clad
adjacent to radial cracks in the pellet, prior to comparison with the
yield stress. This allowance was evaluated using a two-dimensional
(r, θ) finite element model.

Slow transient power increases can result in large clad strains without exceeding the clad yield stress because of clad creep and stress relaxation.   Therefore, in addition to the yield stress criterion, a criterion on allowable clad strain is necessary.   Based upon high strain rate burst and tensile test data on irradiated tubing, 1 percent strain was determined to be a conservative lower limit on irradiated clad ductility and thus adopted as a design criterion.

A comprehensive review of the available strain-fatigue models was conducted by Westinghouse as early as 1968.   This included the Langer-O'Donnell model (O'Donnell et al 1964), the Yao-Munse model, and the Manson-Halford model.   Upon completion of this review and using the results of the Westinghouse experimental programs discussed subsequently, it was concluded that the approach defined by Langer-O'Donnell would be retained and the empirical factors of their correlation modified in order to conservatively bound the results of the Westinghouse testing program.

The Langer-O'Donnell empirical correlation has the following form:

$$S_a = \frac{E}{4\sqrt{N}} \ln\left(\frac{100}{100 - RA}\right) + S_e$$

(4.2-1)

where:

S_a = $1/2\ E\Delta\varepsilon_t$ = pseudo - stress amplitude which causes failure in N_f cycles (lb/in^2)

$\Delta\varepsilon_t$ =   total strain range (in/in)

E =   Young's Modulus (lb/in^2)

N_f =   number of cycles to failure

RA =   reduction in area at fracture in a uniaxial tensile test (%)

S_e =   endurance limit (lb/in^2)

Both RA and S_e are empirical constants which depend on the type of material, the temperature, and irradiation.   The Westinghouse testing program was subdivided into the following subprograms:

1.   A rotating bend fatigue experiment on unirradiated Zircaloy-4 specimens at room temperature and at 725°F.   Both hydrided and nonhydrided Zircaloy-4 cladding were tested.

2.   A biaxial fatigue experiment in gas autoclave on unirradiated Zircaloy-4 cladding both hydrided and nonhydrided.

3.   A fatigue test program on irradiated cladding from the Carolina-Virginia Tube Reactor and Yankee Core V conducted at Battelle Memorial Institute.

The results of these test programs provided information on different cladding conditions including the effect of irradiation, hydrogen level, and temperature.

The design equations followed the concept for the fatigue design criterion according to the ASME Code, Section III. Namely,

1.   The calculated pseudo-stress amplitude (S_a) has to be multiplied by a factor of 2 in order to obtain the allowable number of cycles (N_f).

2.   The allowable cycles for a given S_a is 5 percent of N_f, or a safety factor of 20 on cycles.

The lesser of the two allowable number of cycles is selected. The cumulative fatigue life fraction is then computed as:

$$\sum^{k} \frac{n_k}{N_{fk}} \leq 1 \qquad\qquad (4.2\text{-}2)$$

where:

n_k =   number of daily cycles of mode k,

N_{fk} =   number of allowable cycles.

It is recognized that a possible limitation to the satisfactory behavior of the fuel rods in a reactor which is subjected to daily load follow is the failure of the clad by low-cycle strain fatigue. During their normal residence time in the reactor, the fuel rod may be subjected to 1,000 or more cycles with typical changes in power level from 50 to 100 percent of their steady state values.

The assessment of the fatigue life of the fuel rod clad is subject to a considerable uncertainty due to the difficulty of evaluating the strain range which results from the cyclic interaction of the fuel pellets and clad. This difficulty arises, for example, from such highly unpredictable phenomena as pellet cracking, fragmentation, and relocation. Nevertheless, since early 1968, this particular phenomenon has been investigated analytically and experimentally (O'Donnell et al 1964). Strain fatigue tests on irradiated and nonirradiated hydrided Zircaloy-4 claddings were performed which permitted a definition of a conservative fatigue life limit and recommendation of a methodology to treat the strain fatigue evaluation of the Westinghouse reference fuel rod designs.

It is believed that the final proof of the adequacy of a given fuel rod design to meet the load follow requirements can only come from incore experiments performed on actual reactors. Experience in load follow operation dates back to early 1970 with the load follow operation of the Saxton reactor. Successful load follow operation has been performed on reactor A (400 load follow cycles) and reactor B (>500 load follow cycles). In both cases, there was no significant reactor coolant activity increase that could be associated with the load follow mode of operation.

1. Irradiation experience - Westinghouse fuel operational experience is presented by Skaritka (1985). Additional test assembly and test rod experience are given in Sections 8 and 23 of Eggleston (1978).

2. Fuel and cladding temperature - The methods used for evaluation of fuel rod temperatures are presented in Section 4.4.2.11.

3. Waterlogging damage of a previously defected fuel rod has occasionally been postulated as a mechanism for subsequent rupture of the cladding. Such damage has been postulated as a consequence of a power increase on a rod after water has entered such a rod through a cladding defect of appropriate size. Rupture is postulated upon power increase if the rod internal pressure increase is excessive due to insufficient venting of water to the reactor coolant. Local cladding deformations typical of waterlogging bursts have been observed in commercial Westinghouse fuel. Experience has shown that the small number of rods which have acquired cladding defects, regardless of primary mechanism, remain intact and do not progressively distort or restrict coolant flow. In fact, such small defects are normally observed through reductions in coolant activity to be progressively closed upon further operation due to the buildup of zirconium oxide and other substances. Secondary failures which have been observed in defective rods are attributed to hydrogen embrittlement of the cladding. Post-irradiation examinations point to the hydriding failure mechanism rather than a waterlogging mechanism; the secondary failures occur as blistering and possibly axial cracks in the cladding and are similar regardless of the primary failure mechanism. Such defects do not result in flow blockage. Hence, the presence of such fuel, the quantity of which must be maintained below technical specification limits, does not in any way exacerbate the effects of any postulated transients.

    Zircaloy clad fuel rods which have failed due to waterlogging (Western New York Nuclear Research Center 1971) indicate that very rapid power transients are required for fuel failure. Normal operational transients are limited to about 40 cal/gm-min (peak rod), while the Spert tests (Stephan 1970) indicate that 120 cal/gm to 150 cal/gm are required to rupture the cladding even with very short transients (5.5 millisec period).

4. Potentially damaging temperature effects during transients
    - A fuel rod experiences many operational transients
    (intentional maneuvers) during its residence in the core.
    A number of thermal effects must be considered when
    analyzing the fuel rod performance.

    The clad can be in contact with the fuel pellet at some
    time in the fuel lifetime. Clad/pellet interaction occurs
    if the fuel pellet temperature is increased after the clad
    is in contact with the pellet. Clad/pellet interaction is
    discussed earlier in this section.

    The potential effects of operation with waterlogged fuel
    are discussed in Section 4.2.3.3, Item 3, which concludes
    that waterlogging is not a concern during operational
    transients.

    Clad flattening as shown by George (et al 1974) has been
    observed in some operating power reactors. Thermal
    expansion (axial) of the fuel rod stack against a flattened
    section of clad could cause failure of the clad. This is
    no longer a concern because clad flattening is precluded
    during the fuel residence in the core (Section 4.2.3.1).

    Potential differential thermal expansion between the fuel
    rods and the guide thimbles during a transient is
    considered in the design. Excessive bowing of the fuel
    rods is precluded because the grid assemblies allow axial
    movement of the fuel rods relative to the grids.
    Specifically, thermal expansion of the fuel rods is
    considered in the grid design so that the axial loads
    imposed on the fuel rods during a thermal transient will
    not result in excessively bowed fuel rods.

5. Fuel element burnout and potential energy release - As
    discussed in Section 4.4.2.2, the core is protected from
    DNB over the full range of possible operating conditions.
    In the extremely unlikely event that DNB should occur, the
    clad temperature will rise due to the steam blanketing at
    the rod surface and the consequent degradation in heat
    transfer. During this time, there is potential for
    chemical reaction between the cladding and the reactor
    coolant. However, because of the relatively good film
    boiling heat transfer following DNB, the energy release
    resulting from this reaction is insignificant compared to
    the power produced by the fuel.

6. Reactor coolant flow blockage effects on fuel rods - This
    evaluation is presented in Section 4.4.4.7.

7.   Provisions for detection of fuel rod failure include high-
      and low-range off-line liquid monitors in the reactor
      coolant letdown line as discussed in Section 11.5.2.5.10.

4.2.3.4 Spacer Grids

The reactor coolant flow channels are established and maintained by
the structure composed of grids and guide thimbles. The lateral
spacing between fuel rods is provided and controlled by the support
dimples of adjacent grid cells. Contact of the fuel rods on the
dimples is maintained through the clamping force of the grid springs.
Lateral motion of the fuel rods is opposed by the spring force and the
internal moments generated between the spring and the support dimples.

Time history numerical integration techniques are used to analyze the
fuel assembly responses resulting from the lateral safe shutdown
earthquake, SSE, and the most limiting main coolant pipe break
accident, LOCA. The reactor vessel motions resulting from the
transient loading are asymmetric with respect to the geometrical
center of the reactor core. The complete fuel assembly core finite
element model is employed to determine the fuel assembly deflections
and grid impact forces.

A comparison of the seismic (SSE) response spectrum at the reactor
vessel supports versus the response spectrum of the time history
indicates that the time history spectrum conservatively bounds the
design acceleration spectrum curves for BVPS-2. The seismic analyses
performed for a number of plants indicate that the maximum impact
response is, in general, influenced by the acceleration level of the
input forcing function at the fuel assembly fundamental mode. Thus,
the data in seismic time histories corresponding to the design
envelope are conservatively used for the fuel evaluation.

The reactor core finite element model consisting of the maximum number
of fuel assemblies across the core diameter was used. The BVPS-2
plant has fifteen 17X17 8-grid fuel assemblies arranged in a planar
array. Gapped elements simulate the clearances between the peripheral
fuel assemblies and the baffle plates.

The fuel assembly finite element model preserves essential dynamic
properties, such as the fuel assembly vibration frequencies, mode
shapes, and mass distribution. The time history motions for the upper
and lower core plates and the motions for the core barrel at the upper
core plate elevation are simultaneously introduced into the simulated
core model. The analytical procedures, the fuel assembly and core
modeling, and the methodology are detailed in Gensinski and Chiang
(1973) and Davidson (et al 1981). The time history inputs
representing the SSE motions and the coolant pipe rupture transients
were obtained from the time history analyses of the reactor vessel
internals.

GRID ANALYSIS

The factor applied to the LOCA grid impact load due to flashing has been demonstrated by Westinghouse to be unrealistic for Westinghouse fuel in Westinghouse plants. Therefore, this factor was not applied to the BVPS-2 analysis results.

The maximum grid impact forces for both the seismic and asymmetric LOCA accidents occur at the peripheral fuel assembly locations adjacent to the baffle wall. To comply with the requirements in SRP Section 4.2 the maximum grid impact responses obtained from the two transient analyses are combined. The square-root-of-sum-ofsquares (SRSS) method is used to calculate the results. The maximum combined impact force for the BVPS-2 fuel assemblies was below the allowable grid strength. The grid strength was established experimentally. It was based on the 95 percent confidence level on the true mean as taken from the distribution of measurements.

NON-GRID COMPONENT ANALYSES

The stresses induced in the various fuel assembly non-grid components are calculated. The calculations are based on the maximum responses obtained from the most limiting seismic and LOCA accident conditions. The fuel assembly axial forces resulting from the LOCA accident are the primary sources of stresses in the thimble guide tube and the fuel assembly nozzles. The induced stresses in the fuel rods result from the relative deflections during the hypothetical seismic and LOCA accidents. The stresses are generally small. The combined seismic and LOCA induced stresses of the various fuel assembly components are below the allowable limit. Consequently, the fuel assembly components are structurally acceptable under the postulated accident design conditions for BVPS-2.

4.2.3.5 Fuel Assembly

4.2.3.5.1 Stresses and Deflections

The fuel assembly component stress levels are limited by the design. For example, stresses in the fuel rod due to thermal expansion and Zircaloy or ZIRLO^{TM} irradiation growth are limited by the relative motion of the rod as it slips over the grid spring and dimple surfaces. Clearances between the fuel rod ends and nozzles are provided so that Zircaloy or ZIRLO^{TM} irradiation growth does not result in the rod end interferences. Stresses in the fuel assembly caused by tripping of the RCCA have little influence on fatigue because of the small number of events during the life of an assembly. Assembly components and prototype fuel assemblies made from production parts have been subjected to structural tests to verify that the design bases requirements are met.

The fuel assembly design loads for shipping have been established at 6g lateral and 4g axial. Accelerometers are permanently placed into the shipping cask to monitor and detect fuel assembly accelerations

that would exceed the criteria.   Past history and experience has indicated that loads which exceed the allowable limits rarely occur. Exceeding the limits requires reinspection of the fuel assembly for damage.   Tests on various fuel assembly components such as the grid assembly, sleeves, inserts, and structure joints have been performed to assure that the shipping design limits do not result in impairment of fuel assembly function.

4.2.3.5.2 Dimensional Stability

A prototype fuel assembly has been subject to column loads in excess of those expected in normal service and faulted conditions (Gesinski and Chiang 1973).   No interference with control rod insertion into thimble tubes will occur during a postulated LOCA transient due to fuel rod swelling, thermal expansion, or bowing.   In the early phase of the transient following the reactor coolant pipe break, the high axial load, which could be generated by the difference in thermal expansion between fuel clad and thimbles, are relieved by slippage of the fuel rods through the grids.   The relatively low drag force restraint on the fuel rods will induce only minor thermal bowing, which is insufficient to close the fuel rod-to-thimble tube gap.

The fuel assemblies will maintain a geometry amenable for cooling during a combined seismic and LOCA accident (refer to Section 4.2.3.4).

4.2.3.6 Reactivity Control Assembly and Wet Annular Burnable Absorber
        (WABA) Rods

   1.   Internal pressure and cladding stress during normal transient and accident conditions - The designs of the burnable absorber and source rods provide a sufficient cold void volume to accommodate the internal pressure increase during operation.

        For the WABA rod, an annular void volume is provided along the length of the rod and between the two tubes at the top end.   For the source rods, a void volume is also provided in order to limit the internal pressure rise.

        The stress analysis of the burnable absorber and source rods assumes 100 percent gas release to the rod void volume in addition to the initial pressure within the rod.   The WABA rod stress analysis assumes a 30 percent maximum gas release to the rod void volume.

        During normal transient and accident conditions, the void volume limits the internal pressures to values which satisfy the criteria in Section 4.2.1.6.

        These limits are established not only to assure that peak stresses do not reach unacceptable values, but to also limit the amplitude of the oscillatory stress component in consideration of the fatigue characteristics of the materials.

Rod, guide thimble, and dashpot flow analyses indicate that the flow is sufficient to prevent coolant boiling. Therefore, clad temperatures at which the clad material has adequate strength to resist reactor coolant operating pressures and rod internal pressures are maintained.

2.   Thermal stability of the absorber material including phase changes and thermal expansion - The radial and axial temperature profiles have been determined by considering gap conductance, thermal expansion, and neutron or gamma heating of the contained material as well as gamma heating of the clad.

The maximum temperature of the Ag-In-Cd absorber material is calculated to be less than 1200°F, and occurs axially at only the highest flux region. This temperature is well below the absorber melting temperature bases of Section 4.2.1.6. The thermal expansion properties of the absorber material and the phase changes are discussed by Beaumont (et al 1978).

The maximum temperature of the Al_2O_3-B_4C burnable absorber pellet is calculated to be <1,200°F and takes place following the initial rise to power. As the operating cycle proceeds, the glass temperature decreases for the following reasons: 1) reduction in power generation due to boron 10 depletion, 2) better gap conductance as the helium produced diffuses to the gap, and 3) gap reduction due to borosilicate glass creep.

Sufficient diametral and end clearances have been provided in the neutron absorber, WABA, and source rods to accommodate the relative thermal expansions between the enclosed material and the surrounding clad and end plug.

3.   Irradiation stability of the absorber material, taking into consideration gas release and swelling - The irradiation stability of the absorber material is discussed by Beaumont (et al 1978) and Christensen (et al 1965). Irradiation produces no deleterious effects in the absorber material. Sufficient diametral and end clearances are provided to accommodate swelling of the absorber material.

Gas release is not a concern for the absorber rod because no gas is released by the absorber material. Sufficient diametral and end clearances are provided to accommodate swelling of the absorber material.

The Al_2O_3-B_4C burnable absorber pellets are designed such that gross swelling or crumbling of the pellets is not expected during reactor operation. Some minor cracking of the pellets may occur, but this cracking should not affect the overall absorber stack integrity.

4. Potential for chemical interaction, including possible waterlogging rupture - The structural materials selected have good resistance to irradiation damage and are compatible with the reactor environment.

Corrosion of the materials exposed to the reactor coolant is quite low, and proper control of chloride and oxygen in the coolant will prevent the occurrence of stress corrosion. The potential for the interference with RCC movement due to possible corrosion phenomena is negligible.

Waterlogging rupture is not a failure mechanism associated with Westinghouse-design control rods. However, a breach of the cladding for any postulated reason does not result in serious consequences. The Ag-In-Cd absorber material is relatively inert and would still remain isolated from high reactor coolant velocity regions. Rapid loss of material resulting in significant loss of reactivity control material would not occur.

4.2.4 Testing and Inspection Plan

4.2.4.1 Quality Assurance Program

The quality assurance program plan of the Westinghouse Nuclear Fuel Division is summarized in Westinghouse Report - WCAP 7800 (1979).

The program provides for control over all activities affecting product quality, commencing with design and development and continuing through procurement, materials handling, fabrication, testing and inspection, storage, and transportation. The program also provides for the indoctrination and training of personnel and for the auditing of activities affecting product quality through a formal auditing program.

Westinghouse drawings and product, process, and material specifications identify the inspections to be performed.

4.2.4.2 Quality Control

Quality control philosophy is generally based on the following inspections being performed to a 95 percent confidence that at least 95 percent of the product meets specification, unless otherwise noted.

1. Fuel system components and parts - The characteristics inspected depend upon the component parts and include dimensional and visual examinations, check audits of test reports, material certification, and nondestructive examination (NDE) such as x-ray and ultrasonic.

   All material used in this core is accepted and released by quality control.

2. Pellets - Inspection is performed for dimensional characteristics such as diameter, density, length, and squareness of ends. Additional visual inspections are performed for cracks, chips, and surface conditions according to approved standards.

    Density is determined in terms of weight per unit length and is plotted on zone charts used in controlling the process. Chemical analyses are taken on a specified sample basis throughout pellet production.

3. Rod inspection - Fuel rod, control rods, burnable absorber, and source rod inspection consists of the following NDE techniques and methods, as applicable.

    a. Leak testing - Each rod is tested using a calibrated mass spectrometer with helium being the detectable gas.

    b. Enclosure welds - Rod welds are inspected by ultrasonic test or X-ray in accordance with a qualified technique and Westinghouse specifications.

    c. Dimensional - All rods are dimensionally inspected prior to final release. The requirements include such items as length, camber, and visual appearance.

    d. Plenum dimensions - All fuel rods are inspected by gamma-scanning or other approved methods to ensure that no significant gaps exist between pellets.

    e. All fuel rods are active gamma scanned to verify enrichment control prior to acceptance for assembly loading.

    f. Traceability - Traceability of rods and associated rod components is established by quality control.

4. Assemblies - Each fuel, control rod, burnable absorber, and source rod assembly is inspected for drawing and/or specification requirements. Other incore control component inspection and specification requirements are given in Section 4.2.4.3.

5. Other inspections - The following inspections are performed as part of the routine inspection operation:

    a. Tool and gage inspection and control including standardization to primary and/or secondary working standards. Tool inspection is performed at prescribed intervals on all serialized tools. Complete records of calibration and conditions of tools are kept.

    b. Audits of inspection activities and records are performed to ensure that prescribed methods are followed and that records are correct and properly maintained.

      c.   Surveillance inspection, where appropriate, and audits of outside contractors are performed to ensure conformance with specified requirements.

    6.   Process control - To prevent the possibility of mixing enrichments during fuel manufacture and assembly, strict enrichment segregation, and other process controls are exercised.

The UO_2 powder is kept in sealed containers. The contents are fully identified both by descriptive tagging and preselected color coding. A Westinghouse identification tag completely describing the contents is affixed to the containers before transfer to powder storage. Isotopic content is confirmed by analysis.

Powder withdrawal from storage can be made by only one authorized group, which directs the powder to the correct pellet production line. All pellet production lines are physically separated from each other and pellets of only a single nominal enrichment and density are produced in a given production line at any given time.

Finished pellets are placed on trays identified with the same color code as the powder containers and transferred to segregated storage racks within the confines of the pelleting area. Samples from each pellet lot are tested for isotopic content and impurity levels prior to acceptance by quality control. Physical barriers prevent mixing of pellets of different nominal densities and enrichments in this storage area. Unused powder and substandard pellets are returned to storage in the original color-coded containers.

Loading of pellets into the clad is performed in isolated production lines and again only one density and enrichment is loaded on a line at a time.

A serialized traceability code is placed on each fuel tube which identifies the contract and enrichment. The end plugs are inserted; the bottom end plug is permanently identified as to the contract and enrichment; the end plugs are then inert gas welded to seal the tube. The fuel tube remains coded, and traceability identified until just prior to installation in the fuel assembly. The traceability code and end plug identification character provides a cross reference of the fuel contained in the fuel rods.

At the time of installation into an assembly, a matrix is generated to identify each rod in its position within a given assembly. After the fuel rods are installed, an inspector verifies that all fuel rods in an assembly carry the correct identification character describing the fuel enrichment and density of the core region being fabricated. The top nozzle is inscribed with a permanent identification number providing traceability to the fuel contained in the assembly.

Similar traceability is provided to burnable absorber, source rods, and control rodlets, as required.

4.2.4.3 Incore Control Component Testing and Inspection

Tests and inspections are performed on each reactivity control component to verify the mechanical characteristics. In the case of the RCCA, prototype testing has been conducted and both manufacturing test/inspections and functional testing at the BVPS-2 site are performed.

During the component manufacturing phase, the following requirements apply to the reactivity control components to assure the proper functioning during reactor operation:

1.   All materials are procured to specifications to attain the desired standard of quality.

2.   A spider from each braze lot is proof tested by applying a 5,000 pound load to the spider body, so that approximately 310 pounds is applied to each vane. This proof load provides a bending moment at the spider body approximately equivalent to 1.4 times the load caused by the acceleration imposed by the CRDM.

3.   All rods are checked for integrity by the methods described in Section 4.2.4.2, Item 3.

4.   To ensure proper fitup with the fuel assembly, the RCC, burnable absorber and source assemblies are installed in the fuel assembly without restriction or binding in the dry condition. Also, a straightness of 0.01 in/ft is required on the entire inserted length of each rod assembly.

The RCCAs are functionally tested, following core loading but prior to criticality, to demonstrate reliable operation of the assemblies. Each assembly is operated (and tripped) one time at no flow/cold conditions and one time at full flow/hot conditions. In addition, selected assemblies are operated at no flow/operating temperature conditions and full flow/ambient conditions. Also, those control rods whose scram times fall outside the two-sigma limit of the scram time data for all control rods will be retested ($\geq$3 times) to ensure proper performance during subsequent plant operation consistent with the guidelines given in Regulatory Guide 1.68, Revision 2.

In order to demonstrate continuous free movement of the RCCAs, and to ensure acceptable core power distributions during operations, partial movement checks are performed on every RCCA, as required by the Technical Specifications. In addition, periodic drop tests of the RCCAs are performed at each refueling shutdown to demonstrate continued ability to meet trip time requirements.

If an RCCA cannot be moved by its mechanism, adjustments in the boron concentration ensure that adequate shutdown margin would be achieved following trip. Thus, inability to move one RCCA can be tolerated. More than one inoperable RCCA could be tolerated, but would impose additional demands on the plant operator. Therefore, the number of inoperable RCCAs has been limited to one.

4.2.4.4 Tests and Inspections by Others

If any tests and inspections are to be performed on core components or fuel subassemblies on behalf of Westinghouse, Westinghouse will review and approve the quality control procedures, inspection plans, etc, to be utilized to ensure that they are equivalent to the description provided in Sections 4.2.4.2 and 4.2.4.3, and are performed to meet all Westinghouse requirements.

4.2.4.5 Inservice Surveillance

Westinghouse has conducted a test and surveillance program to examine detailed aspects of the 17 by 17 fuel assembly. The test program described in Section 23 of Eggleston's (1978) report was successfully completed. Skaritka's (1985) report is periodically updated in order to provide recent results of the surveillance and operating experience with Westinghouse fuel and incore control components.

4.2.4.6 Onsite Inspection

Detailed written procedures are used for receipt inspection of new fuel assemblies and associated components, such as control rods, plugs, and inserts. Loaded fuel containers, are visually inspected upon receipt for possible evidence of damage or improper handling. Shock indicators attached to the interior of the container are inspected to verify that excessive forces caused by movement have not been applied to the fuel assemblies. The fuel assemblies and associated components are subjected to inspections which verify sufficient attributes to assure that damage or deterioration during shipping was avoided.

Post-irradiation fuel inspections are routinely conducted during refueling. These inspections include a qualitative visual examination of some discharged fuel assemblies from each refueling. Gross problems of structural integrity, fuel rod failure, rod bowing and crud deposition are identified. Additional surveillance is provided if the visual examination identifies unusual behavior or if the plant instrumentation indicates gross fuel failures.

4.2.4.7 On-line Fuel System Monitoring

Reactor coolant letdown radiation monitors which can detect conditions which indicate fuel rod failure are discussed in Section 11.5.2.2.

4.2.5 References for Section 4.2

Beaumont, M. D. et al 1978. Properties of Fuel and Core Component Materials. WCAP-9179, Revision 1 (Proprietary) and WCAP-9224 (Non-Proprietary), and Appendix B (Al_2O_3-B_4C) 1980.

Burian, R. J.; Fromui, E. O.; and Gates, J. E. 1963. Effect of High Burnups on B_4C and ZrB_2 Dispersions in the Al_2O_3 and Zircaloy. BMI 1627.

Christensen, J. A.; Allio, R. J.; and Biancheria, A. 1965. Melting Point of Irradiated UO_2 WCAP-6065.

Cohen, J. 1959. Development and Properties of Silver Base Alloys as Control Rod Materials for Pressurized Water Reactors; WAPD-214.

Davidson, S. L. et al 1981. Verification Testing and Analysis of the 17 x 17 Optimized Fuel Assembly, WCAP-9401-P-A (Proprietary) and WCAP-9402-A (Non-Proprietary).

Davidson, S. L. (Ed.), et al, "Reference Core Report VANTAGE 5 Fuel Assembly," WCAP-10444-P-A, September 1985.

Davidson, S. L., et al, "Extended Burnup Evaluation of Westinghouse Fuel," WCAP-10125-P-A and WCAP-10126-NP-A, December 1985.

Davidson, S. L., Nuhfer, D. L. (Ed.), "VANTAGE+ Fuel Assembly Reference Core Report," WCAP-12610 and Appendices A through D, June 1990.

Davidson, S. L., (Ed.), "Westinghouse Fuel Criteria Evaluation Process," WCAP-12488-A, October 1994.

DeMario, E. E. 1974. Hydraulic Flow Test of the 17 x 17 Fuel Assembly. WCAP-8278 (Proprietary) and WCAP-8279 (Non-Proprietary).

Eggleston, F. T. 1978. Safety-Related Research and Development for Westinghouse Pressurized Water Reactors, Program Summaries - Winter 1977 Summer 1978. WCAP-8768, Revision 2.

Gesinski, L. and Chiang, D. 1973. Safety Analysis of the 17 x 17 Fuel Assembly for Combined Seismic and Loss-of-Coolant Accident. WCAP-8236 (Proprietary) and WCAP-8288 (Non-Proprietary).

Hellman, J. M. (Ed.) 1975. Fuel Densification Experimental Results and Model for Reactor Application. WCAP-8218-P-A (Proprietary) and WCAP-8219-A (Non-Proprietary).

Kersting, P. J. et al, "Assessment of Clad Flattening and Densification Power Spike Factor Elimination in Westinghouse Nuclear Fuel," WCAP-13589-A, March 1995.

Miller, J. V. (Ed.) 1976. Improved Analytical Models Used in Westinghouse Fuel Rod Design Computations. WCAP-8720 (Proprietary) and WCAP-8785 (Non-Proprietary).

O'Donnell, W. J. and Langer, B. F. 1964. Fatigue Design Basis for Zircaloy Components. Nuclear Science and Engineering, 20, 1-12.

Risher, D. et al 1977. Safety Analysis for the Revised Fuel Rod Internal Pressure Design Basis. WCAP-8963 (Proprietary) and WCAP-8964 (Non-Proprietary).

Skaritka, J. (Ed.) 1979. Fuel Rod Bow Evaluation. WCAP-8691, Revision 1 (Proprietary) and WCAP-8692, Revision 1 (Non-Proprietary).

Skaritka, J. et al 1983. Westinghouse Wet Annular Burnable Absorber Evaluation Report. WCAP-10021-P-A, Revision 1 (Proprietary).

Slagle, W. H. "Operational Experience with Westinghouse Cores" (updated annually). WCAP-8183, Revision 23, January 1996.

Stephen, L. A. 1970. The Effects of Cladding Material and Heat Treatment on the Response of Waterlogged UO_2 Fuel Rods to Power Bursts. IN-ITR-111.

Weiner, R. A., et al, "Improved Fuel Performance Models for Westinghouse Fuel Rod Design and Safety Evaluations," WCAP-10851-P-A and WCAP-11873-A, August 1988.

Western New York Nuclear Research Center 1971. Correspondence with the USAEC on February 11 and August 27, 1971, Docket 50-57.

Westinghouse Electric Corporation 1979. Nuclear Fuel Division Quality Assurance Program Plan. WCAP-7800, Revision 5A.

Foster, J. P. and Siderer, S. 2000. "Westinghouse Improved Performance Analysis and Design Model (PAD 4.0)." WCAP-15063-P-A, Revision 1 with Errata, July 2000.

▲ GUIDE THIMBLE DIMENSIONS
AT TOP NOZZLE ADAPTOR PLATE

FUEL ASSEMBLY WITH ROD CONTROL CLUSTER

11.973 FUEL ASSEMBLY AND RCCA PITCH

8.426 REF.

.530

.245

16 SPACES @ .496=7.936

.122

.058

.495

1.485

.078

2.970

8.466 TYP.

.04 TYP.

GUIDE THIMBLE

INSTRUMENTATION SHEATH

FUEL ASSEMBLY WITHOUT ROD CLUSTER CONTROL

CONTROL CLUSTER ELEMENT

FUEL ROD (264 PER FUEL ASSEMBLY)
OD = .374
CLAD THICKNESS = .0225
CLAD MATERIAL = ZIRC-4/ZIRLO™
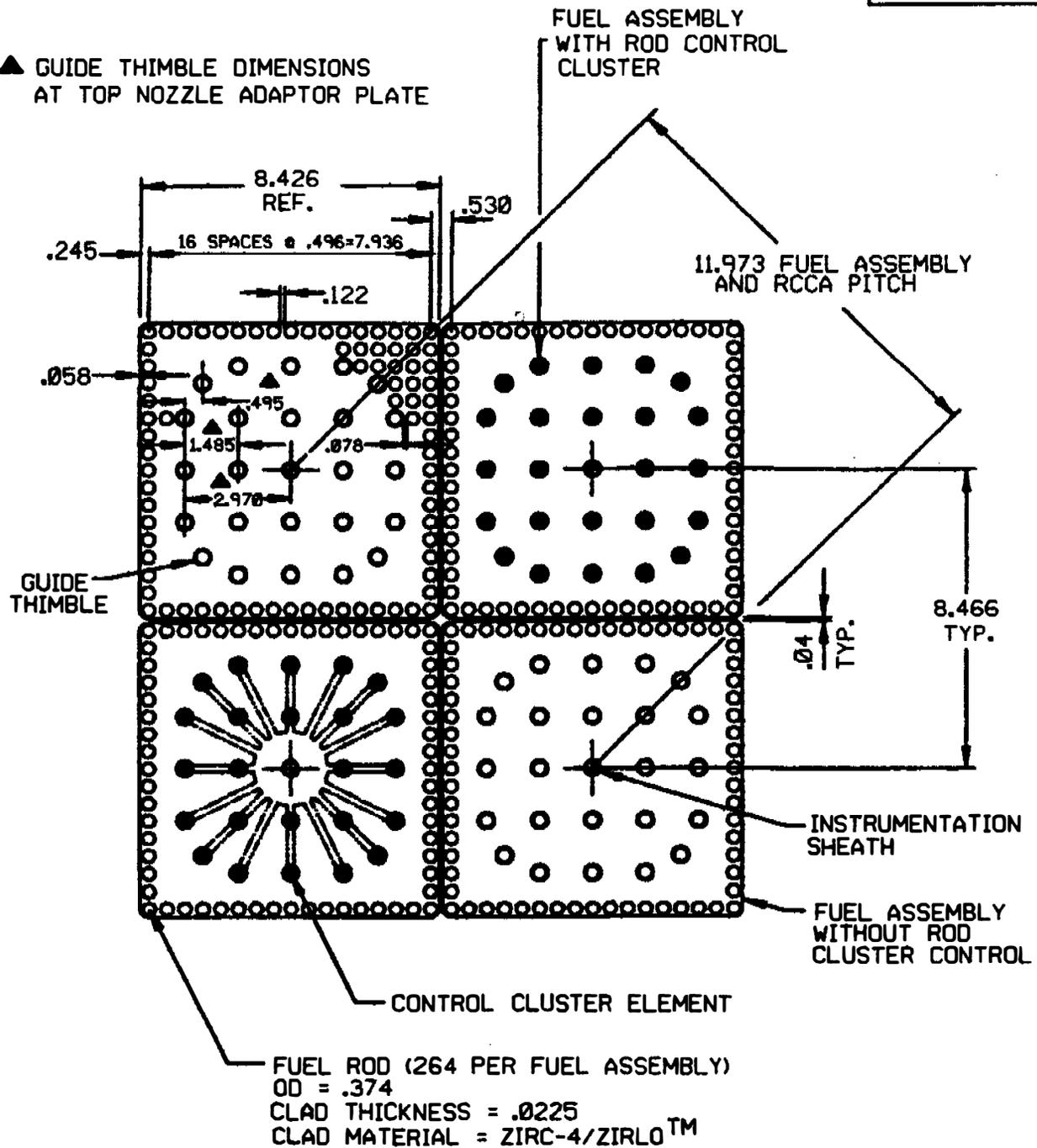
FIGURE 4.2-1
FUEL ASSEMBLY CROSS
SECTION 17 X 17
BEAVER VALLEY POWER STATION-UNIT 2
UPDATED FINAL SAFETY ANALYSIS REPORT

TOP VIEW

BOTTOM VIEW

0.875 ø TYP REF

0.875 ø TYP REF

7.162 TYP REF

8.404 TYP REF

8.750 TYP REF

8.424 TYP REF

.578 ø REF

159.975

152.200

3.475

2.383

GRID 8 GRID 7 GRID 6 GRID 5 GRID 4 GRID 3 GRID 2 GRID 1

1.522
GRIDS 1 & 8

1.500
GRIDS 2 - 7

153.60

133.10

112.55

92.00

71.45

50.90

30.35

5.835
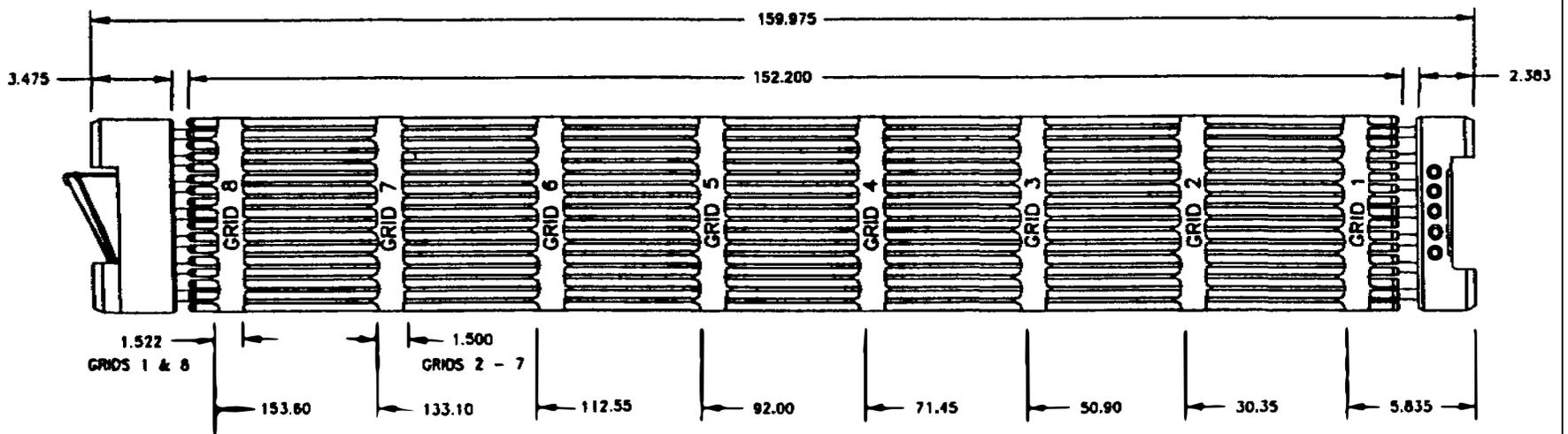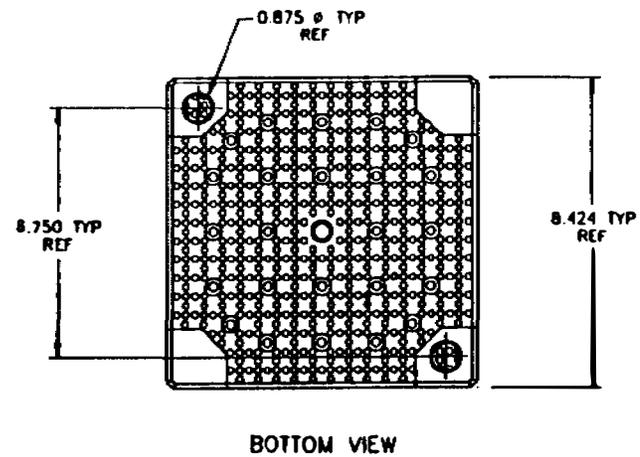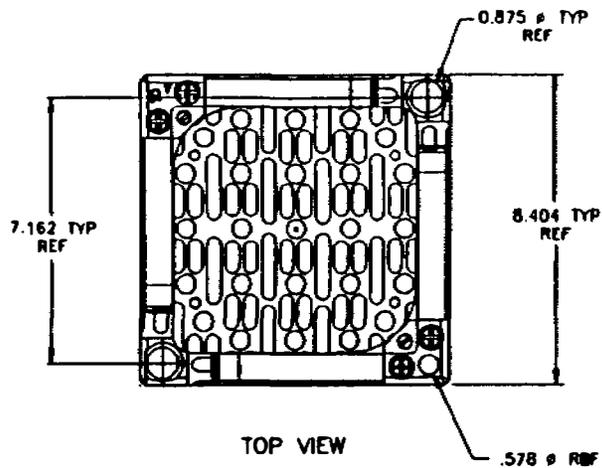
FIGURE 4.2-2

FUEL ASSEMBLY OUTLINE 17 X 17

BEAVER VALLEY POWER STATION-UNIT 2

FINAL SAFETY ANALYSIS REPORT

REV. 4
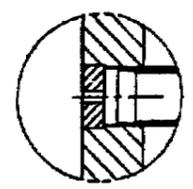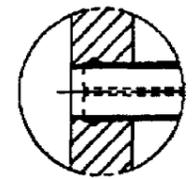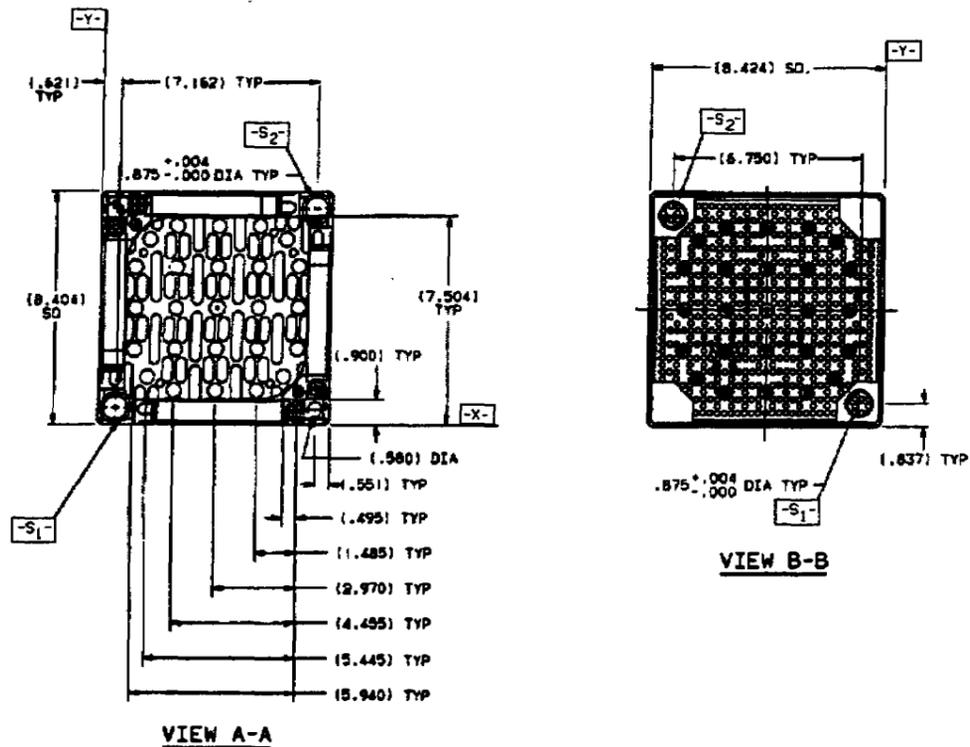
BILL OF MATERIAL

REQ'D 01	ITEM	NOTE	PART NAME	SIZED REFERENCE INFORMATION	MAT'L SIZE CODE PART NUMBER OR REF DWG
1	01	-	BOTTOM NOZZLE, DEBRIS FILTER	STAINLESS STEEL	
1	02	-	TOP NOZZLE	STAINLESS STEEL	
4	03	-	NOZZLE SPRING SET	INCONEL	
24	04	-	GUIDE THIMBLE	ZIRLO	
2	05	-	GRID ASSEMBLY (TOP & BOTTOM)	INCONEL	
1	06	-	INSTRUMENT TUBE	ZIRLO	
6	07	-	GRID ASSEMBLY (MID)	ZIRLO	
1	08	-	PROTECTIVE GRID ASSEMBLY	INCONEL	

DETAIL "A"

DETAIL "B"

SECTION "A-A"

NOTES:

1. DIMENSIONS SHOWN ARE PRIOR TO IRRADIATION.

2. THESE FUEL ASSEMBLIES MAY CONTAIN INTEGRAL FUEL BURNABLE ABSORBER (IFBA) RODS. THESE FUEL RODS ARE IDENTICAL TO OTHER FUEL RODS EXCEPT FOR A THIN COATING OF ZrB_2 ON THE CIRCUMFERENTIAL SURFACE OF THE UO_2 PELLET. THE QUANTITY AND LOCATION OF IFBA RODS MAY VARY AMONG FUEL ASSEMBLIES.

3. THESE FUEL ASSEMBLIES MAY CONTAIN ROTATED MID-GRIDS. GRIDS 3, 5 AND 7 ARE ROTATED 90° CCW AS VIEWED FROM ABOVE.

4. .13 MIN ALLOWANCE REQUIRED ALL AROUND FOR PROTECTION COVER DURING DRY SHIPPING AND STORAGE.

VIEW A-A

VIEW B-B
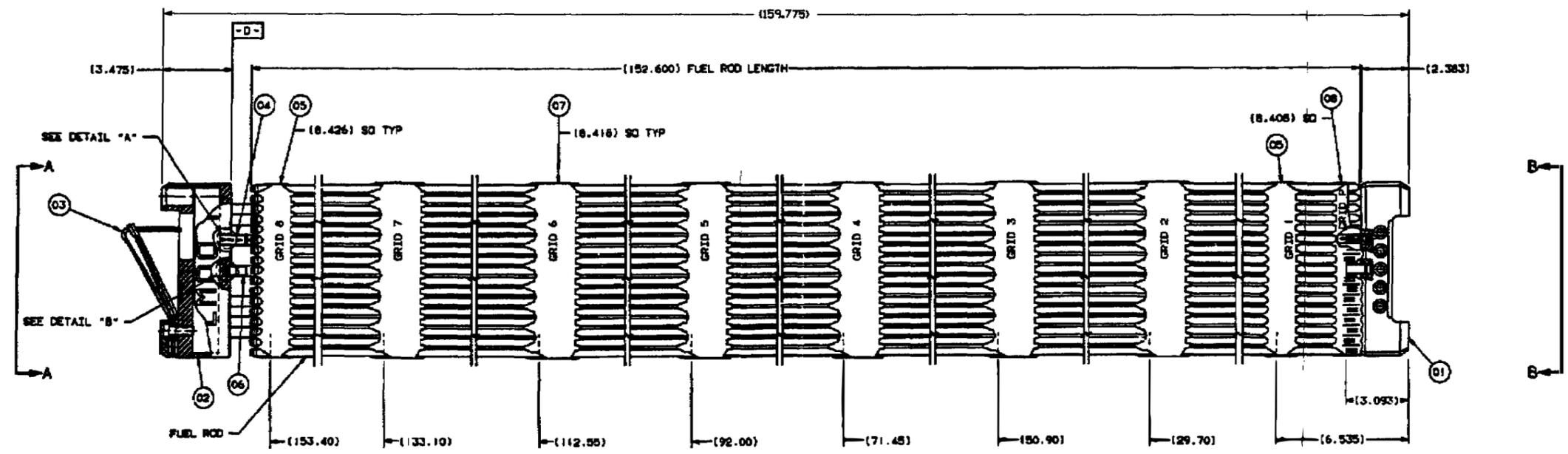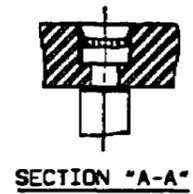
ESTIMATED WEIGHT OF MATERIALS IN FUEL ASSEMBLY:	
TOTAL	1436 LBS

FIGURE 4.2-2b

17 x 17 V5H + ZIRLO

FUEL ASSEMBLY OUTLINE

BEAVER VALLEY POWER STATION-UNIT 2
UPDATED FINAL SAFETY ANALYSIS REPORT
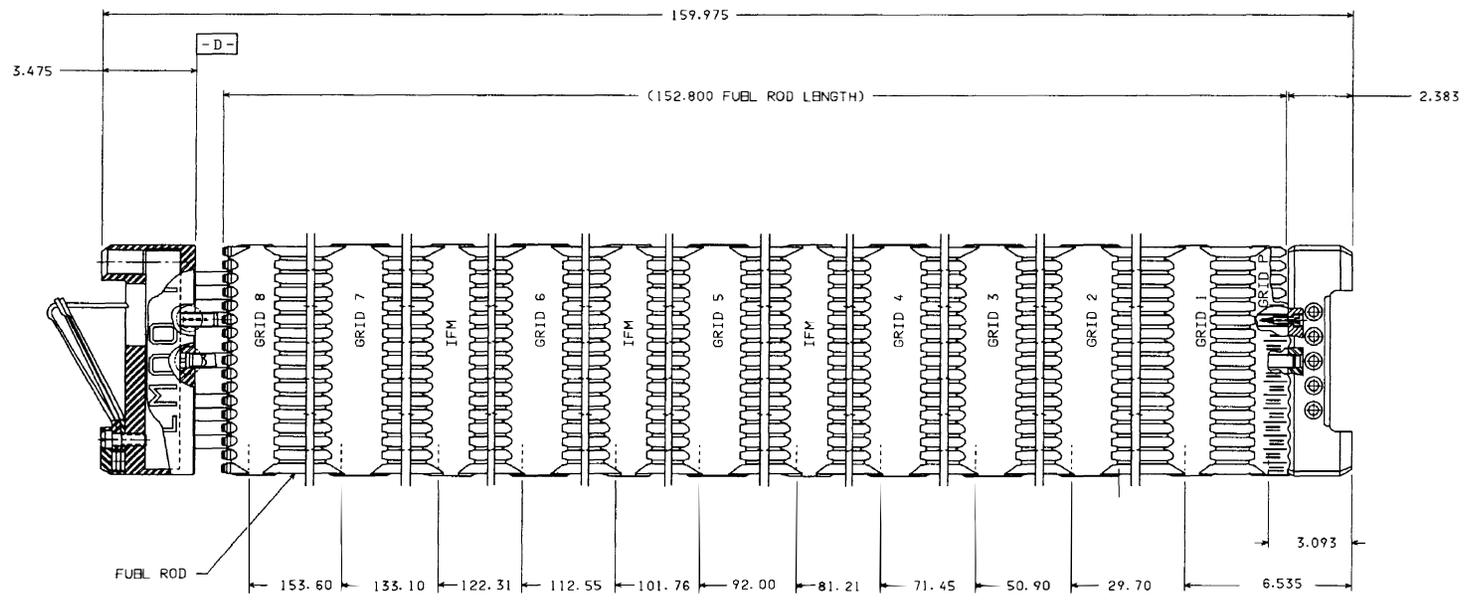
FIGURE 4.2-2b
17 X 17 STD. Z+2
ROBUST FUEL ASSEMBLY OUTLINE
BEAVER VALLEY POWER STATION UNIT NO. 2
UPDATED FINAL SAFETY ANALYSIS REPORT
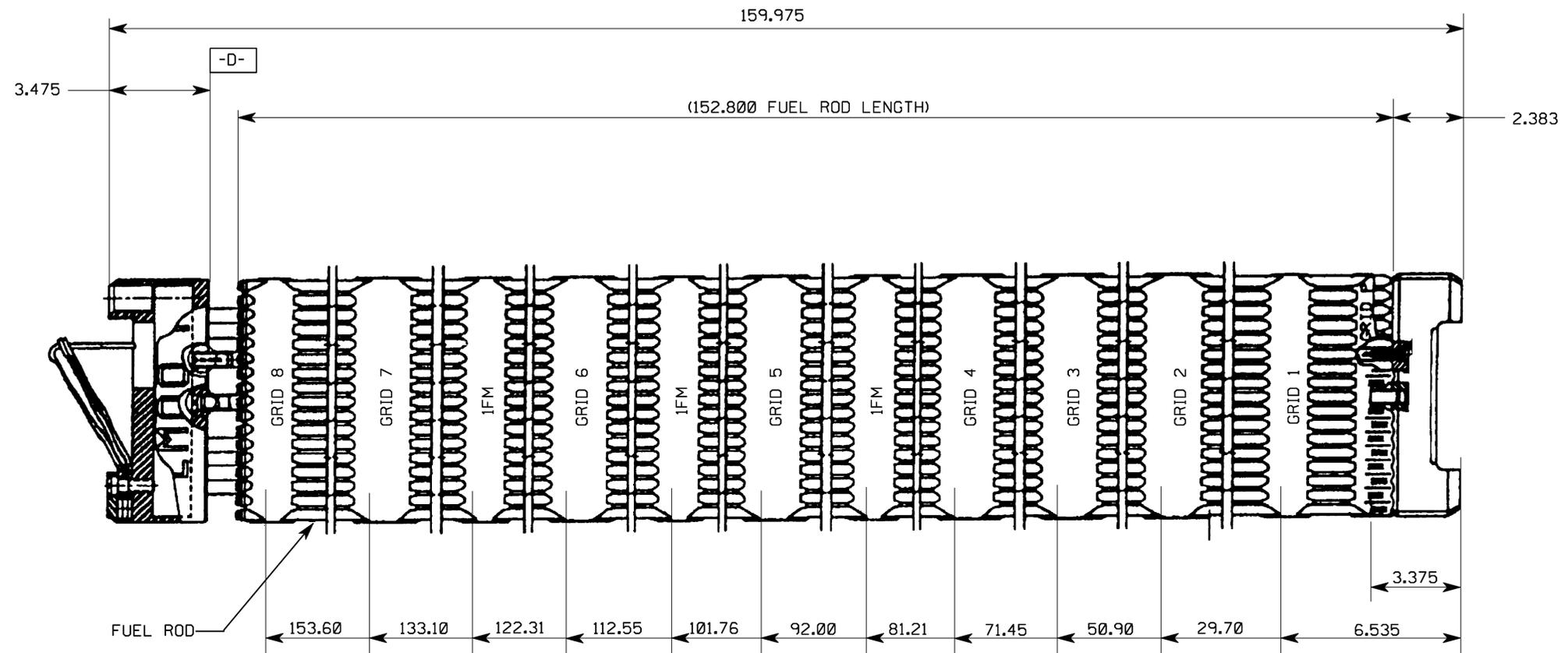
FIGURE 4.2-2C

17x17 ROBUST FUEL ASSEMBLY
WITH STANDARDIZED DEBRIS
FILTER BOTTOM NOZZLE AND
ROBUST PROTECTIVE GRID

BEAVER VALLY POWER STATION UNIT NO. 2
UPDATED FINAL SAFETY ANALYSIS REPORT

SEAL WELD

GIRTH WELD

7.440
PLENUM

SPRING

152.200
FUEL ROD LENGTH

UO$_2$ PELLET

144.00
FUEL STACK LENGTH

PELLET—CLAD GAP

ZIRCALOY CLAD

GIRTH WELD

BOTTOM END PLUG ILLUSTRATES
INTERNAL GRIP CONNECTION
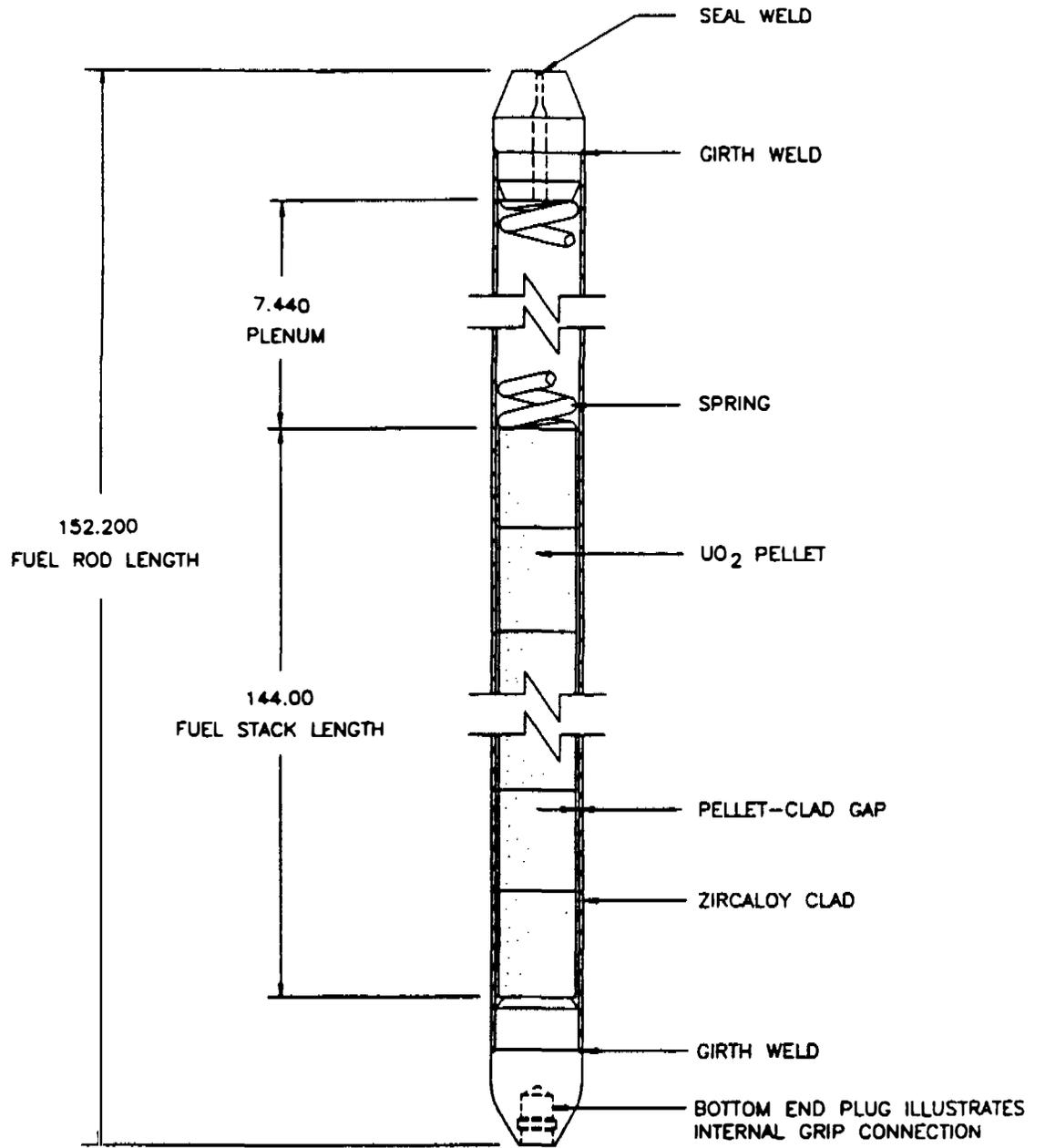
FIGURE 4.2-3
FUEL ROD SCHEMATIC
BEAVER VALLEY POWER STATION-UNIT 2
FINAL SAFETY ANALYSIS REPORT

.385 MAX
WELD DIA.

.383 MAX
WELD DIA.

ZR-4 END PLUG

STAINLESS STEEL
SPRING (VARIABLE PITCH)

ZIRLO TUBE
(.374) OD
(.0225) WALL

TYP.

URANIUM DIOXIDE PELLET

(.450)

(.450)

(7.790)

(144.00)
FUEL COLUMN LENGTH

ZR-4 END PLUG

(152.600)
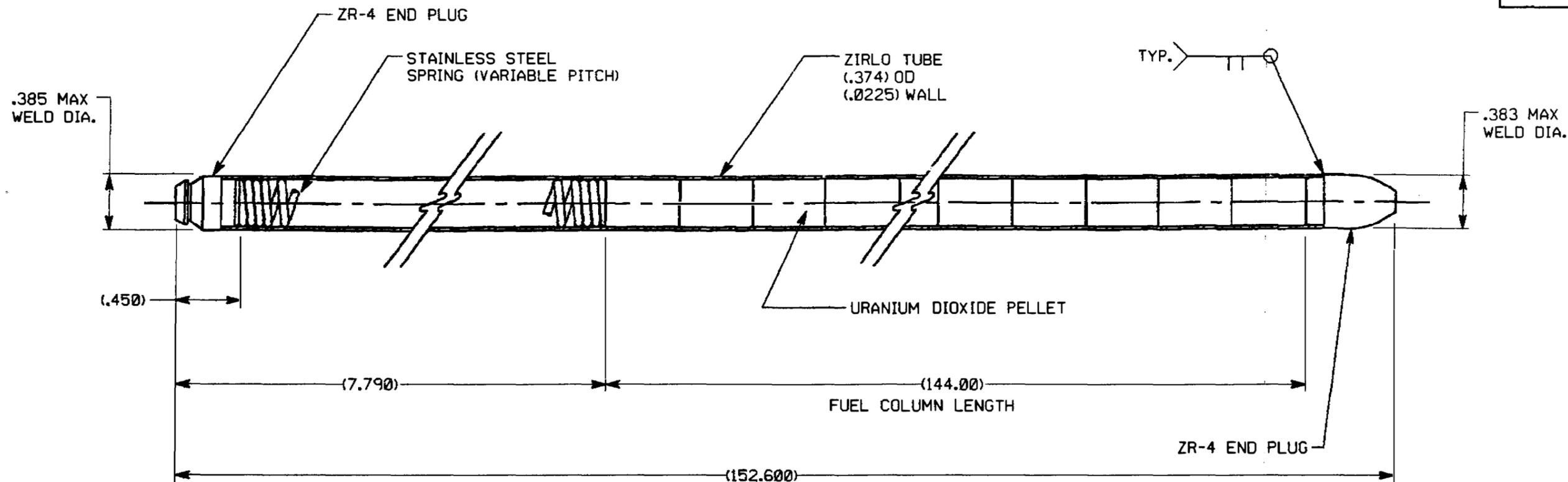
NOTES:

1. DIMENSIONS SHOWN ARE PRIOR TO IRRADIATION.

2. FUEL ROD ASSEMBLY IS PRESSURIZED.

3. SOME FUEL PELLETS MAY CONTAIN A THIN COATING OF
   NATURAL OR ENRICHED Zr-B_2 ON THE CIRCUMFERENTIAL
   SURFACE OF THE PELLET.

4. THE FUEL ROD ASSEMBLIES MAY CONTAIN NATURAL OR ENRICHED UO_2
   ANNULAR AXIAL BLANKET PELLETS AT THE TOP AND BOTTOM OF THE FUEL
   COLUMN LENGTH.

5. SOME FUEL RODS MAY CONTAIN THE DEBRIS RESISTANT
   OXIDE COATING.

6. THE ESTIMATED WEIGHT OF THE MATERIAL IN A FUEL
   ROD ASSEMBLY IN POUNDS IS:

ZIRLO	0.88
ZR-4	0.03
STAINLESS STEEL	0.01
URANIUM DIOXIDE	4.27
TOTAL	5.19

FIGURE 4.2-3b

17 x 17 V5H, VANTAGE+
FUEL ROD ASSEMBLY OUTLINE
BEAVER VALLEY POWER STATION-UNIT 2
UPDATED FINAL SAFETY ANALYSIS REPORT

STAINLESS STEEL SPRING
(VARIABLE PITCH)

ZIRLO TUBE
(.374) OD

ZR-4 END PLUG

ZR-4 END PLUG

URANIUM DIOXIDE PELLET

(7.66)

(144.00)
FUEL COLUMN LENGTH

(152.800)
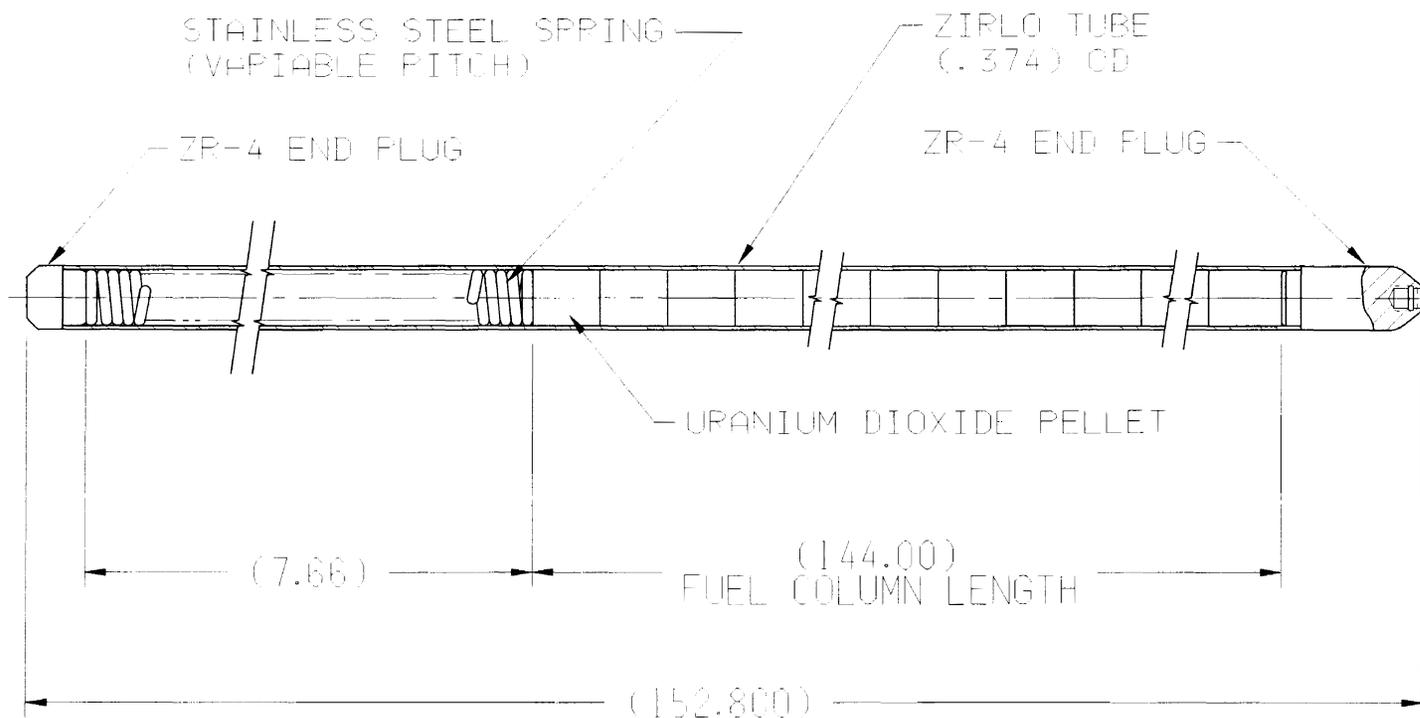
FIGURE 4.2-3b
17 X 17 STD. P+, Z+2
FUEL ROD ASSEMBLY OUTLINE
BEAVER VALLEY POWER STATION UNIT NO. 2
UPDATED FINAL SAFETY ANALYSIS REPORT

GRID STRAP

ZIRCALOY SLEEVE

ZIRCALOY THIMBLE

FUEL ROD

EXPANSION LOBE

EXPANSION
DIAMETER
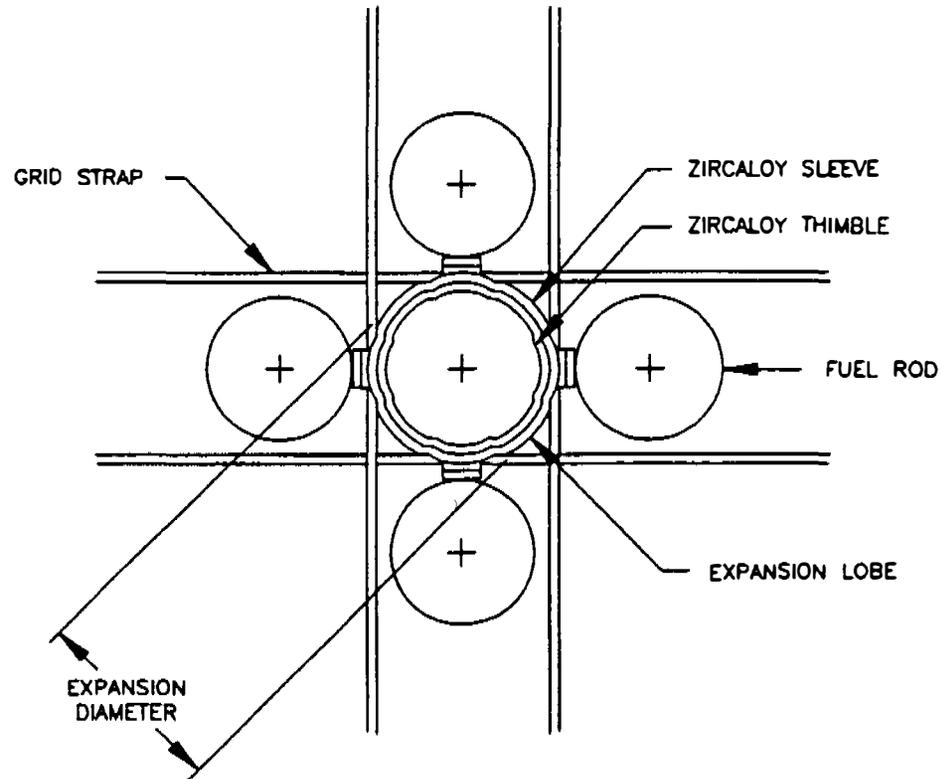
FIGURE 4.2-4
PLAN VIEW MID GRID EXPANSION
JOINT DESIGN
BEAVER VALLEY POWER STATION-UNIT 2
FINAL SAFETY ANALYSIS REPORT

GUIDE THIMBLE TUBE

MIXING VANE

MID GRID

1.500

MID GRID SLEEVE

WELD
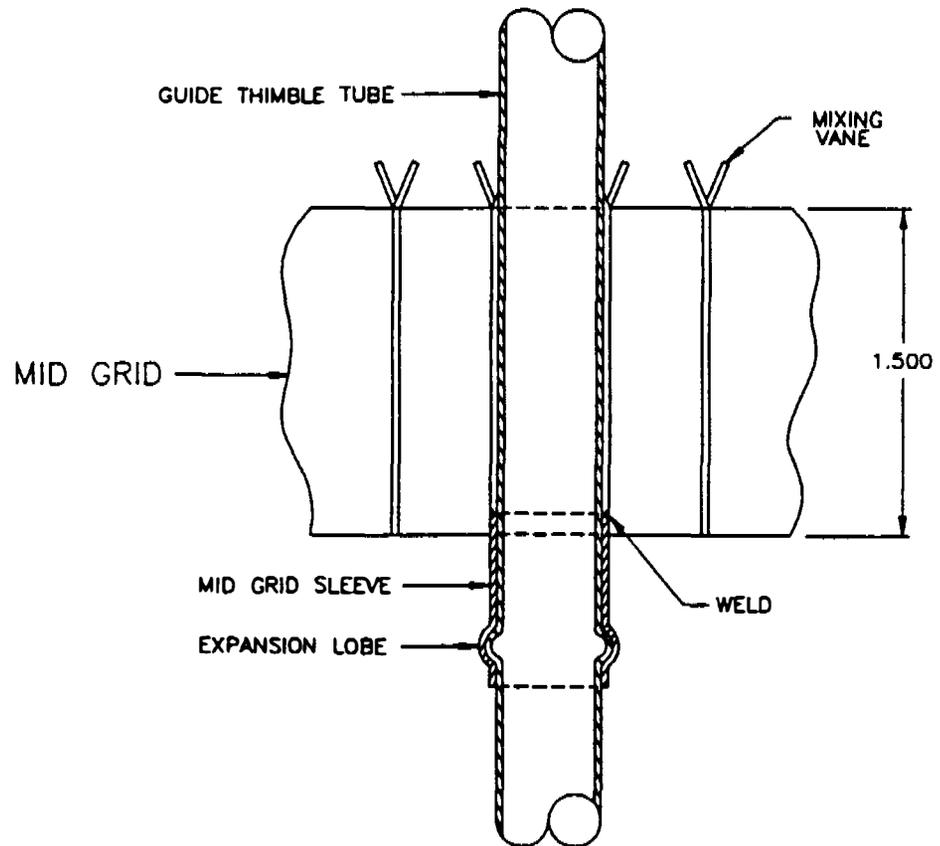
EXPANSION LOBE

FIGURE 4.2-5
MID GRID EXPANSION JOINT
ELEVATION VIEW
BEAVER VALLEY POWER STATION-UNIT 2
FINAL SAFETY ANALYSIS REPORT

LOCK TUBE

ADAPTOR PLATE

GROOVE

ADAPTOR PLATE THRU HOLE

NOZZLE INSERT

E   E

BULGE JOINTS (4 LOBES EACH)

THIMBLE TUBE

SECTION E-E

(TYPICAL)

TOP GRID

TOP GRID SLEEVE

UNASSEMBLED

ASSEMBLED
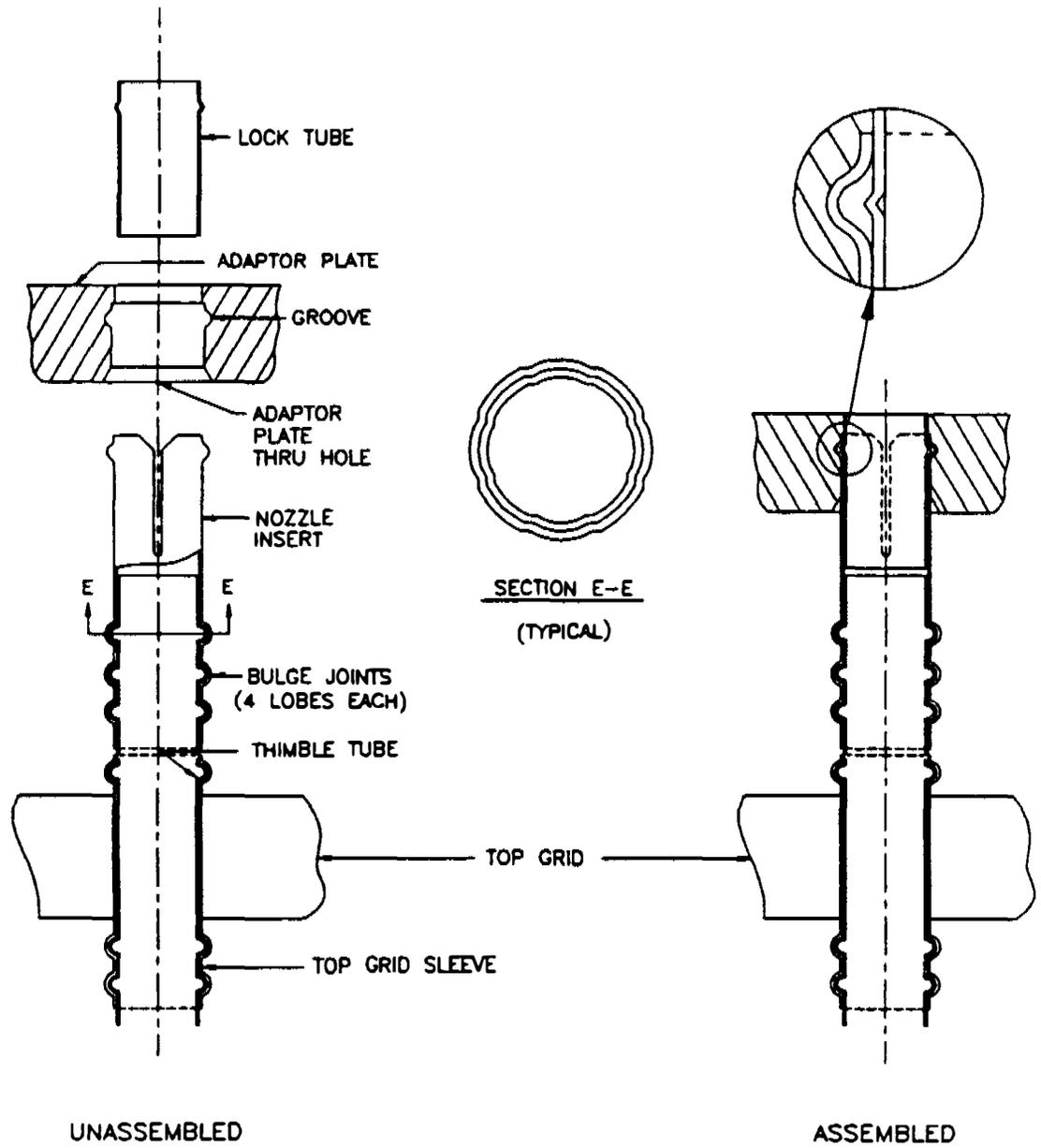
FIGURE 4.2-6
TOP GRID TO NOZZLE ATTACHMENT
BEAVER VALLEY POWER STATION-UNIT 2
FINAL SAFETY ANALYSIS REPORT

BOTTOM GRID

ZIRCALOY GUIDE THIMBLE

SPOT WELDS

BOTTOM GRID SS INSERT

ZIRCALOY GUIDE THIMBLE
THREADED END PLUG

THIMBLE TO END
PLUG WELD

INSERT TO END
PLUG WELD

SS BOTTOM NOZZLE
TOP PLATE

SS THIMBLE SCREW WITH
INTEGRAL LOCKING CUP
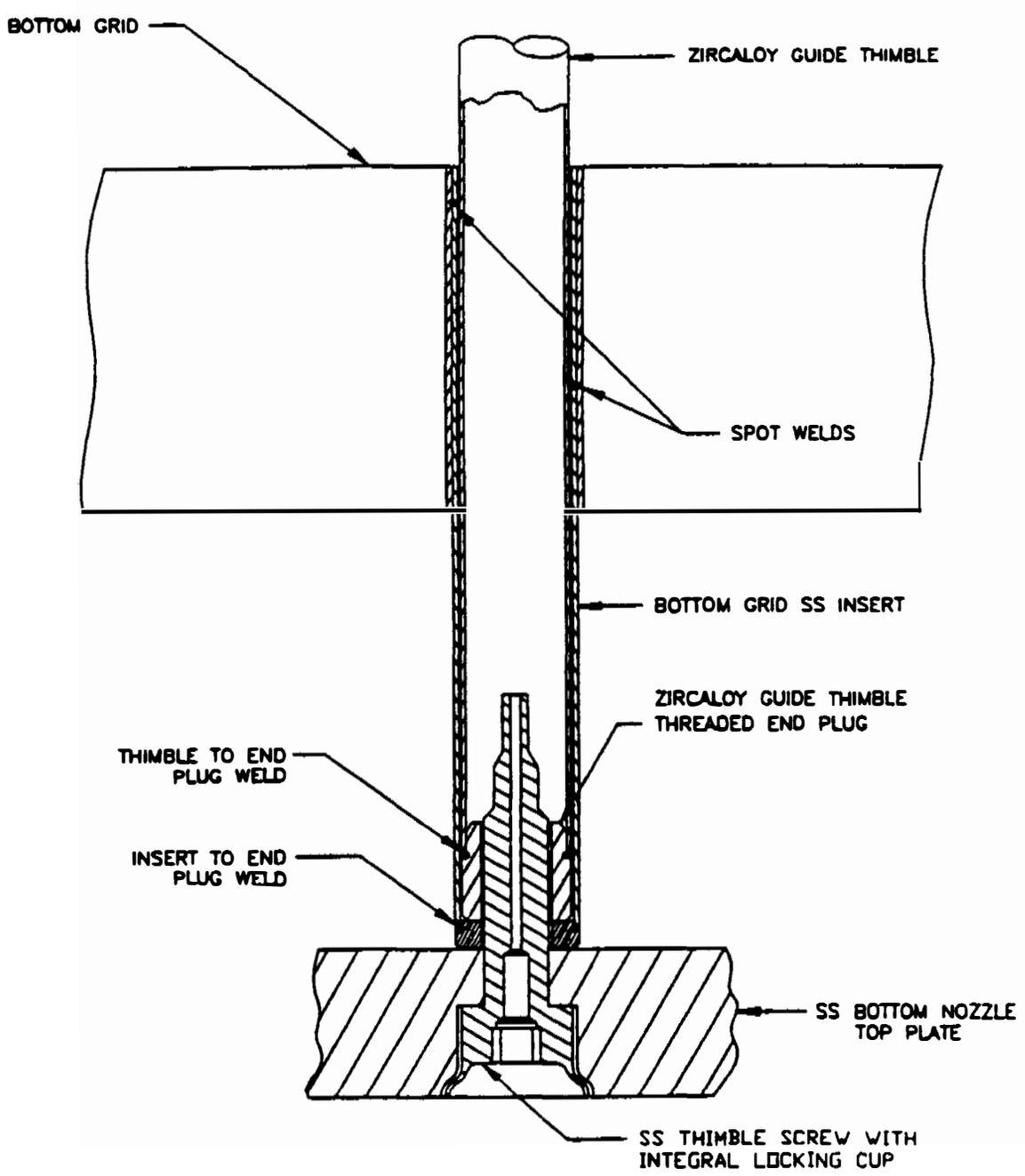
FIGURE 4.2-7
GUIDE THIMBLE TO BOTTOM
NOZZLE JOINT
BEAVER VALLEY POWER STATION-UNIT 2
FINAL SAFETY ANALYSIS REPORT

RCC ASSEMBLY WITHDRAWN

RCC ASSEMBLY INSERTED

CRDM

DRIVE ROD ASSEMBLY

FULL LENGTH RCC ASSEMBLY

GUIDE TUBE ASSEMBLY
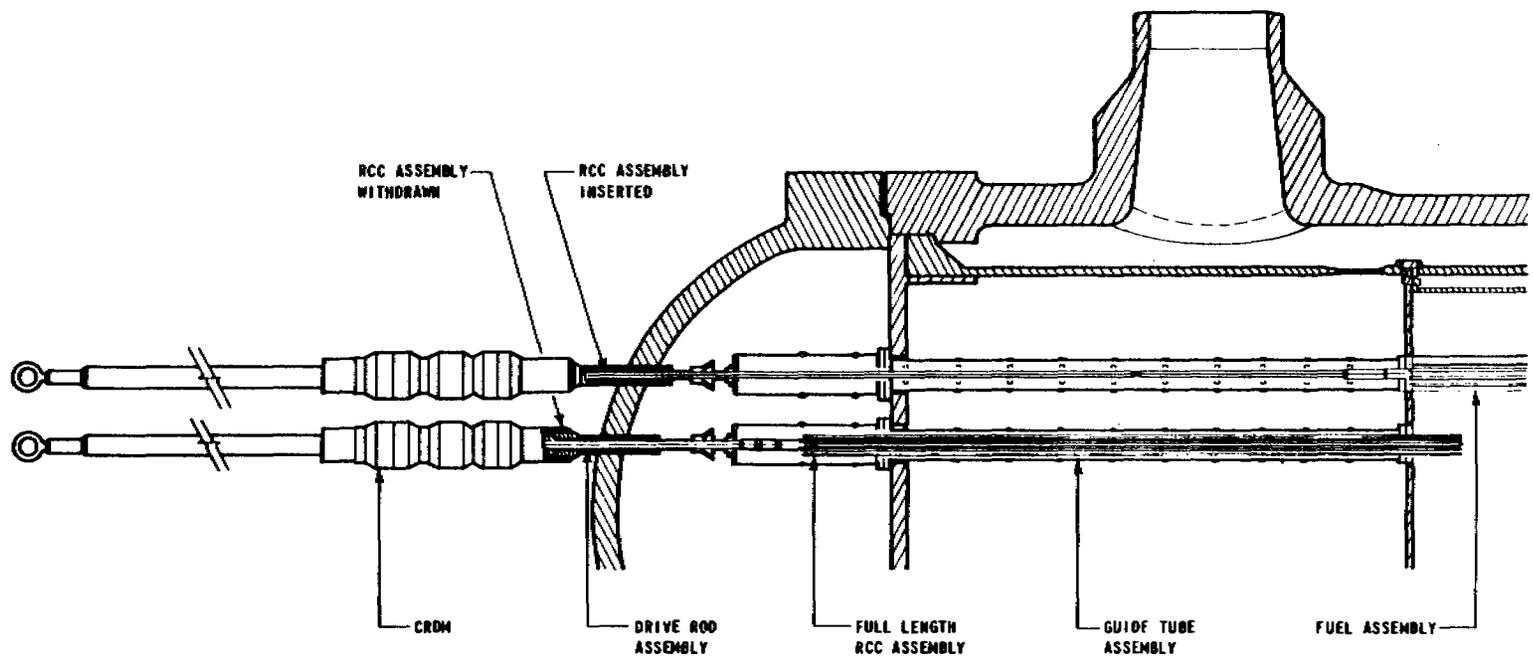
FUEL ASSEMBLY

FIGURE 4. 2-8
ROD CLUSTER CONTROL AND
DRIVE ROD ASSEMBLY WITH
INTERFACING COMPONENTS
BEAVER VALLEY POWER STATION-UNIT 2
FINAL SAFETY ANALYSIS REPORT

INCONEL
SPRING

SPRING RETAINER

SPIDER BODY

ABSORBER (SILVER,
INDIUM, CADMIUM)
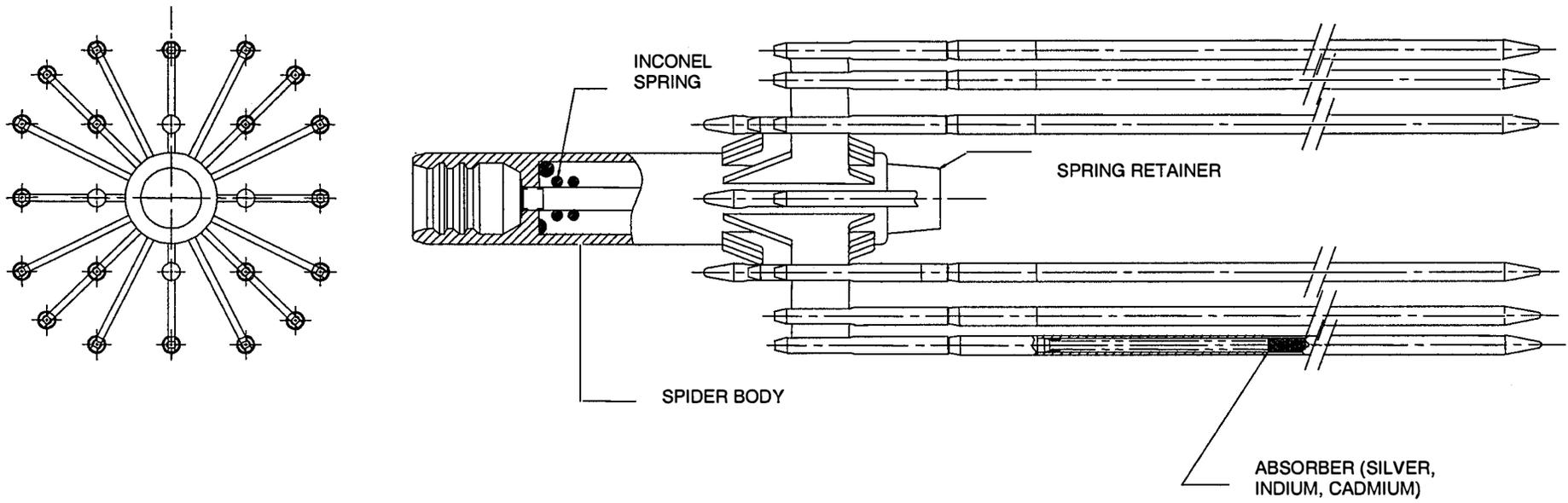
FIGURE 4.2-9
ROD CLUSTER CONTROL ASSEMBLY OUTLINE
BEAVER VALLEY POWER STATION-UNIT 2
FINAL SAFETY ANALYSIS REPORT

.385 DIA
MAXIMUM

TOP END PLUG

3.900

142.0 ABSORBER MATERIAL

TYPE 304 STAINLESS
STEEL

Ag-In-Cd

BOTTOM END PLUG

151.885
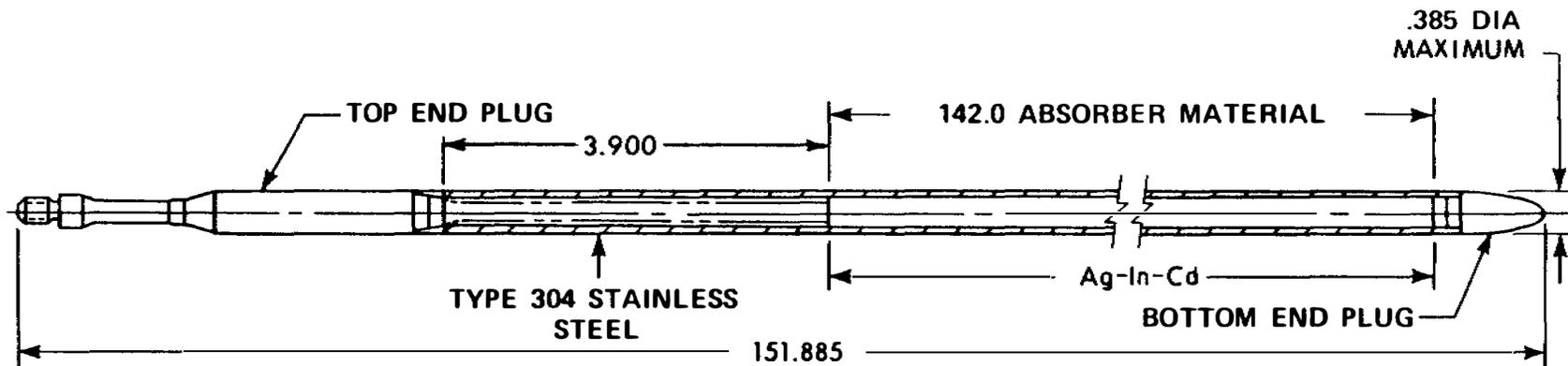
FIGURE 4. 2-10
ABSORBER ROD
BEAVER VALLEY POWER STATION-UNIT 2
FINAL SAFETY ANALYSIS REPORT
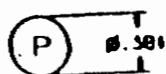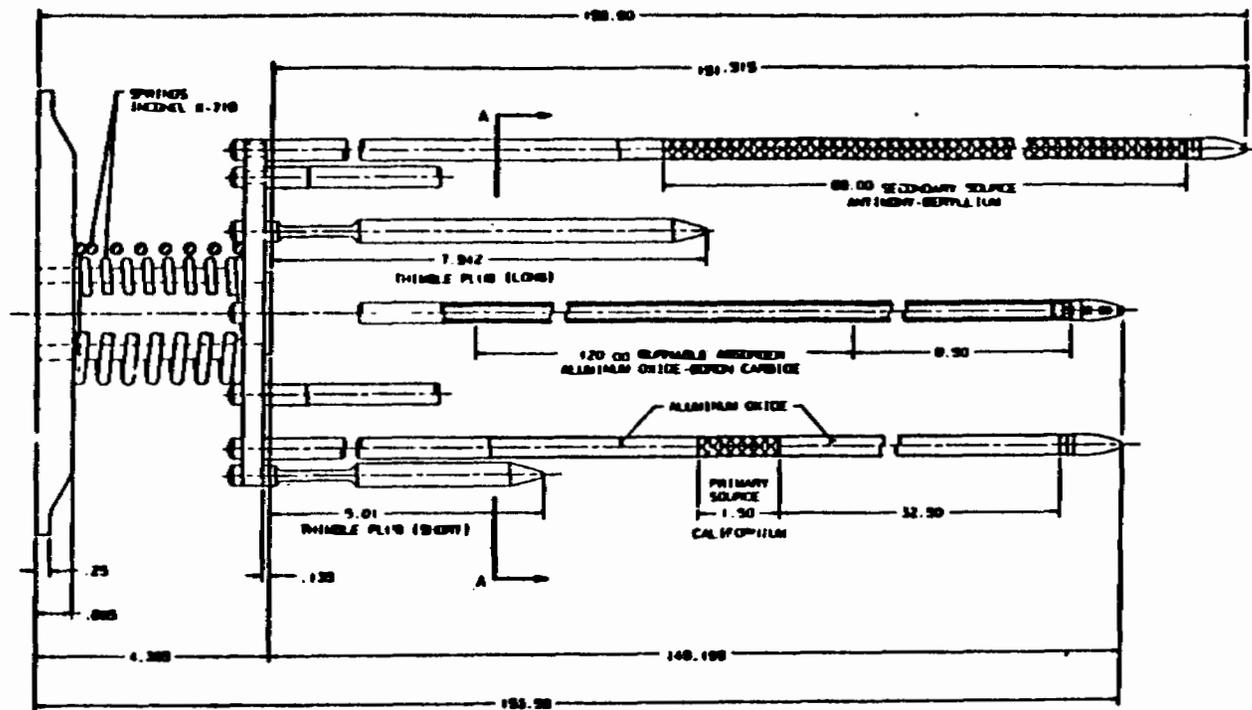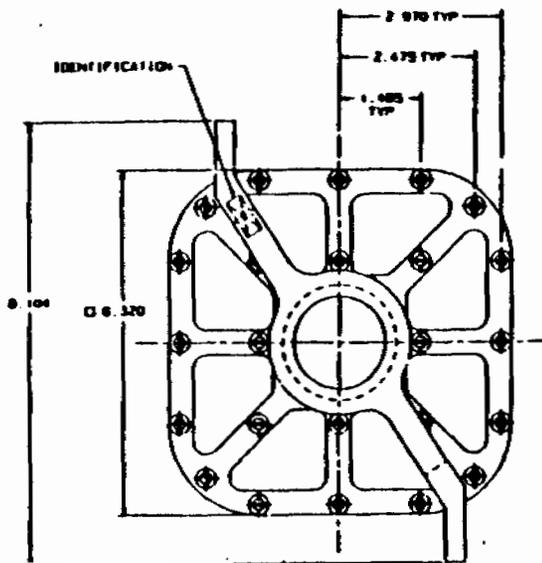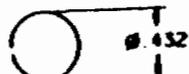
FIGURE 4.2-11
COMPOSITE CORE COMPONENT RODS
BEAVER VALLEY POWER STATION-UNIT 2
FINAL SAFETY ANALYSIS REPORT

4.3 NUCLEAR DESIGN

4.3.1 Design Bases

This section describes the design bases and functional requirements used in the nuclear design of the fuel and reactivity control system and relates these design bases to the General Design Criteria (GDC) presented in 10CFR50, Appendix A. Where applicable, supplemental criteria, such as the "Final Acceptance Criteria for Emergency Core Cooling Systems," are addressed. Before discussing the nuclear design bases, it is appropriate to briefly review the four major categories ascribed to conditions of plant operation.

The full spectrum of plant conditions is divided into four categories, in accordance with the anticipated frequency of occurrence and risk to the public:

     1.   ANS Condition I - Normal Operation

     2.   ANS Condition II - Incidents of Moderate Frequency

     3.   ANS Condition III - Infrequent Faults

     4.   ANS Condition IV - Limiting Faults

In general, the ANS Condition I occurrences are accommodated with margin between any plant parameter and the value of that parameter which would require either automatic or manual protective action. ANS Condition II incidents are accommodated with, at most, a shutdown of the reactor with the plant capable of returning to operation after corrective action. Fuel damage (fuel damage, as used here, is defined as penetration of the fission product barrier, i.e., the fuel rod clad) is not expected during ANS Condition I and ANS Condition II events. It is not possible, however, to preclude a very small number of rod failures, resulting in the release of small quantities of fission products. The chemical and volume control system (CVCS) is designed to remove the fission products from the reactor coolant, keeping the reactor coolant activity within the plant design bases limits.

ANS Condition III incidents shall not cause more than a small fraction of the fuel elements in the reactor to be damaged, although sufficient fuel element damage might occur to preclude immediate resumption of operation. The release of radioactive material due to ANS Condition III incidents should not be sufficient to interrupt or restrict public use of those areas beyond the exclusion area. Furthermore, an ANS Condition III incident shall not, by itself, generate an ANS Condition IV fault or result in a consequential loss of function of the reactor coolant or reactor containment barriers.

ANS Condition IV occurrences are faults that are not expected to occur but are defined as limiting faults which must be designed

against.   ANS Condition IV faults shall not cause a release of
radioactive material that results in an undue risk to public health
and safety.

The core design power distribution limits related to fuel integrity
are met for ANS Condition I occurrences through conservative design
and maintained by the action of the control system.   The requirements
for ANS Condition II occurrences are met by providing an adequate
protection system which monitors reactor parameters.   The control and
protection systems are described in Chapter 7, and the consequences of
ANS Condition II, III, and IV occurrences are given in Chapter 15.

4.3.1.1 Fuel Burnup

     Basis

The fuel rod design basis is described in Section 4.2. The nuclear
design basis is to install sufficient reactivity in the fuel to attain
a region discharge burnup of 45,000 MWD/MTU or higher.   The above,
along with the design basis in Section 4.3.1.3, satisfies GDC-10.

     Discussion

Fuel burnup is a measure of fuel depletion which represents the
integrated energy output of the fuel (MWD/MTU) and is a convenient
means for quantifying fuel exposure criteria.

The core design lifetime or design discharge burnup is achieved by
installing sufficient initial excess reactivity in each fuel region
and by following a fuel replacement program (such as that described in
Section 4.3.2.1) that meets all safety-related criteria in each cycle
of operation.

Initial excess reactivity installed in the fuel, although not a design
basis, must be sufficient to maintain core criticality at full power
operating conditions throughout cycle life with equilibrium xenon,
samarium, and other fission products present.   The end of design cycle
life is defined to occur when the chemical shim concentration is
essentially zero with control rods present to the degree necessary for
operational requirements (e.g., the controlling bank at the "bite"
position).   In terms of chemical shim boron concentration, this
represents approximately 10 ppm with no control rod insertion.

A limitation on initial installed excess reactivity is not required
other than as is quantified in terms of other design bases, such as
core negative reactivity feedback and shutdown margin, discussed
below.

4.3.1.2 Negative Reactivity Feedbacks (Reactivity Coefficient)

    Basis

The total reactivity defect is composed of the reactivity defects due to fuel and moderator effects. As the core power and temperature increase, the total reactivity defect is always negative, even when the moderator defect is positive as a result of implementing a positive MTC limit. Therefore, the cumulative reactivity feedback as the core power approaches 100 percent is always negative, even with a part-power positive moderator temperature coefficient of reactivity. The design basis meets GDC-11.

    Discussion

When compensation for a rapid increase in reactivity is considered, there are two major effects. These are the resonance absorption effects (Doppler) associated with changing fuel temperature and the neutron spectrum effect resulting from changing moderator density. These basic physics characteristics are often identified by reactivity coefficients. The use of slightly enriched uranium ensures that the Doppler coefficient of reactivity is negative. This coefficient provides the most rapid reactivity compensation. The core is also designed to have an overall moderator temperature coefficient of reactivity which is non-positive at 100 percent power, less than +2.0 pcm/°F below 70 percent power, and less than a linearly decreasing limit of +2.0 pcm/°F to 0.0 pcm/°F between 70 percent power to 100 percent power, respectively. At full power, void content provides another, slower compensatory effect. The moderator temperature coefficient is maintained within the above limits through use of burnable absorbers and/or control rods, which decrease the concentration of soluble boron for criticality, while maintaining reactivity control.

Burnable absorber content (quantity and distribution) is not stated as a design basis other than as it relates to the accomplishment of the moderator temperature coefficient limits discussed above.

4.3.1.3 Control of Power Distribution

    Basis

The nuclear design basis is that, with at least a 95 percent confidence level:

    1. The fuel will not be operated at greater than 13.74 kW/ft
        (based on F_Q of 2.40) under normal operating conditions,
        including an allowance of 0.6 percent for calorimetric error
        and not including power spike factor due to densification.

    2. Under abnormal conditions, including the maximum overpower
        condition, the fuel peak power will not cause melting, as
        defined in Section 4.4.1.2.

3. The fuel will not operate with a power distribution that violates the departure from nucleate boiling (DNB) design basis (i.e., the DNBR shall not be less than 1.30, as discussed in Section 4.4.1) under ANS Condition I and II events, including the maximum overpower condition

4. Fuel management will be such as to produce rod powers and burnups consistent with the assumptions in the fuel rod mechanical integrity analysis of Section 4.2.

The above basis meets GDC-10.

Discussion

Calculation of extreme power shapes which affect fuel design limits is performed with proven methods and verified frequently with measurements from operating reactors. The conditions, under which limiting power shapes are assumed to occur are chosen conservatively with regard to any permissible operating state.

Even though there is good agreement between calculated peak power and measurements, a nuclear uncertainty (Section 4.3.2.2) is applied to the calculated peak local power. Such a margin is provided both for the analyses for normal operating states and for anticipated transients.

4.3.1.4 Maximum Controlled Reactivity Insertion Rate

Basis

The maximum reactivity insertion rate due to withdrawal of rod cluster control assemblies at power or by boron dilution is limited. During normal at power operation, the maximum controlled reactivity insertion rate is less than 35 pcm/sec (1 pcm = $10^{-5}\Delta\rho$). A maximum reactivity change rate of 75 pcm/sec for accidental withdrawal of control banks is set such that peak heat generation rate and DNBR do not exceed the maximum allowable at overpower conditions. This satisfies GDC-25.

The maximum reactivity worth of control rods and the maximum rates of reactivity insertion employing control rods are limited so as to preclude rupture of the reactor coolant pressure boundary or disruption of the core internals to a degree which would impair core cooling capacity due to a rod withdrawal or ejection accident (see Chapter 15).

Following any ANS Condition IV event, the reactor can be brought to the shutdown condition and the core will maintain acceptable heat transfer geometry. This satisfies GDC-28.

Discussion

Reactivity addition associated with an accidental withdrawal of a control bank (or banks) is limited by the maximum rod speed (or travel rate) and by the worth of the bank(s). The maximum control rod speed is 45 inches per minute, and the maximum rate of reactivity change considering two control banks moving is less than 75 pcm/sec. During normal operation at power and with control rod overlap, the maximum reactivity change rate is less than 35 pcm/sec.

The reactivity change rates are conservatively calculated, assuming unfavorable axial power and xenon distributions. The peak xenon burnout rate is 25 pcm/min, which is lower than the maximum reactivity addition rate of 35 pcm/sec for normal operation and 75 pcm/sec for accidental withdrawal of two banks.

4.3.1.5 Shutdown Margins

Basis

Minimum shutdown margin, as specified in the Technical Specifications, is required in all modes of operation.

In all analyses involving reactor trip, the single, highest worth rod cluster control assembly is postulated to remain untripped in its full-out position (stuck rod criterion). This satisfies GDC-26.

Discussion

Two independent reactivity control systems are provided: control rods and soluble boron in the coolant. The control rod system can compensate for the reactivity effects of the fuel and water temperature changes accompanying power level changes over the range from full-load to no-load. In addition, the control rod system provides the minimum shutdown margin under ANS Condition I events and is capable of making the core subcritical rapidly enough to prevent exceeding acceptable fuel damage limits, assuming that the highest worth control rod is stuck out upon trip.

The boron concentration can compensate for all xenon burnout reactivity changes and will maintain the reactor in the cold shutdown condition. Thus, backup and emergency shutdown provisions are provided by a mechanical and a chemical shim control system which satisfies GDC-26.

Basis

When fuel assemblies are in the pressure vessel and the vessel head is not in place, K_{eff} will be maintained at or below 0.95 by control rods and soluble boron. Further, the fuel will be maintained sufficiently subcritical that removal of all rod cluster control assemblies will not result in criticality.

Discussion

The methodology contained in Holtec Report HI-2084175, ''Licensing Report for Beaver Valley Unit 2 Rerack,'' Revision 8, dated February 2011, demonstrates a K_{eff} less than 1.0 in the spent fuel storage racks if fully flooded with unborated water. ANSI Standard N18.2 specifies a K_{eff} not to exceed 0.98 in normally dry new fuel storage racks, assuming optimum moderation. No criterion is given for the refueling operation.

The boron concentration required to meet the refueling shutdown criteria is specified in the Technical Specifications. Verification that these shutdown criteria are met, including uncertainties is achieved using standard Westinghouse design methods. The subcriticality of the core is continuously monitored as described in the Technical Specifications.

4.3.1.6 Stability

Basis

The core will be inherently stable to power oscillations at the fundamental mode. This satisfies GDC-12.

Spatial power oscillations within the core with a constant core power output, should they occur, can be reliably and readily detected and suppressed.

Discussion

Oscillations of the total power output of the core, from whatever cause, are readily detected by the reactor coolant loop temperature sensors and by the nuclear instrumentation. The core is protected by these systems, and a reactor trip would occur if power increased unacceptably, preserving the design margins to fuel design limits. The stability of the turbine/steam generator/core systems and the reactor control system is such that total core power oscillations are not normally possible. The redundancy of the protection circuits ensures an extremely low probability of exceeding design power levels.

The core is designed so that diametral and azimuthal oscillations due to spatial xenon effects are self-damping, and no operator action or control action is required to suppress them. The stability to diametral oscillations is so great that this excitation is highly improbable. Convergent azimuthal oscillations can be excited by prohibited motion of individual control rods. Such oscillations are readily observable and alarmed, using the excore power range ion chambers. Indications are also continuously available from incore thermocouples and loop temperature measurements. Movable incore

detectors can be activated to provide more detailed information. In all proposed cores, these horizontal plane oscillations are self-damping by virtue of reactivity feedback effects designed into the core.

Axial xenon spatial power oscillations may occur late in core life. The control bank and excore detectors are provided for control and monitoring of axial power distributions. Assurance that fuel design limits are not exceeded is provided by reactor overpower ΔT and overtemperature ΔT trip functions. Overtemperature ΔT uses the measured axial power imbalance as an input.

4.3.1.7 Anticipated Transients Without Trip

The effects of anticipated transients with failure to trip are not considered in the design bases of the plant. Analysis has shown that the likelihood of such a hypothetical event is negligibly small. Furthermore, analysis of the consequences of a hypothetical failure to trip following anticipated transients has shown that no significant core damage would result, system peak pressures would be limited to acceptable values, and no failure of the reactor coolant system would result (Westinghouse 1974).

In compliance with 10 CFR 50.62, Anticipated Transient Without Scram Mitigating System Actuation Circuitry (AMSAC) has been added to the unit design. The scenario for which AMSAC is designed and required is a complete loss of normal feedwater coupled with a common mode failure of the Reactor Protection System that results in its failure to trip the reactor, failure to initiate Auxiliary Feedwater and failure to initiate Turbine Trip. Under such a scenario without AMSAC, the RCS pressure could exceed the 3200 psig ASME Boiler and Pressure Vessel Code Level C service limit stress criteria.

AMSAC design is primarily based upon 49FR26036 (Federal Register June 26, 1984), WCAP-10858P-A Revision 1 (Westinghouse 1987) and NRC Generic Letter 85-06, "Quality Assurance Guidance for ATWS Equipment That Is Not Safety-Related." AMSAC itself is not safety-related but the output isolation relays located in the AMSAC panel that operate to start the auxiliary feedwater pumps and trip the turbine are safety-related.

AMSAC monitors normal feedwater flow in each of the three (3) loops. Any two-out-of-three loops indicating a loss of feedwater flow (i.e., less than 25% of nominal flow at 100% power) will initiate AMSAC provided that the C-20 permissive is met. This C-20 permissive is met when the turbine load is at 40% or greater, as sensed by two-out-of-two turbine first stage pressure channels. Failure of one or more of the three feedwater signals (as evidenced by an out-of-range signal) will automatically block AMSAC actuation in order to preclude spurious operation.   When AMSAC is initiated, a variable time delay proportional to turbine load is introduced to allow the Reactor Protection System to initiate appropriate action first.   After the delay, AMSAC will initiate auxiliary feedwater flow by starting both motor driven and the steam driven auxiliary feedwater pumps and also

initiate a turbine trip. To ensure AMSAC remains available long enough to perform its function in the event of a turbine trip, the C-20 permissive signal is maintained for an appropriate period of time after the turbine first stage pressure drops below 40% turbine load.

Isolated input signals to AMSAC originate in the Primary Process Racks. Isolated output signals from AMSAC originate from qualified electro-mechanical isolation relays in the rear of the AMSAC panel. The AMSAC panel is located on elevation 707'-6" of the Control Building.

The AMSAC system may be bypassed to allow for testing, calibration or repair while at power. Control Room indication is provided if the AMSAC system is bypassed.

4.3.2 Description

4.3.2.1 Nuclear Design Description

The reactor core consists of a specified number of fuel rods which are held in bundles by spacer grids and top and bottom nozzles. The fuel rods are constructed of cylindrical Zircaloy or Zirlo^{TM} tubes containing UO$_2$ fuel pellets. The bundles, known as fuel assemblies, are arranged in a pattern which approximates a right circular cylinder. Some fuel assemblies may contain non-fueled rods. For a description of non-fueled rods see Section 4.1.

Each fuel assembly contains a 17 x 17 rod array composed of 264 fuel rods, 24 rod cluster control thimbles, and an incore instrumentation thimble. Figure 4.2-1 shows a cross-sectional view of a 17 x 17 fuel assembly and the related rod cluster control locations. Further details of the fuel assembly are given in Section 4.2.

The fuel rods within a given assembly have the same uranium enrichment in the radial plane. However, the uranium enrichment may change with fuel height (e.g., the fuel assemblies may use unenriched uranium fuel in the top and bottom six inches of the fuel rods. The middle 132 inches of each assembly would then contain the enriched uranium fuel). Fuel assemblies of several different enrichments are used in the core loading to establish a favorable radial power distribution.

The reference reloading pattern is typically similar to Figure 4.3-1 with depleted fuel interspersed checkerboard style in the center and burned fuel on the periphery. The core will normally operate approximately eighteen months between refuelings, accumulating 18,000 MWD/MTU or more per cycle. The exact reloading pattern, initial and final burnups of the assemblies, and the number of fresh assemblies and their placement are dependent on the energy requirement for the next cycle and burnup and power histories of the previous cycles.

The core average enrichment is determined by the amount of fissionable material required to provide the desired core lifetime and energy requirements, namely a region average discharge burnup of 45,000 MWD/MTU or higher. The physics of the burnout process is such that operation of the reactor depletes the amount of fuel available due to the absorption of neutrons by the U-235 atoms and their subsequent fission. The rate of U-235 depletion is directly proportional to the power level at which the reactor is operated. In addition, the fission process results in the formation of fission products, some of which readily absorb neutrons. These effects, depletion, and the buildup of fission products, are partially offset by the buildup of plutonium, as shown on Figure 4.3-2 for a typical 17 x 17 fuel assembly, which occurs due to the nonfission absorption of neutrons in U-238. Therefore, at the beginning of any cycle, a reactivity reserve equal to the depletion of the fissionable fuel and the buildup of fission product poisons over the specified cycle life must be "built" into the reactor. This excess reactivity is controlled by removable neutron absorbing material in the form of boron dissolved in the primary coolant and burnable absorber.

The concentration of boric acid in the reactor coolant is varied to provide control and to compensate for long-term reactivity requirements. The concentration of the soluble neutron absorber is varied to compensate for reactivity changes due to fuel burnup; fission product poisoning, including xenon and samarium; burnable poison depletion; and the cold-to-operating moderator temperature change. Using its normal makeup path, the chemical and volume control system (CVCS) is capable of inserting negative reactivity at a rate of approximately 25 pcm/min when the reactor coolant boron concentration is 2,000 ppm, approximately 30 pcm/min when the reactor coolant boron concentration is 1000 ppm and approximately 35 pcm/min when reactor coolant boron concentration is 100 ppm. If the emergency boration path is used, the CVCS is capable of inserting negative reactivity at a rate of approximately 55 pcm/min when the reactor coolant concentration is 2,000 ppm, approximately 65 pcm/min when the reactor coolant concentration is 1000 ppm and approximately 75 pcm/min when the reactor coolant boron concentration is 100 ppm. The peak burnout rate for xenon is 25 pcm/min (Section 9.3.4 discusses the capability of the CVCS to counteract xenon decay). Rapid transient reactivity requirements and safety shutdown requirements are met with control rods.

As the boron concentration is increased, the moderator temperature coefficient becomes less negative. The use of a soluble boron in the moderator alone would result in a moderator temperature coefficient more positive than that permitted by the Technical Specifications. Therefore, burnable absorber rods are used to reduce the soluble boron concentration sufficiently to ensure that the

moderator temperature coefficient remains more negative than the Technical Specification limit as a function of power level. The use of control rods may be required early in the cycle at low power to maintain the moderator temperature coefficient more negative than the Technical Specification limit. During operation, the poison content in the burnable absorbers is depleted, adding positive reactivity to offset some of the negative reactivity from fuel depletion and fission product buildup. The depletion rate of the burnable absorber is not critical because chemical shim is always available and flexible enough to cover any possible deviations in the expected burnable absorber depletion rate. Figure 4.3-3 shows plots of typical core depletion with and without burnable absorber rods.

In addition to reactivity control, the burnable absorber rods or Integral Fuel Burnable Absorbers (IFBAs) are strategically located to provide a favorable radial power distribution. Figures 4.3-4, 4.3-4a, 4.3-4b and 4.3-4c show typical burnable absorber distributions within a fuel assembly for the several burnable absorber patterns used in a 17 x 17 array. A typical reload core integral burnable absorber loading pattern is shown in Figure 4.3-5.

Tables 4.3-1, 4.3-2 and 4.3-3 contain summaries of the reactor core design parameters for the first fuel cycle, including reactivity coefficients, delayed neutron fraction, and neutron lifetimes. Sufficient information is included to permit an independent calculation of the nuclear performance characteristics of the core.

4.3.2.2 Power Distributions

The accuracy of power distribution calculations has been confirmed through approximately 1,000 flux maps during some 20 years of operation under conditions very similar to those expected. Details of this confirmation are given in Langford and Nath (1971) and in Section 4.3.2.2.7.

4.3.2.2.1 Definitions

Power distributions are quantified in terms of hot channel factors. These factors are a measure of the peak pellet power within the reactor core and the total energy produced in a coolant channel, relative to the total reactor power output, and are expressed in terms of quantities related to the nuclear or thermal design, namely:

   1. Power density - the thermal power produced per unit volume of the core (kW/liter).

   2. Linear power density - the thermal power produced per unit length of active fuel (kW/ft). Because fuel assembly geometry is standardized, this is the unit of power density

most commonly used. For all practical purposes, it differs
from kW/liter by a constant factor which includes geometry
and the fraction of the total thermal power which is
generated in the fuel rod.

3. Average linear power density - the total thermal power
    produced in the fuel rods divided by the total active fuel
    length of all rods in the core.

4. Local heat flux - the heat flux at the surface of the
    cladding (Btu-ft^{-2} hr^{-1}). For nominal rod parameters, this
    differs from linear power density by a constant factor.

5. Rod power or rod integral power - the length integrated
    linear power density in one rod (kW).

6. Average rod power - the total thermal power produced in the
    fuel rods divided by the number of fuel rods (assuming all
    rods have equal length).

The hot channel factors used in the discussion of power distributions
in this section are defined as follows:

1. F_Q, heat flux hot channel factor - the maximum local heat
    flux on the surface of a fuel rod divided by the average fuel
    rod heat flux, allowing for manufacturing tolerances on fuel
    pellets and rods.

2. F^N_Q, nuclear heat flux hot channel factor - the maximum local
    fuel rod linear power density divided by the average fuel rod
    linear power density, assuming nominal fuel pellet and rod
    parameters.

3. F^E_Q, engineering heat flux hot channel factor - the allowance
    on heat flux required for manufacturing tolerances. The
    engineering factor allows for local variations in enrichment,
    pellet density and diameter, surface area of the fuel rod,
    and eccentricity of the gap between pellet and clad.
    Combined statistically, the net effect is a factor of 1.03 to
    be applied to fuel rod surface heat flux.

4. $F^N_{\Delta H}$, nuclear enthalpy rise hot channel factor - the ratio of
    the integral of linear power along the rod with the highest
    integrated power to the average rod power.

Manufacturing tolerances, hot channel power distribution, and
surrounding channel power distributions are explicitly treated in the
calculation of the DNBR described in Section 4.4.

It is convenient for the purposes of discussion to define subfactors of F_Q. However, design limits are set in terms of the total peaking factor.

F_Q = Total peaking factor or heat flux hot channel factor

$$= \frac{\text{Maximum kW / ft}}{\text{Average kW / ft}}$$

$$F_Q = F_Q^N \times F_Q^E$$

$$F_Q = \max\left[F_{XY}^N(Z) \times P(Z)\right] \times F_U^N \times F_Q^E$$

where:

   F_Q^N and F_Q^E are defined above

   F_U^N = Factor for measurement uncertainties, assumed to be 1.05

   $F_{XY}^N(Z)$ = Ratio of peak power density to average power density in the horizontal plane of peak local power

   $P(Z)$ = Ratio of the power per unit core height in the horizontal plane at height Z to the average value of power per unit core height

4.3.2.2.2 Radial Power Distributions

The power shape in horizontal sections of the core at full power is a function of the fuel and burnable absorber loading patterns, and the presence or absence of a single bank of control rods. Thus, at any time in the cycle, a horizontal section of the core can be characterized as unrodded or with group D control rods. These two situations, combined with burnup effects, determine the radial power shapes which can exist in the core at full power. The effect on radial power shapes of power level, xenon, samarium, and moderator density effects are also considered but these are quite small. The effect of nonuniform flow distribution is negligible. While radial power distributions in various planes of the core are often illustrated, the core radial enthalpy rise distribution, as determined by the integral of power up each channel, is of greater interest. Figures 4.3-6, 4.3-7, 4.3-8, 4.3-9 and 4.3-10 show typical radial power distributions for l/8th of the core for representative operating conditions.   These conditions are: 1) hot full power (HFP) at beginning-of-life (BOL), no xenon, 2) HFP at BOL, unrodded, equilibrium xenon, 3) HFP near BOL, bank D partially in, equilibrium xenon 4) HFP near middle-of-life (MOL), unrodded, equilibrium xenon, and 5) HFP near end-of-life (EOL), unrodded, equilibrium xenon.

Because the position of the hot channel varies from time to time, a single reference radial design power distribution is selected for DNB calculations.   This reference power distribution is conservatively chosen to concentrate power in one area of the core, minimizing the benefits of flow redistribution.   Assembly powers are normalized to core average power.   The radial power distribution within a fuel rod and its variation with burnup as utilized in thermal calculations and fuel rod design is discussed in Section 4.4.

4.3.2.2.3 Assembly Power Distributions

For the purpose of illustration, typical assembly power distributions for the BOL and EOL conditions, corresponding to Figures 4.3-7 and 4.3-10, respectively, are given for the same assembly in Figures 4.3-11 and 4.3-12, respectively.

Because the detailed power distribution surrounding the hot channel varies from time to time, a conservatively flat assembly power distribution is assumed in the DNB analysis, described in Section 4.4, with the rod of maximum integrated power artificially raised to the design value of $F_{\Delta H}^{N}$. Care is taken in the nuclear design of all fuel cycles and all operating conditions to ensure that

a flatter assembly power distribution does not occur with limiting values of $F_{\Delta H}^{N}$.

4.3.2.2.4 Axial Power Distributions

The shape of the power profile in the axial, or vertical direction is largely under the control of the operator through the automatic (insertion) or manual (withdrawal) motion of the control rods responding to manual operation of the CVCS. Nuclear effects which cause variations in the axial power shape include moderator density, Doppler effect on resonance absorption, spatial distribution of xenon, and burnup. Automatically (insertion) or manually (withdrawal) controlled variations in total power output and control rod motion are also important in determining the axial power shape at any time. Signals are available to the operator from the excore ion chambers, which are power range ion chambers outside the reactor vessel running parallel to the axis of the core. Separate signals are taken from the top and bottom halves of the chambers. The difference between top and bottom signals from each of four pairs of detectors is displayed on the main control board and called the flux difference, ΔI. Calculations of the core average peaking factor for many plants and measurements from operating plants under many operating situations are associated with either ΔI or axial offset in such a way that an upper bound can be placed on the peaking factor. For these correlations, axial offset is defined as:

$$\text{axial offset} = \frac{\Psi_t - \Psi_b}{\Psi_t + \Psi_b}$$

and Ψ_t and Ψ_b are the top and bottom detector readings.

Representative axial power shapes for BOL, MOL, and EOL conditions are shown in Figures 4.3-13, 4.3-14, 4.3-15. These figures cover a wide range of axial offset, including values not permitted at full power.

The radial power distribution shown in Figure 4.3-8 involving the partial insertion of control rods represents a synthesis of power shapes from the rodded and unrodded planes. The applicability of the separability assumption upon which this procedure is based, is ensured through extensive three-dimensional calculations of possible rodded conditions. As an example, Figure 4.3-16 compares the axial power distribution for several assemblies at different distances from inserted control rods with the core average distribution. The only significant difference from the average occurs in the low power peripheral assemblies, thus confirming the validity of the separability assumption.

4.3.2.2.5 DELETED

4.3.2.2.6   Limiting Power Distributions

According to the ANSI classification of plant conditions (see Chapter 15), ANS Condition I occurrences are those which are frequently or regularly expected in the course of power operation, maintenance, or maneuvering of the plant. As such, ANS Condition I occurrences are accommodated with margin between any plant parameter and the value of that parameter which would require either automatic or manual protective action. Inasmuch as ANS Condition I occurrences occur frequently or regularly, they must be considered from the point of view of affecting the consequences of fault conditions (ANS Conditions II, III, and IV). In this regard, analysis of each fault condition described is generally based on a conservative set of initial conditions corresponding to the most adverse set of conditions which can occur during ANS Condition I operation.

The list of steady-state and shutdown conditions, permissible deviations, and operational transients is given in Chapter 15. Implicit in the definition of normal operation is proper and timely action by the reactor operator. That is, the operator follows recommended operating procedures for maintaining appropriate power distributions and takes any necessary remedial actions when alerted to do so by the plant instrumentation. Thus, as stated above, the worst or limiting power distribution which can occur during normal operation is to be considered as the starting point for analysis of ANS Conditions II, III, and IV events.

Improper procedural actions or errors by the operator are assumed in the design as occurrences of moderate frequency (ANS Condition II). Some of the consequences which might result are discussed in Chapter 15. Therefore, the limiting power shapes which result from such ANS Condition II events are those power shapes which deviate from the normal operating condition at the recommended axial offset band, e.g., due to lack of proper action by the operator during a xenon transient following a change in power level brought about by control rod motion. Power shapes which fall in this category are used for determination of the reactor protection system setpoints so as to maintain margin to overpower or DNB limits.

The means for maintaining power distributions within the required hot channel factor limits are described in the Technical Specifications and the Licensing Requirements Manual. A complete discussion of power distribution control in Westinghouse pressurized water reactors is included in Moore (1971). Detailed background information on the following design constraints on local power density in a Westinghouse pressurized water reactor, the defined operating procedures, and on the measures taken to preclude exceeding design limits is presented in the Westinghouse topical report on power distribution control and load following procedures (Morita et al 1974). The following paragraphs summarize these reports and describe the calculations used to establish the upper bound on peaking factors.

The calculations used to establish the upper bound on peaking factors F_Q and $F_{\Delta H}^N$, include all of the nuclear effects which influence the radial and/or axial power distributions throughout core life for various modes of operation, including load follow, reduced power operation, and axial xenon transients.

Radial power distributions are calculated for the full power conditions and fuel and moderator temperature feedback effects are included for the average enthalpy plane of the reactor. The steady state nuclear design calculations are done for normal flow with the same mass flow in each channel and flow redistribution effects neglected. The effect of flow redistribution is calculated explicitly where it is important in the DNB analysis of accidents. The effect of xenon on radial power distribution is small (compare Figures 4.3-6 and 4.3-7) but is included as part of the normal design process. Radial power distributions are relatively fixed and easily bounded with upper limits.

The core average profile, however, can experience significant changes which can rapidly occur as a result of rod motion and load changes, and more slowly due to xenon distribution, and core burnup. For the study of points of closest approach to axial power distribution limits, several thousand cases are examined. Because the properties of nuclear design dictate what axial shapes can occur, boundaries on the limits of interest can be set in terms of the parameters which are readily observed on the plant. Specifically, the nuclear design parameters which are significant to the axial power distribution analysis are:

1. Core power level,

2. Core height,

3. Reactor coolant temperature and flow,

4. Reactor coolant temperature program as a function of reactor power,

5. Fuel cycle lifetimes,

6. Rod bank worths, and

7. Rod bank overlaps.

Normal operation of the plant assumes compliance with the following conditions:

1. Control rods in a single bank move together with no individual rod insertion differing by more than 13 steps (indicated) from the bank demand position.

2. Control banks are sequenced with overlapping banks.

3. The control rod bank insertion limits are not violated.

4. Axial power distribution control procedures, which are given in terms of flux difference control and control bank position, are observed.

The axial power distribution procedures referred to above are part of the required operating procedures which are followed in normal operation. Limits placed on the axial flux difference are designed to assure that the heat flux hot channel factor F_Q is maintained within acceptable limits. The constant axial offset control (CAOC) operating procedures described in Morita, et al. (1974), require control of the axial flux difference at all power levels within a permissible operating band about a target value corresponding to the equilibrium full power value. The Relaxed Axial Offset Control (RAOC) procedures to be implemented in Unit 2 Cycle 13 and beyond, described in Miller, et al. (1994), were developed to provide wider control band widths and, consequently, more operating flexibility. These wider operating limits, particularly at lower power levels, can increase plant availability by allowing quicker plant startups and increased maneuvering flexibility.

Further operating flexibililty is achieved by combining RAOC operation with an F_Q Surveillance Technical Specification. $F_{XY}(Z)$ Surveillance requires periodic plant surveillance on the height-dependent radial peaking factor, $F_{XY}(Z)$, for partial verification that operation will not cause the $F_Q(Z)$ limit to be exceeded. In the F_Q Surveillance Technical Specification to be implemented in Unit 2 Cycle 13, $F_{XY}(Z)$ Surveillance will be replaced by $F_Q(Z)$ Surveillance. Monitoring $F_Q(Z)$ and increasing the measured value for expected plant maneuvers provides a more convenient form of assuring plant operating below the $F_Q(Z)$ limit while retaining the intent of using a measured parameter to verify Technical Specification compliance.

In standard CAOC analysis described in Morita, et. al. (1974), the generation of the normal operation power distribution is constrained by the rod insertion limits (RIL) and the ΔI band limits. The purpose of RAOC is to find the widest permissible ΔI-Power operating space by analyzing a wide range of ΔI. Therefore, the generation of normal operation power distributions is constrained only by the RIL for RAOC.

For a CAOC analysis, load-follow simulations are performed covering the allowed CAOC operating space to generate a typical range of allowed axial xenon distributions, which in turn are used to calculate axial power distributions in both normal operation and Condition II accident conditions. For an RAOC analysis, however, a reconstruction model described in Miller, et. al. (1994) is used as a more practical method to create axial xenon distributions covering the wider ΔI-Power operating space allowed with RAOC operation. Each resulting power shape is analyzed to determine if LOCA constraints are met or

exceeded.   The total peaking factor, F_Q^T is determined using standard
syntheis methods as described in Morita, et. al. (1974).

The calculated points are synthesized from axial calculations combined
with radial factors appropriate for rodded and unrodded planes.   In
these calculations, the effects on the unrodded radial peak of xenon
redistribution that occurs following the withdrawal of a control bank
(or banks) from a rodded region is obtained from two-dimensional X-Y
calculations. A 1.03 factor to be applied on the unrodded radial peak
was   obtained   from   calculations   in   which   xenon   distribution   was
preconditioned by the presence of control rods and then allowed to
redistribute for several hours.   A detailed discussion of this effect
may be found in Morita et al (1974).   The calculated values have been
increased by a factor of 1.05 for conservatism and a factor of 1.03
for the engineering factor F_Q^E.

The envelope drawn over the calculated points (max F_Q x power) in
Figure 4.3-20 represents an upper bound envelope on local power
density versus elevation in the core.   It should be emphasized that
this envelope is a conservative representation of the bounding values
of local power density.   Expected values are considerably smaller,
and, in fact, less conservative bounding values may be justified with
additional analysis or surveillance requirements.   For example, Figure
4.3-20 bounds both BOL and EOL conditions but without consideration of
radial power distribution flattening with burnup, i.e., both BOL and
EOL points presume the same radial peaking factor.   Inclusion of the
burnup flattening effect would reduce the local power densities
corresponding to EOL conditions which may be limiting at the higher
core elevations.

Accident analyses are presented in Chapter 15.   The results of these
analyses determined a limiting value of total peaking factor, F_Q, of
2.40 under normal operation, including load following maneuvers.   This
value is derived from the conditions necessary to satisfy the limiting
conditions specified in the LOCA analyses of Section 15.6.5.   As noted
previously in this section, an upper bound envelope of F_Q x power
equal to 2.40 x K(Z), as shown on Figure 4.3-20, results from
operation in accordance with constant axial offset control procedures
using ex-core surveillance only.

The surveillance of the core hot channel factors, in accordance with
the above, is presented in the Technical Specifications.

Allowing for fuel densification effects, the average linear power at
2,900 MWt is 5.69 kW/ft.   From Figure 4.3-20, the conservative upper
bound value of normalized local power density, including uncertainty
allowances, is 2.40.

To determine reactor protection system setpoints, with respect to
power distributions, three categories of events are considered, namely
rod control equipment malfunctions, operator errors of commission, and
operator errors of omission.   In evaluating these three categories of
events, the core is assumed to be operating within the four
constraints described above.

The first category comprises uncontrolled rod withdrawal (with rods moving in the normal bank sequence). Also included are motions of the rod banks below their insertion limits, which could be caused, for example, by uncontrolled dilution or reactor coolant cooldown. Power distributions were calculated throughout these occurrences, assuming short term corrective action; that is, no transient xenon effects were considered to result from the malfunction. The event was assumed to occur from typical normal operating situations, which include normal xenon transients. It was further assumed in determining the power distributions that the total core power level would be limited by reactor trip below 118 percent. Because the study is to determine protection limits with respect to power and axial offset, no credit was taken for trip setpoint reduction due to flux difference. Results are given in Figure 4.3-21 in units of kW/ft. The peak power density which can occur in such events, assuming reactor trip at or below 118 percent, is less than that required for center line melt, including uncertainties and densification effects.

The second category, also appearing on Figure 4.3-21, assumes that the operator mispositions the control rod bank in violation of the insertion limits and creates short-term conditions not included in normal operating conditions.

The third category assumes that the operator fails to take action to correct a flux difference violation. Figure 4.3-22 illustrates the behavior of the peak power under these conditions. The points represent the calculated F_Q multiplied by 100% power plus the calorimetric error. The calorimetric error is 0.6% using a Leading Edge Flow Meter (LEFM) for calorimetric power. If the LEFM is unavailable, then the calorimetric error is 2%, with decreased RTP (Refer to Licensing Requirements Manual). The behavior of the peak power is essentially as illustrated, with the actual peak power values remaining below 20 kw/ft. The figure shows that provided the assumed error in operation does not continue for a period which is long compared to the xenon time constant, the peak linear power does not exceed that required for fuel centerline melt.

Analyses of possible operating power shapes show that the appropriate hot channel factors F_Q and $F_{\Delta H}^N$ for peak local power density and for DNB analysis at full power are the values given in Table 4.3-2 and are described in the Beaver Valley Unit 2 Core Operating Limits Report (COLR), part of the plant Licensing Requirements Manual documentation.

F_Q can be increased with decreasing power as shown in the Technical Specifications. Increasing $F_{\Delta H}^N$ with decreasing power is permitted by the DNB protection setpoints and allows radial power shape changes with rod insertion to the insertion limits as described in Section 4.4.4.3. The allowance for increased $F_{\Delta H}^N$ permitted is $F_{\Delta H}^N$ = 1.62 (1 + 0.3(1-P)). This becomes a design basis criterion which is used for establishing acceptable control rod patterns and control bank sequencing. Likewise, fuel loading patterns for each cycle are

selected with consideration of this design criterion. The worst values of $F_{\Delta H}^N$ for possible rod configurations occurring in normal operation are used in verifying that this criterion is met. Typical radial factors and radial power distributions are shown in Figure 4.3-6 through 4.3-10. The worst values generally occur when the rods are assumed to be at their insertion limits. Maintenance of constant axial offset control establishes rod positions which are above the allowed rod insertion limits, thus providing increasing margin to the $F_{\Delta H}^N$ criterion. As discussed in Section 3.2 of McFarlane (1975), it has been determined that the Technical Specification limits are met, provided the above conditions are observed. These limits are taken as input to the thermal-hydraulic design basis, as described in Section 4.4.4.3.1.

When a situation is possible in normal operation which could result in local power densities in excess of those assumed as the precondition for a subsequent hypothetical accident, but which would not itself cause fuel failure, administrative controls and alarms are provided for returning the core to a safe condition. These alarms are described in detail in Chapters 7 and 16.

4.3.2.2.7 Experimental Verification of Power Distribution Analysis

This subject is discussed in depth in Langford and Nath (1971). A summary of this report is given below. It should be noted that power distribution related measurements are incorporated into the evaluation of calculated power distribution information, using the INCORE Code described in Meyer and Stover (1975). A detailed description of this code's input and output is included in this reference. The measured versus calculational comparison is normally performed periodically throughout the cycle lifetime of the reactor, as required by Technical Specifications.

In a measurement of the heat flux hot channel factor, F_Q, with the movable detector system described in Sections 7.7.1 and 4.4.6, the following uncertainties have to be considered:

1. Reproducibility of the measured signal,

2. Errors in the calculated relationship between detector current and local flux, and

3. Errors in the calculated relationship between detector flux and peak rod power some distance from the measurement thimble.

The appropriate allowance for Category 1 above has been quantified by repetitive measurements made with several intercalibrated detectors by using the common thimble features of the incore detector system. This system allows more than one detector to access any thimble. Errors in Category 2 above are quantified to the extent possible, by using the fluxes measured at one thimble location to predict fluxes

at another location, which is also measured. Local power distribution predictions are verified in critical experiments on arrays of rods with simulated guide thimbles, control rods, burnable absorbers, etc. These critical experiments provide quantification of errors of Categories 1 and 3 above.

Langford and Nath (1971) describe critical experiments performed at the Westinghouse Reactor Evaluation Center and measurements taken on two Westinghouse plants with incore systems of the same type as used in BVPS-2. The report concludes that the uncertainty associated with F (heat flux) is 4.58 percent at the 95-percent confidence level with only 5 percent of the measurements greater than the inferred value. This is the equivalent of a 1.645 limit on a normal distribution and is the uncertainty to be associated with a full core flux map with movable detectors reduced with a reasonable set of input data incorporating the influence of burnup on the radial power distribution. The uncertainty is usually rounded up to 5 percent.

In comparing measured power distributions (or detector currents) with calculations for the same operating conditions, it is not possible to subtract out the detector reproducibility. Thus, a comparison between measured and predicted power distributions has to include some measurement error. Such a comparison is given in Figure 4.3-23 for one of the maps used in Langford and Nath (1971). Since the first publication of the report, hundreds of maps have been taken on these and other reactors. The results confirm the adequacy of the 5-percent uncertainty allowance on the calculated F_Q. An additional increase to the uncertainty of F_Q for reduced flux thimble availability is discussed in Sections 3.3.7 and 5.1.6 of the Licensing Requirements Manual.

A similar analysis for the uncertainty in $F_{\Delta H}^N$ (rod integral power) measurements results in an allowance of 3.65 percent at the equivalent of a 1.645 σ confidence level. For historical reasons, an 8 percent uncertainty factor is allowed in the nuclear design calculational basis; that is, the predicted rod integrals at full power must not exceed the design $F_{\Delta H}^N$ less 8 percent. This 8 percent may be reduced in final design to 4 percent to allow wider range of acceptable axial power distributions in the DNB analysis and still meet the design bases of Section 4.3.1.3. An additional increase to the uncertainty of $F_{\Delta H}^N$ for reduced flux thimble availability is discussed in Sections 3.3.7 and 5.1.7 of the Licensing Requirements Manual.

A recent measurement in the second cycle of a 121 fuel assembly, 12 foot core is compared with a simplified one-dimensional core average calculation in Figure 4.3-24. This calculation does not give explicit representation to the fuel grids.

The accumulated data on power distributions in actual operation is basically of three types:

   1. Much of the data is obtained in steady-state operation at constant power in the normal operating configuration.

2. Data with unusual values of axial offset are obtained as part of the excore detector calibration exercise which is performed monthly.

3. Special tests have been performed in load follow and other transient xenon conditions which have yielded useful information on power distributions.

These data are presented in detail in Meyer and Stover (1975) and Westinghouse (1976). Figure 4.3-25 contains a summary of measured values of F_Q as a function of axial offset for several plants from these reports.

4.3.2.2.8 Testing

An extensive series of physics tests are performed on the first core. These tests and the criteria for satisfactory results are described in Chapter 14. Because not all limiting situations can be created at BOL, the main purpose of the tests is to provide a check on the calculational methods used in the predictions for the conditions of the test.

4.3.2.2.9 Monitoring Instrumentation

The adequacy of instrument numbers, spatial deployment, required correlations between readings and peaking factors, calibration, and errors are described in Langforth and Nath (1971); Moore (1971); and McFarlane (1975). The relevant conclusions are summarized in Sections 4.3.2.2.7 and 4.4.6.

Provided the limitations given in Section 4.3.2.2.6 on rod insertion and flux difference are observed, the excore detector system provides adequate on-line monitoring of power distributions. Further details of specific limits on the observed rod positions and flux difference are given in the Technical Specifications and the Licensing Requirements Manual, together with a discussion of their bases.

Limits for alarms, reactor trip, etc., are given in the Technical Specifications and the Licensing Requirements Manual. Descriptions of the systems provided are given in Section 7.7.

4.3.2.3 Reactivity Coefficients

The kinetic characteristics of the reactor core determine the response of the core to changing plant conditions or to operator adjustments made during normal operation, as well as the core response during abnormal or accidental transients. These kinetic characteristics are quantified in reactivity coefficients. The reactivity coefficients reflect the changes in the neutron multiplication due to varying plant conditions such as power, moderator or fuel temperatures, or less significantly, due to a change in pressure or void conditions. Because reactivity coefficients change during the life of the core, ranges of coefficients are employed in transient analysis to determine the response of the plant throughout life. The results of such simulations and the reactivity coefficients used are presented in

Chapter 15. The reactivity coefficients are calculated on a corewise
basis by radial and axial diffusion theory methods and with nodal
analysis methods. The effect of radial and axial power distribution
on core average reactivity coefficients is implicit in those
calculations and is not significant under normal operating conditions.
For example, a skewed xenon distribution which results in changing
axial offset by 5 percent, changes the moderator and Doppler
temperature coefficients by less than 0.01 pcm/°F and 0.03 pcm/°F,
respectively. An artificially skewed xenon distribution which results
in changing the radial $F_{\Delta H}^{N}$ by 3 percent, changes the moderator and Doppler
temperature coefficients by less than 0.03 pcm/°F and 0.001 pcm/°F,
respectively. The spatial effects are accentuated in some transient
conditions; for example, in the postulated rupture of the main steam line and
rupture of a rod cluster control assembly mechanism housing described in
Sections 15.1.5 and 15.4.8, and are included in these analyses.

The analytical methods and calculational models used in calculating
the reactivity coefficients are given in Section 4.3.3. These models
have been confirmed through extensive testing of more than 30 cores
similar to the plant described herein; results of these tests are
discussed in Section 4.3.3.

Quantitative information for calculated reactivity coefficients,
including fuel-Doppler coefficient, moderator coefficients (density,
temperature, pressure, and void), and power coefficient is given in
the following sections.

4.3.2.3.1 Fuel Temperature (Doppler) Coefficient

The fuel temperature (Doppler) coefficient is defined as the change in
reactivity per degree change in effective fuel temperature and is
primarily a measure of the Doppler broadening of U-238 and PU-240
resonance absorption peaks. Doppler broadening of other isotopes,
such as U-236 and Np-237, is also considered but their contribution to
the Doppler effect is small. An increase in fuel temperature
increases the effective resonance absorption cross-section of the fuel
and produces a corresponding reduction in reactivity.

The fuel temperature coefficient is calculated by performing two-group
X-Y calculations using the Advanced Nodal Code (ANC) (Liu, et.al.,
1986). Moderator temperature is held constant, and the power level is
varied. Spatial variation of fuel temperature is taken into account
by calculating the effective fuel temperature as a function of power
density, as discussed in Section 4.3.3.1.

A typical Doppler temperature coefficient is shown in Figure 4.3-26 as
a function of the effective fuel temperature (at BOL and EOL
conditions). The effective fuel temperature is lower than the volume
averaged fuel temperature, since the neutron flux distribution is non-
uniform through the pellet and gives preferential weight to the
surface temperature. A typical Doppler-only contribution to the

power coefficient, defined later, is shown in Figure 4.3-27 as a
function of relative core power. The integral of the differential
curve on Figure 4.3-27 is the Doppler contribution to the power defect
and is shown in Figure 4.3-28 as a function of relative power. The
Doppler coefficient becomes more negative as a function of life as the
Pu-240 content increases, thus increasing the Pu-240 resonance
absorption, but the overall value becomes less negative since the fuel
temperature changes with burnup, as described in Section 4.3.3.1. The
upper and lower limits of Doppler coefficient used in accident
analyses are given in Chapter 15.

4.3.2.3.2 Moderator Coefficients

The moderator coefficient is a measure of the change in reactivity due
to a change in specific reactor coolant parameters, such as density,
temperature, pressure, or void. The coefficients so obtained are
moderator density, temperature, pressure, and void coefficients.

Moderator (Density) Temperature Coefficients

The moderator temperature (density) coefficient is defined as the
change in reactivity per degree change in the moderator temperature.
Generally, the effects of the changes in moderator density, as well as
the temperature, are considered together. A decrease in moderator
density means less moderation which results in a negative moderator
coefficient. An increase in reactor coolant temperature, keeping the
density constant, leads to a hardened neutron spectrum and results in
an increase in resonance absorption in U-238, Pu-240 and other
isotopes. The hardened spectrum also causes a decrease in the fission
to capture ratio in U-235 and Pu-239. Both of these effects make the
moderator coefficient more negative. Because water density changes
more rapidly with temperature as temperature increases, the moderator
temperature (density) coefficient becomes more negative with
increasing temperature.

The soluble boron used in the reactor as a means of reactivity control
also has an effect on moderator density coefficient, since the soluble
boron poison density, as well as the water density, is decreased when
the coolant temperature rises. A decrease in the soluble poison
concentration introduces a positive component in the moderator
coefficient. If the concentration of soluble poison is large enough,
the net value of the coefficient may be positive. With discrete
and/or integral burnable absorber rods present, however, the beginning
of life hot boron concentration is sufficiently low that the moderator
temperature coefficient is non-positive at 100 percent power, less
than +2.0 pcm/°F below 70 percent power, and less than a linearly
decreasing limit of +2.0 pcm/°F to 0.0 pcm/°F between 70 percent power
to 100 percent power, respectively. The effects of control rods is to
make the moderator coefficient more negative by increasing the
"leakage" of the core.

With burnup, the moderator coefficient becomes more negative, primarily as a result of boric acid dilution, but also to a significant extent from the effects of the buildup of plutonium and and fission products.

The moderator coefficient is calculated for the various plant conditions by performing two-group dimensional calculations, varying the moderator temperature (and density) by about ±5°F about each of the mean temperatures. The moderator coefficient is shown as a function of core temperature and boron concentration for a typical unrodded and rodded core in Figures 4.3-29, 4.3-30, 4.3-31. The temperature range covered is from cold (50°F) to about 600°F. The contribution due to Doppler coefficient (because of change in moderator temperature) has been subtracted from these results. Figure 4.3-32 shows the hot, full power moderator temperature coefficient for a typical core plotted as a function of first cycle lifetime for the just critical boron concentration condition based on the design boron concentration reduction as a function of burnup (Figure 4.3-3.).

The moderator coefficients presented here are calculated on a corewide basis, since they are used to describe the core behavior in normal and accident situations when the moderator temperature changes can be considered to affect the entire core.

Moderator Pressure Coefficient

The moderator pressure coefficient relates the changes in moderator density, resulting from a reactor coolant pressure change, to the corresponding effect on neutron production. This coefficient is of much less significance in comparison with the moderator temperature coefficient.

A change of 50 psi in pressure has approximately the same effect on reactivity as a 1/2 degree change in moderator temperature. This coefficient can be determined from the moderator temperature coefficient by relating change in pressure to the corresponding change in density. The moderator pressure coefficient may be negative over a portion of the moderator temperature range at BOL (- 0.004 pcm/psi, BOL) but is always positive at operating conditions and becomes more positive during life (+0.3 pcm/psi, EOL).

Moderator Void Coefficient

The moderator void coefficient relates the change in neutron multiplication to the presence of voids in the moderator. In a pressurized water reactor, this coefficient is not very significant because of the low void content in the coolant. The core void content is less than 1/2 of 1 percent and is due to local or statistical boiling. The void coefficient varies from 50 pcm/percent void at BOL and at low temperatures to -250 pcm/percent void at EOL and at operating temperatures. The negative void coefficient at operating temperature becomes more negative with fuel burnup.

4.3.2.3.3 Power Coefficient

The combined effect of moderator temperature and fuel temperature
change as the core power level changes is called the total power
coefficient and is expressed in terms of reactivity change per percent
power change. A typical power coefficient at BOL and EOL conditions
is given in Figure 4.3-33.

It becomes more negative with burnup, reflecting the combined effect
of moderator and fuel temperature coefficients with burnup. The power
defect (integral reactivity effect) at BOL and EOL is given in Figure
4.3-34.

4.3.2.3.4   Comparison of Calculated and Experimental Reactivity
Coefficients

Section 4.3.3 describes the comparison of calculated and experimental
reactivity coefficients in detail. Based on the data presented there,
the accuracy of the current analytical model is:

    1. $\pm$0.2 percent $\Delta\rho$ for Doppler and power defect

    2. $\pm$2 pcm/°F for the moderator coefficient

Experimental evaluation of the calculated reactivity coefficients will
be performed during the physics startup tests described in Chapter 14.

4.3.2.3.5 Reactivity Coefficients Used in Transient Analysis

Table 4.3-2 gives the limiting values, as well as the best estimate
values, for the reactivity coefficients. The limiting values are used
as design limits in the transient analysis. The exact values of the
coefficient used in the analysis depend on whether the transient of
interest is examined at the BOL or EOL, whether the most negative or
the most positive (least negative) coefficients are appropriate, and
whether spatial non-uniformity must be considered in the analysis.
Conservative values of coefficients, considering various aspects of
analysis, are used in the transient analysis. This is described in
Chapter 15.

The reactivity coefficients shown in Figures 4.3-26, 4.3-27, 4.3-28,
4.3-29, 4.3-30, 4.3-31, 4.3-32, 4.3-33 and 4.3-34 are typical best
estimate values calculated for a first cycle. The limiting values
shown in Table 4.3-2 are chosen to encompass the best estimate
reactivity coefficients, including the uncertainties given in Section
4.3.3.3 over appropriate operating conditions calculated for this
cycle and the expected values for the subsequent cycles. The most
positive, as well as the most negative, values are selected to form
the design basis range used in the transient analysis. In many
instances, the most conservative combination of reactivity
coefficients is used in the

transient analysis even though the extreme coefficients assumed may
not simultaneously occur at the conditions of lifetime, power level,
temperature and boron concentration assumed in the analysis. The need
for a reevaluation of any accident in a subsequent cycle is contingent
upon whether or not the coefficients for that cycle fall within the
identified range used in the analysis presented in Chapter 15 with due
allowance for the calculational uncertainties given in Section
4.3.3.3. Control rod requirements are given in Table 4.3-3 for both a
first cycle and a typical reload.

4.3.2.4 Control Requirements

To ensure the shutdown margin stated in the Technical Specifications
under conditions where a cooldown to ambient temperature is required,
concentrated soluble boron is added to the reactor coolant. Boron
concentrations for several core conditions are listed in Table 4.3-2.
For all core conditions including refueling, the boron concentration
is well below the solubility limit. The rod cluster control
assemblies are employed to bring the reactor to the hot standby
condition. The minimum required shutdown margin is given in the
Technical Specifications.

The ability to accomplish the shutdown for hot conditions is
demonstrated in Table 4.3-3 by comparing the difference between the
rod cluster control assembly reactivity available with an allowance
for the worst struck rod with that required for control and protection
purposes. The shutdown margin includes an allowance of 10 percent for
analytical uncertainties (see Section 4.3.2.4.9). The largest
reactivity control requirement appears at the EOL when the moderator
temperature coefficient reaches its peak negative value as reflected
in the larger power defect.

The control rods are required to provide sufficient reactivity to
account for the power defect from full power to zero power and to
provide the required shutdown margin. The reactivity addition
resulting from power reduction consists of contributions from Doppler,
variable average moderator temperature, flux redistribution, and
reduction in void content, as discussed below.

4.3.2.4.1 Doppler

The Doppler effect arises from the broadening of U-238 and Pu-240
resonance cross-section peaks with an increase in effective pellet
temperature. This effect is most noticeable over the range of zero
power to full power due to the large pellet temperature increase with
power generation.

4.3.2.4.2 Variable Average Moderator Temperature

When the core is shut down to the hot, zero power condition, the average moderator temperature changes from the equilibrium full-load value determined by the steam generator and turbine characteristics (steam pressure, heat transfer, tube fouling, etc.) to the equilibrium no-load value, which is based on the steam generator shell side design pressure. The design change in temperature is conservatively increased by 4°F to account for the control dead band and measurement errors.

When the moderator coefficient is negative (except for early in core life, when higher boron concentrations may result in a moderator temperature coefficient value as high as +2.0 pcm/°F below 70 percent power, and a value decreasing linearly to 0.0 pcm/°F at 100 percent power), there is a reactivity addition with power reduction. The moderator coefficient becomes more negative as the fuel depletes because the boron concentration is reduced. This effect is the major contributor to the increased requirement at EOL.

4.3.2.4.3 Redistribution

During full power operation, the reactor coolant density decreases with core height, and this, together with partial insertion of the control rods, results in less fuel depletion near the top of the core. Under steady-state conditions, the relative power distribution will be slightly asymmetric toward the bottom of the core. On the other hand, with a constant moderator temperature at equilibrium, no load value, the reactor coolant density is uniform up the core, and there is no flattening due to Doppler. The result will be a flux distribution which, at zero power, can be skewed toward the top of the core. The reactivity insertion due to the skewed distribution is calculated with an allowance for effects of xenon distribution.

4.3.2.4.4 Void Content

A small void content in the core is due to nucleate boiling at full power. The void collapse, coincident with power reduction, makes a small reactivity contribution.

4.3.2.4.5 Rod Insertion Allowance

At full power, the control bank is operated within a prescribed band of travel to compensate for small periodic changes in boron concentration, changes in temperature, and very small changes in the xenon concentration not compensated for by a change in boron concentration. When the control bank reaches either limit of this band, a change in boron concentration is required to compensate for additional reactivity changes. Because the insertion limit is set by a rod travel limit, a conservatively high calculation of the inserted worth is made which exceeds the normally inserted reactivity. The withdrawal limit is an all rods out condition.

4.3.2.4.6   Installed Excess Reactivity for Depletion

Excess reactivity of approximately 10 percent Δρ (hot) is installed at
the beginning of each cycle to provide sufficient reactivity to
compensate for fuel depletion and fission product buildup throughout
the cycle. This reactivity is controlled by the addition of soluble
boron to the reactor coolant and by burnable absorbers. The soluble
boron concentration for several core configurations, the unit boron
worth, and burnable absorber worth are given in Tables 4.3-1 and 4.3-
2. Because the excess reactivity for burnup is controlled by soluble
boron and/or burnable absorber, it is not included in control rod
requirements.

4.3.2.4.7 Xenon and Samarium Poisoning

Changes in xenon and samarium concentrations in the core occur at a
sufficiently slow rate, even following rapid power level changes, that
the resulting reactivity change is normally controlled by changing the
soluble boron concentration.

4.3.2.4.8 pH Effects

Changes in reactivity due to a change in coolant pH, if any, are
sufficiently small in magnitude and occur slowly enough to be
controlled by the boron system. Further details are provided in
Cermak et al (1968).

4.3.2.4.9 Experimental Confirmation

Following a normal shutdown, the total core reactivity change during
cooldown with a stuck rod has been measured on a 121 fuel assembly
10-foot-high core, and 121 fuel assembly, 12-foot-high core. In each
case, the core was allowed to cool down until it reached criticality
simulating the steam line break accident. For the 10-foot core, the
total reactivity change associated with the cooldown is overpredicted
by about 0.3 percent Δρ with respect to the measured result. This
represents an error of about 5 percent in the total reactivity change
and is about half the uncertainty allowance for this quantity. For
the 12-foot core, the difference between the measured and predicted
reactivity change was an even smaller 0.2 percent Δρ. These
measurements and others demonstrate the ability of the methods
described in Section 4.3.3.

4.3.2.4.10 Control

Core reactivity is controlled by means of a chemical poison dissolved
in the reactor coolant, rod cluster control assemblies, and burnable
absorber rods, as described below.

4.3.2.4.11 Chemical Poison

Boron in solution as boric acid is used to control relatively slow
reactivity changes associated with:

1. The moderator temperature defect in going from cold shutdown
    at ambient temperature to a constant moderator temperature at
    equilibrium no load value.

2. The transient xenon and samarium poisoning, such as that
    following power changes or changes in rod cluster control
    position.

3. The excess reactivity required to compensate for the effects
    of fissile inventory depletion and buildup of long-life
    fission products.

4. The absorber poison depletion.

The boron concentrations for various core conditions are presented in
Table 4.3-2.

4.3.2.4.12 Rod Cluster Control Assemblies

The number of rod cluster control assemblies is shown in Table 4.3-1.
The rod cluster control assemblies are used for shutdown and control
purposes to offset fast reactivity changes associated with:

1. The required shutdown margin in the hot zero power, stuck
    rods condition.

2. The reactivity compensation as a result of an increase in
    power above hot zero power (power defect, including Doppler,
    and moderator reactivity changes).

3. Unprogrammed fluctuations in boron concentration, reactor
    coolant temperature, or xenon concentration (with rods not
    exceeding the allowable rod insertion limits).

4. Reactivity ramp rates resulting from load changes.

The allowed control bank reactivity insertion is limited at full power
to maintain shutdown capability. As the power level is reduced,
control rod reactivity requirements are also reduced, and more rod
insertion is allowed. The control bank position is monitored, and the
operator is notified by an alarm if the limit is approached. The
determination of the insertion limit uses conservative xenon
distributions and axial power shapes. In addition, the rod cluster
control assembly withdrawal pattern determined from these analyses is
used in determining power distribution factors and in determining the
maximum worth of an inserted rod cluster control assembly ejection
accident. For further

discussion, refer to the Technical Specifications on rod insertion limits.

Power distribution, rod ejection, and rod misalignment analyses are based on the arrangement of the shutdown and control groups of the rod Cluster control assemblies shown in Figure 4.3-35. All shutdown rod cluster control assemblies are withdrawn before withdrawal of the control banks is initiated. In going from zero to 100-percent power, control banks A, B, C, and D are sequentially withdrawn. The limits of rod positions and further discussion on the basis for rod insertion limits are provided in the Technical Specifications.

4.3.2.4.13 Burnable Absorbers

Burnable absorbers provide partial control of the excess reactivity available at the beginning of the cycle. In doing so, these absorbers ensure the moderator temperature coefficient is non-positive at 100 percent power, less than +2.0 pcm/°F below 70 percent power, and less than a linearly decreasing limit of +2.0 pcm/°F to 0.0 pcm/°F between 70 percent power to 100 percent power, respectively. They perform this function by reducing the requirement for soluble poison in the moderator at the beginning of the cycle, as previously described. For purposes of illustration, a typical burnable absorber pattern in the core is shown in Figure 4.3-5, while the arrangement within an assembly is displayed in Figure 4.3-4. The reactivity worth of this burnable absorber is shown in Table 4.3-1. The boron in the absorber is depleted with burnup, but at a sufficiently slow rate so that the resulting critical concentration of soluble boron is such that the moderator temperature coefficient remains within the above limits at all times for power operating conditions.

4.3.2.4.14 Peak Xenon Startup

Compensation for the peak xenon buildup is accomplished using a chemical shim control system. Startup from the peak xenon condition is accomplished with a combination of rod motion and boron dilution. The boron dilution may be made at any time, including during the shutdown period, provided the shutdown margin is maintained.

4.3.2.4.15 Load Follow Control and Xenon Control

During load follow maneuvers, power changes are accomplished using control rod motion and dilution or boration by the chemical shim control system as required. Control rod motion is limited by the control rod insertion limits on the control rods, as provided in the Technical Specifications and discussed in Section 4.3.2.4.12. The power distribution is maintained within acceptable limits through location of the control rod bank. Reactivity changes due to the changing xenon concentration can be controlled by rod motion and/or changes in the soluble boron concentration.

Rapid power increases (5 percent/min) are accomplished with a combination of rod motion and boron dilution. Compensation for the rapid power increase is initially accomplished by a combination of rod withdrawal and moderator temperature reduction. As the slower boron dilution takes effect after the initial rapid power increase, the moderator temperature returns to the programmed value.

4.3.2.4.16 Burnup

Control of the excess reactivity for burnup is accomplished, using soluble boron and/or burnable absorbers. The boron concentration must be limited during operating conditions to ensure that the moderator temperature coefficient is non-positive at 100 percent power, less than +2.0 pcm/°F below 70 percent power, and less than a linearly decreasing limit of +2.0 pcm/°F to 0.0 pcm/°F between 70 percent power to 100 percent power, respectively. Sufficient burnable poison is installed at the beginning of a cycle to give the desired cycle lifetime and limit the boron concentration to assure that moderator temperature coefficient limits are achieved. The practical minimum boron concentration is 10 ppm.

4.3.2.5 Control Rod Patterns and Reactivity Worth

The rod cluster control assemblies are designated by function as the control groups and the shutdown groups. The terms "group" and "bank" are used synonymously throughout this report to describe a particular grouping of control assemblies. The rod cluster assembly pattern is displayed in Figure 4.3-35, which is not expected to change during the life of the plant. The control banks are labeled A, B, C, and D and the shutdown banks are labeled SA and SB. Each bank, although operated and controlled as a unit, is comprised of two subgroups. The axial position of the rod cluster control assemblies may be manually or automatically controlled. The rod cluster control assemblies are all dropped into the core following actuation of reactor trip signals.

Two criteria have been employed for selection of the control groups. First, the total reactivity worth must be adequate to meet the requirements specified in Table 4.3-3. Second, in view of the fact that these rods may be partially inserted at power operation, the total power peaking factor should be low enough to ensure that the power capability requirements are met. Analyses indicate that the first requirement can be met either by a single group or by two or more banks whose total worth equals at least the required amount. The axial power shape would be more peaked, following movement of a single group of rods worth 3 to 4-percent Δρ. Therefore, four banks (described as A, B, C, and D in Figure 4.3-35), each worth approximately 1 percent Δρ, have been selected.

The position of control banks for criticality under any reactor condition is determined by the concentration of boron in the reactor coolant. On an approach to criticality, boron is adjusted to ensure that criticality will be achieved with control rods above the insertion limit set by shutdown and other considerations (see the Technical Specifications). Early in the cycle, there may also be a rod withdrawal limit at low power to maintain the moderator temperature coefficient to a value that is less than 0.0 pcm/°F at 100 percent power, less than +2.0 pcm/°F below 70 percent power, and less than a linearly decreasing limit of +2.0 pcm/°F to 0.0 pcm/°F between 70 percent power to 100 percent power, respectively.

Ejected rod worths are given in Section 15.4.8 for several different conditions.

Allowable deviations due to misaligned control rods are discussed in the Technical Specifications.

A representative calculation for two banks of control rods simultaneously withdrawn(rod withdrawal accident) is given in Figure 4.3-36.

Calculation of control rod reactivity worth versus time following reactor trip involves control rod velocity and differential reactivity worth. The rod position versus time of travel after rod release normalized to "Distance to Top of Dashpot" and "Drop Time to Top of Dashpot" is given on Figure 4.3-37. For nuclear design purposes, the reactivity worth versus rod position is calculated by a series of steady-state calculations at various control rod positions, assuming all rods out of the core as the initial position in order to minimize the initial reactivity insertion rate. Also, to be conservative, the rod of highest worth is assumed stuck out of the core, and the flux distribution (and thus reactivity importance) is assumed to be skewed to the bottom of the core. The result of these calculations is shown on Figure 4.3-38.

The shutdown groups provide additional negative reactivity to assure an adequate shutdown margin. Shutdown margin is defined as the amount by which the core would be subcritical at hot shutdown if all rod cluster control assemblies are tripped, but assuming that the highest worth assembly remains fully withdrawn and no changes in xenon or boron take place. The loss of control rod worth due to the material irradiation is negligible, since only bank D may be in the core under normal operating conditions (near full power). The values given in Table 4.3-3 show that the available reactivity in withdrawn rod cluster control assemblies provides the design bases minimum shutdown margin, allowing for the highest worth cluster to be at its fully withdrawn position. An allowance for the uncertainty in the calculated worth of N-1 rods is made before determination of the shutdown margin.

4.3.2.6 Criticality of the Reactor During Refueling and Criticality of Fuel Assemblies

Criticality of fuel assemblies outside the reactor is precluded by adequate design of fuel transfer, shipping and storage facilities, and by administrative control procedures. The principal methods of preventing criticality are by limiting the fuel assembly array size and configuration, limiting assembly interaction by fixing the minimum separation between assemblies and by utilizing boron as a neutron poison where appropriate.

For storage of fuel in the spent fuel racks, the design basis for preventing criticality outside the reactor is that there is a 95 percent probability at a 95 percent confidence level, without soluble boron, that the effective multiplication factor (K_{eff}) of the fuel assembly array will be less than 1.0 including uncertainties and tolerances as documented in Holtec Report HI-2084175, ''Licensing Report for Beaver Valley Unit 2 Rerack,'' Revision 8, dated February 2011 for Metamic racks.

Conditions assumed in meeting this design basis for Metamic racks are:

1. Limiting fuel characteristics from the spectrum of fuel used at BVPS-2 were used to develop the design basis fuel assembly model. The model bounds Westinghouse fuel products with a 0.3740-inch fuel pin, such as the Westinghouse Standard design, the V5H product, as well as the Robust Fuel Assembly (RFA) and RFA-2 products.

2. The fuel assemblies were conservatively modeled with a UO2 density of 10.6312 g/cm^3 (97% of theoretical density).

3. The fuel assemblies were conservatively modeled as containing solid right cylindrical pellets and uniformly enriched over the entire length of the fuel stack height.

4. The reactivity effects of operating fuel with IFBA configurations up to 200 rods per fuel assembly were analyzed down to an enrichment of 3.8 weight percent U235. IFBA configurations up to 128 rods per fuel assembly were analyzed down to an enrichment of 3.0 weight percent U235.

5. The design basis limit for K_{eff} at the zero soluble boron condition was conservatively reduced from 1.0 to 0.995 for Region 2 and 0.992 for Region 3 in the analysis.

6. Fuel assembly storage is analyzed for the highest permitted enrichment in defined configurations. Credit is taken for fuel assembly burnup. No credit is taken for control rods or burnable absorbers.

7. The moderator is unborated water at a temperature of 39.2°F. A conservative value of 1.0 gm/cm^3 is used for the density of water.

8. The array is either infinite in lateral extent or is surrounded by a conservatively chosen reflector, whichever is appropriate for the design.

9. Manufacturing tolerances are addressed using a combination of bounding values and sensitivity studies.

10. Regionalized loading, fuel assembly burnup, fixed neutron absorber (Metamic) and soluble boron credit ensure that K_{eff} is maintained less than or equal to 0.95, including uncertainties, tolerances, and accident conditions.

The principal method for the criticality analysis of the spent fuel storage racks is the use of the three-dimensional Monte Carlo code MCNP4a. MCNP4a calculations use continuous energy cross-section data predominantly based on ENDF/B-V and ENDF/B-VI. Exceptions are included in the Holtec Report HI-2084175, ``Licensing Report for Beaver Valley Unit 2 Rerack,'' Revision 8.

Benchmark calculations were performed to determine the bias and bias uncertainty for MCNP4a, evaluated with a 95% probability at the 95% confidence level. The calculations for the analysis utilize the same computer platform and cross-section libraries used for the benchmark calculations.

Fuel depletion analyses during core operation were performed with CASMO-4 (using the 70-group cross-section library). CASMO-4 is used to determine the isotopic composition of the spent fuel. In addition, the CASMO-4 calculations are restarted in the storage rack geometry, yielding the two-dimensional infinite multiplication factor (k_{inf}) for the storage rack to determine the reactivity effect of fuel and rack tolerances, temperature variation, and to perform various studies. For all calculations in the spent fuel pool racks, the Xe-135 concentration in the fuel is conservatively set to zero.

Benchmark calculations were also performed for CASMO-4 to determine the bias and bias uncertainty, evaluated with a 95% probability at the 95% confidence level. Since CASMO-4 was used to determine reactivity differences, the bias was not applied to the results of the calculations. However, the bias uncertainty was included with the other uncertainties when determining the maximum K_{eff} values.

The maximum K_{eff} is determined from the MCNP4a calculated K_{eff}, the calculation bias, the temperature bias, and the applicable uncertainties and tolerances (bias uncertainty, calculation uncertainty, rack tolerances, fuel tolerances, depletion uncertainty, LFP uncertainty, Metamic coupon measurement uncertainty) using the following formula:

$$\text{Max } K_{eff} = \text{Calculated } k_{calc} + \text{biases} + [\textstyle\sum_i (\text{Uncertainty})^2]^{1/2}$$

In the geometric models used for the calculations, each fuel rod and its cladding were described explicitly, and reflecting or periodic boundary conditions were used in the radial direction which has the effect of creating an infinite radial array of storage cells.

When two separate, independent MCNP calculations are compared to determine a delta k_{calc}, the uncertainty associated with each individual calculation is statistically combined and added to the k_{calc} calculation according to the following equation:

$$\text{Delta } k_{calc} = (k_{calc2} - k_{calc1}) + 2 * \sqrt{(\sigma 2^2 + \sigma 1^2)}$$

For new fuel storage, the design basis for preventing criticality outside the reactor is that, including uncertainties, there is a 95 percent probability at a 95 percent confidence level that the effective neutron multiplication factor, K_{eff}, of the fuel assembly array will be less than 0.95 as recommended by ANSI 57.2-1983, ANSI 57.3-1983, and NRC guidance (Regulatory Guide 1.13). Criticality of fuel assemblies in a fuel storage rack is prevented by the design of the rack, which limits fuel assembly interaction. This is done by fixing the minimum separation between fuel assemblies.

Spatial calculations are performed using KENO-Va to quantify the multiplication factor for the storage racks under flooded and optimum moderation conditions in accordance with ANSI N18.2. The maximum rack K_{eff} under optimum density moderation conditions occurs at 0.075 gm/cm^3 water density. For all conditions, i.e. normal and accident, the K_{eff} values are less than 0.95 for average fuel assembly enrichments up to 5.00 weight percent U-235.

4.3.2.7 Stability

4.3.2.7.1 Introduction

The stability of the pressurized water reactor cores against xenon-induced spatial oscillations and the control of such transients are extensively discussed in Moore (1971); Poncelet and Christie (1968); Skogen and McFarlane (1969a); and Skogen and McFarlane (1969b). A summary of these reports is given in the following discussion, and the design bases are given in Section 4.3.1.6.

In a large reactor core, xenon-induced oscillations can take place with no corresponding change in the total power of the core. The oscillation may be caused by a power shift in the core which rapidly occurs by comparison with the xenon-iodine time constants. Such a power shift occurs in the axial direction when a plant load change is made by control rod motion and results in a change in the moderator density and fuel temperature distributions. Such a power shift could occur in the diametral plane of the core as a result of abnormal control action.

Due to the negative power coefficient of reactivity, pressurized water reactor cores are inherently stable to oscillations in total power. Protection against total power instabilities is provided by the control and protection system, as described in Section 7.7. Hence, the discussion on the core stability will be limited here to xenon-induced spatial oscillations.

4.3.2.7.2 Stability Index

Power distributions, either in the axial direction or in the X-Y plane, can undergo oscillations due to perturbations introduced in the equilibrium distributions without changing the total core power. The overtones in the current pressurized water reactors and the stability of the core against xenon-induced oscillations can be determined in terms of the eigenvalues of the first flux overtones. Writing, either in the axial direction or in the X-Y plane, the eigenvalue ε of the first flux harmonic as:

$$\varepsilon = b + ic \qquad\qquad\qquad (4.3-1)$$

then b is defined as the stability index and $T = \pi/c$ as the oscillation period of the first harmonic. The time-dependence of the first harmonic $\delta\phi$ in the power distribution can now be represented as:

$$\delta\Phi(t) + Ae^{\varepsilon t} = ae^{bt}\cos(ct) \qquad\qquad (4.3\text{-}2)$$

where A and a are constants. The stability index can also be obtained approximately by:

$$b - \frac{1}{T}\ln\frac{A_{n+1}}{A_n} \qquad\qquad (4.3\text{-}3)$$

where A and A_{n+1} are the successive peak amplitudes of the oscillation and T is the time period between the successive peaks.

4.3.2.7.3 Prediction of the Core Stability

Analysis of both the axial and X-Y xenon transient tests, discussed in Section 4.3.2.7.5, shows that the calculational model is adequate for the prediction of core stability.

4.3.2.7.4 Stability Measurements

   1. Axial measurements

      Two axial xenon transient tests conducted in a pressure water reactor with a core height of 12 feet and 121 fuel assemblies are reported in Lee et al (1971) and will be briefly discussed here. The tests were performed at approximately 10 percent and 50 percent of cycle life.

      Both a free-running oscillation test and a controlled test were performed during the first test. The second test at mid-cycle consisted of a free-running oscillation test only. In each of the free-running oscillation tests, a perturbation was introduced to the equilibrium power distribution through an impulse motion of the control bank D and the subsequent oscillation was monitored to measure the stability index and the oscillation period. The axial offset of power was obtained from the excore ion chamber readings (which had been calibrated against the incore flux maps) as a function of time for both free-running tests, as shown in Figure 4.3-39.

The total core power was maintained constant during these spatial xenon tests, and the stability index and the oscillation period were obtained from a least-square fit of the axial offset data in the form of Equation 4.3-2. The axial offset of power is the quantity that properly represents the axial stability in the sense that it essentially eliminates any contribution from even-order harmonics, including the fundamental mode. The conclusions of the tests are:

a. The core was stable against induced axial xenon transients, both at the core average burnups of 1,550 MWD/MTU and 7,700 MWD/MTU. The measured stability indices are -0.041 hr^{-1} for the first test (Curve 1 of Figure 4.3-39) and -0.014 hr^{-1} for the second test (Curve 2 of Figure 4.3-39). The corresponding oscillation periods are 32.4 and 27.2 hours, respectively.

b. The reactor core becomes less stable as fuel burnup progresses and the axial stability index was essentially zero at 12,000 MWD/MTU.

2. Measurements in the X-Y plane

Two X-Y xenon oscillation tests were performed at a pressurized water reactor plant with a core height of 12 feet and 157 fuel assemblies. The first test was conducted at a core average burnup of 1540 MWD/MTU and the second at a core average burnup of 12,900 MWD/MTU. The X-Y xenon tests show that the core was stable in the X-Y plane at both burnups. The second test shows that the core became more stable as the fuel burnup increased, and all Westinghouse pressurized water reactors are expected to be stable throughout their burnup cycles.

In each of the two X-Y tests, a perturbation was introduced to the equilibrium power distribution through an impulse motion of one rod cluster control unit located along the diagonal axis. Following the perturbation, the uncontrolled oscillation was monitored, using the movable detector and thermocouple system and the excore power range detectors. The quadrant tilt difference (QTD) is the quantity that properly represents the diametral oscillation in the X-Y plane of the reactor core in that the differences of the quadrant average powers over two symmetrically opposite quadrants essentially eliminates the contribution to the oscillation from the aximuthal mode. The QTD data were fitted in the form of Equation 4.3-2 through a least-square method. A stability index of -0.076 hr^{-1} with a period of 29.6 hours was obtained from the thermocouple data shown in Figure 4.3-40.

It was observed in the second X-Y xenon test that the pressurized water reactor core with 157 fuel assemblies had become more stable due to an increased fuel depletion, and the stability index was not determined.

4.3.2.7.5 Comparison of Calculations with Measurements

The analysis of the axial xenon transient tests was performed in an axial slab geometry, using a flux synthesis technique. The direct simulation of the axial offset data was carried out using the PANDA Code (Barry et al 1975). The analysis of the X-Y xenon transient tests was performed in an X-Y geometry, using a modified TURTLE Code (Barry and Altomare 1975). Both the PANDA and TURTLE Codes solve the two-group time-dependent neutron diffusion equation with time-dependent xenon and iodine concentration. The fuel temperature and moderator density feedback is limited to a steady-state model. All the X-Y calculations were performed in an average enthalpy plane. Current designs use ANC, a two group time dependent neutron diffusion equation solution. Iodine, Xenon, and feedback modeling has been preserved from prior methods.

The basic nuclear cross-sections used in this study were generated from a unit cell depletion program which has evolved from the codes LEOPARD (Barry 1963) and CINDER (England 1962). The detailed experimental data during the tests, including the reactor power level, enthalpy rise, and the impulse motion of the control rod assembly, as well as the plant follow burnup data, were closely simulated in the study. Current designs use NEXUS/PARAGON. This code has been extensively benchmarked against prior methods and actual data.

The results of the stability calculation for the axial tests are compared with the experimental data in Table 4.3-5. The calculations show conservative results for both of the axial tests with a margin of approximately -0.01 hr^{-1} in the stability index.

An analytical simulation of the first X-Y xenon oscillation test shows a calculated stability index of -0.081 hr^{-1}, in good agreement with the measured value of -0.076 hr^{-1}. As indicated earlier, the second X-Y xenon test showed that the core had become more stable compared to the first test, and no evaluation of the stability index was attempted. This increase in the core stability in the X-Y plane due to increased fuel burnup is due mainly to the increased magnitude of the negative moderator temperature coefficient.

Previous studies of the physics of xenon oscillations, including three-dimensional analysis, are reported in the series of topical reports: Poncelet and Christie (1968); Skogen and McFarlane (1969a); and Skogen and McFarlane (1969b). A more detailed description of the experimental results and analysis of the axial and X-Y xenon transient tests is presented in Lee et al (1971) and Section 1 of Eggleston (1977).

4.3.2.7.6 Stability Control and Protection

The excore detector system is utilized to provide indications of xenon-induced spatial oscillations. The readings from the excore detectors are available to the operator and also form part of the protection system.

    1. Axial power distribution

        For maintenance of proper axial power distributions, the operator is instructed to maintain an axial offset within a prescribed operating band, based on the excore detector readings. Should the axial offset be permitted to move far enough outside this band, the protection limit will be reached, and the power will be automatically reduced.

        Twelve-foot pressurized water reactor cores become less stable to axial xenon oscillations as fuel burnup progresses. However, free xenon oscillations are not allowed to occur, except for special tests. The full-length control rod banks are sufficient to dampen and control any axial xenon oscillations present. Should the axial offset be inadvertently permitted to move far enough outside the control band due to an axial xenon oscillation, or any other reason, the protection limit on axial offset will be reached and the power will be automatically reduced.

    2. Radial power distribution

        The core described herein is calculated to be stable against X-Y xenon-induced oscillations at all times in life.

        The X-Y stability of large pressurized water reactors has been further verified as part of the startup physics test program for pressurized water reactor cores with 193 fuel assemblies. The measured X-Y stability of the cores with 157 and 193 assemblies was in good agreement with the calculated stability, as discussed in Sections 4.3.2.7.4 and 4.3.2.7.5. In the unlikely event that X-Y oscillations occur, backup actions are possible and would be implemented, if necessary, to increase the natural stability of the core. This is based on the fact that several actions could be taken to make the moderator temperature coefficient more negative, which will increase the stability of the core in the X-Y plane.

        Provisions for protection against nonsymmetric perturbations in the X-Y power distribution that could result from equipment malfunctions are made in the protection system design. This includes control rod drop, rod misalignment, and asymmetric loss-of-coolant flow.

        A more detailed discussion of the power distribution control in pressurized water reactor cores is presented in Moore (1971) and Morita (1974).

4.3.2.8 Vessel Irradiation

A brief review of the methods and analyses used in the determination of neutron and gamma ray flux attenuation between the core and the pressure vessel is given below. A more complete discussion on the pressure vessel irradiation and surveillance program is given in Section 5.3.

The materials that serve to attenuate neutrons originating in the core and gamma rays from both the core and structural components consist of the core baffle, core barrel, neutron pads, and associated water annuli, all of which are within the region between the core and the pressure vessel.

In general, few group neutron diffusion theory and nodal analysis codes are used to determine fission power density distributions within the active core, and the accuracy of these analyses is verified by incore measurements on operating reactors. Region and rodwise power sharing information from the core calculations is then used as source information in two-dimensional S_N transport calculations which compute the flux distributions throughout the reactor.

The neutron flux distribution and spectrum in the various structural components varies significantly from the core to the pressure vessel. Representative values of the neutron flux distribution and spectrum are presented in Table 4.3-6. The values listed are based on time-averaged equilibrium cycle reactor core parameters and power distributions, and, thus, are suitable for long-term fluence projections and for correlation with radiation damage estimates.

As discussed in Section 5.3, the irradiation surveillance program utilizes actual test samples to verify the accuracy of the calculated fluxes at the vessel.

4.3.3 Analytical Methods

Calculations required in nuclear design consist of three distinct types, which are performed in sequence:

    1.   Determination of effective fuel temperatures

    2.   Generation of macroscopic few-group parameters

    3.   Space-dependent, few-group diffusion calculations

These calculations are carried out by computer codes which can be individually executed. However, at Westinghouse, most of the codes required have been linked to form an automated design sequence which minimizes design time, avoids errors in transcription of data, and standardizes the design methods.

4.3.3.1 Fuel Temperature (Doppler) Calculations

Temperatures vary radially within the fuel rod, depending on the heat generation rate in the pellet, the conductivity of the materials in the pellet, gap, and clad, and the temperature of the reactor coolant.

The fuel temperatures for use in the BVPS-2 nuclear design Doppler calculations are obtained from a simplified version of the Westinghouse fuel rod design model described in Section 4.2.1.3 which considers the effect of radial variation of pellet conductivity, expansion coefficient and heat generation rate, elastic deflection of the clad, and a gap conductance which depends on the initial fill gap, the hot open gap dimension, and the fraction of the pellet over which the gap is closed. The fraction of the gap assumed closed represents an empirical adjustment used to produce good agreement with observed reactivity data at BOL. Further gap closure occurs with burnup and accounts for the decrease in Doppler defect with burnup which has been observed in operating plants.

Radial power distributions in the pellet as a function of burnup are obtained from LASER (Poncelet 1966) calculations.

The effective U-238 temperature for resonance absorption is obtained from the radial temperature distribution by applying a radially dependent weighting function. The weighting function was determined from REPAD (Olhoeft 1962) Monte Carlo calculations of resonance escape probabilities in several steady-state and transient temperature distributions. In each case, a flat pellet temperature was determined which produced the same resonance escape probability as the actual distribution. The weighting function was empirically determined from these results.

The effective Pu-240 temperature for resonance absorption is determined by a convolution of the radial distribution of Pu-240 densities from LASER burnup calculations and the radial weighting function. The resulting temperature is burnup dependent, but the difference between U-238 and Pu-240 temperatures, in terms of reactivity effects, is small.

The effective pellet temperature for pellet dimensional change is that value which produces the same outer pellet radius in a virgin pellet as that obtained from the temperature model. The effective clad temperature for dimensional change is its average value.

The temperature calculational model has been validated by plant Doppler defect data, as shown in Table 4.3-7, and Doppler coefficient data, as shown in Figure 4.3-41. Stability index measurements also

provide a sensitive measure of the Doppler coefficient near full power (see Section 4.3.2.7).   It can be seen that Doppler defect data is typically within 0.2 percent Δρ of prediction.

4.3.3.2 Macroscopic Group Constants

There are three lattice codes used for the generation of macroscopic group constants for use in the spatial few group diffusion codes. The first code is a linked version of LEOPARD (Barry 1963) and CINDER (England 1962), the second code is PHOENIX-P (Nguyen, et. al., 1988), and the third is NEXUS/PARAGON (Zhang, et. al. 2005, Ouisloumen et. al. 2004). A description of each code follows.

Macroscopic few-group constants and consistent microscopic cross-sections (needed for feedback and microscopic depletion calculations) can be generated for fuel cells by a Westinghouse version of the LEOPARD (Barry 1963) and CINDER (England 1962) codes, which are internally linked and provide burnup-dependent cross-sections. Normally, a simplified approximation of the main fuel chains is used. However, where needed, a complete solution for all the significant isotopes in the fuel chains, from Th-232 to Cm-244, is available (Nodvik et al 1969).   Fast and thermal cross-section library tapes contain microscopic cross-sections taken for the most part from the ENDF/B (Drake 1970) library, with a few exceptions where other data provided better agreement with critical experiments, isotopic measurements, and plant critical boron values. The effect on the unit fuel cell of nonlattice components in the fuel assembly is obtained by supplying an appropriate volume fraction of these materials in an extra region which is homogenized with the unit cell in the fast (MUFT) and thermal (SOFOCATE) flux calculations.   In the thermal calculation, the fuel rod, clad, and moderator are homogenized by energy-dependent disadvantage factors derived from an analytical fit to integral transport theory results.

Group constants for guide thimbles, instrument thimbles, and interassembly gaps are generated in a manner analogous to the fuel cell calculations. Reflector group constants are taken from-infinite medium LEOPARD calculations. Baffle group constants are calculated from an average of core and radial reflector microscopic group constants for stainless steel.

Group constants for control rods and burnable absorbers are calculated in a linked version of the HAMMER (Suich and Honeck 1967) and AIM (Flatt and Buller 1960) codes. The Doppler broadened cross sections of the control rod and burnable absorber materials are represented as smooth cross sections in the 54-group LEOPARD fast group structure and in 30 thermal groups. The four-group constants in the rod cell and appropriate extra region are generated in the coupled space-energy transport HAMMER calculation. A corresponding AIM calculation of the homogenized rod cell with extra region is used to adjust the absorption cross-sections of the rod cell to match the reaction rates in HAMMER. These transport-equivalent group constants are reduced to two-group constants for use in space-dependent

diffusion calculations. In discrete X-Y calculations, only one mesh interval per cell is used, and the rod group constants are further adjusted for use in this standard mesh by reaction rate matching the standard mesh unit assembly to a fine mesh unit assembly calculation.

Nodal group constants are obtained by a flux-volume homogenization of the fuel cells, burnable absorber cells, guide thimbles, instrumentation thimbles, interassembly gaps, and control rod cells from one mesh interval per cell X-Y unit fuel assembly diffusion calculations.

Validation of the cross-section method is based on analysis of critical experiments, as shown in Table 4.3-4, isotopic data, as shown in Table 4.3-8, plant critical boron (C_B) values at HZP, BOL, as shown in Table 4.3-9, and at HFP as a function of burnup, as shown in Figures 4.3-42, 4.3-43, 4.3-44. Control rod worth measurements are shown in Table 4.3-10.

Confirmatory critical experiments on burnable absorbers are described in Moore (1971a).

The PHOENIX-P computer code is a two-dimensional, multigroup, transport based lattice code and capable of providing all necessary data for PWR analysis. Being a dimensional lattice code, PHOENIX-P does not rely on predetermined spatial/spectral interaction assumptions for a heterogeneous fuel lattice, hence, will provide a more accurate multi-group flux solution than versions of LEOPARD/CINDER. The PHOENIX-P computer code is approved by the USNRC as the lattice code for generating macroscopic and microscopic few group cross sections for PWR analysis (Nguyen 1988).

The solution for the detailed spatial flux and energy distribution is divided into two major steps in PHOENIX-P (Nguyen 1988 and Mildrum 1985). In-the first step, a two-dimensional fine energy group nodal solution is obtained which couples individual subcell regions (pellet, clad and moderator) as well as surrounding pins. PHOENIX-P uses a method based on the Carlvik's collision probability approach and heterogeneous response fluxes which preserves the heterogeneity of the pin cells and their surroundings. The nodal solution provides accurate and detailed local flux distribution which is then used to spatially homogenize the pin cells to fewer groups.

The second step in the solution process solves for the angular flux distribution using a standard S4 discrete ordinates calculation. This step is based on the group-collapsed and homogenized cross sections obtained from the first step of the solution. The S4 fluxes are then used to normalize the detailed spatial and energy nodal fluxes. The normalized nodal fluxes are used to compute reaction rates, power distribution and to deplete the fuel and burnable absorbers. A standard B1 calculation is employed to evaluate the fundamental mode critical spectrum and to provide an improved fast diffusion coefficient for the core spatial codes.

The PHOENIX-P code employs a 42 energy group library which has been derived mainly from ENDF/B-V files. The PHOENIX-P cross sections library was designed to properly capture integral properties of the multi-group data during group collapse, and enabling proper modeling of important resonance parameters. The library contains all neutronic data necessary for modeling fuel, fission products, cladding and structural, coolant, and control/burnable absorber materials present in Light Water Reactor cores.

Group constants for burnable absorber cells, guide thimbles, instrument thimbles, control rod cells and other non-fuel cells can be obtained directly from PHOENIX-P without any adjustments such as those required in the cell or 1D lattice codes.

PARAGON has been approved by the NRC as the new generation of Westinghouse lattice code (Ouisloumen 2004). PARAGON is a replacement for PHOENIX-P and its primary use will be to provide the same types of input data that PHOENIX-P generates for use in three dimensional core simulator codes. This includes macroscopic cross sections, microscopic cross sections for feedback adjustments to the macroscopic cross sections, pin factors for pin power reconstruction calculations, discontinuity factors for a nodal method solution, and other data needed for safety analysis or other downstream applications.

PARAGON is based on collision probability - interface current cell coupling methods. PARAGON provides flexibility in modeling that was not available in PHOENIX-P including exact cell geometry representation instead of cylinderization, multiple rings and regions within the fuel pin and the moderator cell geometry, and variable cell pitch. The solution method permits flexibility in choosing the quality of the calculation through both increasing the number of regions modeled within the cell and the number of angular current directions tracked at the cell interfaces.

The calculation scheme in PARAGON is based on the conventional lattice modules: resonance calculation, flux solution, leakage correction and depletion. The cross-section resonance calculation module is based on the space dependent Dancoff method (Ouisloumen 2004); it is a generalization of the PHOENIX-P methodology that permits to subdivide the fuel pin into many rings and therefore generates space dependent self-shielded isotopic cross-sections. The flux solution module uses the interface current collision probability method and permits a detailed representation of the fuel cells (Ouisloumen 2004). The other two modules (leakage and depletion) are similar to the ones used in PHOENIX-P.

The current PARAGON cross section library is a 70-group library, based on the ENDF/B basic nuclear data, with the same group structure as the library currently used with PHOENIX-P. The PARAGON qualification library has been improved through the addition of more explicit fission products and fission product chains (Ouisloumen 2004). PARAGON is however designed to employ any number of energy groups.

The new NEXUS cross-section generation system uses PARAGON as the lattice code (Zhang 2005).

4.3.3.3 Spatial Few-Group Diffusion Calculations

Spatial few-group diffusion calculations have historically consisted
of two-group X-Y calculations using an updated version of the TURTLE
code, and two-group axial calculations using an updated version of the
PANDA code. However, with the advent of VANTAGE 5 fuel and, hence,
axial features such as axial blankets and part length burnable
absorbers, there is a greater reliance on three dimensional nodal
codes such as 3D ANC (Advanced Nodal Code) (Liu, 1986). The three
dimensional nature of the nodal codes provides both the radial and
axial power distributions.

Nodal three dimensional calculations are carried out to determine the
critical boron concentrations and power distributions. The moderator
coefficient is evaluated by varying the inlet temperature in the same
calculations used for power distribution and reactivity predictions.

ANC is used in two-dimensional and three-dimensional calculations.
ANC can be used for safety analyses and to calculate critical boron
concentrations, control rod worths, reactivity coefficients, etc.

Axial calculations are used to determine differential control rod
worth curves (reactivity versus rod insertion) and axial power shapes
during steady-state and transient xenon conditions (flyspeck curve).
Group constants and the radial buckling used in the axial calculation

are obtained from the three dimensional ANC calculation from which constants are homogenized by flux-volume weighting.

Validation of the spatial codes for calculating power distributions involves the use of incore and excore detectors and is discussed in Section 4.3.2.2.7.

Based on comparison with measured data, it is estimated that the accuracy of current analytical methods is:

$\pm$0.1 percent $\Delta\rho$ for Doppler defect

$\pm$2 x 10^{-5}/°F for moderator coefficient

$\pm$50 ppm for critical boron concentration with depletion

$\pm$3 percent for power distributions

$\pm$0.2 percent $\Delta\rho$ for rod bank worth

$\pm$4 pcm/step for differential rod worth

$\pm$0.5 pcm/ppm for boron worth

$\pm$0.1 percent $\Delta\rho$ for moderator defect

4.3.4 Revisions

The design methods for the criticality of fuel assemblies outside the reactor use the continuous energy 3D Monte Carlo code MCNP4a and CASMO-4 depletion code for Metamic racks as described in Section 4.3.2.6.

4.3.5 References for Section 4.3

Adler, M. R., "AMSAC Generic Design Package" WCAP-10858P-A Revision 1 (Proprietary) July, 1987.

Liu, Y. S., et.al., "ANC: A Westinghouse Advanced Nodal Computer Code," WCAP-10965-P-A, December, 1985.

Nguyen, T.Q., et.al., "Qualification of the PHOENIX-P/ANC Nuclear Design System for Pressurized Water Reactor Cores,'' WCAP-11596-P-A, June, 1988.

Mildrum, C.M., Mayhue, L.T., et.al., "Qualification of the PHOENIX/POLCA Nuclear Design and Analysis Program for Boiling Water Reactors," WCAP-10841 (Proprietary) and WCAP-10842 (Non-proprietary), June, 1985.

Strawbridge, L.E., and Barry, R. F., "Criticality Calculation Uniform Water-Moderated Lattices," Nuclear Science and Eng. 23, 58 (1965).

Nodvik, R.J., "Saxton Core II Fuel Performance Evaluation, "WCAP-3385-56 Part 11, "Evaluation of Mass Spectrometric and Radiochemical Analyses of Irradiated Saxton Plutonium Fuel," July, 1970.

Barry, R.F. 1963. LEOPARD - A Spectrum Dependent Non-Spatial Depletion Code for the IBM-7094. WCAP-3269-26.

Barry, R.F. et al 1975. The PANDA Code. WCAP-7048-P-A (Proprietary) and WCAP-7757-A (Nonproprietary).

Barry, R.F. and Altomare, S. 1975. The TURTLE 24.0 Diffusion Depletion Code. WCAP-7213-P-A (Proprietary) and WCAP-7758-A (Nonproprietary).

Baldwin M.N.; Critical Experiments Supporting Close Proximity-Water Storage of Power Reactor Fuel, BAW-1484-7, July 1979.

Cermak, J.O. et al 1968. Pressurized Water Reactor pH - Reactivity Effect Final Report. WCAP-3696-8 (EURAEC-2074).

Drake, M.K. (Ed) 1970. Data Formats and Procedure for the ENDF/B Neutron Cross Section Library BNL-50274, ENDF-102 Vol. 1.

Eggleston, F.T. 1977. Safety-Related Research and Development for Westinghouse Pressurized Water Reactors Program Summaries - winter 1976, WCAP-8768, Revision 1.

England, T.R. 1962. CINDER - A One-Point Depletion and Fission Product Program. WAPD-TM-334.

Flatt, H.P. and Buller, D.C. 1960. AIM-5, A Multigroup, one Dimensional Diffusion Equation Code. NAA-SR-4694.

Ford, W.E., III, CSRL-V: Processed ENDFIB-V 227-Neutron-Group and Pointwise Cross-Section Libraries for Criticality Safety, Reaction and Shielding Studies, ORNL/CSD/TM-160, June 1982.

Greene, N.H. et al 1976. AMPX: A Modular Code System for Generating Coupled Multigroup Neutron-Gamma Libraries from ENDF/B. ORNL/TM-06.

Holtec Report HI-2084175, Revision 8, Licensing Report for Beaver Valley Unit 2 Rerack," as submitted to the NRC in support of License Amendment 173, Unit 2 Fuel Storage Pool Rerack.

Langford, F.L. and Nath, R.J. 1971. Evaluation of Nuclear Hot Channel Factor Uncertainties. WCAP-7308-L (Proprietary) and WCAP-7810 (Nonproprietary).

Leamer, R.D. et al 1967. PUO_2-UO_2 Fueled Critical Experiments. WCAP-3726-1.

Lee, J.C. et al 1971. Axial Xenon Transient Tests at the Rochester Gas and Electric Reactor. WCAP-7964.

McFarlane, A.F. 1975. Power Peaking Factors, WCAP-7912-P-A (Proprietary) and WCAP-7912-A (Nonproprietary).

Miller, R. W., et al., "Relaxation of Constant Axial Offset Control; Fq Surveillance Technical Specification," WCAP-10216-P-A Revision 1A (Proprietary), and WCAP-10217-A Revision 1A (Nonproprietary), February 1994.

Moore, J.S. 1971. Power Distribution Control of Westinghouse Pressurized Water Reactors. WCAP-7811.

Moore, J.S. 1971a. Nuclear Design of Westinghouse Pressurized Water Reactors with Burnable Poison Rods. WCAP-7806.

Morita, T., et al 1974. Power Distribution Control and Load Follow Procedures. WCAP-8385 (Proprietary) and WCAP-8403 (Nonproprietary).

Nodvik, R.J. et al 1969. Supplementary Report on Evaluation of Mass Spectrometric and Radiochemical Analyses of Yankee Core I Spent Fuel, Including Isotopes of Elements Throium Through Curium WCAP-6086.

Nuclear Regulatory Commission, Letter to all Power Reactor Licensees, from B.K. Grimes OT Position for Review and Acceptance of Spent Fuel Storage and Handling Applications, April 14, 1978.

Olhoeft, J.E. 1962. The Doppler Effect for Non-Uniform Temperature Distribution in Reactor Fuel Elements WCAP-2048.

Ouisloumen, M. et al., ''Qualification of the Two-Dimensional Transport Code PARAGON,'' WCAP-16045-P-A, Westinghouse 2004.

Petrie, L.M. and Cross, N.F. 1975. KENO IV - An Improved Monte Carlo Criticality Program. 0RNL-4938.

Poncelet, C.G. 1966. LASER - A Depletion Program for Lattice Calculations Based on MUFT and THERMOS. WCAP-6073.

Poncelet, C.G. and Christie, A.M. 1968. Xenon-Induced Spatial Instabilities in Large PWRs WCAP-3680-20 (EURAEC-1974).

Skogen, F.B. and McFarlane, A.F. 1969a. Control Procedures for Xenon-Induced X-Y Instabilities in Large PWRS. WCAP-3680-21 (EURAEC-2111).

Skogen, F.B. and McFarlane, A.F. 1969b. Xenon-Induced Spatial Instabilities in Three-Dimensions. WCAP-3680-22 (EURAEC-2116).

Suich, J.E. and Honeck, H.C. 1967. The HAMMER System Heterogeneous Analysis by Multigroup Methods of Exponential and Reactors. DP-1064.

Thomas, J.T. 1973. Critical Three-Dimensional Arrays of U (93.2) - Metal Cylinders. Nuclear Science and Engineering, Volume 52, pp. 350-359.

U.S. Nuclear Regulatory Commission - Safety Evaluation related to Amendment No. 173 Regarding the Spent Fuel Pool Rerack for Facility Operating License No. NPF-73, dated April 29, 2011.

Westinghouse 1974. Westinghouse Anticipated Transients Without Reactor Trip Analysis. WCAP-8330.

Westinghouse 1976. Augmented Startup and Cycle 1 Physics Program Supplement 1. WCAP-8575 Supplement 1 (Westinghouse Proprietary) and WCAP-8576 (Nonproprietary).

Zhang, B. et al., ''Qualification of the NEXUS Nuclear Data Methodology,'' WCAP-16045-P-A, Addendum 1, Westinghouse 2005.

Tables for Section 4.3

TABLE 4.3-1

REACTOR CORE DESCRIPTION
(First Cycle)

Active Core

Equivalent diameter (in)	119.7
Core average active fuel height, first core (in) (nominal)	144
Height-to-diameter ratio	1.20
Total cross section area (ft^2)	78.14
H_2O/U molecular ratio, lattice (cold)	2.42

Reflector Thickness and Composition

Top - water plus steel (in)	10
Bottom - water plus steel (in)	10
Side - water plus steel (in)	15

Fuel Assemblies

Number	157
Rod array	17 x 17
Rods per assembly	264
Rod pitch (in)	0.496
Overall transverse dimensions (in)	8.426 x 8.426
Fuel Weight, as UO_2 (lb)	181,200
Zircaloy weight (lb)	41,400
Number of grids per assembly	8-R Type
Composition of Grids	Inconel-718
Weight of grids, (effective in core) (lb)	1885
Number of guide thimbles per assembly	24
Composition of guide thimbles	Zircaloy-4
Diameter of guide thimbles, upper part (in)	0.450 I.D. x 0.482 O.D.
Diameter of guide thimbles, lower part (in)	0.397 I.D. x 0.430 O.D.
Diameter of instrument guide thimbles (in)	0.450 I.D. x 0.482 O.D.

Fuel Rods

Number	41,448
Outside diameter (in)	0.374
Diameter gap (in)	0.0065
Clad thickness (in)	0.0225
Clad material	Zircaloy-4

TABLE 4.3-1 (Cont)

Fuel Pellets

Material	UO_2 Sintered
Density (percent of theoretical)	95
Fuel enrichments (weight percent) (see Figure 4.3-10)	
Region 1	2.10
Region 2	2.60
Region 3	3.10
Diameter (in)	0.3225
Length (in)	0.530
Mass of UO_2 per foot of fuel rod (lb/ft)	0.364

Rod Cluster Control Assemblies

Neutron Absorber	Ag-In-Cd
Composition	80%-15%-5%
Diameter (in)	0.341
Density (lb/in^3)	0.367
Cladding material	Type 304, cold worked stainless steel
Clad thickness (in)	0.0185
Number of clusters	48
Number of absorber rods per cluster	24
Rod cluster control assembly weight (dry) lb	149

Burnable Absorber Rods (First Core)

Number	1072
Material	Al_2O_3-B_4C
Outside diameter (in)	0.381
Inner tube, O.D. (in)	0.267
Clad material	Zircaloy
Inner tube material	Zircaloy
Boron loading (wt% B_4C in glass rod)	14.0
Weight of boron-10 per foot of rod (gm/cm)	0.006
Initial reactivity worth (percent $\Delta\rho$)	6.7 (hot) 5.0 (cold)

<u>Excess Reactivity</u>

    Maximum fuel assembly K∞   <1.6
      (cold, clean unborated water)
    Maximum core reactivity   1.22
      (cold, zero power, beginning of
    cycle,
      zero soluble boron)

TABLE 4.3-2

NUCLEAR DESIGN PARAMETERS
(First Cycle)

Core average linear power, including densification   5.2
effects (kW/ft)

Total heat flux hot channel factor, F_Q 2.32

Nuclear enthalpy rise hot channel factor, $F^N_{\Delta H}$ 1.55

Reactivity Coefficients**

   Doppler-only power coefficients, (pcm/percent power)

     Upper limit (Figure 15.0-2)   -19.4 to -12.6

     Lower limit (Figure 15.0-2)   -10.2 to -6.7

   Doppler temperature coefficient (pcm/°F)   -2.9 to -1.4

   Moderator temperature coefficient (pcm/°F)   See Figure
                                                   4.3-29, 4.3-30
                                                  and 4.3-31

   Boron coefficient (pcm/ppm)   -16 to -7

   Rodded moderator density coefficient (pcm/gm/cm^3) 0.43×10^5

Delayed Neutron Fraction and Lifetime

B_{eff} BOL, (EOL)   0.0075
                                                     (0.0044)

1*, BOL, (EOL) μ sec   19.4 (18.1)

Control Rods

   Rod requirements   See Table 4.3-3

   Maximum bank worth (pcm)***   <2300

   Maximum ejected rod worth   See Chapter 15

Boron Concentrations (ppm)

   Zero power, k_{eff} = 1.00, cold, rod cluster control   1444

     assemblies out, 1 percent Δρ uncertainty included

   Zero power, k_{eff} = 1.00, hot, rod cluster control   1435

     assemblies out, 1 percent Δρ uncertainty included

TABLE 4.3-2 (Cont)

Design basis refueling boron concentration	2000
Zero power, $k_{eff} \leq 0.95$, cold, rod cluster control assemblies in, 1 percent $\Delta\rho$ uncertainty included	1339
Zero power, $k_{eff} = 1.00$, hot, rod cluster control assemblies out	1335
Full power, no xenon, $k_{eff} = 1.00$, hot, rod cluster control assemblies out	1236
Full power, equilibrium xenon, $k_{eff} = 1.00$, hot rod cluster control assemblies out	937
Reduction with fuel burnup	
First cycle (ppm/GWD/MTU)****	See Figure 4.3-3
Reload cycle (ppm/GWD/MTU)	~100

NOTES:

  **Uncertainties are given in Section 4.3.3.3.

 ***1 pcm = 10^{-5} $\Delta\rho$ where $\Delta\rho$ is calculated from two statepoint values of K_{eff} by $\ln(k_2/k_1)$.

****Gigawatt day (GWD) = 1000 megawatt day (1000 MWD). During the first cycle, fixed burnable poison rods are present which significantly reduce the boron depletion rate compared to reload cycles.

TABLE 4.3-3

REACTIVITY REQUIREMENTS FOR ROD CLUSTER CONTROL ASSEMBLIES

Reactivity Effects (percent)	Beginning-of-Life (first Cycle)	End-of-Life (First Cycle)	End-of-Life (Equilibrium Cycle)
1. Control requirements			
Fuel temperature, (Doppler) (percent $\Delta\rho$)**	1.23	1.11	1.12
Moderator temperature (percent $\Delta\rho$)	0.19	0.86	0.89
Void (percent $\Delta\rho$)	0.05	0.05	0.05
Redistribution (percent $\Delta\rho$)	0.50	0.85	0.95
Rod insertion allowance (percent $\Delta\rho$)	0.50	0.50	0.50
2. Total control (percent $\Delta\rho$)	2.47	3.37	3.51
3. Estimated rod cluster control assembly worth (48 rods)			
a. All assemblies inserted (percent $\Delta\rho$)	9.30	8.87	8.19
b. All but one (highest worth) assemblies inserted (percent $\Delta\rho$)	7.32	7.60	7.32
4. Estimated rod cluster control assembly credit with 10 percent adjustment to accommodate uncertainties, (Item 3b minus 10 percent) (percent $\Delta\rho$)	6.59	6.84	6.59
5. Shutdown margin available (Item 4 minus Item 2), (percent $\Delta\rho$)*	4.12	3.47	3.08

NOTES:

*The design basis minimum shutdown is 1.77 percent $\Delta\rho$.
**Includes 0.1% $\Delta\rho$ uncertainty.

TABLE 4.3-4
BENCHMARK CRITICAL EXPERIMENTS

	General Description	Enrichment Percent U235	Reflector	Separating material	Soluble Boron ppm	K_{eff}
1.	UO_2 rod lattice	2.46	water	water	0	0.9057 ± .0028
2.	UO_2 rod lattice	2.46	water	water	1037	0.9906 ± .0018
3.	UO_2 rod lattice	7.46	water	water	764	0.9896 ± .0015
4.	UO_2 rod lattice	2.46	water	84C pins	0	0.9914 ± .0025
5.	UO_2 rod lattice	2.46	water	84C pins	0	0.9891 ± .0026
6.	UO_2 rod lattice	2.46	water	84C pins	0	0.9955 ± .0020
7.	UO_2 rod lattice	2.46	water	84C pins	0	0.9889 ± .0026
8.	UO_2 rod lattice	2.46	water	84C pins	0	0.9983 ± .0025
9.	UO_2 rod lattice	2.46	water	water	0	0.9931 ± .0028
10.	UO_2 rod lattice	2.46	water	water	143	0.9928 ± .0025
11.	UO_2 rod lattice	2.46	water	stainless steel	514	0.9967 ± .0020
12.	UO_2 rod lattice	2.46	water	stainless steel	217	0.9943 ± .0019
13.	UO_2 rod lattice	2.46	water	borated aluminum	15	0.9692 ± .0023
14.	UO_2 rod lattice	2.46	water	borated aluminum	92	0.9884 ± .0023
15.	UO_2 rod lattice	2.46	water	borated aluminum	395	0.9832 ± .0021
16.	UO_2 rod lattice	2.46	water	borated aluminum	121	0.9848 ± .0024
17.	UO_2 rod lattice	2.46	water	borated aluminum	487	0.9895 ± .0020
18.	UO_2 rod lattice	2.46	water	borated aluminum	197	0.9885 ± .0022
19.	UO_2 rod lattice	2.46	water	borated aluminum	634	0.9921 ± .0019
20.	UO_2 rod lattice	2.46	water	borated aluminum	320	0.9920 ± .0020
21.	UO_2 rod lattice	2.46	water	borated aluminum	72	0.9939 ± .0020
22.	U metal cylinders	93.2	air	air	0	0.9905 ± .0020
23.	U metal cylinders	93.2	air	air	0	0.9976 ± .0020
24.	U metal cylinders	93.2	air	air	0	0.9947 ± .0025
25.	U metal cylinders	93.2	air	air	0	0.9928 ± .0019
26.	U metal cylinders	93.2	air	air	0	0.9922 ± .0026
27.	U metal cylinders	93.2	air	air	0	0.9950 ± .0027
28.	U metal cylinders	93.2	air	plexiglass	0	0.9941 ± .0030
29.	U metal cylinders	93.2	paraffin	plexiglass	0	0.9929 ± .0041
30.	U metal cylinders	93.2	paraffin	plexiglass	0	0.9928 ± .0018
31.	U metal cylinders	93.2	paraffin	plexiglass	0	1.0042 ± .0019
32.	U metal cylinders	93.2	paraffin	plexiglass	0	0.9963 ± .0030
33.	U metal cylinders	93.2	paraffin	plexiglass	0	0.9919 ± .0032

TABLE 4.3-5

AXIAL STABILITY INDEX PRESSURIZED WATER
REACTOR CORE WITH A 12 FOOT HEIGHT

Burnup (MWD/MTU)	F_z	C_B (ppm)	Stability Index (hr⁻¹) Exp	Calc
1550	1.34	1065	-0.041	-0.032
7700	1.27	700	-0.014	-0.006
		Difference	+0.027	+0.026

TABLE 4.3-6

TYPICAL NEUTRON FLUX LEVELS (n/cm^2-sec) AT FULL POWER

	E >1.0 MeV	5.53 KeV <E <1.0 MeV	0.625 eV ≤E <5.33 KeV	0.625 eV < (nv)o
Core center	6.73×10^{13}	1.18×10^{14}	8.92×10^{13}	3.14×10^{13}
Core outer radius at mid-height	3.39×10^{13}	6.03×10^{13}	4.85×10^{13}	9.03×10^{13}
Core top, on axis	1.60×10^{13}	2.54×10^{13}	2.20×10^{13}	1.71×10^{12}
Core bottom, on axis	2.48×10^{13}	4.13×10^{13}	3.67×10^{13}	1.53×10^{13}
Pressure vessel Inner wall azimuthal peak, core mid-height	2.90×10^{10}	6.03×10^{10}	6.32×10^{10}	8.78×10^{11}

TABLE 4.3-7

COMPARISON OF MEASURED AND CALCULATED DOPPLER DEFECTS

Plant	Fuel Type	Core Burnup (MWD/MTU)	Measured (pcm)*	Calculated (pcm)
1	Air-filled	1,800	1,700	1,710
2	Air-filled	7,700	1,300	1,440
3	Air and helium-filled	8,460	1,200	1,210

NOTE:

* $pcm = 10^5 \times \ln(K_1/K_2)$

TABLE 4.3-8

SAXTON CORE II ISOTOPES
ROD MY, AXIAL ZONE 6

Atom Ratio	Measured*	2 Precision (%)	LEOPARD Calculation
U-234/U	4.65×10^{-5}	±29	4.60×10^{-5}
U-235/U	5.74×10^{-3}	±0.9	5.73×10^{-3}
U-236/U	3.55×10^{-4}	±5.6	3.74×10^{-4}
U-238/U	0.99386	±0.01	0.99385
Pu-238/Pu	1.32×10^{-3}	±2.3	1.222×10^{-3}
Pu-239/Pu	0.73971	±0.03	0.74497
Pu-240/Pu	0.19302	±0.2	0.19102
Pu-241/Pu	6.014×10^{-2}	±0.3	5.74×10^{-2}
Pu-242/Pu	5.81×10^{-3}	±0.9	5.38×10^{-3}
Pu/U**	5.938×10^{-2}	±0.7	5.970×10^{-2}
Np-237/U-238	1.14×10^{-4}	±15	0.86×10^{-4}
Am-241/Pu-239	1.23×10^{-2}	±15	1.08×10^{-2}
Cm-242/Pu-239	1.05×10^{-4}	±10	1.11×10^{-4}
Cm-244/Pu-239	1.09×10^{-4}	±20	0.98×10^{-4}

NOTES:

 *Reported in Nodvik (1970)
**Weight ratio.

TABLE 4.3-9

CRITICAL BORON CONCENTRATIONS, HZP*, BOL

Plant Type		Measured (ppm)	Calculated (ppm)
2-loop, assemblies 10 foot core	121	1583	1589
2-loop, assemblies 12 foot core	121	1625	1624
2-loop, assemblies 12 foot core	121	1517	1517
3-loop, assemblies 12 foot core**	157	1169	1161
3-loop, assemblies 12 foot core	157	1344	1319
4-loop, assemblies 12 foot core	193	1370	1355
4-loop, assemblies 12 foot core	193	1321	1306

NOTES:

 *HZP = hot zero power = constant moderator temperature at
                     equilibrium no load value
**Beaver Valley Power Station - Unit 2 design

TABLE 4.3-10

COMPARISON OF MEASURED AND CALCULATED ROD WORTH

BENCHMARK CRITICAL EXPERIMENT
HAFNIUM CONTROL ROD WORTH

Control Rod Configuration	No. of Fuel Rods	Measured*,** Worth (ppm B-10)	Calculated*,** Worth (ppm B-10)
9 Hafnium Rods	1192	138.3	141.0

NOTE:

 *Reported in Leamer et al (1967).
**Calculated and measured worths are given in terms of an equivalent change in B-10 concentration.

TABLE 4.3-11

COMPARISON OF MEASURED AND CALCULATED MODERATOR
COEFFICIENTS AT HZP*, BOL

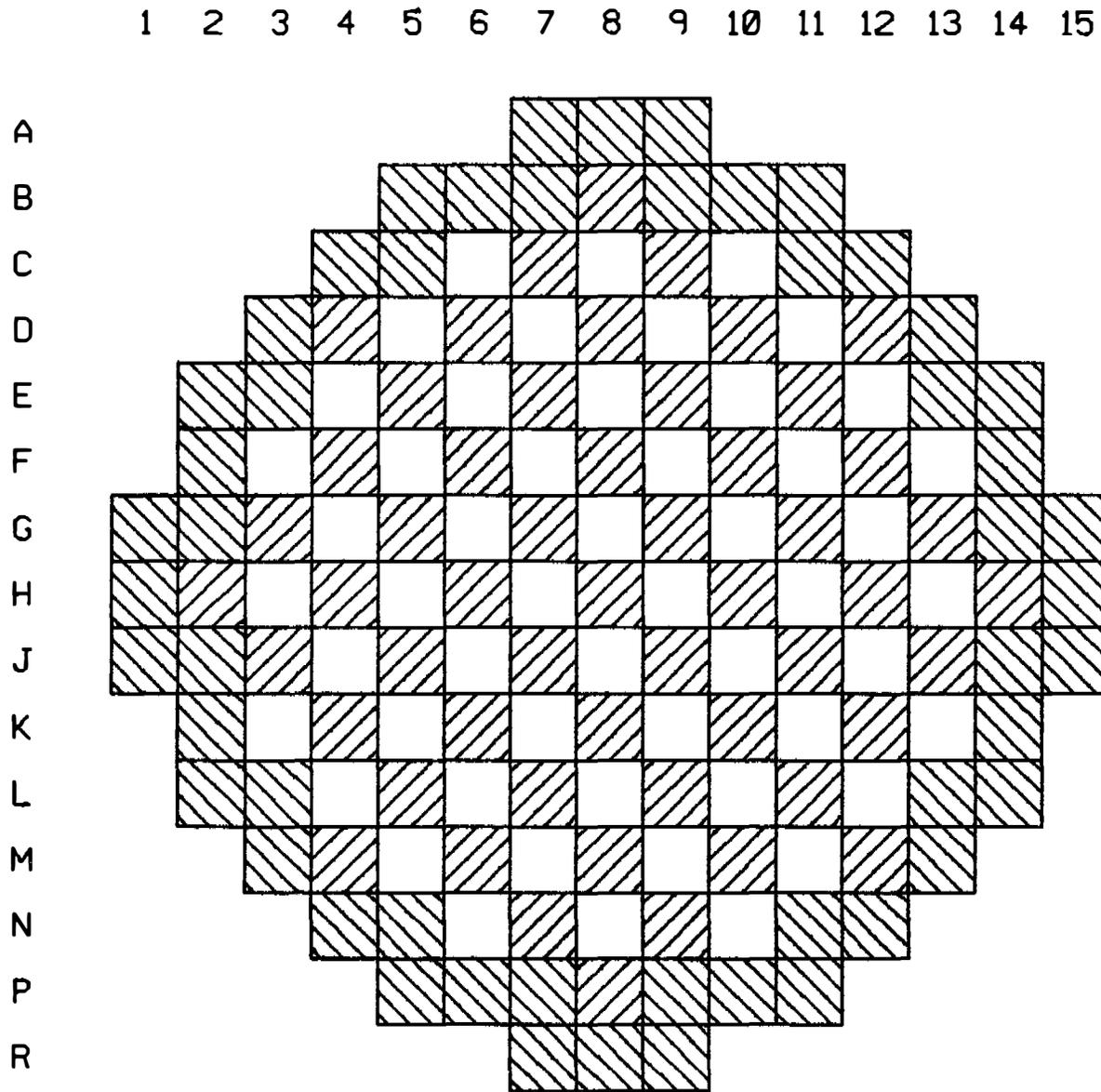| Plant Type/ Control Bank Configuration	Measured 150** (pcm/°F)	Calculated 150 (pcm/°F)
2-loop, 121 assemblies, 12 foot core		
D at 180 steps	+0.85	+1.02
D in, C at 180 steps	-2.40	-1.90
C and D in, B at 165 steps	-4.40	-5.58
B, C and D in, A at 174 steps	-8.70	-8.12
3-loop, 157 assemblies, 12 foot core***		
D at 160 steps	-0.50	-0.50
D in, C at 190 steps	-3.01	-2.75
D in, C at 28 steps	-7.67	-7.02
B, C, and D in	-5.16	-4.45
4-loop, 193 assemblies 12-foot core		
ARO	-0.52	-1.2
D in	-4.35	-5.7
D and C in	-8.59	-10.0
D, C, and B in	-10.14	-10.55
D, C, B, and A in	-14.63	-14.45

NOTES:

 *HZP = hot zero power = constant moderator temperature at
                equilibrium no load value.

**Isothermal coefficients, which include the Doppler effect in the
fuel.

$$\alpha_{150} = 10^5 \ln \frac{k_2}{k_1}/\rho T°F$$

***Beaver Valley Power Station - Unit No. 2 design.

FIRST CORE

⬜ REGION 1

⬜ REGION 2

⬜ REGION 3

RELOAD CORE

ONCE OR TWICE
BURNED FUEL

FRESH FUEL

ONCE OR TWICE
BURNED FUEL

FIGURE 4.3-1
TYPICAL FUEL LOADING ARRANGEMENT
BEAVER VALLEY POWER STATION-UNIT 2
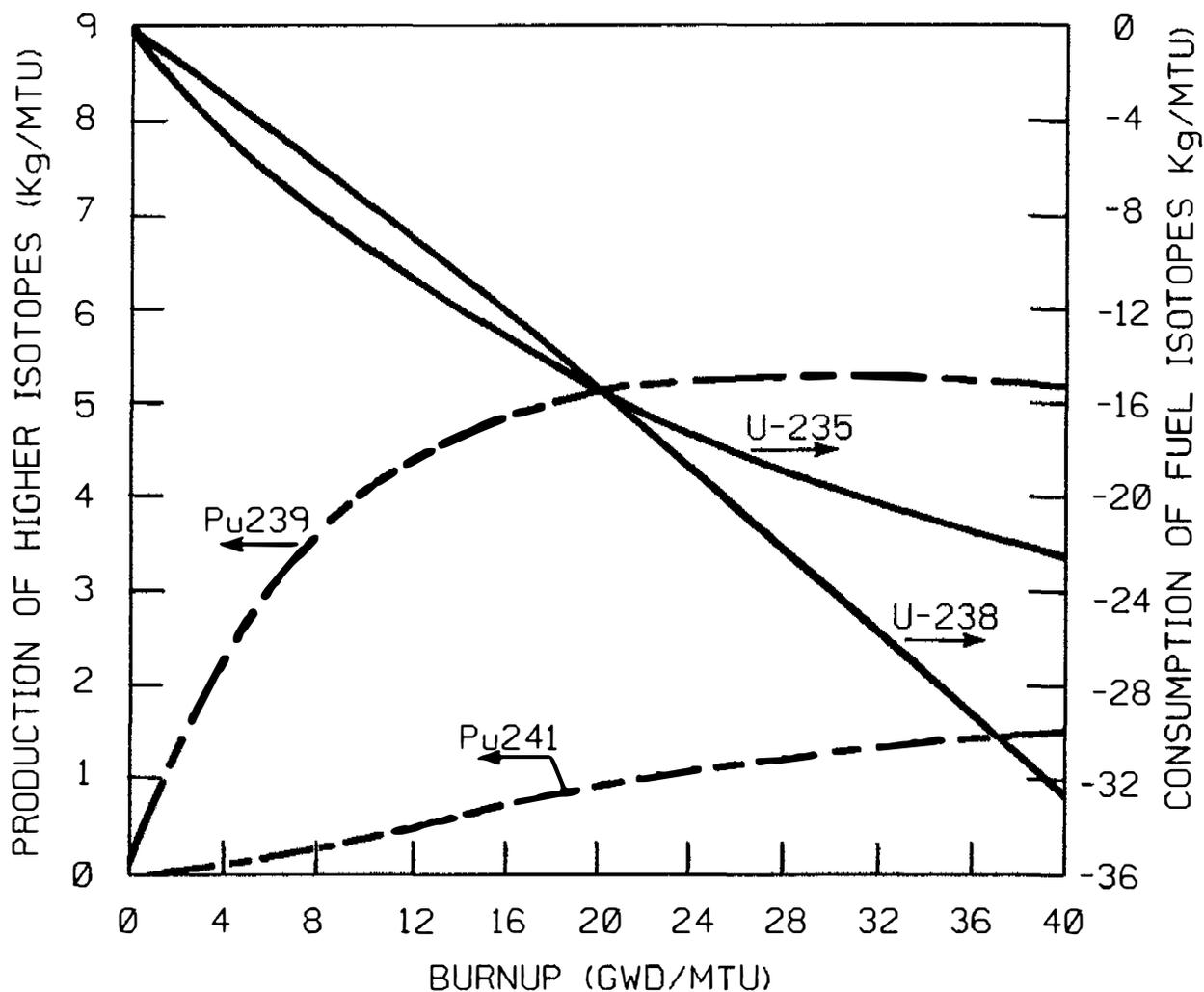UPDATED FINAL SAFETY ANALYSIS REPORT

FIGURE 4.3-2

TYPICAL PRODUCTION AND CONSUMPTION
OF HIGHER ISOTOPES
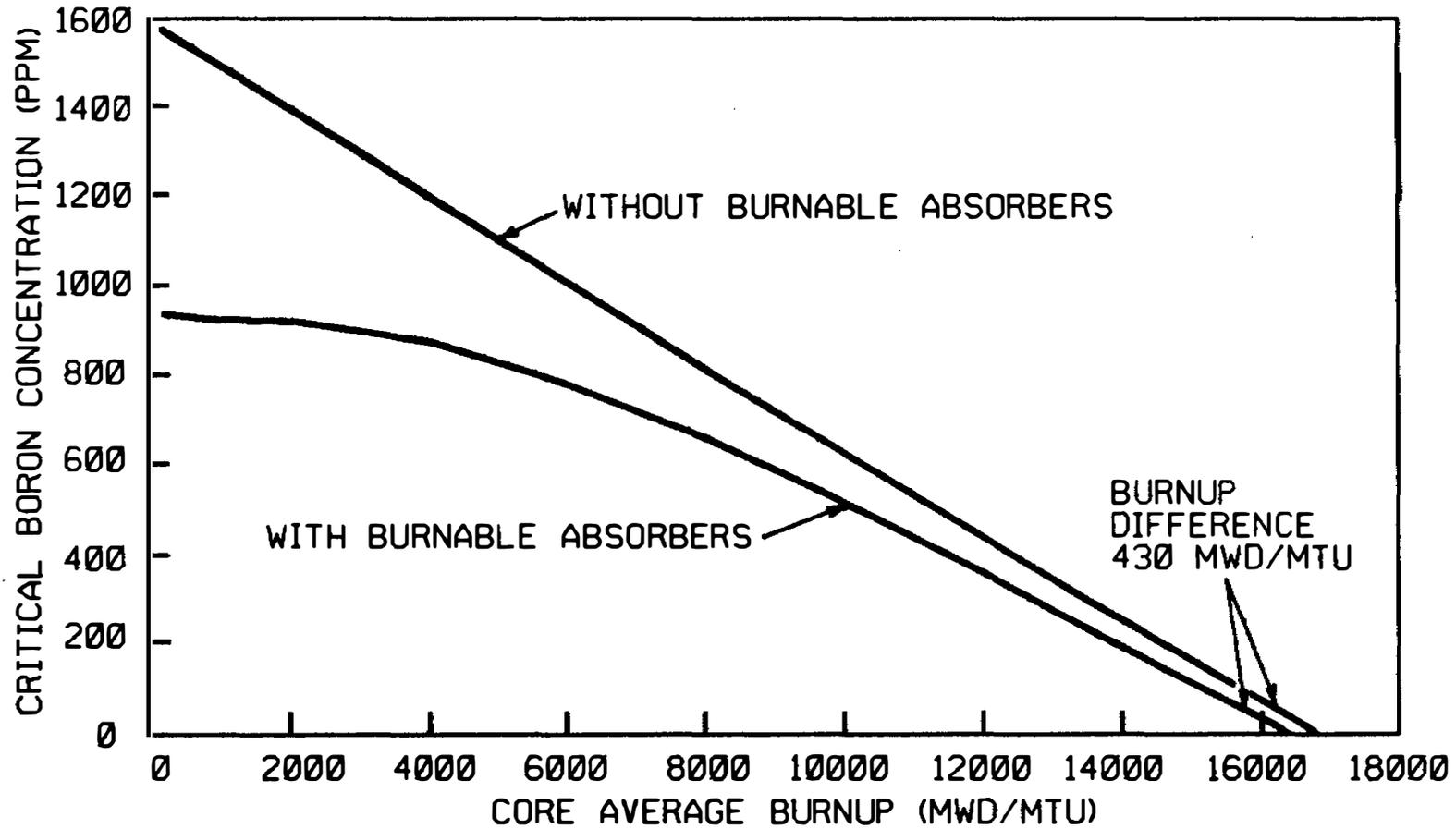BEAVER VALLEY POWER STATION-UNIT 2
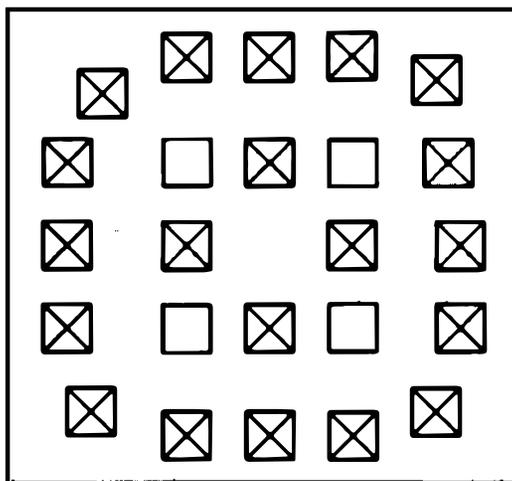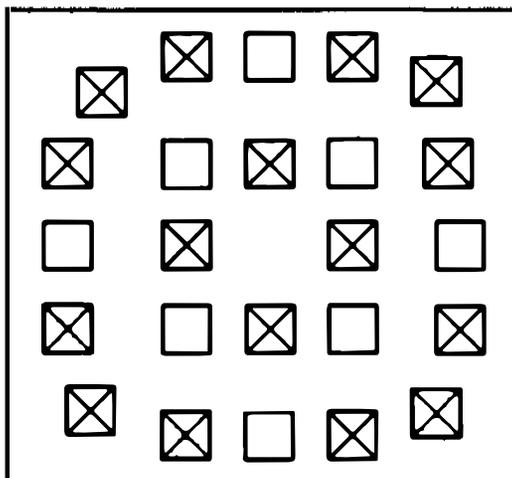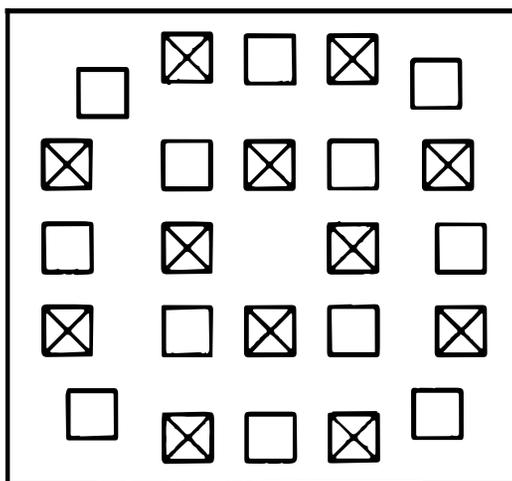UPDATED FINAL SAFETY ANALYSIS REPORT

FIGURE 4.3-3
TYPICAL BORON CONCENTRATION
VERSUS FIRST CYCLE BURNUP WITH &
WITHOUT BURNABLE ABSORBER RODS
BEAVER VALLEY POWER STATION-UNIT 2
UPDATED FINAL SAFETY ANALYSIS REPORT

20 BP

16 BP

12 BP

FIGURE 4.3-4
TYPICAL BURNABLE ABSORBER ROD
ARRANGEMENT WITHIN AN ASSEMBLY
BEAVER VALLEY POWER STATION-UNIT 2
UPDATED FINAL SAFETY ANALYSIS REPORT

CONFIGURATION FOR 16 IFBA ROD ASSEMBLY (17×17)

○ FUEL ROD

● FUEL ROD WITH IFBA

◯ GUIDE TUBE/INST TUBE

FIGURE 4.3-4a

TYPICAL BURNABLE ABSORBER ROD
ARRANGEMENT WITHIN AN ASSEMBLY
BEAVER VALLEY POWER STATION-UNIT 2
UPDATED FINAL SAFETY ANALYSIS REPORT

17×17 DEFAULT BURNABLE ABSORBER PATTERNS

32 IFBA'S

48 IFBA'S

64 IFBA'S

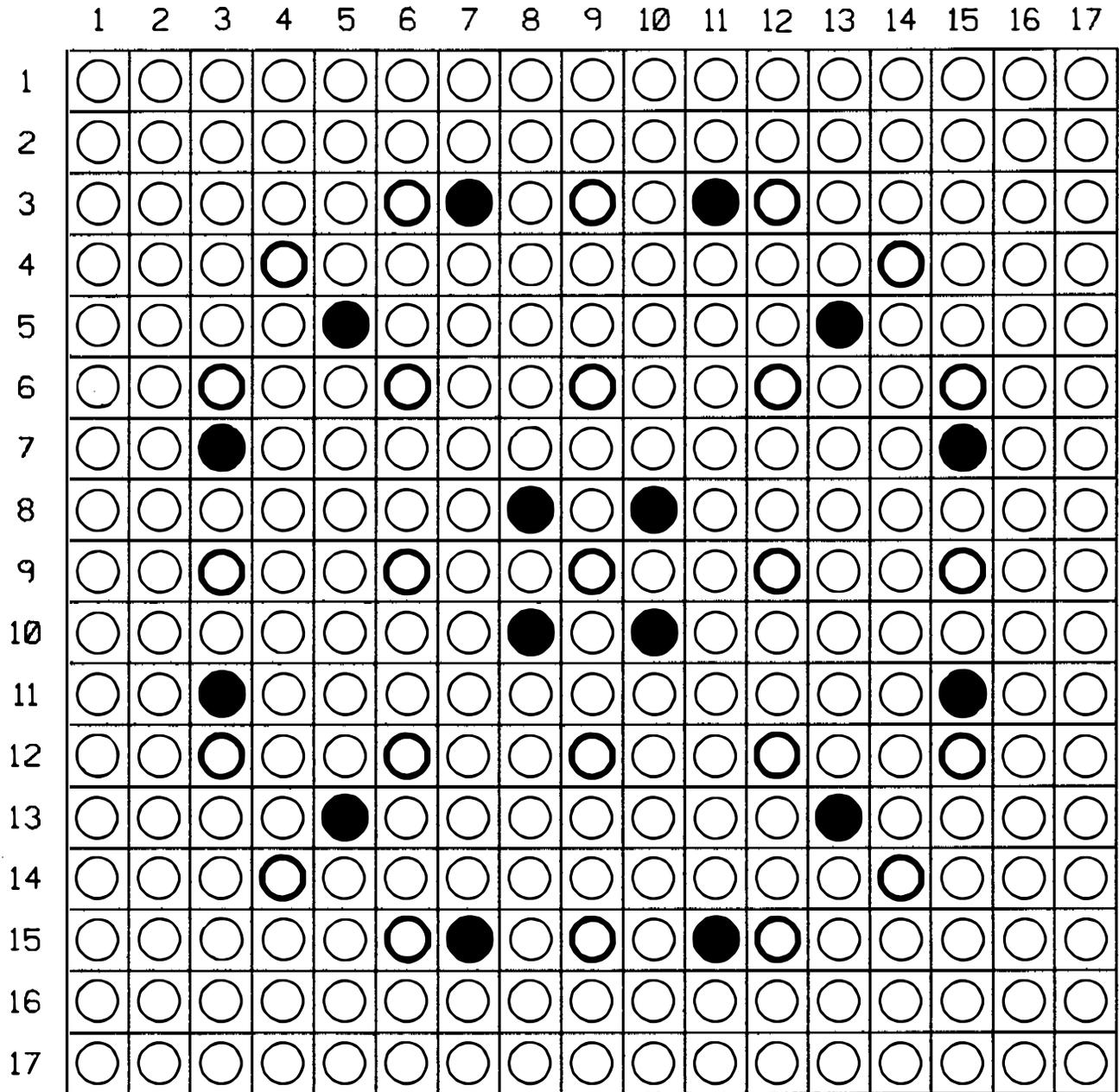80 IFBA'S

○ FUEL ROD

● FUEL ROD WITH IFBA

○ GUIDE TUBE/INST TUBE

FIGURE 4.3-4b

TYPICAL BURNABLE ABSORBER ROD
ARRANGEMENT WITHIN AN ASSEMBLY
BEAVER VALLEY POWER STATION-UNIT 2
UPDATED FINAL SAFETY ANALYSIS REPORT

17x17 DEFAULT BURNABLE ABSORBER PATTERNS

104 IFBA'S

128 IFBA'S
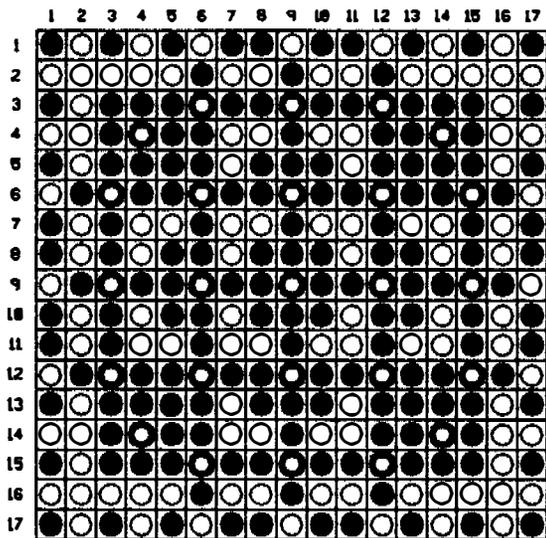
156 IFBA'S

○ FUEL ROD

● FUEL ROD WITH IFBA

◯ GUIDE TUBE/INST TUBE

FIGURE 4.3-4c
TYPICAL BURNABLE ABSORBER ROD ARRANGEMENT WITHIN AN ASSEMBLY
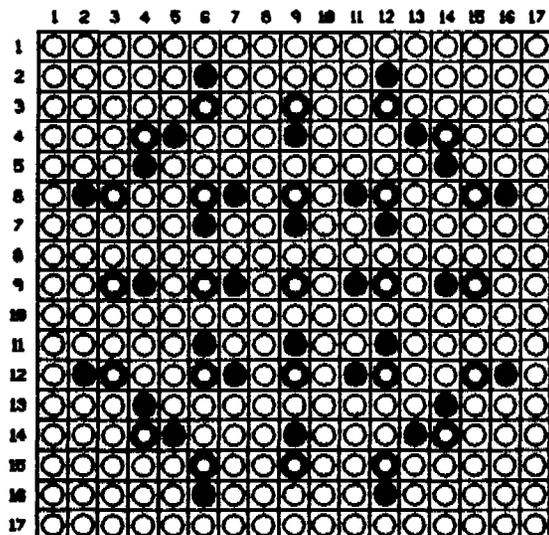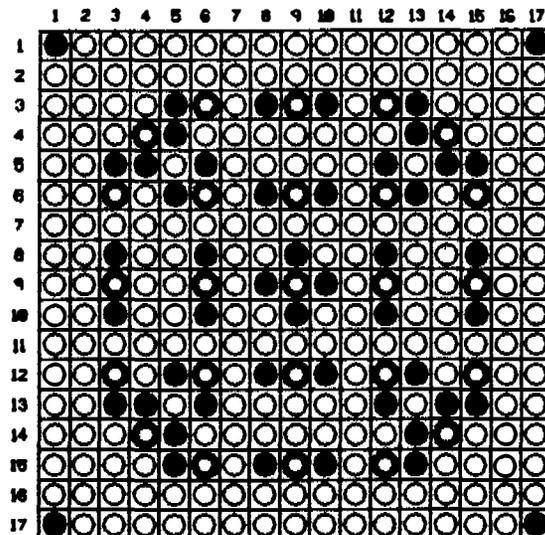BEAVER VALLEY POWER STATION-UNIT 2
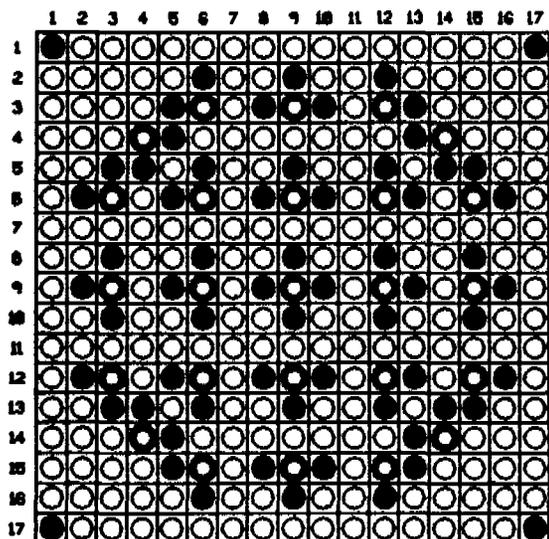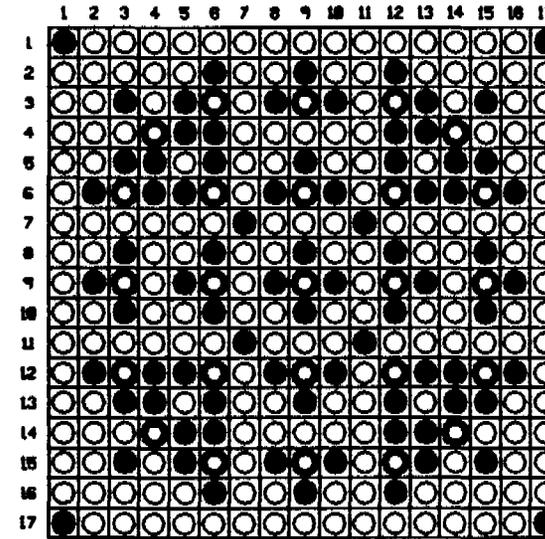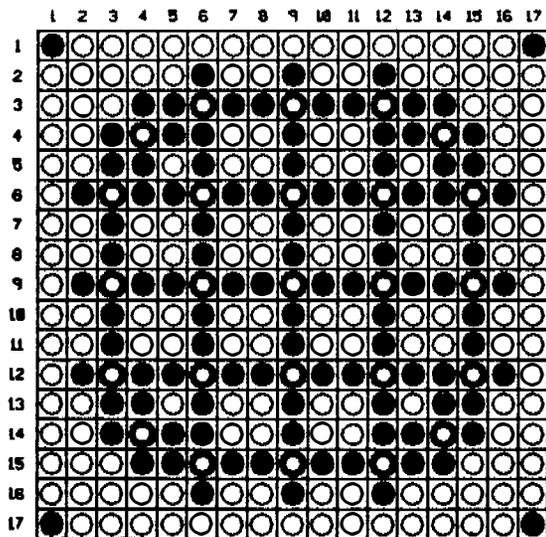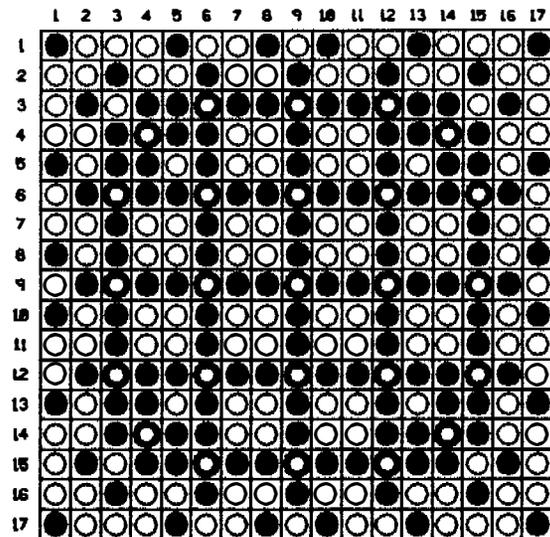UPDATED FINAL SAFETY ANALYSIS REPORT

180°

	R	P	N	M	L	K	J	H	G	F	E	D	C	B	A	
1																
2							P 80	48	80							
3			64			128		SS	128		64					
4				80		128		S		128		80				
5			64		128			128			128		64			
6				128		128			128			128				
7		80	128			128		128		128			128	80		
8		48			128		128		128		128			48		
9		80	128			128		128		128			128	80		
10				128			128		128			128				
11			64		128			128			128		64			
12				80		128		S		128		80				
13					64		128	SS	128		64					
14						80	48	P 80								
15																
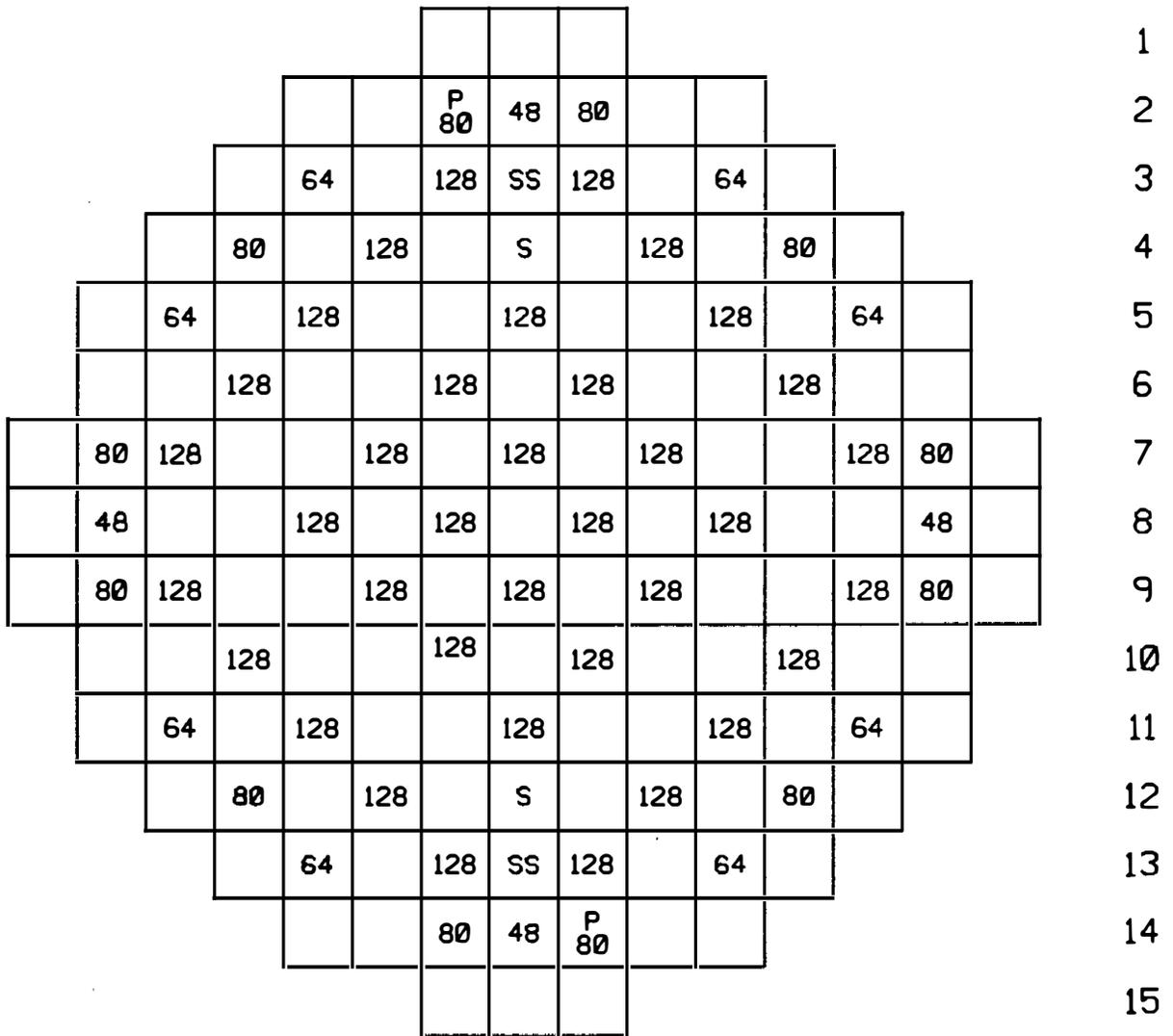
0°

NUMBER INDICATES NUMBER OF IFBA RODS
S INDICATES SECONDARY SOURCE RODS
P INDICATES PRIMARY RODS
SS INDICATES SECONDARY SOURCE RODS
   IN LATER CYCLES

} FIRST CORE ONLY

FIGURE 4.3-5
TYPICAL INTEGRAL FUEL BURNABLE ABSORBER LOADING PATTERN
BEAVER VALLEY POWER STATION-UNIT 2
UPDATED FINAL SAFETY ANALYSIS REPORT

CALCULATED $F_{\Delta H}^N$ = 1.33

KEY:
VALUE REPRESENTS ASSEMBLY
RELATIVE POWER

FIGURE 4.3-6
TYPICAL NORMALIZED POWER DENSITY
DISTRIBUTION NEAR BEGINNING OF LIFE,
UNRODDED CORE, HOT FULL POWER,
NO XENON
BEAVER VALLEY POWER STATION-UNIT 2
UPDATED FINAL SAFETY ANALYSIS REPORT

	H	G	F	E	D	C	B	A
8	1.14							
9	1.11	1.18						
10	1.18	1.19	1.20					
11	1.13	1.19	1.16	1.11				
12	1.19	1.15	1.11	.99	.85			
13	1.18	1.12	1.00	.91	.63			
14	1.03	1.00	.88	.59				
15	.78	.60						

CALCULATED $F_{\Delta H}^{N} = 1.31$

KEY:
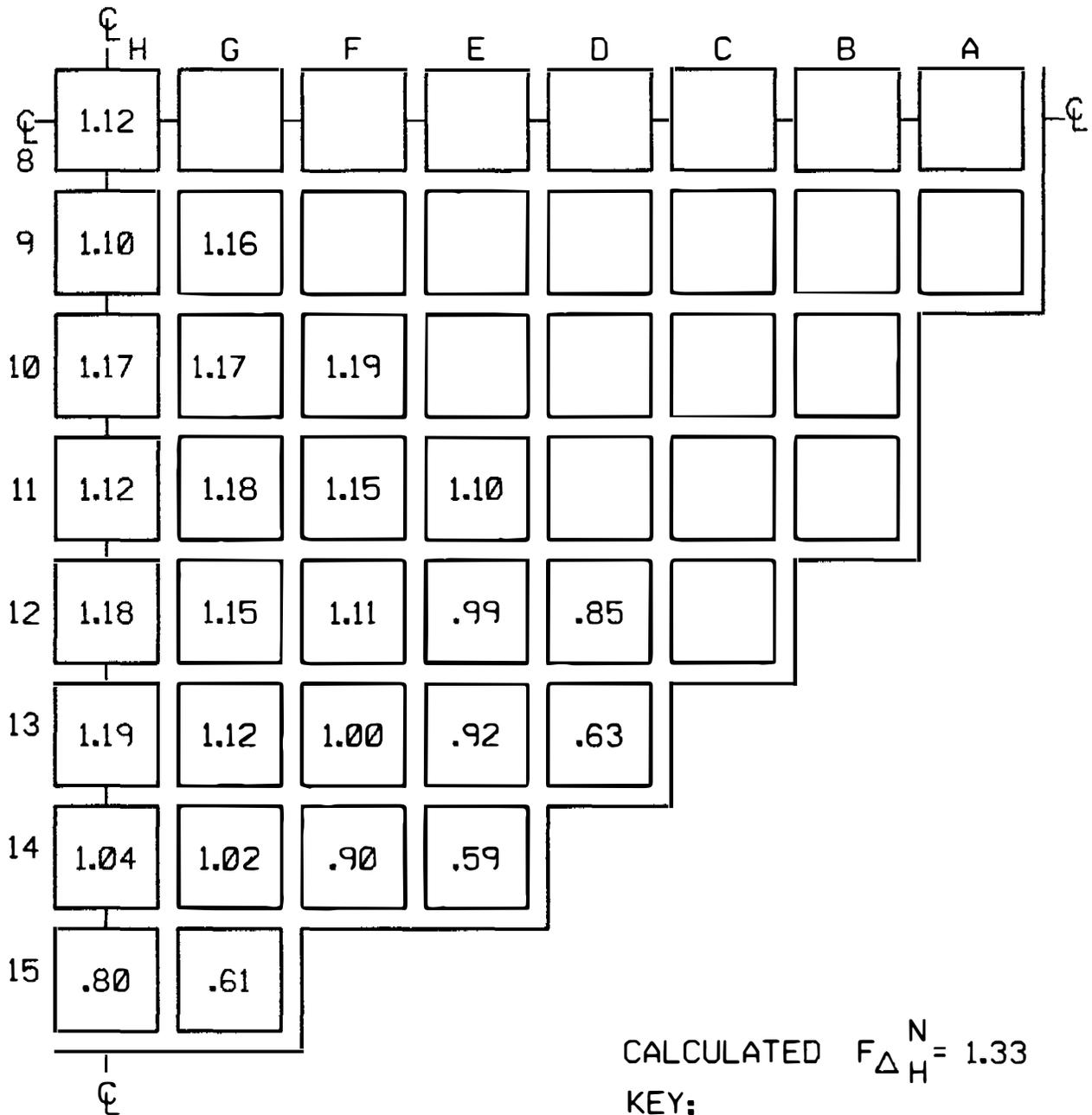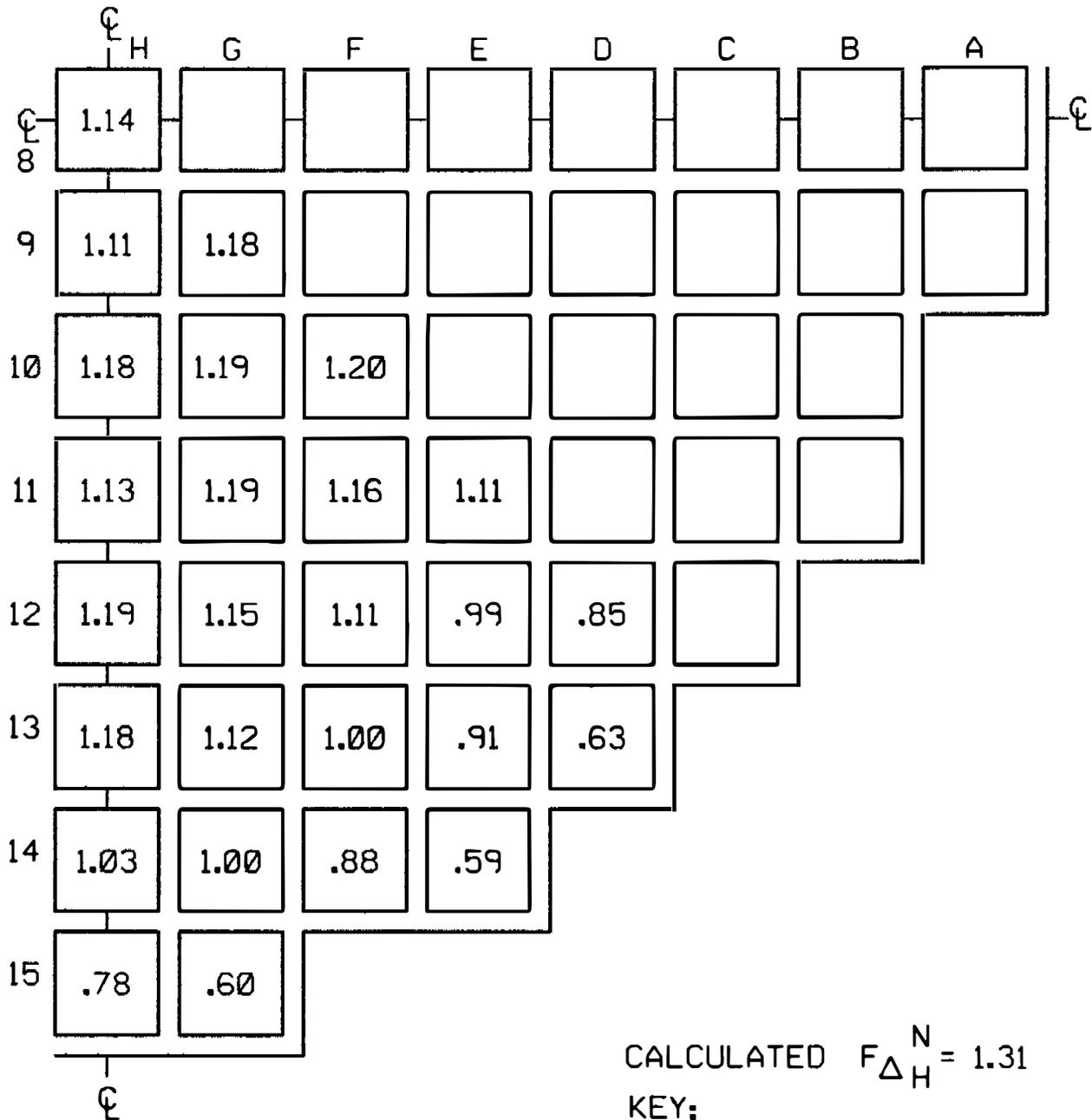VALUE REPRESENTS ASSEMBLY
RELATIVE POWER

FIGURE 4.3-7
TYPICAL NORMALIZED POWER DENSITY
DISTRIBUTION NEAR BEGINNING OF LIFE,
UNRODDED CORE, HOT FULL POWER,
EQUILIBRIUM XENON
BEAVER VALLEY POWER STATION-UNIT 2
UPDATED FINAL SAFETY ANALYSIS REPORT

	H	G	F	E	D	C	B	A
8	1.18							
9	1.14	1.21						
10	1.22	1.20	1.15					
11	1.16	1.22	1.17	1.14				
12	1.23	1.19	1.15	1.02	.85			
13	1.20	1.14	1.01	.93	.59			
14	.95	.98	.87	.53				
15	.70	.51						

CALCULATED $F_{\Delta H}^{N} = 1.332$

KEY:
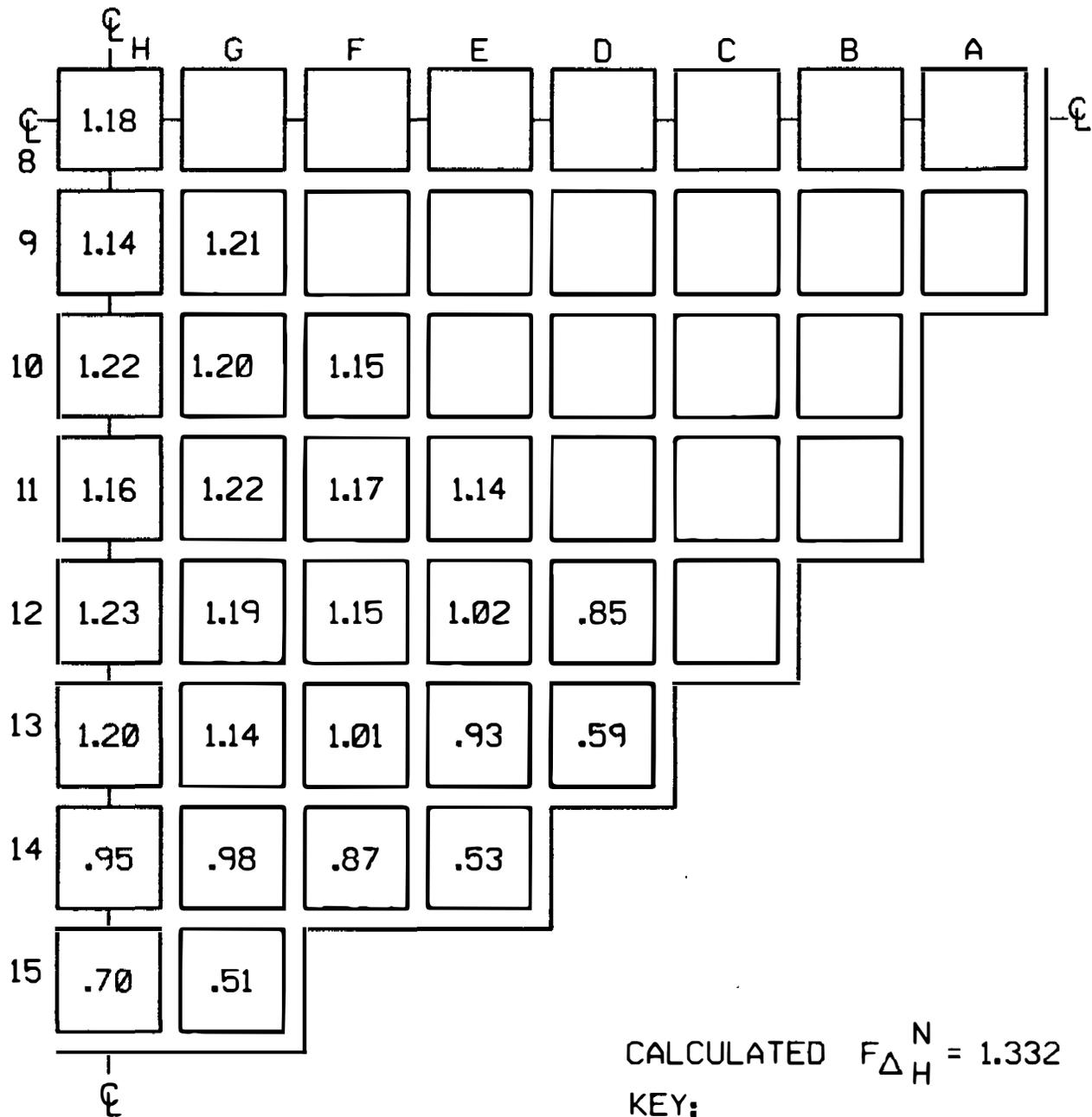VALUE REPRESENTS ASSEMBLY
RELATIVE POWER

FIGURE 4.3-8

TYPICAL NORMALIZED POWER DENSITY
DISTRIBUTION NEAR BEGINNING OF LIFE,
GROUP D 30% INSERTED, HOT FULL POWER,
EQUILIBRIUM XENON

BEAVER VALLEY POWER STATION-UNIT 2
UPDATED FINAL SAFETY ANALYSIS REPORT

	H	G	F	E	D	C	B	A
8	1.14							
9	1.22	1.14						
10	1.14	1.23	1.14					
11	1.21	1.13	1.21	1.09				
12	1.11	1.19	1.09	1.10	.87			
13	1.15	1.05	1.07	.99	.65			
14	.92	.98	.84	.59				
15	.68	.55						

CALCULATED $F_{\Delta H}^{N}$ = 1.26

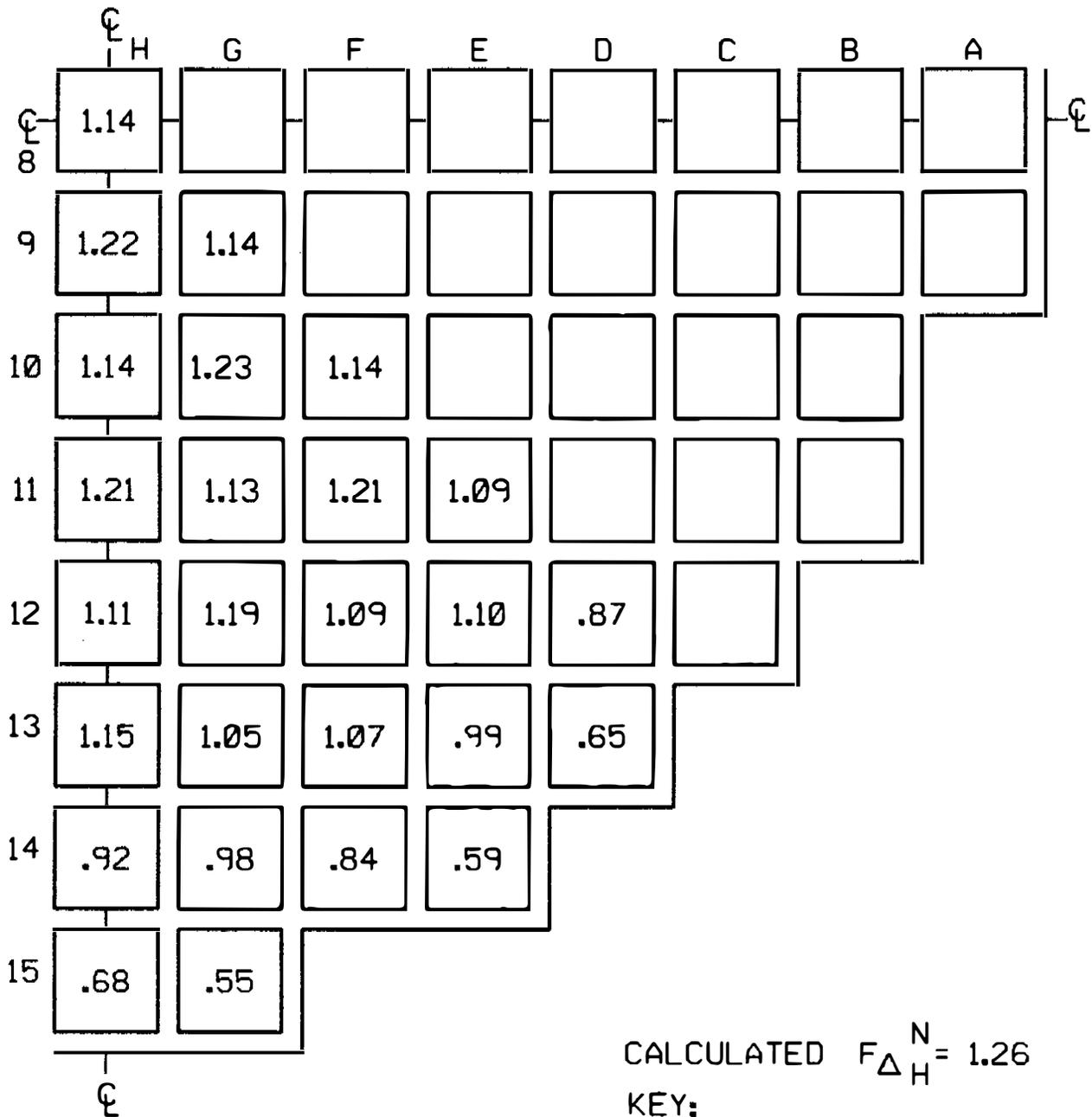KEY:
VALUE REPRESENTS ASSEMBLY
RELATIVE POWER

FIGURE 4.3-9
TYPICAL NORMALIZED POWER DENSITY
DISTRIBUTION NEAR MIDDLE OF LIFE,
UNRODDED CORE, HOT FULL POWER,
EQUILIBRIUM XENON
BEAVER VALLEY POWER STATION-UNIT 2
UPDATED FINAL SAFETY ANALYSIS REPORT

	H	G	F	E	D	C	B	A
8	1.04							
9	1.12	1.04						
10	1.05	1.13	1.05					
11	1.14	1.06	1.15	1.06				
12	1.06	1.15	1.07	1.13	.92			
13	1.14	1.05	1.10	1.06	.71			
14	.97	1.06	.89	.65				
15	.75	.63						

CALCULATED $F_{\Delta H}^{N} = 1.21$

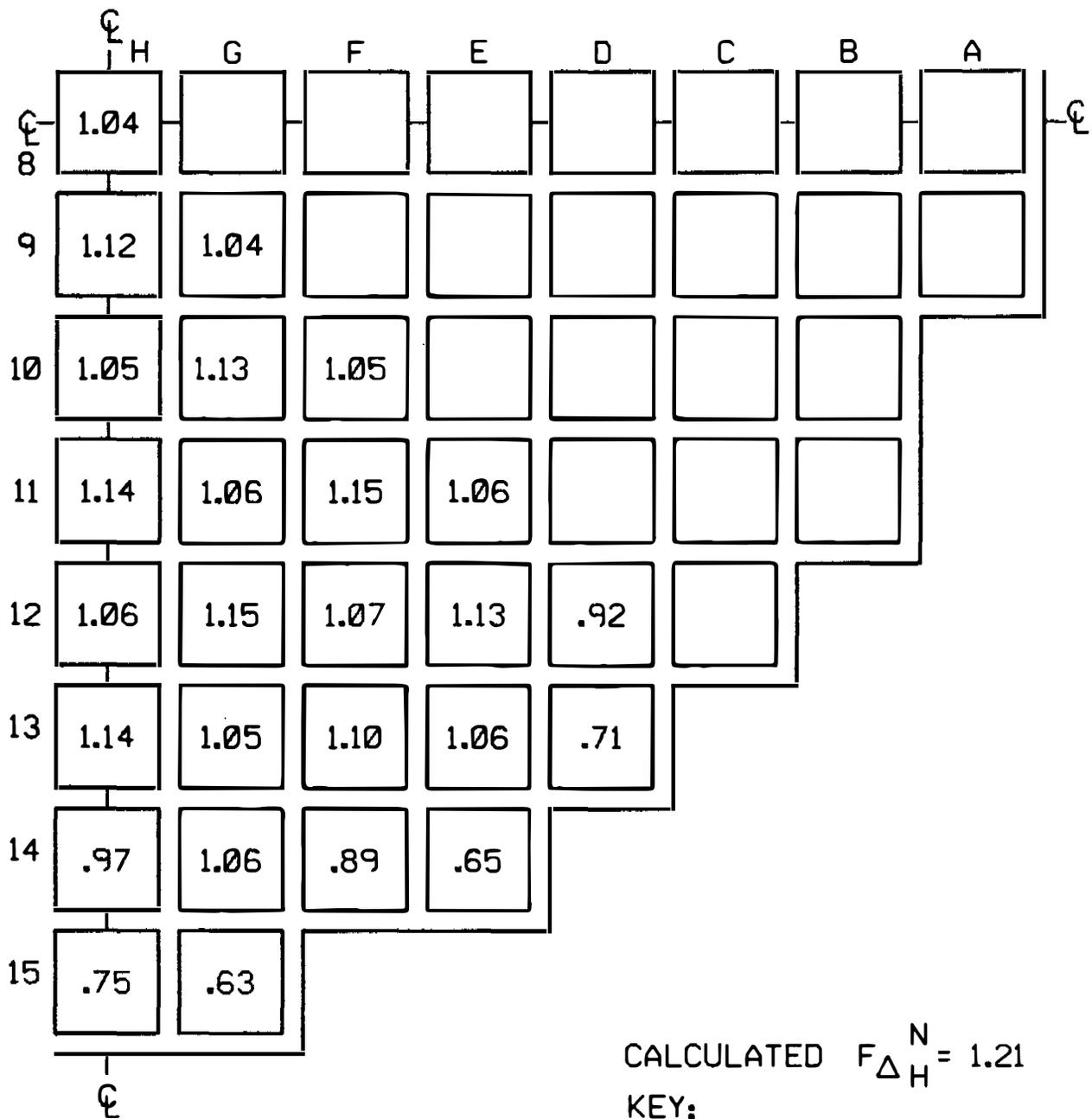KEY:
VALUE REPRESENTS ASSEMBLY
RELATIVE POWER

FIGURE 4.3-10
TYPICAL NORMALIZED POWER DENSITY
DISTRIBUTION NEAR END OF LIFE,
UNRODDED CORE, HOT FULL POWER,
EQUILIBRIUM XENON
BEAVER VALLEY POWER STATION-UNIT 2
UPDATED FINAL SAFETY ANALYSIS REPORT

L125

L123	L133

L124	L147	L179

L128	L165	L223	X

L134	L179	L241	L264	L255

L141	L203	X	L265	L271	X

L143	L167	L239	L234	L243	L270	L247

L148	L188	L239	L232	L241	L269	L247	1.248

L154	L208	X	L254	L264	X	L271	L271	X

L147	L187	L238	L238	L239	L268	L246	L246	L269	L244

L141	L185	L237	L232	L248	L267	L244	L244	L267	L242	L240

L139	L201	X	L261	L267	X	L265	L264	X	L262	L260	X

L131	L176	L237	L260	L258	L265	L236	L234	L256	L231	L231	L257	L248

L125	L160	L218	X	L258	L258	L226	L223	L245	L228	L221	L250	L247	X

L120	L142	L173	L216	L233	X	L230	L228	X	L226	L224	X	L222	L202	L157

L118	L127	L140	L157	L171	L184	L176	L177	L195	L174	L170	L185	L160	L143	L124	L108

L119	L116	L117	L120	L125	L131	L131	L135	L140	L132	L125	L122	L113	L105	L099	L096	L096

FIGURE 4.3-11
TYPICAL RODWISE POWER DISTRIBUTION
IN A TYPICAL ASSEMBLY (F-10)
NEAR BOL, HFP, EQUILIBRIUM
XENON, UNRODDED CORE
BEAVER VALLEY POWER STATION-UNIT 2
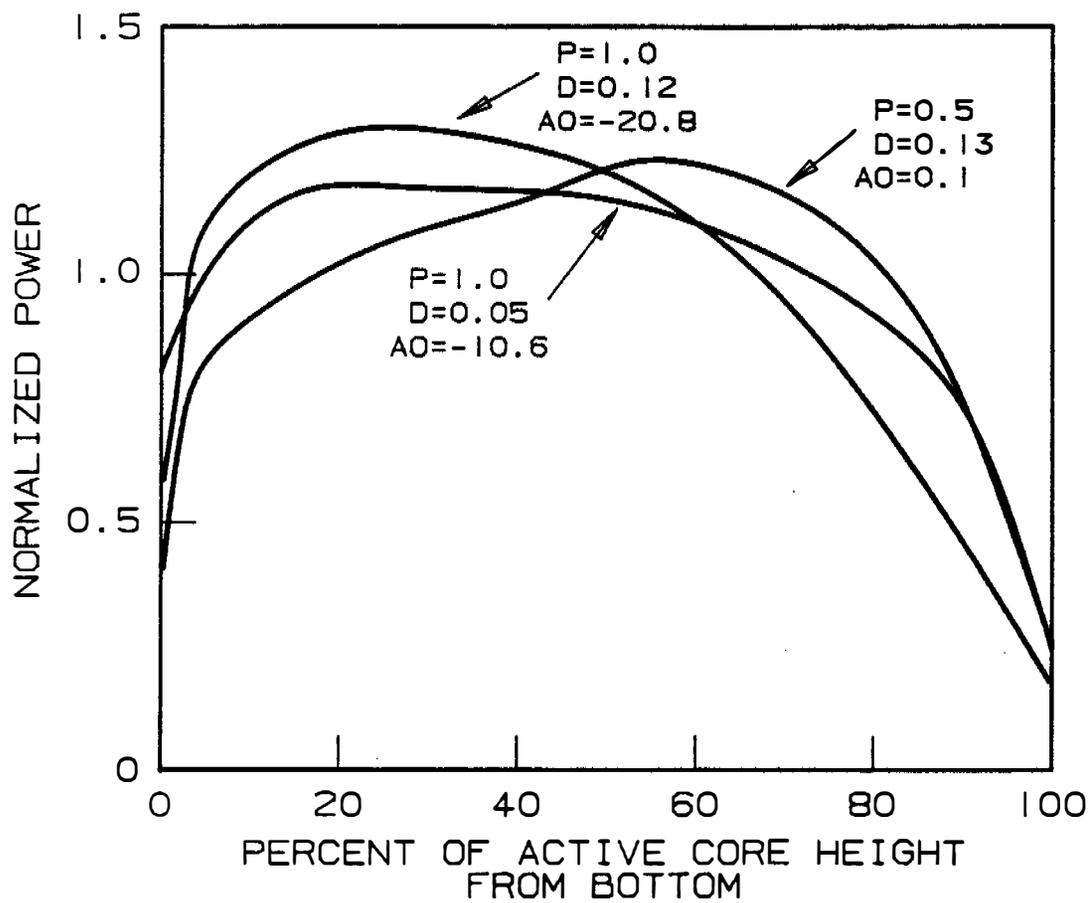UPDATED FINAL SAFETY ANALYSIS REPORT

0.988															
0.979	0.984														
0.983	0.997	1.024													
0.992	1.015	1.065	X												
1.002	1.030	1.082	1.098	1.085											
1.011	1.055	X	1.097	1.098	X										
1.009	1.036	1.078	1.085	1.089	1.093	1.069									
1.010	1.037	1.077	1.062	1.067	1.092	1.089	1.089								
1.016	1.057	X	1.086	1.090	X	1.093	1.093	X							
1.011	1.038	1.078	1.063	1.068	1.093	1.070	1.070	1.095	1.071						
1.011	1.038	1.080	1.067	1.071	1.095	1.071	1.071	1.095	1.072	1.073					
1.014	1.058	X	1.100	1.101	X	1.096	1.096	X	1.097	1.099	X				
1.005	1.034	1.086	1.102	1.089	1.102	1.073	1.071	1.095	1.072	1.075	1.105	1.093			
0.997	1.020	1.070	X	1.103	1.102	1.070	1.068	1.091	1.069	1.072	1.105	1.108	X		
0.989	1.003	1.030	1.071	1.088	X	1.084	1.083	X	1.084	1.086	X	1.092	1.077	1.035	
0.985	0.991	1.003	1.022	1.037	1.062	1.043	1.044	1.064	1.045	1.045	1.065	1.041	1.026	1.009	0.997
0.987	0.986	0.991	0.999	1.009	1.019	1.017	1.018	1.023	1.019	1.018	1.021	1.013	1.004	0.996	0.992

FIGURE 4.3-12
TYPICAL RODWISE POWER DISTRIBUTION
IN A TYPICAL ASSEMBLY (F-10)
NEAR EOL, HFP, EQUILIBRIUM
XENON, UNRODDED CORE
BEAVER VALLEY POWER STATION-UNIT 2
UPDATED FINAL SAFETY ANALYSIS REPORT

FIGURE 4.3-13
TYPICAL AXIAL POWER SHAPES
OCCURING AT BEGINNING-OF-LIFE
BEAVER VALLEY POWER STATION-UNIT 2
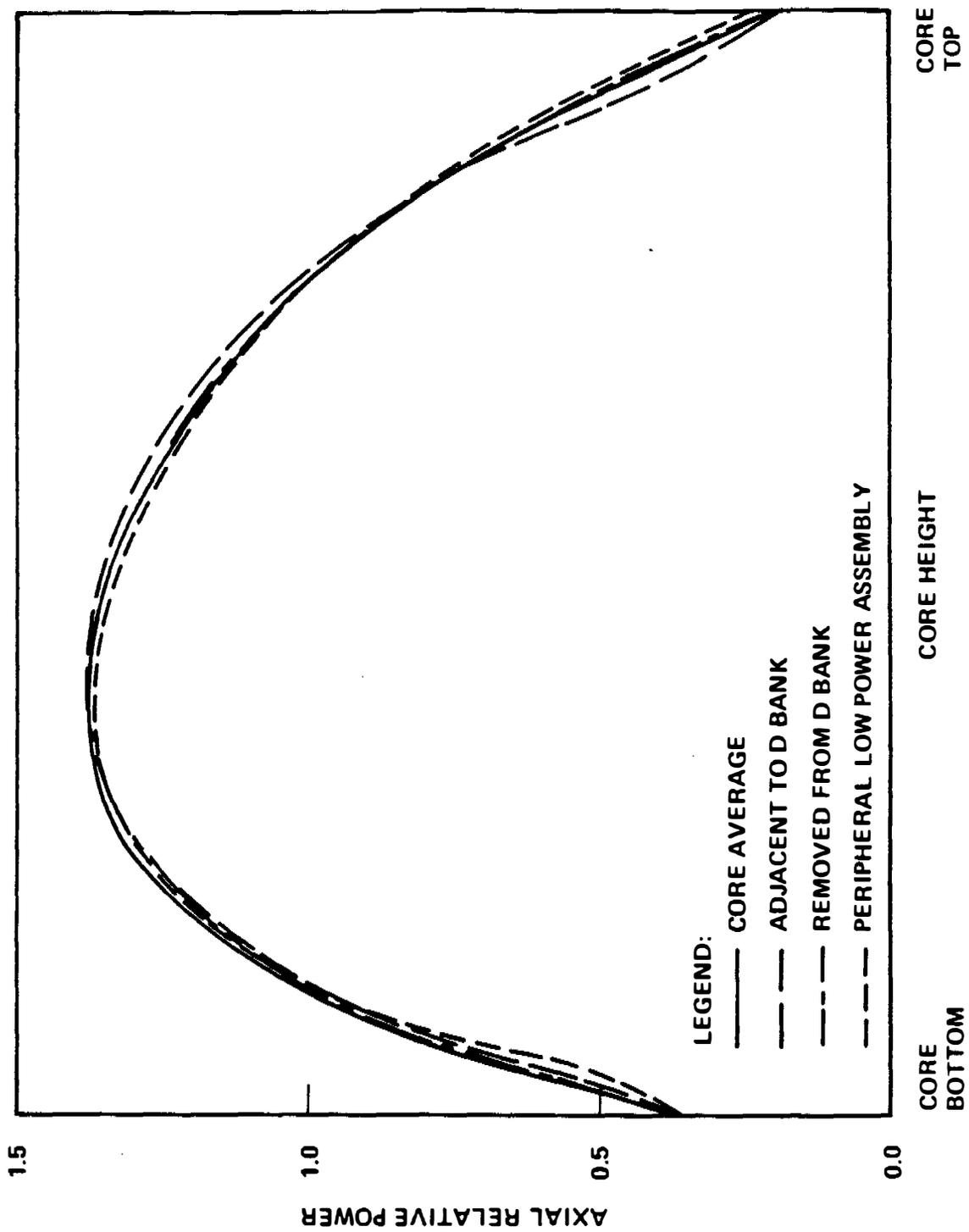FINAL SAFETY ANALYSIS REPORT

016-A-20921-1
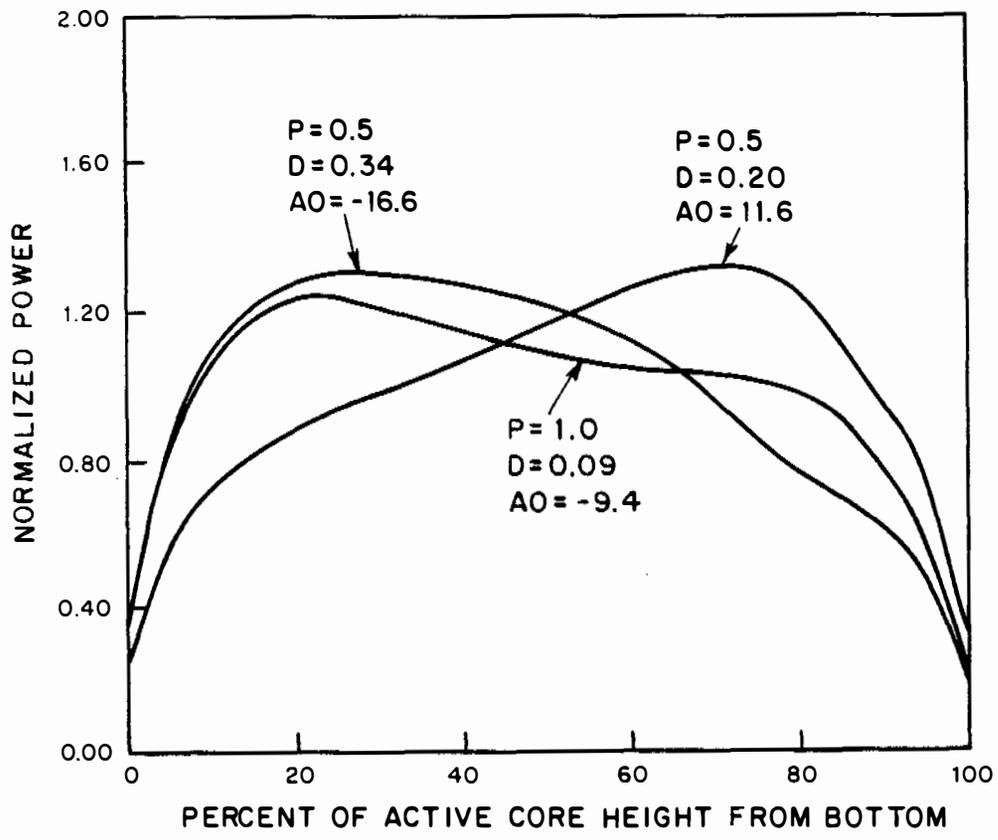
FIGURE 4.3-14
**TYPICAL AXIAL POWER SHAPES
OCCURING AT MIDDLE-OF-LIFE**
BEAVER VALLEY POWER STATION-UNIT 2
FINAL SAFETY ANALYSIS REPORT
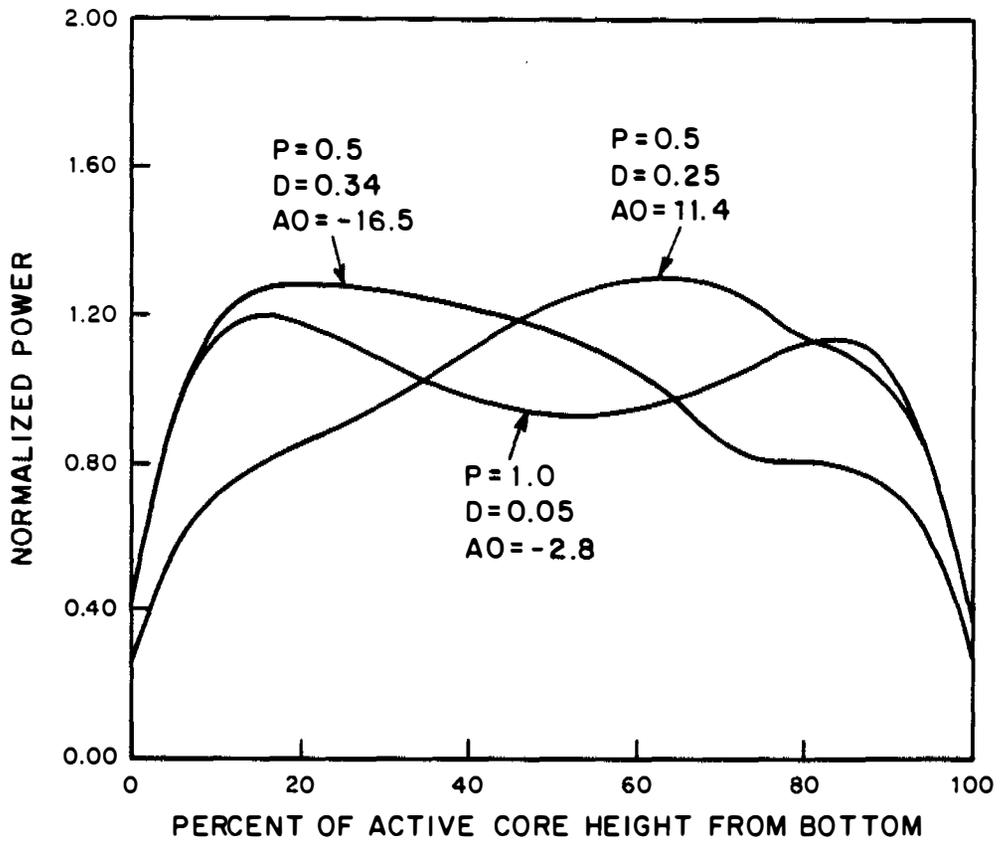
FIGURE 4.3-15
TYPICAL AXIAL POWER SHAPES
OCCURING AT END-OF-LIFE
BEAVER VALLEY POWER STATION-UNIT 2
FINAL SAFETY ANALYSIS REPORT

LEGEND:
——— CORE AVERAGE
— — ADJACENT TO D BANK
— - — REMOVED FROM D BANK
— - - — PERIPHERAL LOW POWER ASSEMBLY

CORE
BOTTOM

CORE HEIGHT

CORE
TOP

AXIAL RELATIVE POWER

1.5
1.0
0.5
0.0

FIGURE 4.3 - 16
COMPARISON OF A TYPICAL ASSEMBLY
AXIAL POWER DISTRIBUTION WITH CORE
AVERAGE AXIAL DISTRIBUTION
BANK SLIGHTLY INSERTED
BEAVER VALLEY POWER STATION-UNIT 2
FINAL SAFETY ANALYSIS REPORT

2.40 - 0 ft.
2.40 - 6 ft.
2.22 - 12 ft.
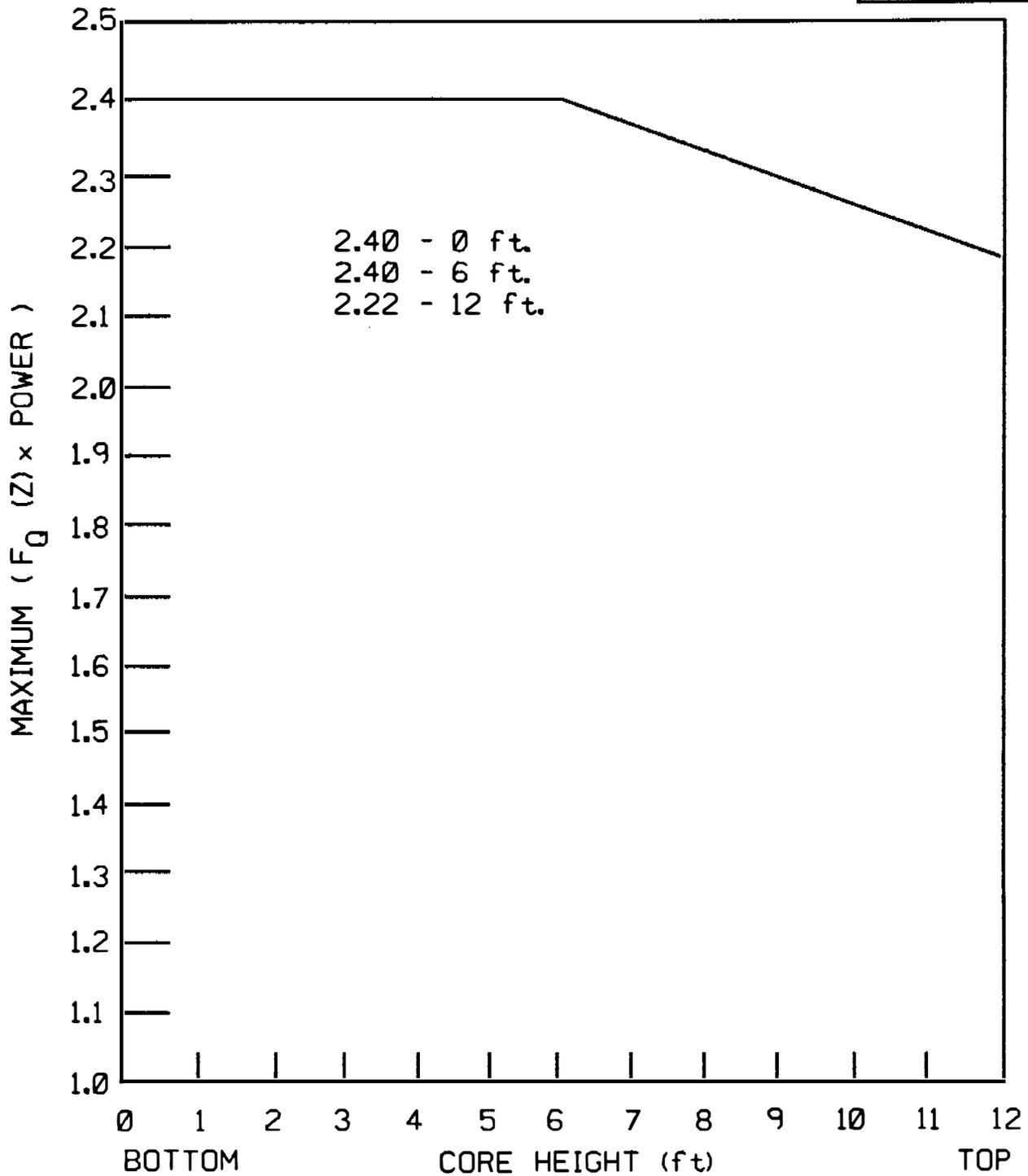
FIGURE 4.3-20

MAXIMUM F_Q × POWER vs. AXIAL
HEIGHT DURING NORMAL OPERATION

BEAVER VALLEY POWER STATION-UNIT 2
UPDATED FINAL SAFETY ANALYSIS REPORT
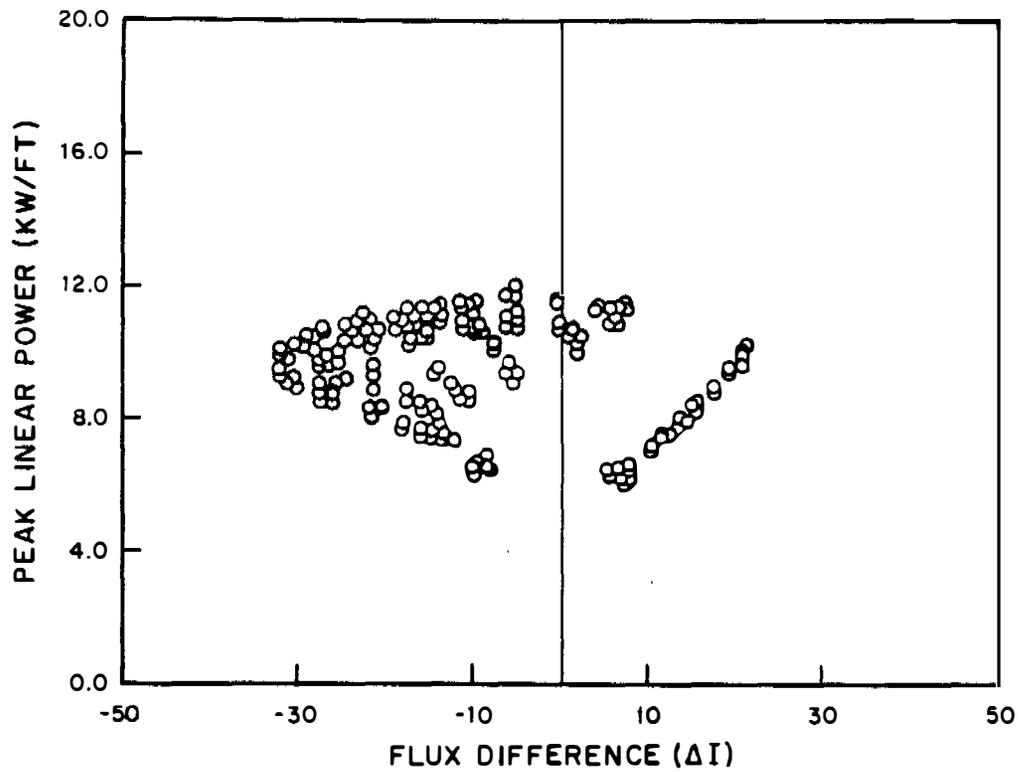
FIGURE 4.3-21
PEAK POWER DURING CONTROL
ROD MALFUNCTION OVERPOWER
TRANSIENTS
BEAVER VALLEY POWER STATION-UNIT 2
FINAL SAFETY ANALYSIS REPORT
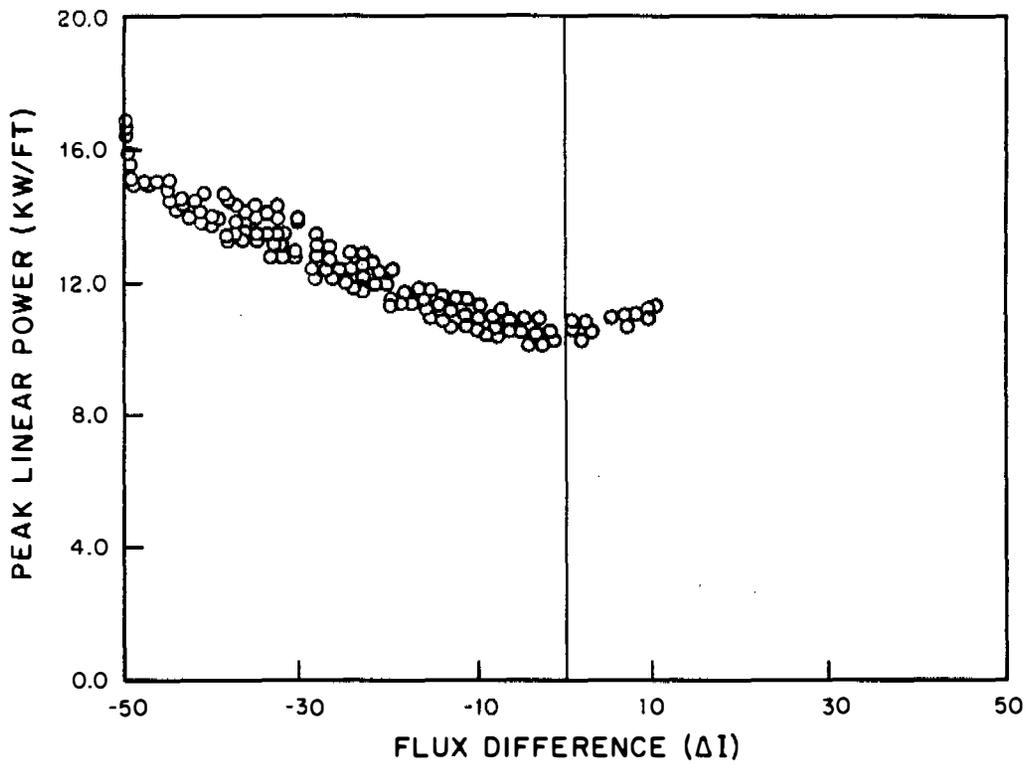
FIGURE 4.3-22
PEAK POWER DURING BORATION/
DILUTION OVERPOWER TRANSIENTS
BEAVER VALLEY POWER STATION-UNIT 2
FINAL SAFETY ANALYSIS REPORT
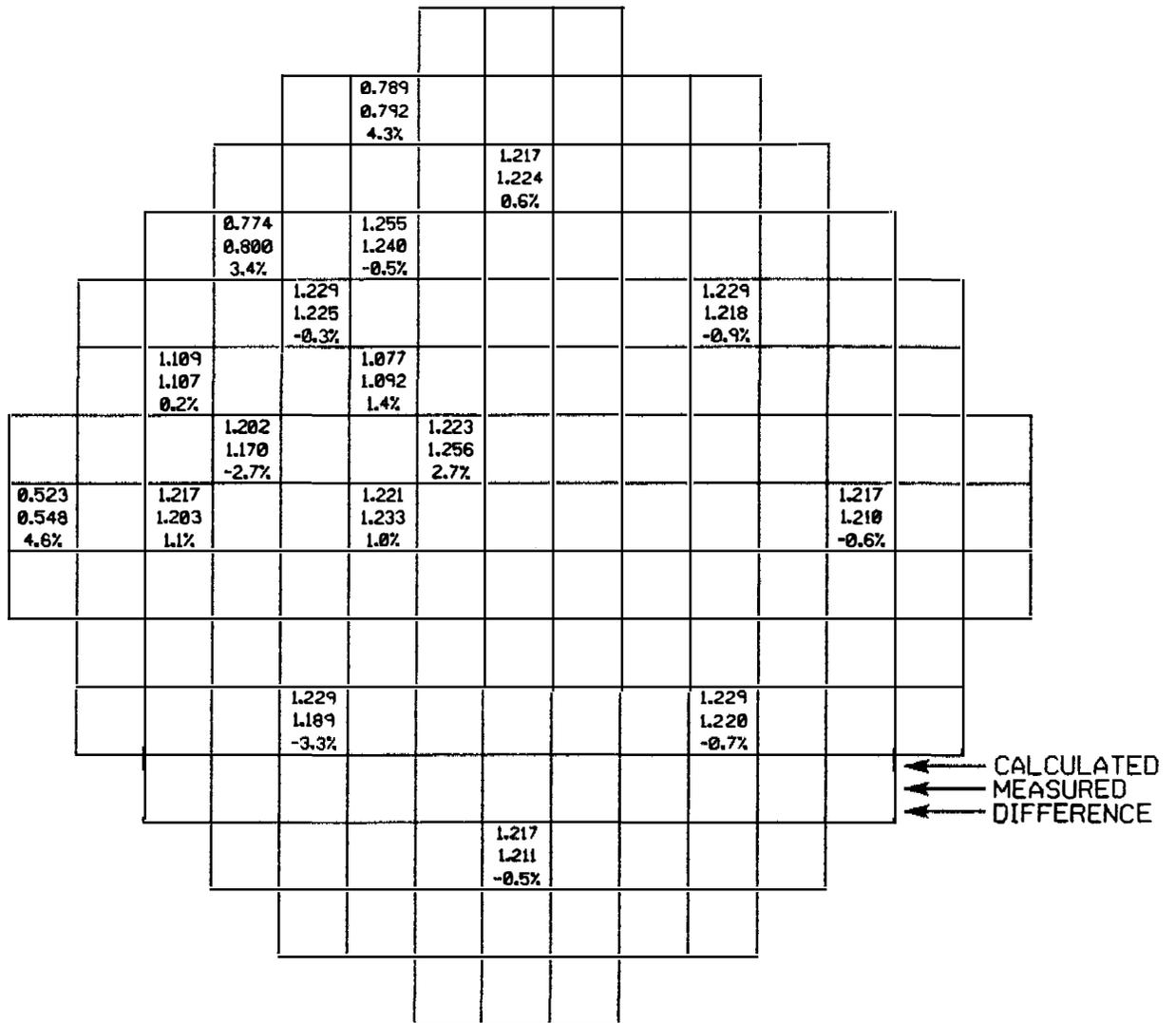
PEAKING FACTORS

$$\overline{F}_Z = 1.5$$

$$F_{\Delta H}^N = 1.357$$

$$F_Q^N = 2.07$$

FIGURE 4.3-23

TYPICAL COMPARISON BETWEEN CALCULATED
AND MEASURED RELATIVE FUEL ASSEMBLY
POWER DISTRIBUTION

BEAVER VALLEY POWER STATION-UNIT 2
UPDATED FINAL SAFETY ANALYSIS REPORT

BOL NO XENON
POWER AT 70%
BANK D 25% INSERTED

CALCULATED
AO = 3%

CORE AVERAGE
FROM INCORE MAP
AO = 2%

PERCENT OF CORE HEIGHT

AXIAL RELATIVE POWER
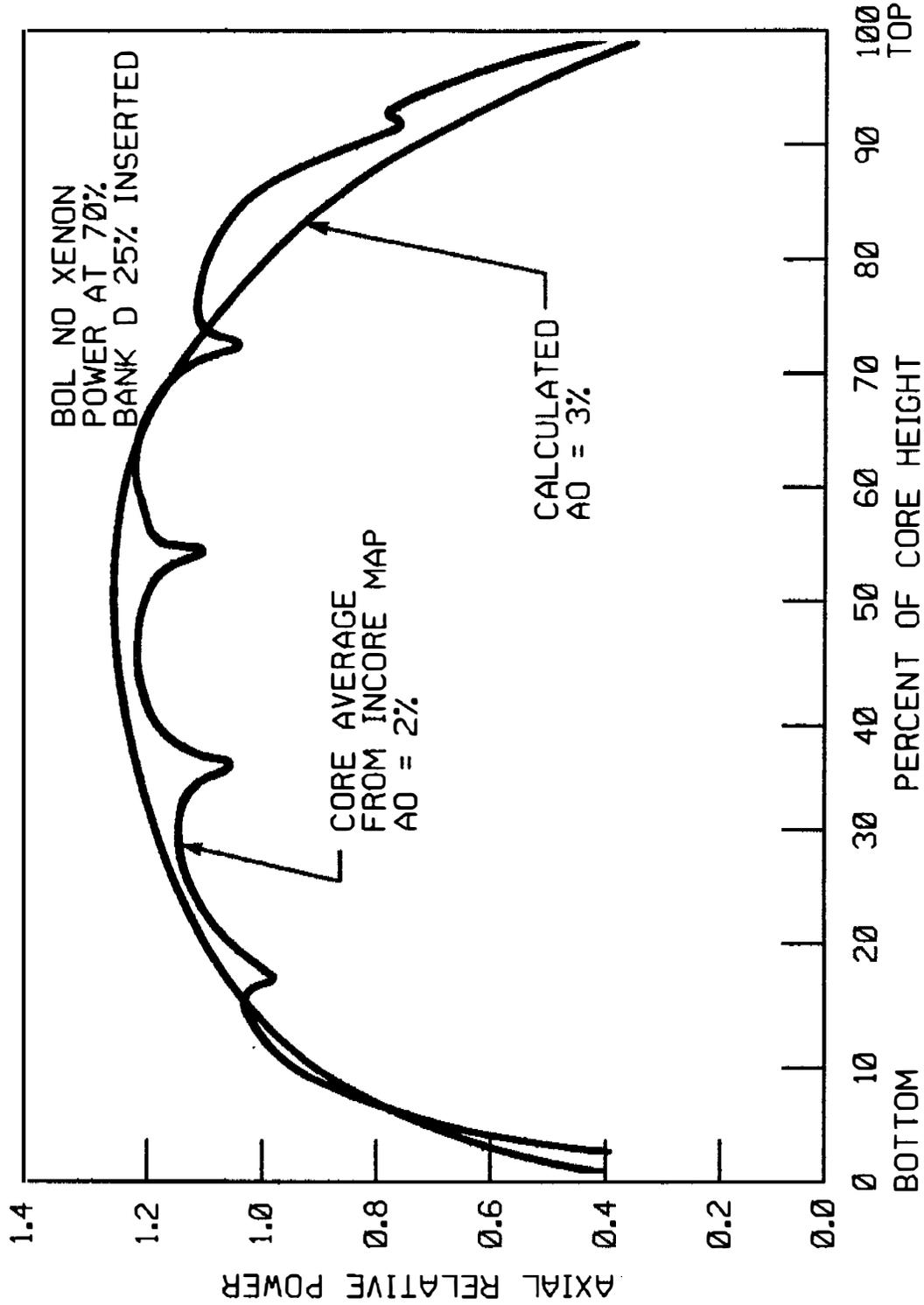
FIGURE 4.3-24

TYPICAL COMPARISON OF TYPICAL
CALCULATED & MEASURED AXIAL SHAPES

BEAVER VALLEY POWER STATION-UNIT 2
UPDATED FINAL SAFETY ANALYSIS REPORT
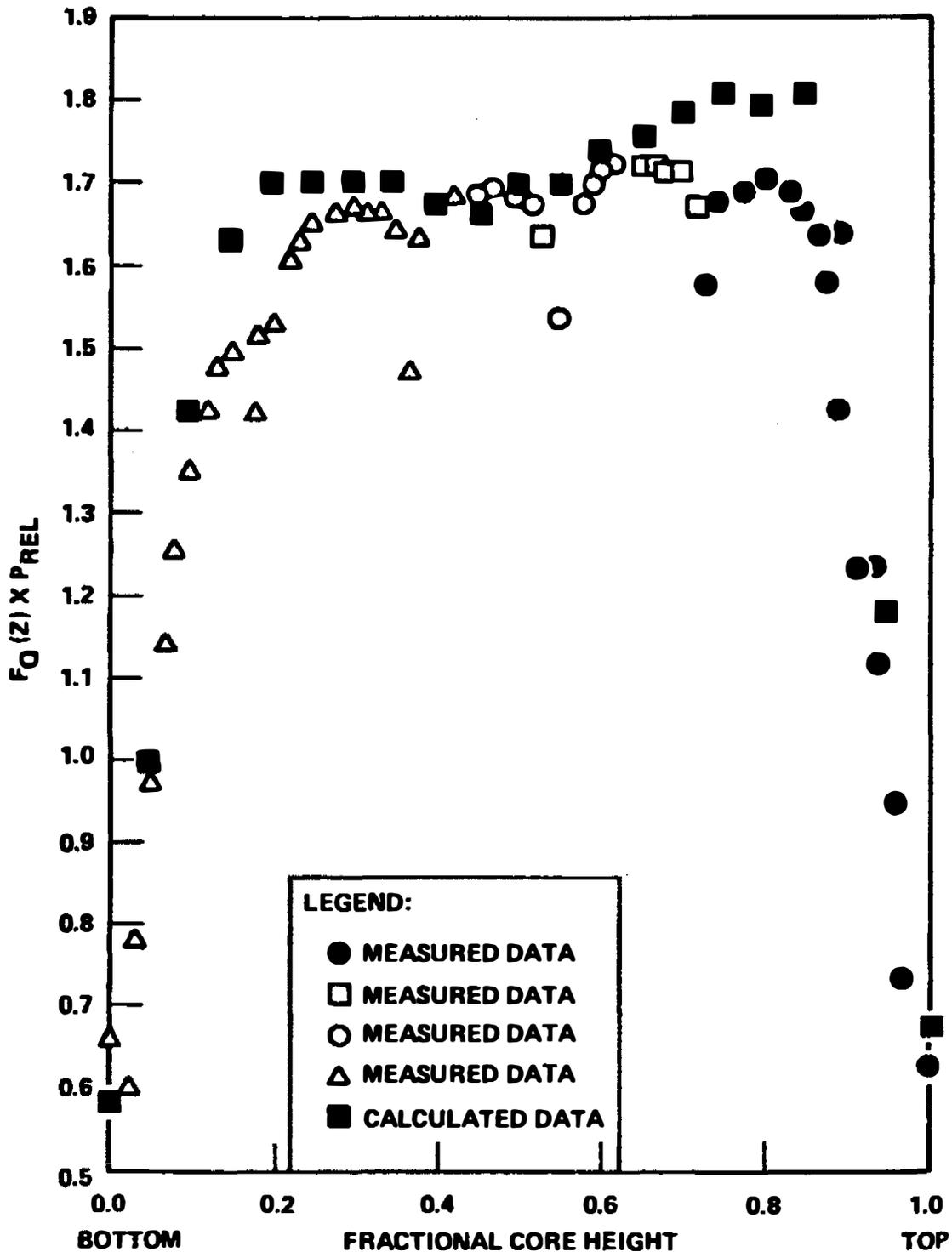
FIGURE 4.3-25

TYPICAL COMPARISON OF CALCULATED
AND MEASURED PEAKING FACTORS,
$F_Q \times P_{REL}$ MAX. ENVELOPE AS A
FUNCTION OF CORE HEIGHT

BEAVER VALLEY POWER STATION-UNIT 2
UPDATED FINAL SAFETY ANALYSIS REPORT
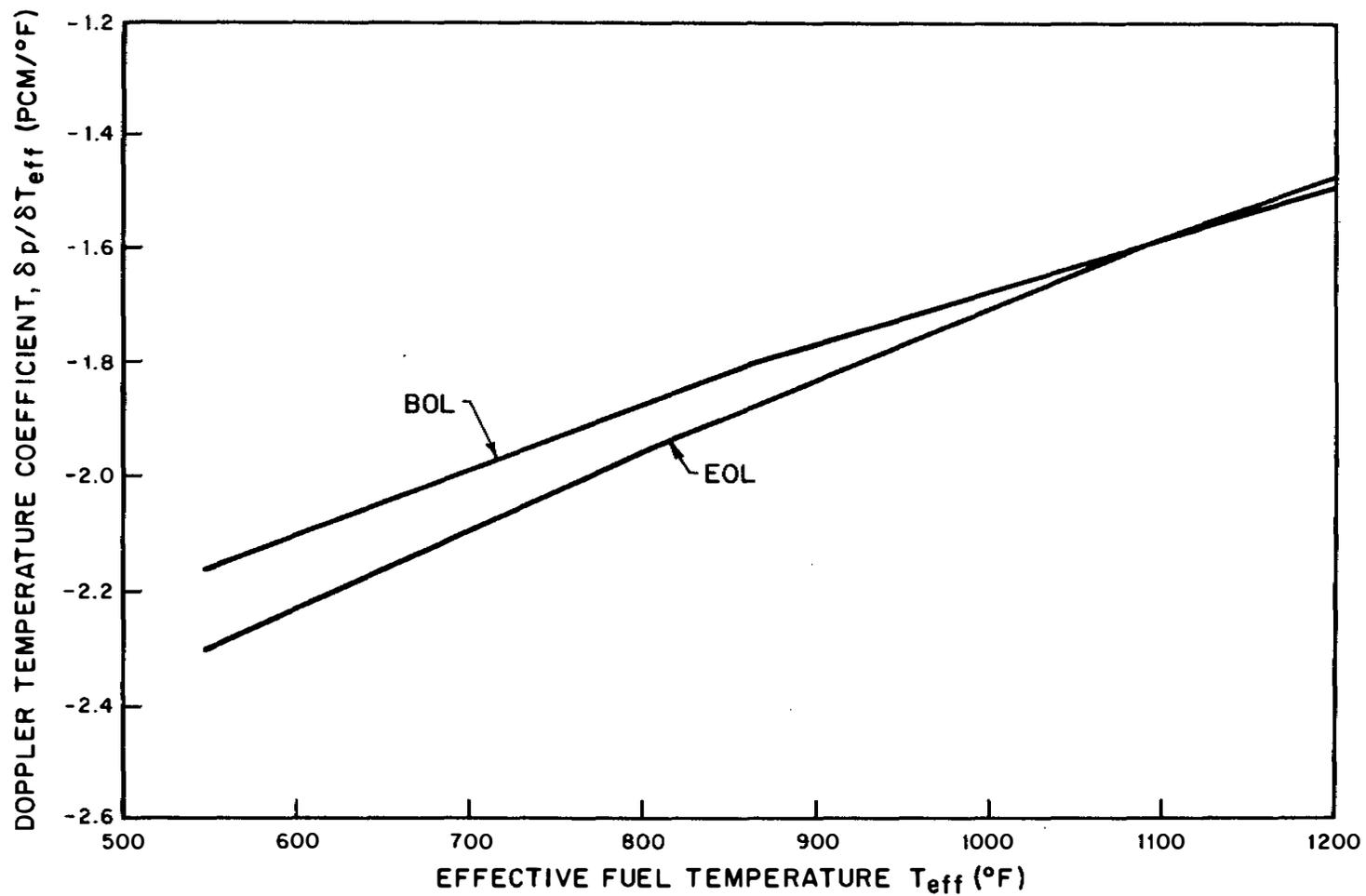
FIGURE 4.3-26
DOPPLER TEMPERATURE COEFFICIENT
AT BOL AND EOL VERSUS T_{EFF}
FOR CYCLE 1
BEAVER VALLEY POWER STATION -UNIT 2
FINAL SAFETY ANALYSIS REPORT
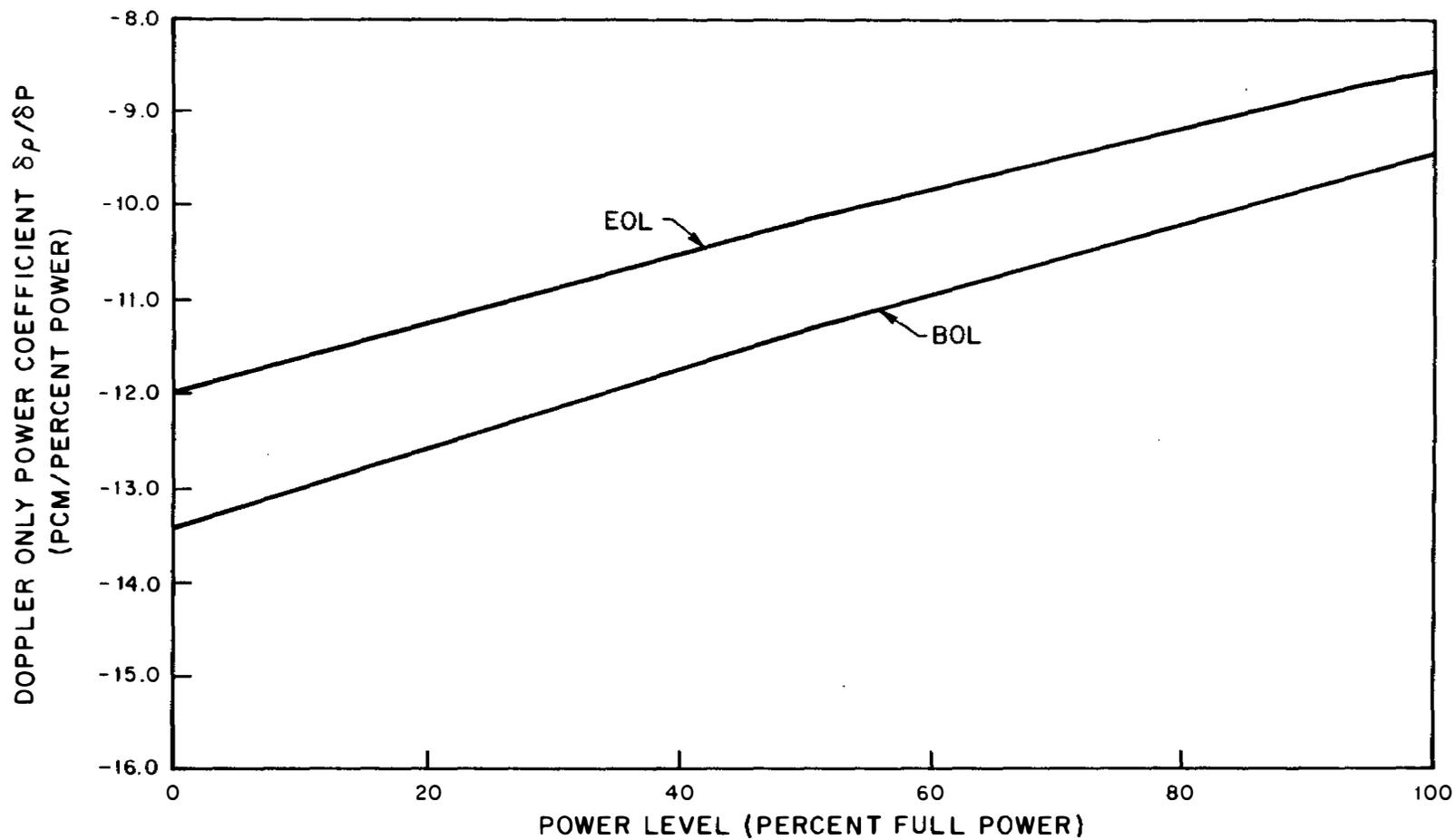
FIGURE 4.3-27
DOPPLER ONLY POWER COEFFICIENT
VERSUS POWER LEVEL AT
BOL AND EOL, CYCLE 1
BEAVER VALLEY POWER STATION-UNIT 2
FINAL SAFETY ANALYSIS REPORT
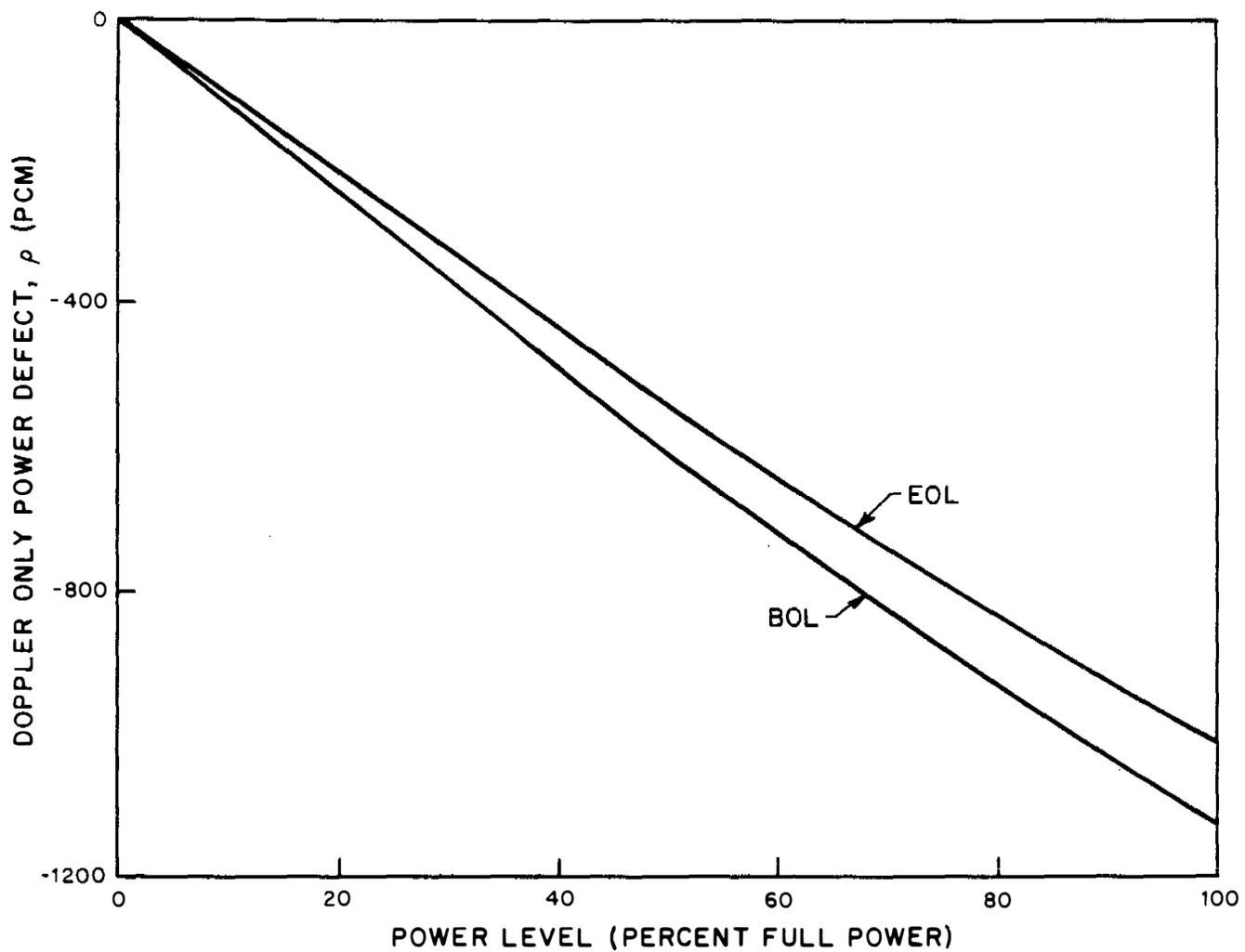
FIGURE 4.3-28
DOPPLER ONLY POWER DEFECT
VERSUS PERCENT POWER,
BOL AND EOL, CYCLE 1
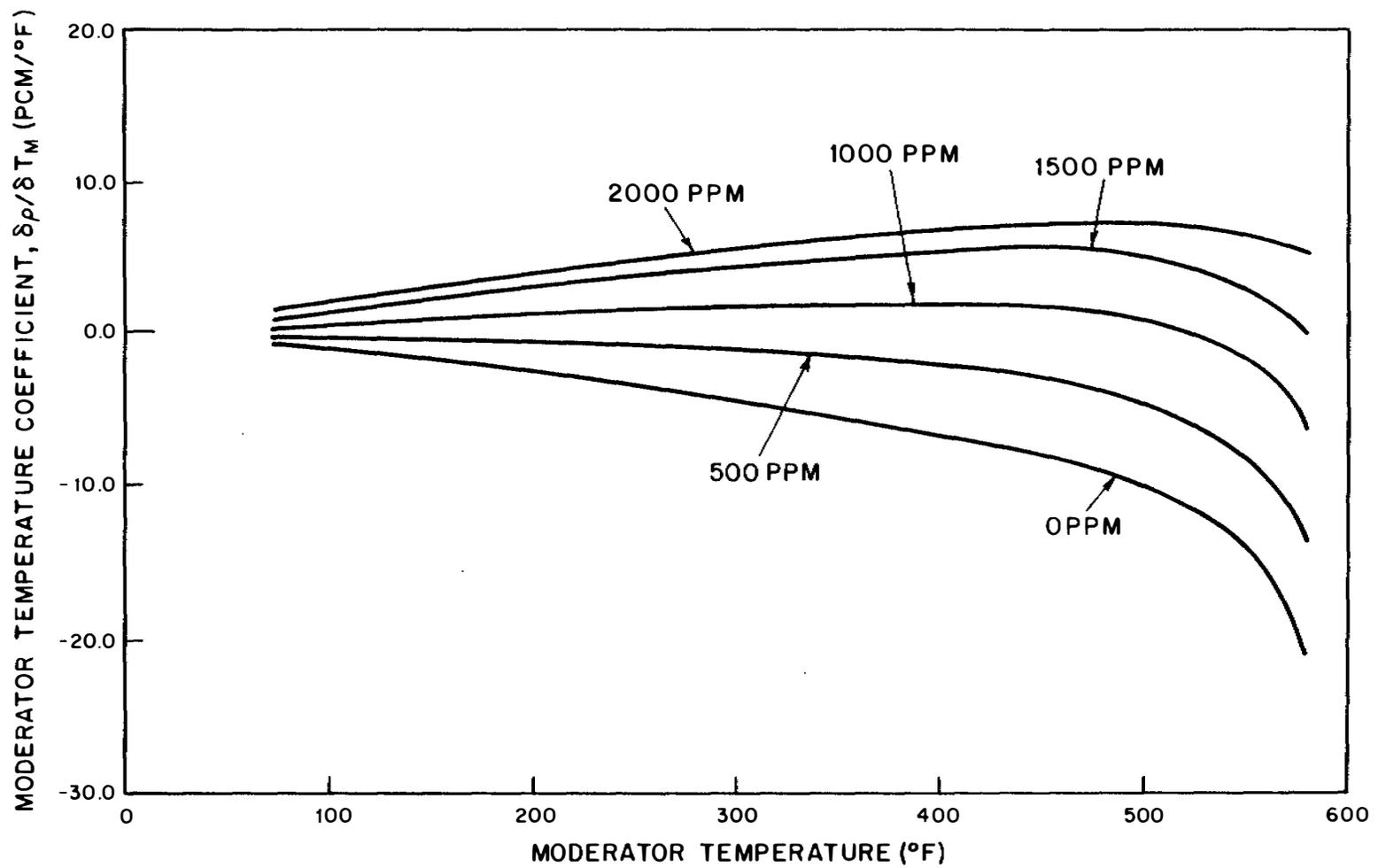BEAVER VALLEY POWER STATION-UNIT 2
FINAL SAFETY ANALYSIS REPORT

FIGURE 4.3-29

TYPICAL MODERATOR TEMPERATURE
COEFFICIENT AT BOL, CYCLE 1 NO RODS
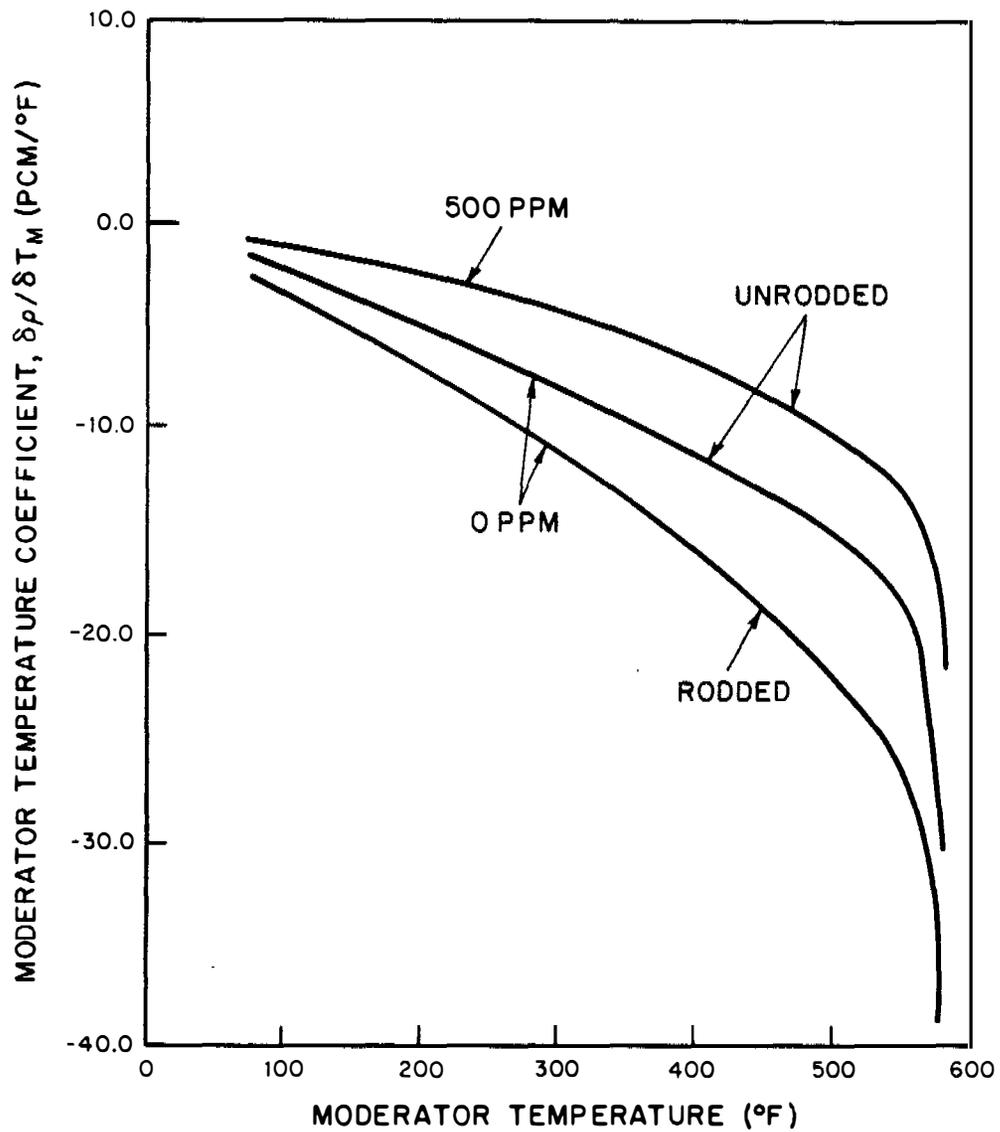BEAVER VALLEY POWER STATION-UNIT 2
FINAL SAFETY ANALYSIS REPORT

FIGURE 4.3-30
TYPICAL MODERATOR TEMPERATURE
COEFFICIENT AT EOL, CYCLE 1
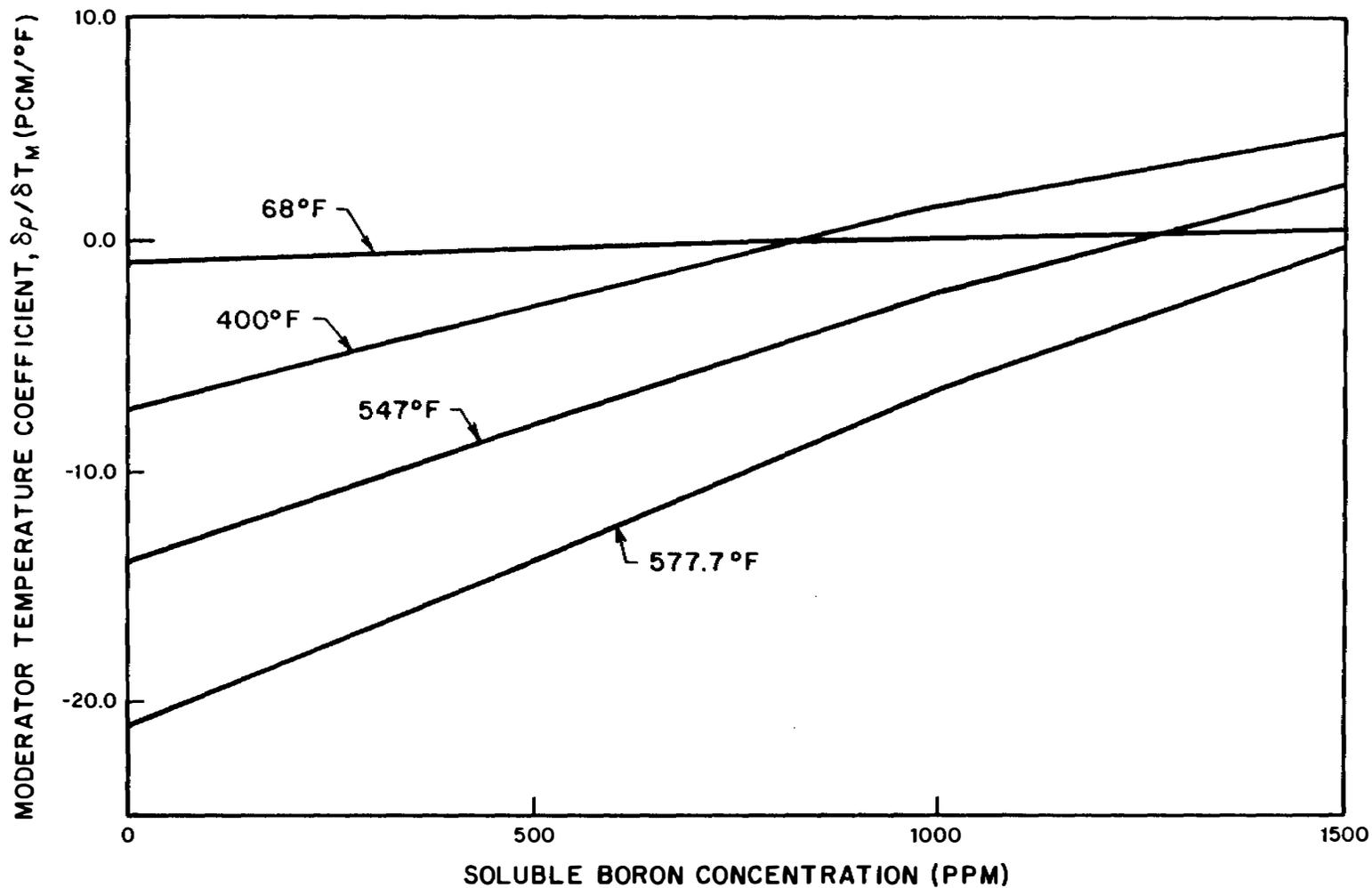BEAVER VALLEY POWER STATION-UNIT 2
FINAL SAFETY ANALYSIS REPORT

FIGURE 4.3-31

TYPICAL MODERATOR TEMPERATURE
COEFFICIENT AS A FUNCTION OF
BORON CONCENTRATION AT BOL,
CYCLE 1, NO RODS
BEAVER VALLEY POWER STATION-UNIT 2
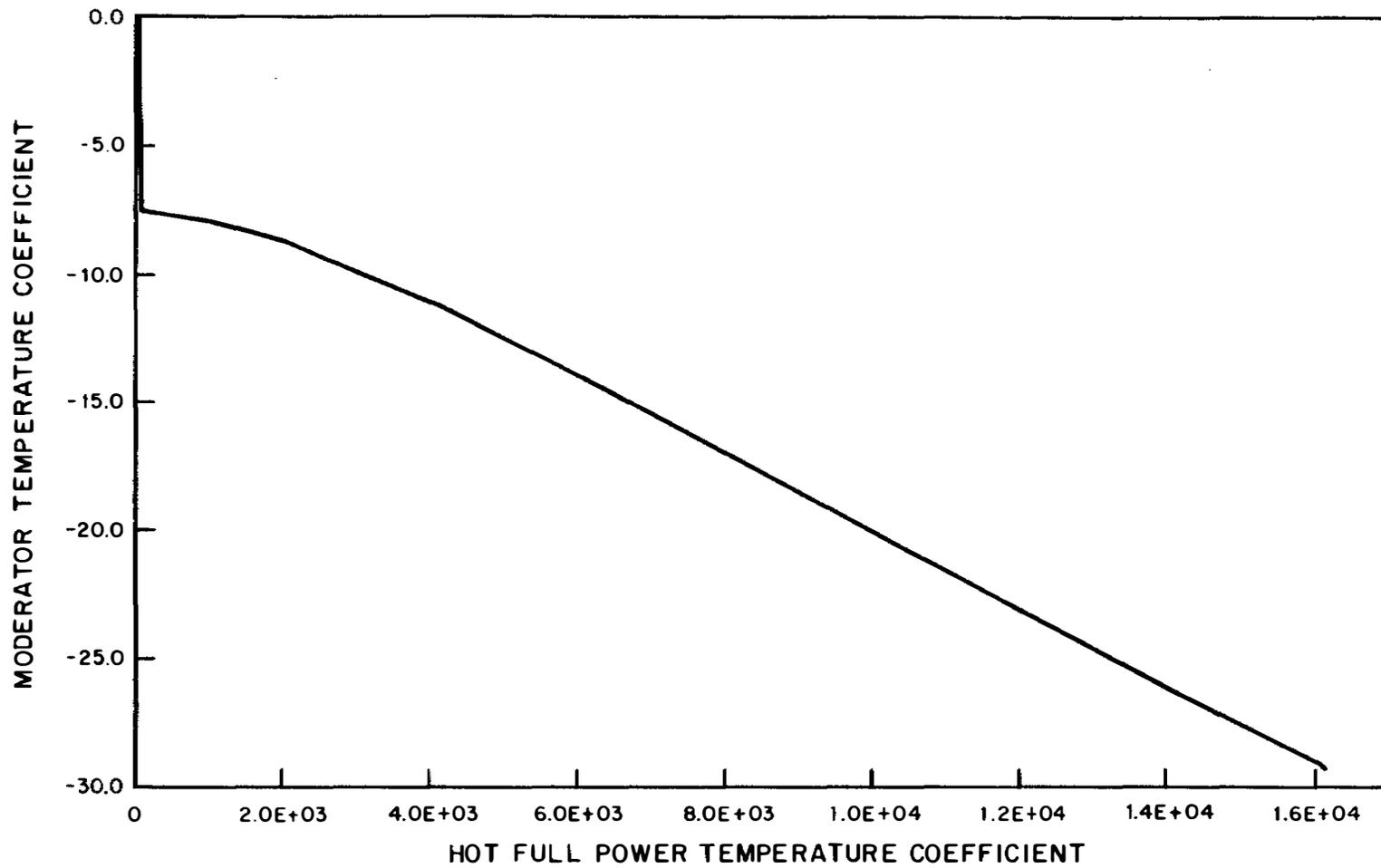FINAL SAFETY ANALYSIS REPORT

FIGURE 4.3-32
HOT FULL POWER TEMPERATURE
COEFFICIENT DURING CYCLE 1 FOR
THE CRITICAL BORON CONCENTRATION
BEAVER VALLEY POWER STATION-UNIT 2
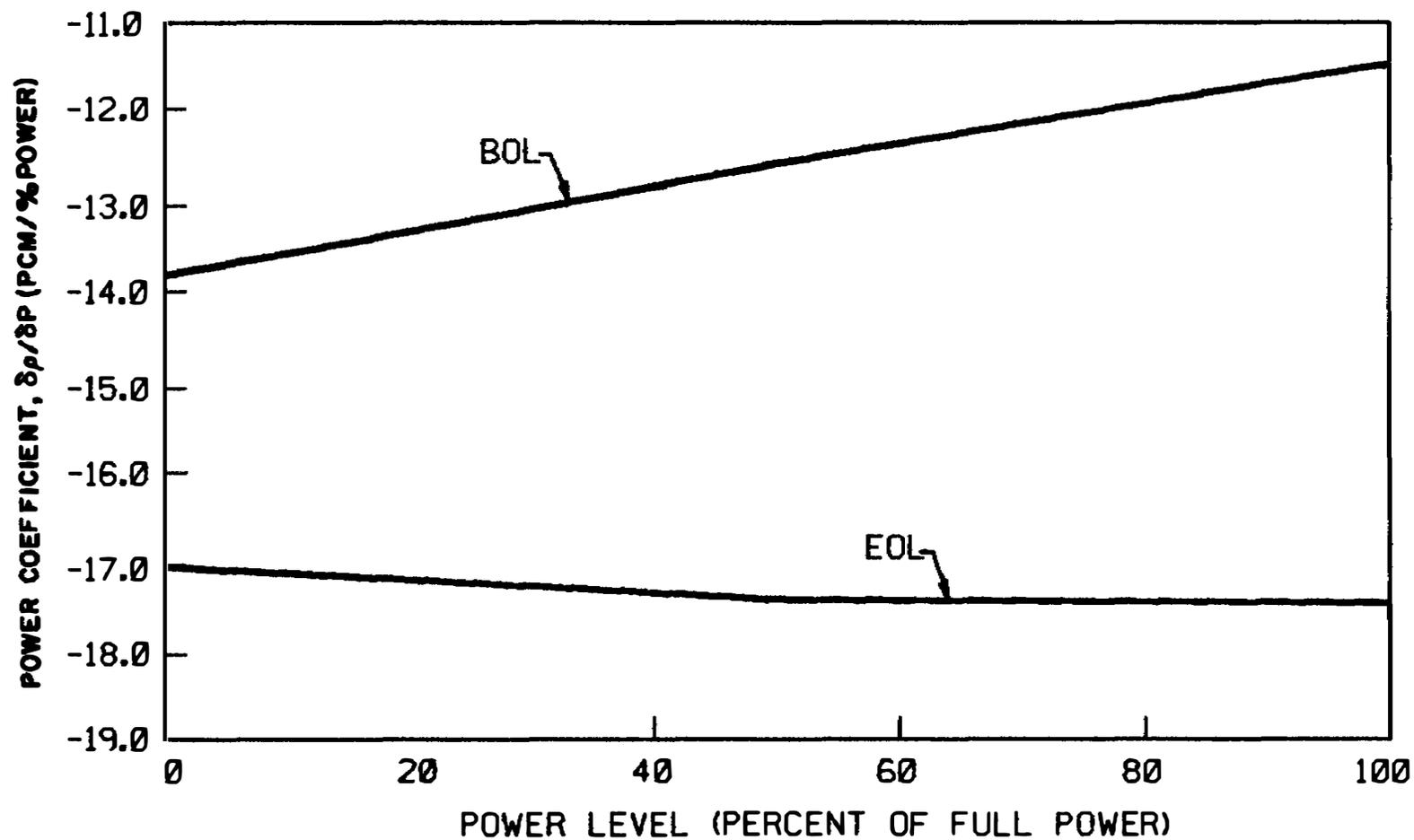FINAL SAFETY ANALYSIS REPORT

FIGURE 4.3-33
TYPICAL POWER COEFFICIENT VERSUS
PERCENT POWER FOR BOL AND EOL
BEAVER VALLEY POWER STATION-UNIT 2
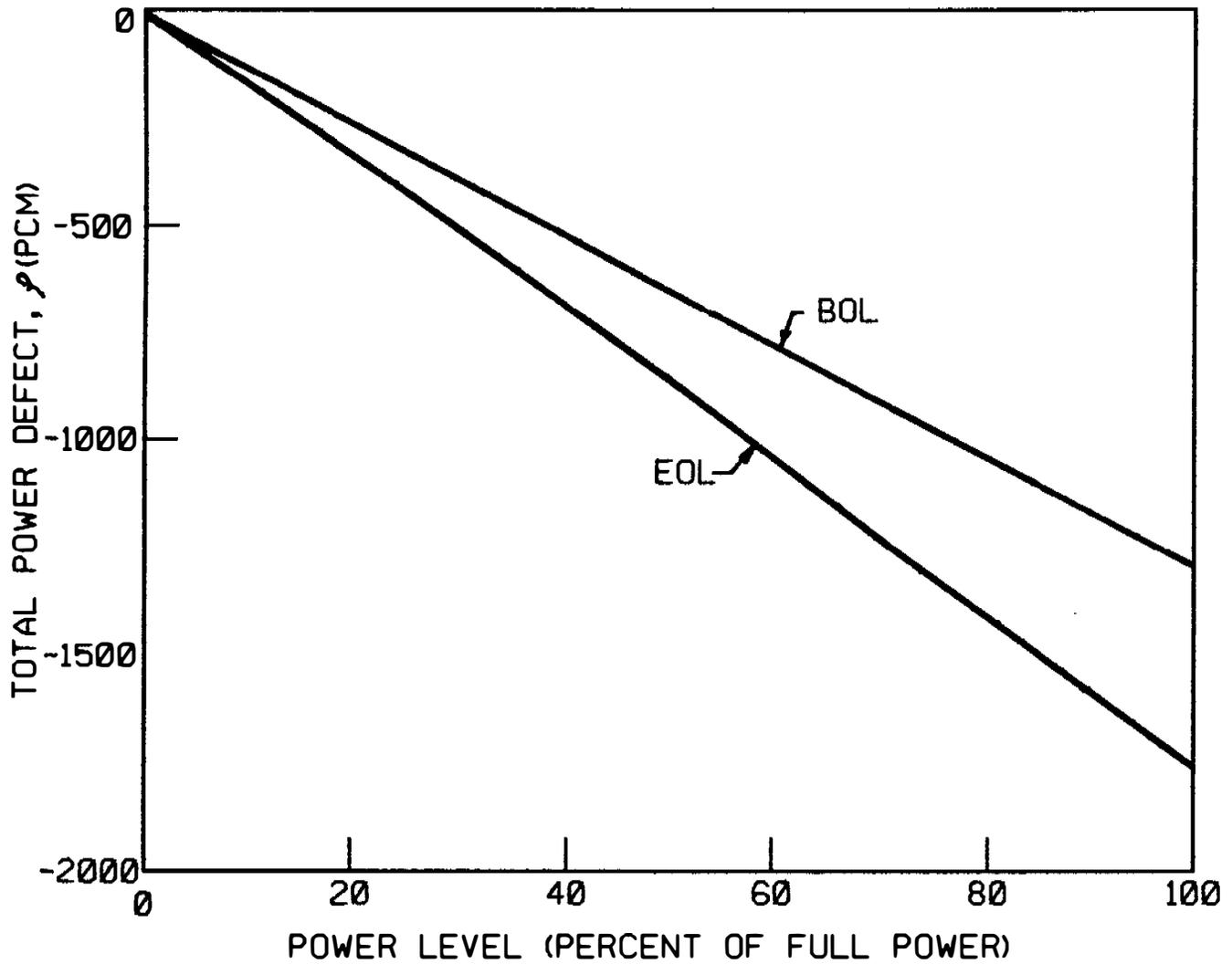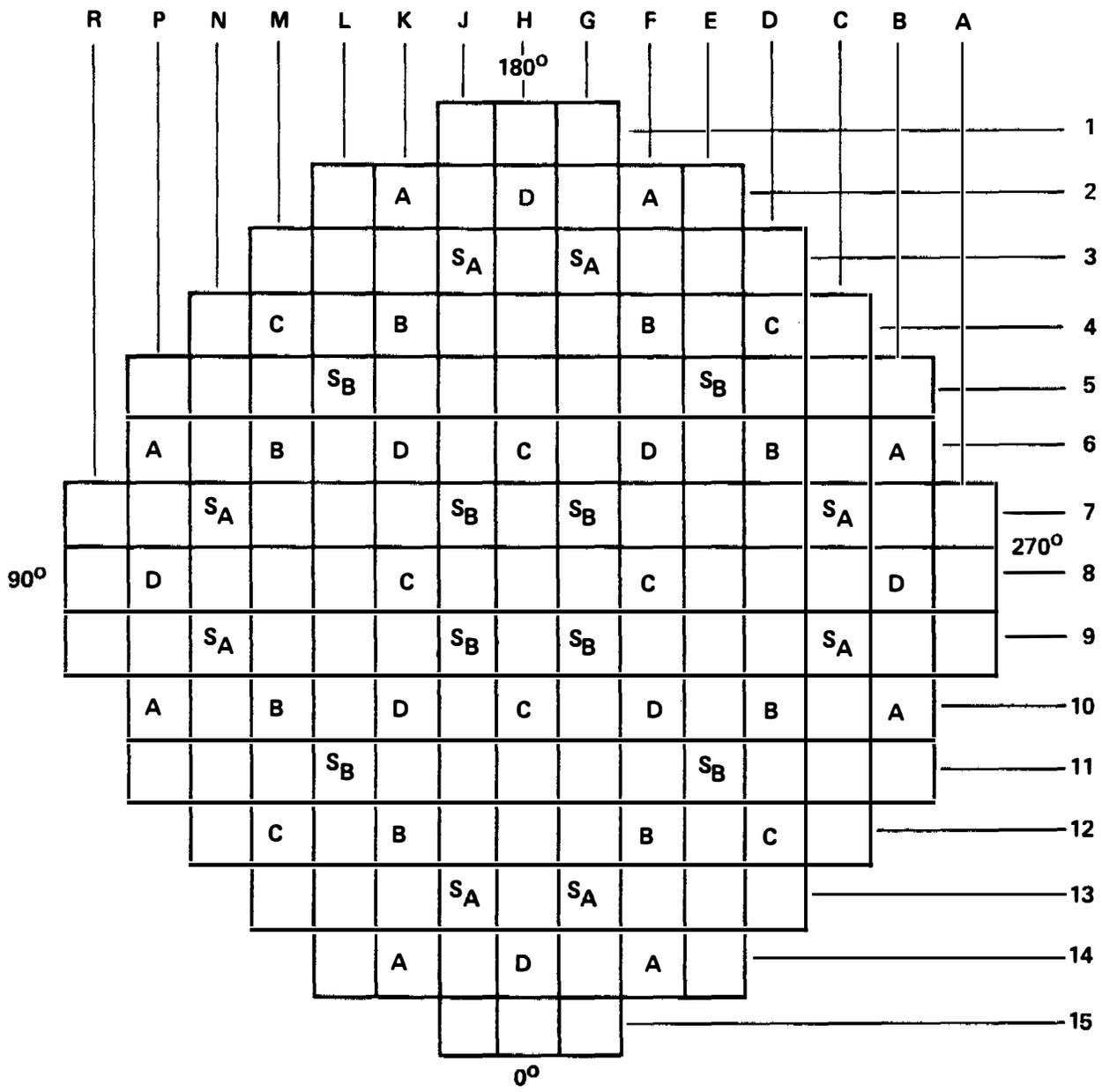UPDATED FINAL SAFETY ANALYSIS REPORT

FIGURE 4.3-34

TYPICAL POWER DEFECT VERSUS
POWER AT BOL AND EOL

BEAVER VALLEY POWER STATION-UNIT 2
UPDATED FINAL SAFETY ANALYSIS REPORT

CONTROL BANK	NUMBER OF RODS	SHUTDOWN BANK	NUMBER OF RODS
CONTROL D	8	SHUTDOWN B	8
CONTROL C	8	SHUTDOWN A	8
CONTROL B	8		
CONTROL A	8		
TOTAL	32 +	TOTAL	16 = 48

FIGURE 4.3-35
ROD CLUSTER CONTROL
ASSEMBLY PATTERN
BEAVER VALLEY POWER STATION-UNIT 2
FINAL SAFETY ANALYSIS REPORT
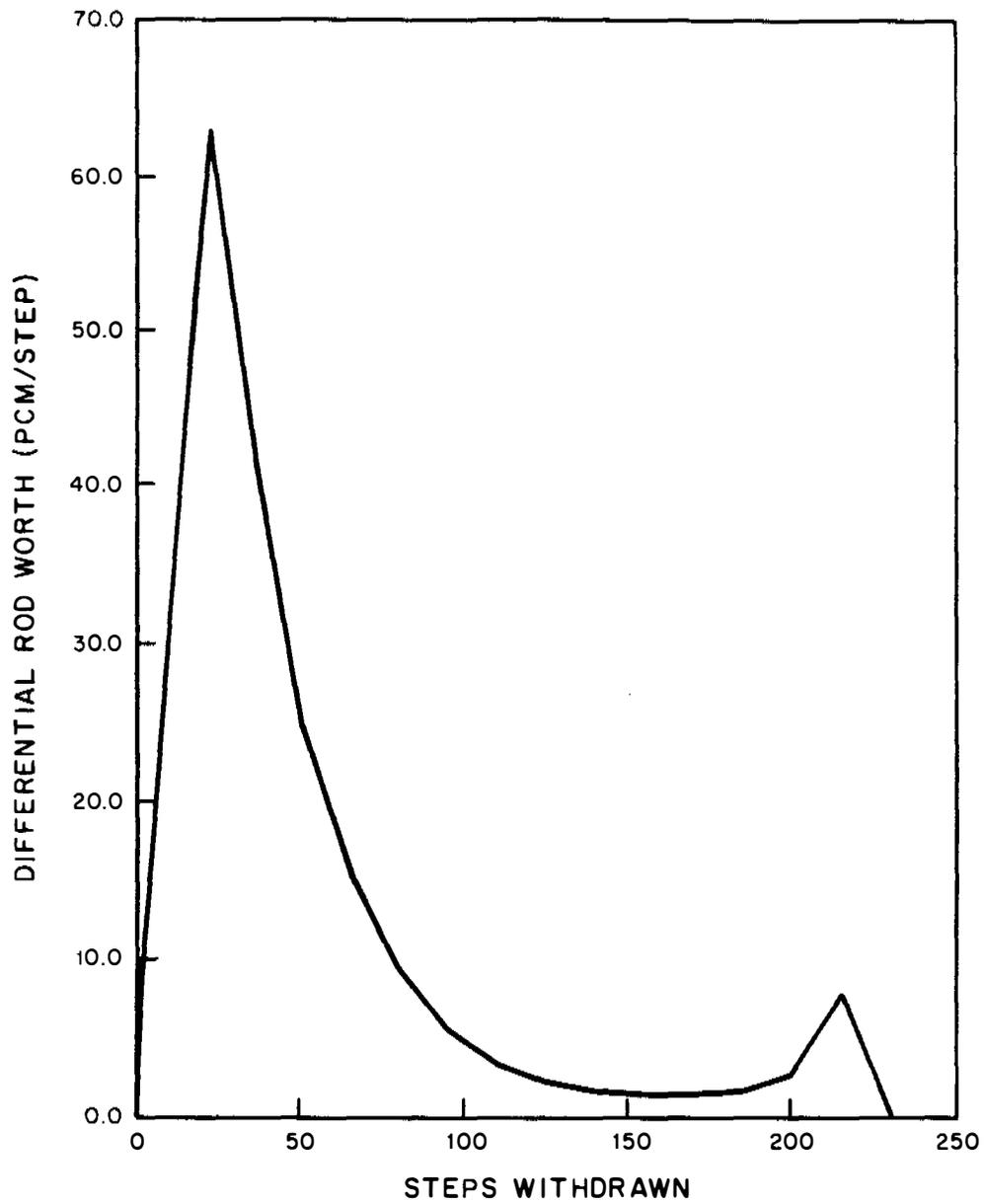
FIGURE 4.3-36
TYPICAL ACCIDENTAL SIMULTANEOUS
WITHDRAWAL OF TWO CONTROL BANKS
AT BOL, HZP, BANKS "A" AND "B"
MOVING IN THE SAME PLANE
BEAVER VALLEY POWER STATION-UNIT 2
FINAL SAFETY ANALYSIS REPORT
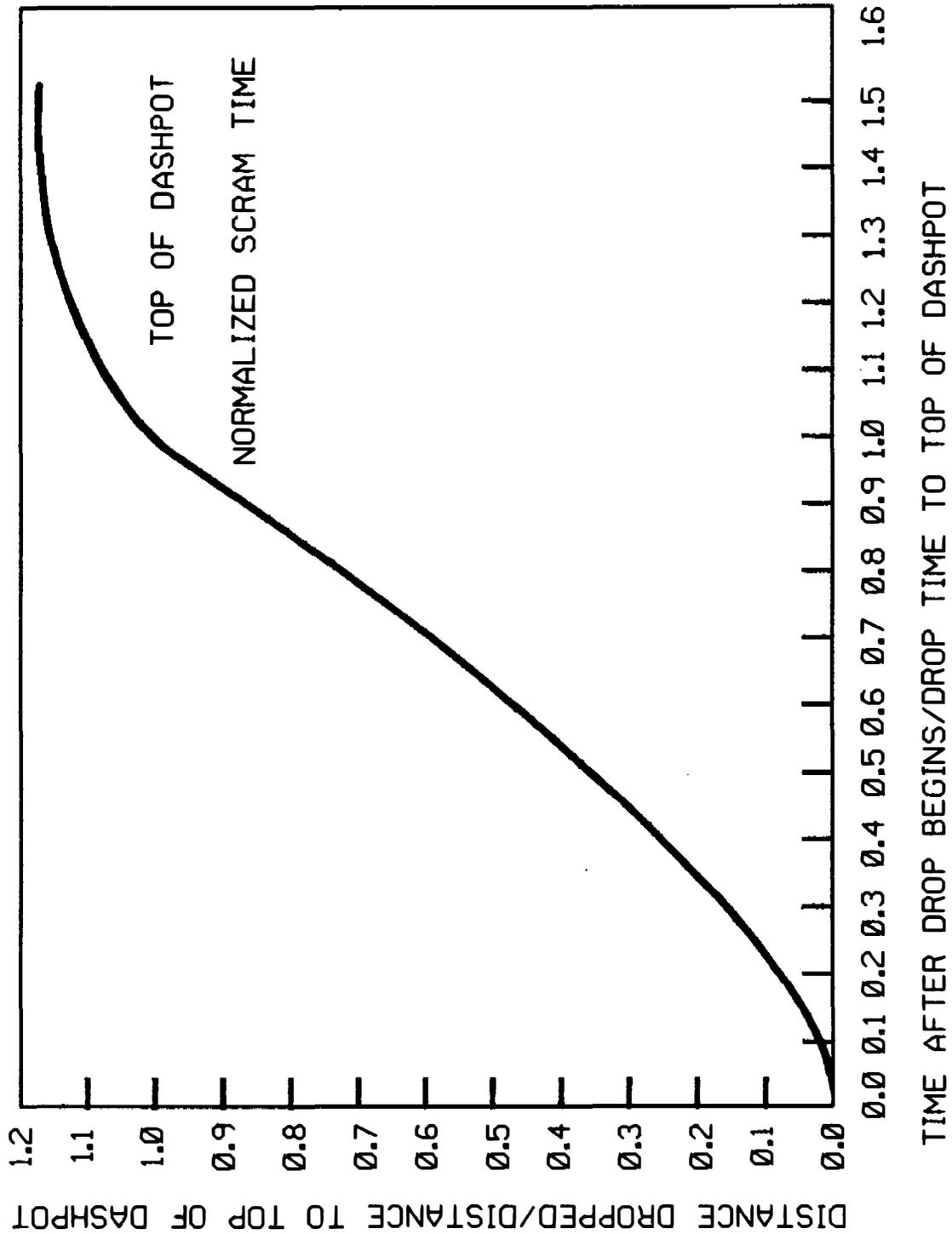
FIGURE 4.3-37
TYPICAL DESIGN TRIP CURVE

BEAVER VALLEY POWER STATION-UNIT 2
UPDATED FINAL SAFETY ANALYSIS REPORT
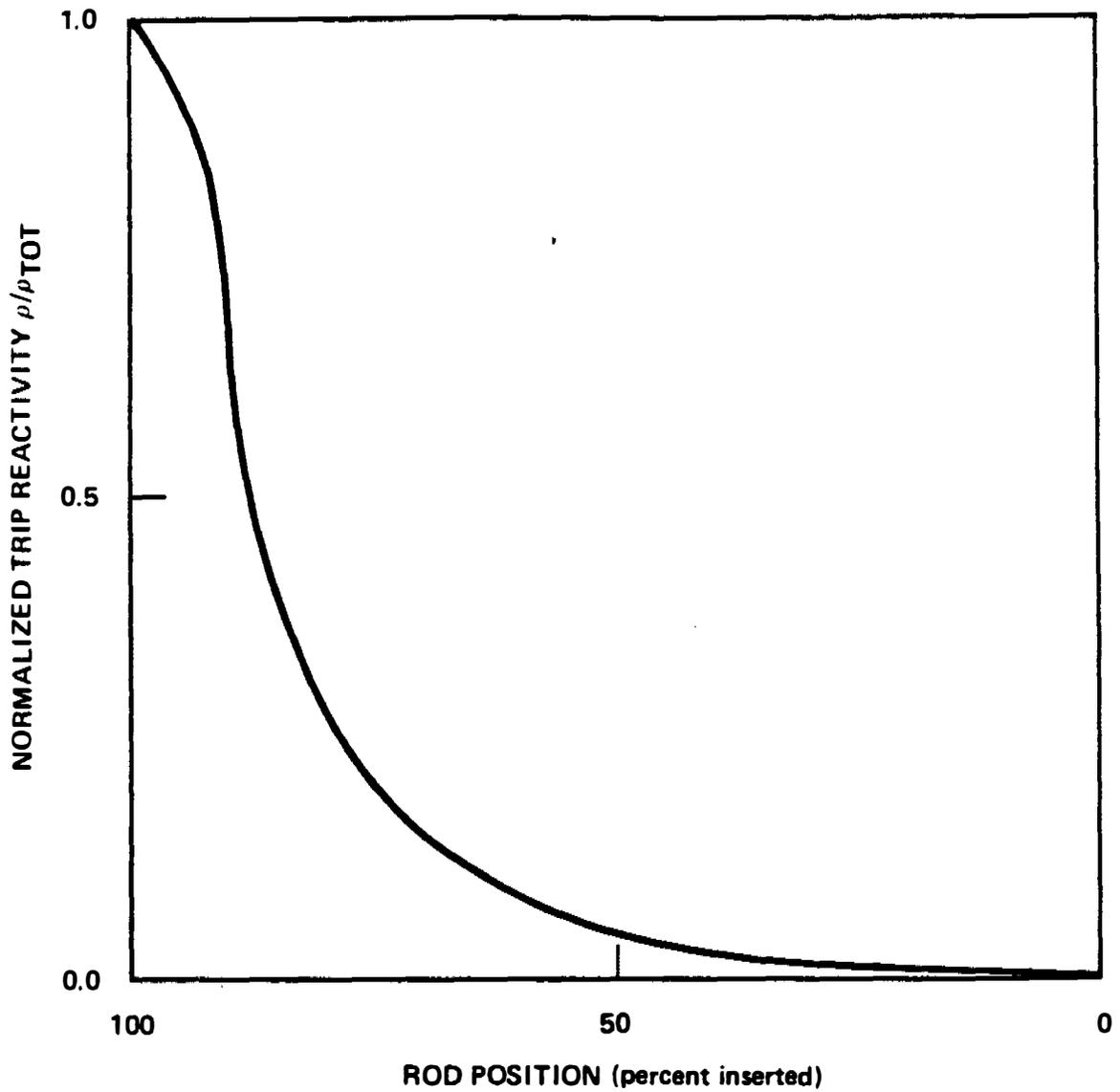
FIGURE 4.3-38
TYPICAL NORMALIZED ROD WORTH
VERSUS PERCENT INSERTION,
ALL RODS OUT BUT ONE
BEAVER VALLEY POWER STATION-UNIT 2
FINAL SAFETY ANALYSIS REPORT

CURVE	BURNUP (MWD MTU)	PERIOD (hours)	STABILITY INDEX (hours^{-1})
1	1550	32.4	-0.041
2	7700	27.2	-0.014
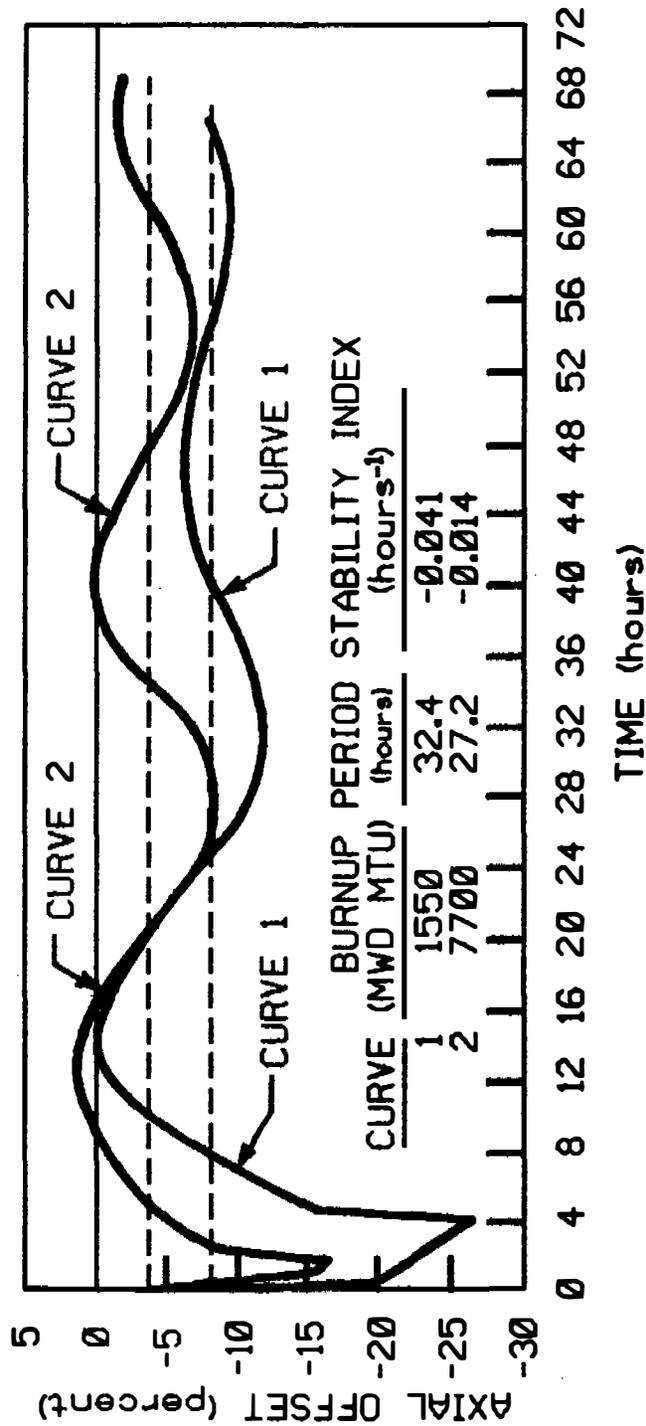
FIGURE 4.3-39

TYPICAL AXIAL OFFSET VERSUS TIME
PWR CORE WITH A 12 FOOT HEIGHT
AND 121 ASSEMBLIES

BEAVER VALLEY POWER STATION-UNIT 2
UPDATED FINAL SAFETY ANALYSIS REPORT
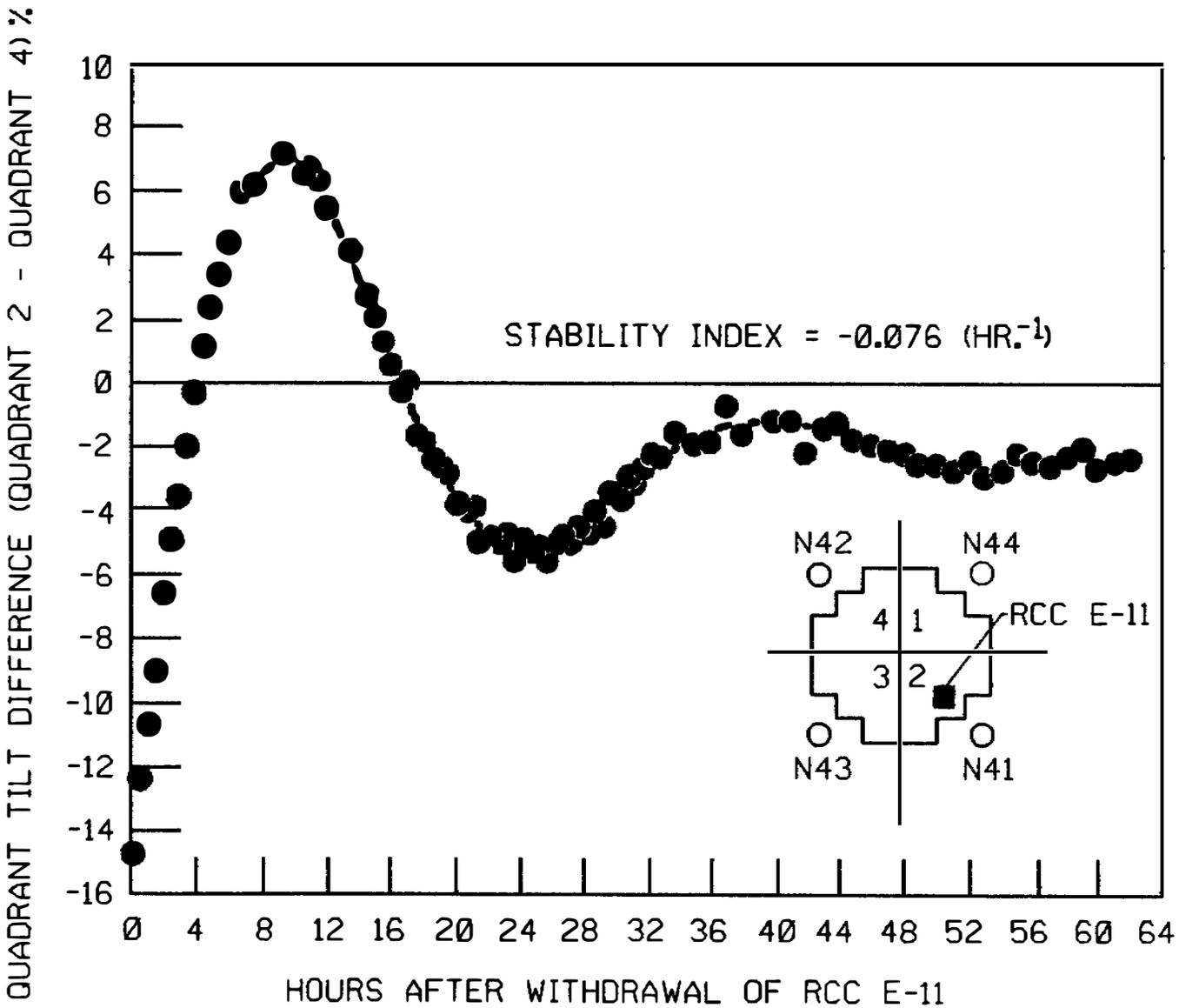
FIGURE 4.3-40

TYPICAL X-Y XENON TEST THERMO-
COUPLE RESPONSE QUADRANT TILT
DIFFERENCE VERSUS TIME

BEAVER VALLEY POWER STATION-UNIT 2
UPDATED FINAL SAFETY ANALYSIS REPORT

REV.10 (97)
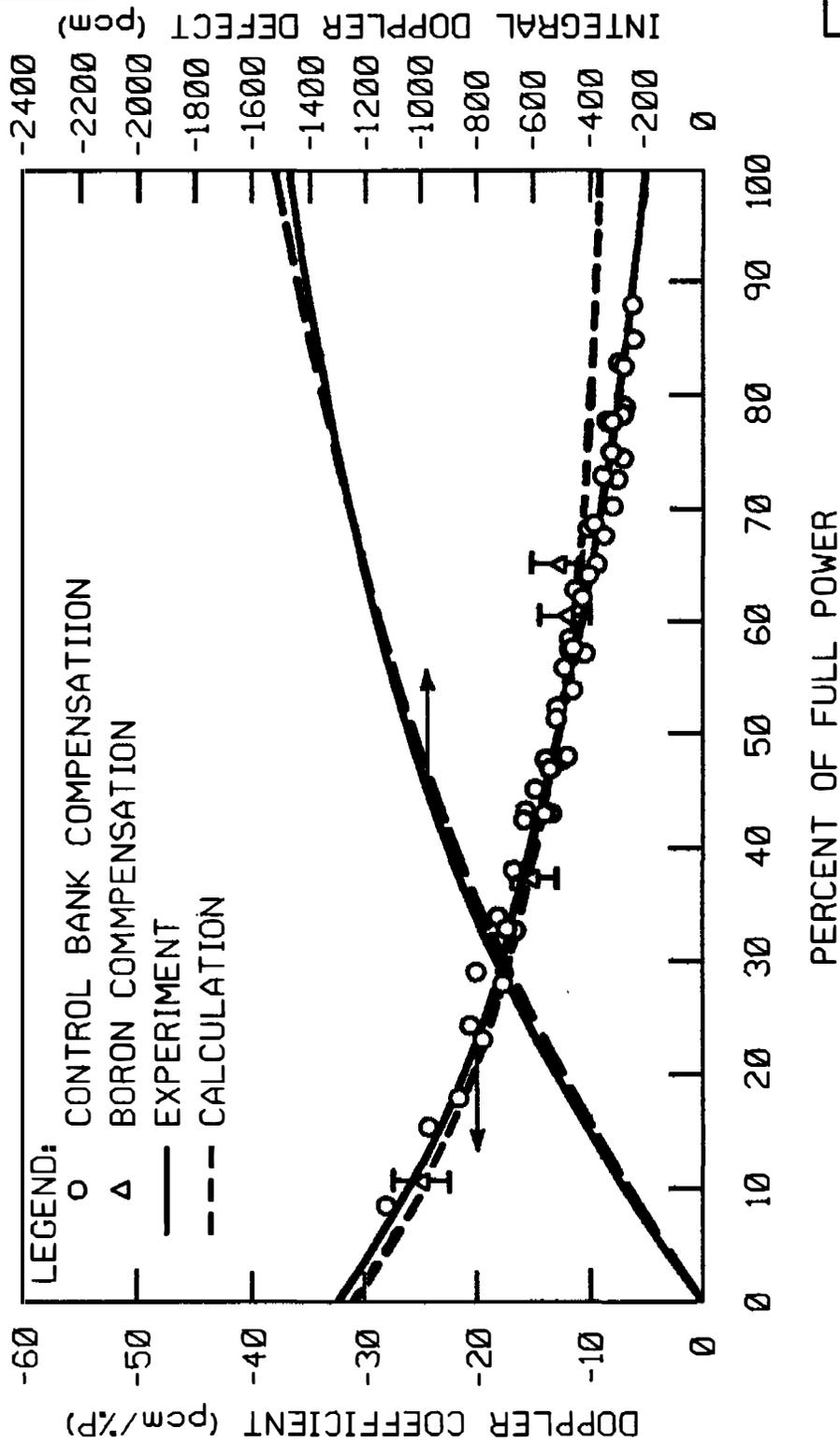
FIGURE 4.3-41

TYPICAL CALCULATED AND MEASURED DOPPLER
DEFECT AND COEFFICIENTS AT BOL,
2-LOOP PLANT,121 ASSEMBLIES 12 FOOT CORE

BEAVER VALLEY POWER STATION-UNIT 2
UPDATED FINAL SAFETY ANALYSIS REPORT
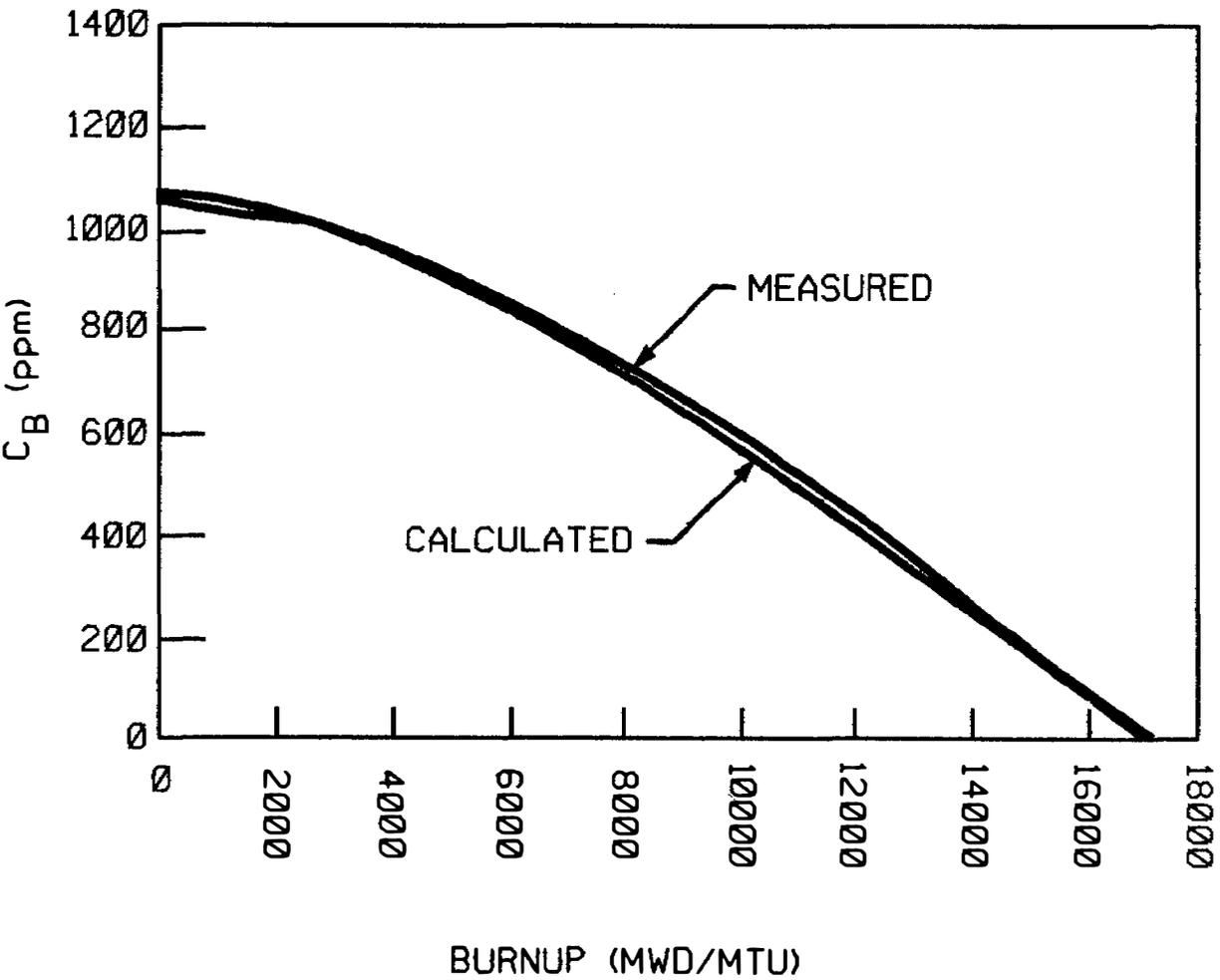
FIGURE 4.3-42

TYPICAL COMPARISON OF CALCULATED
CONCENTRATION MEASURED BORON
CONCENTRATION 2-LOOP PLANT,
121 ASSEMBLIES, 12 FOOT CORE

BEAVER VALLEY POWER STATION-UNIT 2
UPDATED FINAL SAFETY ANALYSIS REPORT

REV. 10 (97)

FIGURE 4.3-43
TYPICAL COMPARISON OF CALCULATED AND
MEASURED C B 3- LOOP PLANT
157 ASSEMBLIES,12 FOOT CORE
BEAVER VALLEY POWER STATION-UNIT 2
UPDATED FINAL SAFETY ANALYSIS REPORT

REV. 10 (97)

FIGURE 4.3-44
TYPICAL COMPARISON OF CALCULATED
AND MEASURED C_B4 - LOOP PLANT
193 ASSEMBLIES,12 FOOT CORE
BEAVER VALLEY POWER STATION-UNIT 2
UPDATED FINAL SAFETY ANALYSIS REPORT

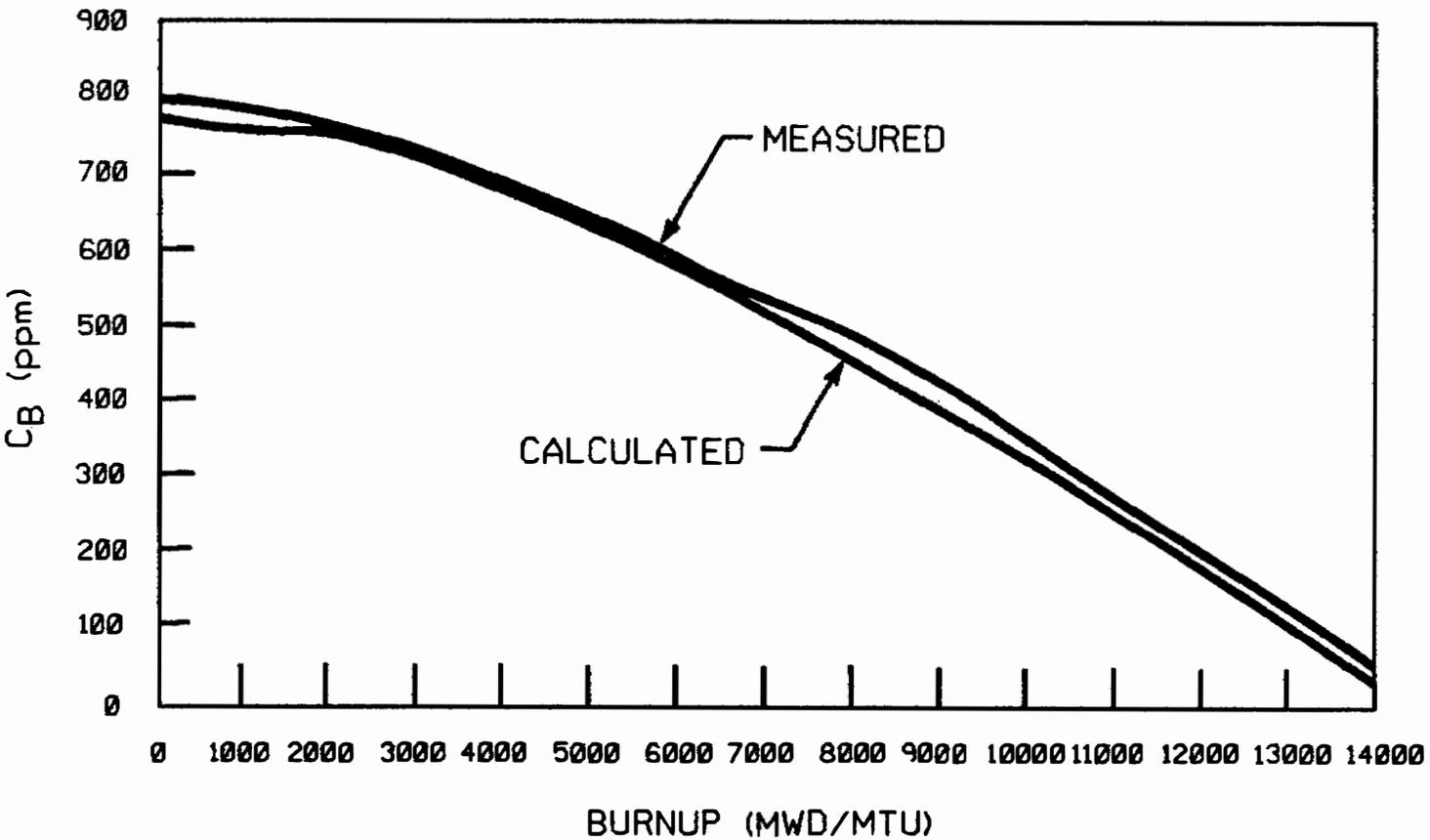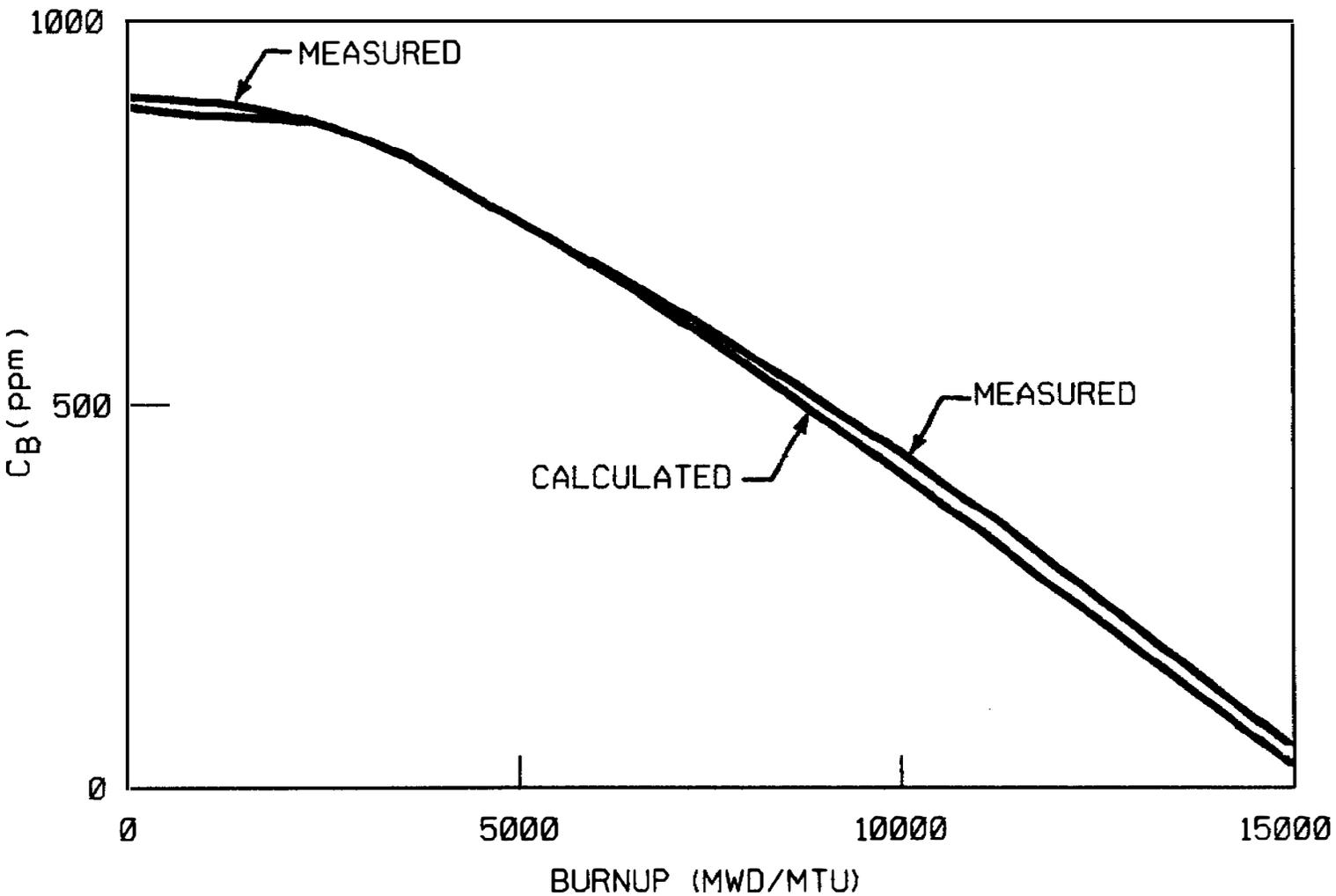4.4 THERMAL AND HYDRAULIC DESIGN

4.4.1 Design Bases

The overall objective of the thermal and hydraulic design of the reactor core is to provide adequate heat transfer which is compatible with the heat generation distribution in the core such that heat removal by the reactor coolant system (RCS) or the emergency core cooling system (ECCS) (when applicable) assures that the following performances and safety criteria requirements are met:

   1. Fuel damage (defined as penetration of the fission product barrier, that is, the fuel rod clad) is not expected during normal operation and operational transients (ANS Condition I) or any transient conditions arising from faults of moderate frequency (ANS Condition II). It is not possible, however, to preclude a very small number of rod failures resulting in the release of fission products. The chemical and volume control system is designed to remove the fission products from the reactor coolant, keeping the reactor coolant activity within plant design bases limits.

   2. The reactor can be brought to a safe state following a Condition III event with only a small fraction of the fuel rods damaged, as defined previously, although sufficient fuel damage might occur to preclude resumption of operation without considerable outage time.

   3. The reactor can be brought to a safe state and the core can be kept subcritical with acceptable heat transfer geometry following transients arising from Condition IV events.

In order to satisfy these requirements, the following design bases have been established for the thermal and hydraulic design of the reactor core.

4.4.1.1 Departure from Nucleate Boiling Design Basis

     Basis

There will be at least a 95 percent probability that departure from nucleate boiling (DNB) will not occur on the limiting fuel rods during normal operation, operational transients, or during transient conditions arising from faults of moderate frequency (ANS Condition I and II events), at a 95 percent confidence level.

Discussion

By preventing DNB, adequate heat transfer is assured between the fuel clad and the reactor coolant, thereby preventing clad damage as a result of inadequate cooling. Maximum fuel rod surface temperature is not a design basis as it will be within a few degrees of the coolant temperature during operation in the nucleate boiling region. Limits provided by the RCS and the reactor protection system are such that this design basis will be met for transients associated with ANS Condition II events, including overpower transients. There is an additional large DNBR margin at rated power operation and during normal operating transients.

Historically, the DNBR limit has been 1.30 for Westinghouse applications. In this application, the WRB-2M (Smith 1999) and the WRB-1 correlations (Motley 1984) are used. With the significant improvement in the accuracy of the critical heat flux prediction by using these correlations instead of the previous correlation, DNBR correlation limits of 1.14 and 1.17 apply to WRB-2M and WRB-1, respectively, with at least a 95% probability with a 95% confidence level.

The design method used to meet the DNB design basis is the revised thermal design procedure (Friedland, Ray 1989). With the RTDP methodology, uncertainties in plant operating parameters (Williams, Reagan, Tuley, 1999), nuclear and thermal parameters, fuel fabrication parameters, computer codes, and DNB correlation predictions are considered statistically to obtain DNB uncertainty factors. Based on the DNB uncertainty factors, RTDP design limit DNBR values are determined such that there is at least a 95 percent probability at a 95 percent confidence level that DNB will not occur on the most limiting fuel rod during normal operation and operational transients and during transient conditions arising from faults of moderate frequency (Condition I and II events as defined in ANSI N18.2).

In the RTDP method, the following uncertainties are statistically combined with the DNB correlation uncertainties to obtain the overall DNBR uncertainty factor used to define the design limit DNBR:

1. Plant operating parameters (vessel coolant flow, core power, coolant temperature, system pressure, effective core flow fraction)

2. Nuclear and thermal parameter $\left(F_{\Delta H}^{N}\right)$

3. Fuel fabrication parameters $\left(F_{\Delta H, 1}^{E}\right)$

4. VIPRE and transient codes

The uncertainty factor obtained is used to define the design limit DNBR which satisfies the DNB design criterion. The DNB design criterion is that the probability that DNB will not occur on the most limiting fuel rod is at least 95 percent at a 95 percent confidence level during normal operation and operational transients (Condition I events) and during transient conditions arising from faults of moderate frequency (Condition II events).

The RTDP design limit DNBR value is 1.22 for both the typical and thimble cells for the Robust Fuel Assemblies (RFA/RFA-2). For the VANTAGE 5H (V5H) and VANTAGE+ fuel assemblies, the RTDP design limit DNBR values for the typical and thimble cells are 1.23 and 1.22, respectively.

In addition to the considerations above, a specific plant allowance has been considered in the present analysis. In particular, a DNBR safety analysis limit value of 1.55 for typical and thimble cells for RFA/RFA-2 and 1.33 and 1.32 for typical and thimble cells, respectively, for V5H and VANTAGE+ fuel assemblies are used in the safety analyses for the plant. The difference between the DNBR value used in the safety analyses and the design DNBR values provides plant-specific DNB margin to offset the rod bow penalty and other DNB penalties that may occur. This DNB margin may also be used for flexibility in the design, operation or analysis of the plant.

The standard thermal design procedure (STDP) is used for those analyses where RTDP is not applicable. In the STDP method, the parameters used in analysis are treated in a conservative way from a DNBR standpoint. The parameter uncertainties are applied directly to the plant safety analyses input values to give the lowest minimum DNBR. The DNBR limit for STDP is the appropriate DNB correlation limit increased by sufficient margin to offset the applicable DNBR penalties.

For conditions outside the range of parameters for the WRB-1 and WRB-2M correlations (refer to Section 4.4.2.2.1), the W-3 correlation is used with a DNBR correlation limit of 1.30 for pressure equal to or greater than 1000 psia. For low pressure applications (500-1000 psia), the W-3 DNBR correlation limit is 1.45 (Hollingsworth, Woods, 1998).

A full region of RFA was used in Cycle 10. The thermal-hydraulically equivalent RFA-2 design was used starting in Cycle 11. The RFA/RFA-2 has a mixing vane grid design that is different from the V5H and VANTAGE+ mixing vane grids. In addition, the RFA/RFA-2 has Intermediate Flow Mixing (IFM) grids located between the top three mid-grid spans. The WRB-2M DNB correlation is applicable to the DNB analysis of the RFA/RFA-2. This correlation is described in Section 4.4.2.2.1.

Tests and analyses have confirmed that the RFA/RFA-2 is hydraulically compatible with the V5H/VANTAGE+ fuel assemblies. The NRC-approved Fuel Criteria Evaluation Process (WCAP-12488-A, October 1994) was used to address the design modifications for the 17 x 17 RFA, SECL-98-056, Rev. 0, September 30, 1998, and Westinghouse letter LTR-ESI-03-35. The modification for RFA-2 was addressed in "Generic - Implementation of Robust Fuel Assembly-2 (RFA-2) Design Changes," EVAL-01-066, August 31, 2001.

The VIPRE-01 computer code (Stewart et al., 1989 and Sung et al., 1999) is used to determine coolant density, mass velocity, enthalpy, vapor void, static pressure, and DNBR distributions along parallel flow channels within a reactor core under expected steady state operating conditions. VIPRE-01 which replaces the THINC-IV computer code, has had extensive experimental verification and comparisons with other licensed codes and is considered a best estimate code. The DNBR predictions are very close to those predicted by THINC-IV. VIPRE-01 is licensed with the NRC as an acceptable model for performing thermal-hydraulic calculations.

4.4.1.2 Fuel Temperature Design Basis

        Basis

During modes of operation associated with ANS Condition I and ANS
Condition II events, there is at least a 95 percent probability at the
95 percent confidence level that the peak kW/ft fuel rods will not
exceed the UO_2 melting temperature. The melting temperature of
unirradiated UO_2 is taken as 5,080°F (Christensen et al 1965), and
decreasing 58°F per 10,000 MWD/MTU. By precluding UO_2 Melting, the
fuel geometry is preserved and possible adverse effects of molten UO_2
on the cladding are eliminated. To preclude center melting and as a
basis for overpower protection system set points, a calculated
centerline fuel temperature of 4,700°F has been selected as the
overpower limit. This provides sufficient margin for uncertainties in
the thermal evaluations as described in Section 4.4.2.9.1.

        Discussion

Fuel rod thermal evaluations are performed at rated power, maximum
overpower and during transients at various burnups. These analyses
assure that this desiqn basis as well as the fuel integrity design
bases given in Section 4.2 are met. They also provide input for the
evaluation of ANS Condition III and IV events given in Chapter 15.

4.4.1.3 Core Flow Design Basis

        Basis

A minimum of 93.5 percent of the thermal flow rate passes through the
fuel rod region of the core and is effective for fuel rod cooling.
Coolant flow through the thimble tubes as well as the leakage from the
core barrel-baffle region into the core are not considered effective
for heat removal.

        Discussion

Core cooling evaluations are based on the thermal flow rate (minimum
flow) entering the reactor vessel. A maximum of 6.5 percent of this
value is allotted as bypass flow. This includes rod cluster control
(RCC) guide thimble cooling flow, head cooling flow, baffle leakage,
and leakage to the vessel outlet nozzle.

4.4.1.4 Hydrodynamic Stability Design Basis

Basis

Modes of operation associated with ANS Condition I and II events shall not lead to hydrodynamic instability.

4.4.1.5 Other Considerations

The above design bases together with the fuel clad and fuel assembly design bases given in Section 4.2.1 are sufficiently comprehensive that no additional limits are required.

Fuel rod diametral gap characteristics, moderator-coolant flow velocity and distribution, and moderator void are not inherently limiting. Each of these parameters is incorporated into the thermal and hydraulic models used to ensure that the design criteria mentioned previously are met. For instance, the fuel rod diametral gap characteristics change with time (Section 4.2.3.3) and the fuel rod integrity is evaluated on that basis. The effect of the moderator flow velocity and distribution (Section 4.4.2.2) and moderator void distribution (Section 4.4.2.4) are included in the core thermal (VIPRE) evaluation and thus affect the design bases.

Meeting the fuel clad integrity criteria covers possible effects of clad temperature limitations. As noted in Section 4.2.3.3, the fuel rod conditions change with time. A single clad temperature limit for ANS Condition I or II events is not appropriate because it would be overly conservative. A clad temperature limit is applied to the loss-of-coolant accident (LOCA), control rod ejection accident, and locked rotor accident.

4.4.2 Description

4.4.2.1 Summary

Values of pertinent parameters, along with critical heat flux ratios, fuel temperatures, and linear heat generation rates, are presented in Table 4.4-1 for all reactor coolant loops in service. The reactor is designed to meet the DNB design criterion of Section 4.4.1.1 as well as no fuel centerline melting during normal operation, operational transients, and faults of moderate frequency.

Fuel densification has been considered in the DNB and fuel temperature evaluations utilizing the methods and models described by Hellman (1975).

4.4.2.2   Critical Heat Flux Ratio and Departure from Nucleate
           Boiling Ratio and Mixing Technology

The minimum DNBRs for the rated power, design overpower, and anticipated transient conditions are given in Table 4.4-1. The core average DNBR is not a safety related item as it is not directly related to the minimum DNBR in the core, which occurs at some elevation in the limiting flow channel. Similarly, the DNBR at the hot spot is not directly safety related. The minimum DNBR in the limiting flow channel is downstream of the peak heat flux location (hot spot) due to the increased downstream enthalpy rise.

Departure from nucleate boiling ratios are calculated by using the correlation and definitions described in Sections 4.4.2.2.1 and 4.4.2.2.2. The VIPRE-01 computer code (Section 4.4.4.5.1) is used to determine the flow distribution in the core and the local conditions in the hot channel for use in the DNB correlation. The use of hot channel factors is discussed in Section 4.4.4.3.1 (nuclear hot channel factor) and in Section 4.4.2.2.4 (engineering hot channel factors).

4.4.2.2.1 Departure from Nucleate Boiling Technology

Early experimental studies of DNB were conducted with fluid flowing inside single heated tubes or channels and with single annulus configurations with one or both walls heated. The results of the experiments were analyzed using many different physical models for describing the DNB phenomenon, but all resultant correlations are highly empirical in nature. The evolution of these correlations is given by Tong 1965, 1972 including the W-3 correlation which is in wide use in the pressurized water reactor industry.

As testing methods progressed to the use of rod bundles, instead of single channels, it became apparent that the bundles average flow conditions cannot be used in DNB correlations. As outlined by Tong 1969, test results showed that correlations based on average conditions were not accurate predictors of DNB heat flux. This indicated that a knowledge of the local subchannel conditions within the bundle is necessary.

It was shown by Tong 1969, that the above approach yielded
conservative predictions particularly in rod bundles with mixing vane
grid spacers.

The WRB-l DNB correlation (Motley, Hill, Cadek, and Shefchek 1984) was
developed based exclusively on the large bank of mixing vane grid rod
bundle CHF data (over 1100 points) that Westinghouse has collected.
The WRB-1 correlation, based on local fluid conditions, represent the
rod bundle data with better accuracy over a wide range of variables
than the previous correlation used in design. This correlation
accounts directly for both typical and thimble cold wall cell effects,
uniform and non-uniform heat flux profiles and variations in rod
heated length and grid spacing. The WRB-1 correlation is applicable
to the 17x17 STD, VANTAGE 5H, and RFA/RFA-2 (Sepp, 1998) fuel.

The applicable range of variables for the WRB-1 correlation is:

    Pressure   : $1440 \leq P \leq 2490$ psia
    Local Mass Velocity   : $0.9 \leq G_{loc}/10^6 \leq 3.7$ lb/ft^2-hr
    Local Quality   : $-0.2 \leq X_{loc} \leq 0.3$
    Heated Length, Inlet to CHF   : $L_h \leq 14$ feet
    Location
    Grid Spacing   : $13 \leq g_{sp} \leq 32$ inches
    Equivalent Hydraulic Diameter   : $0.37 \leq d_e \leq 0.60$ inches
    Equivalent Heated Hydraulic   : $0.46 \leq d_h \leq 0.68$ inches
    Diameter

Figure 4.4-1 shows the measured critical heat flux plotted against
predicted critical heat flux using the WRB-1 correlation.

The WRB-2M DNB correlation is applicable to the RFA/RFA-2. This
correlation gives improved DNBR predictions compared to the WRB-1 DNB
correlation.

In order to meet the design criterion that DNB will not occur at a 95
percent probability with a 95 percent confidence level, a limiting
value of DNBR is determined by the method of Owen 1963. Owen has
prepared tables which give values of K such that "at least a
proportion P of the population is greater than M/P - K_ps with
confidence γ," where M/P and s are the sample mean and standard
deviation. When this method was carried out using the data on Figure
4.4-1, the results indicated that a reactor core with these fuel
geometries may operate with a minimum DNBR of 1.17 with the WRB-1
correlation and 1.14 with the WRB-2M correlation and satisfy the
design criterion.

The WRB-2M DNB correlation (WCAP-15025-P-A, April 1999) was developed to take advantage of the benefit seen in DNB test data of the mixing vane grids and intermediate flow mixers (IFM) associated with the Robust Fuel Assembly (RFA). This correlation is based on 241 data points and local fluid conditions and is applicable to both typical and thimble cells, non-uniform heat flux profiles and variation in rod heated length and grid spacing. The DNB correlation limit for the WRB-2M DNB correlation is 1.14 compared to the value of 1.17 for the WRB-1 correlation. The WRB-2 or the W-3 DNB correlation is used wherever the WRB-2M correlation is not applicable. The applicable range of variables for the WRB-2M correlation is:

Pressure : $1495 \leq P \leq 2425$ psia

Local Mass Velocity : $0.97 \leq G_{loc}/10^6 \leq 3.1$ lb/ft^2-hr

Local Quality : $-0.1 \leq X_{loc} \leq 0.29$

Heated Length, Inlet to CHF Location : $L_h \leq 14$ feet

Grid Spacing : $10 \leq g_{sp} \leq 20.6$ inches

Equivalent Hydraulic Diameter : $0.37 \leq d_e \leq 0.46$ inches

Equivalent Heated Hydraulic Diameter : $0.46 \leq d_h \leq 0.54$ inches

Effects of Fuel Densification on DNB/Effect of Heat Flux Spikes

As discussed in Section 4.3.2.2.5 and Hellman 1973, a gap or combination of gaps results in a heat flux spike on the individual or adjacent fuel rods. Recent Westinghouse high pressure DNB Water Tests (Hill, Motley, and Cadek 1973) on a 14 foot axially non-uniformly heated 4x4 rod bundle were carried out to measure the effect of heat flux spikes. The rod bundle incorporated mixing vane grids on a 26 inch spacing. A 20% heat flux spike was placed on three adjacent rods at the axial location where DNB is most likely to occur. This test series was run at the same conditions as those of two earlier test series which had unspiked rods so that a comparison of spiked and unspiked data could be made and the spike effects isolated. Figure 4.4-1A shows the relative positions of the three spiked rods. Figure 4.4-2 shows the heat flux profile of the spiked rods.

The test facilities consisted of a high pressure loop capable of supplying water at pressures up to 2400 psia with flow rates up to 400 GPM and inlet temperatures in excess of 600°F. The power supply was capable of delivering up to 4.5 MW.

Using these test facilities, a 14 foot, 16 rod test section can be operated over a wide range of test parameters. For the present tests, these ranges were:

1. Pressure   1500 - 2400 psia
2. Inlet Temperature   401 - 569°F
3. Mass Velocity   1.5 - 3.5 x 10^6 lb/hr-ft^2

The results of the spike test series indicated that the spike effect
on DNB is so small that it lies within the repeatability of DNB
measurements. The spike geometry modeled in the above rod bundle
experiment was also more severe than that presently ascribed to fuel
densification effects, and hence, the absence of a spike effect
indicated that a special spike factor in DNB need not be incorporated
into the BVPS-2 reactor design.

Effects of Pellet Eccentricity and Clad Ovality on DNB

Individual fuel pellets can be eccentrically located in the clad at
BOL. The clad may also assume an oval shape at some later time in
life. Both of these cases will produce azimuthal variations of the
pellet clad gap. However, these local heat flux peaks will have
limited axial lengths at any azimuthal angle.

For the eccentric case the local heat flux peak at a given azimuthal
angle will have a maximum length equal to several pellet lengths.
This is due to the randomness of the angle of contact of the pellets
in the rod at BOL. The randomness has been verified by observation of
radiographs of Beznau Unit 1 fuel rods and is due in part to the
variation in pellet diameter.

For the clad ovality case, the local heat flux peak also has a maximum
length equal to several pellets at a given azimuthal angle. This is
due to the randomness of the azimuthal location of the cracked pellet
fragments in the axial direction.

The recent spike DNB tests (Hill, Motley, and Cadek 1973) described
previously indicate that for 360 circumferential heat flux spikes at
20% magnitude and 6" long, a special spike factor on DNB need not be
incorporated into Westinghouse reactor designs which incorporate the
Westinghouse type mixing vane grids. Since the 6 inch length is
equivalent to 10 pellet lengths, no reduction in DNBR due to pellet
eccentricity or clad ovality is applied in DNB evaluations.
Similarly, the heat flux engineering hot channel factor, F(E,Q) of
1.03 which allowed for variations in manufacturing tolerances and was
used to determine the local maximum linear heat generation rate at a
point, the "hot spot", is no longer considered in DNB evaluations.
This subfactor was determined by statistically combining the
tolerances for the fuel pellet diameter, density, enrichment,
eccentricity and the fuel rod diameter. F(E,Q) continues to be
applied in determining the peak power and in fuel pellet temperature
evaluations.

The effect of manufacturing tolerances which affect the integrated
values along a channel, i. e., enthalpy rise engineering hot channel
subfactor corresponding to pellet diameter, density and enrichment,
and fuel rod diameter, pitch and bowing, are still considered in all
DNB evaluations as described in Section 4.4.2.2.4.1.

4.4.2.2.2 Definition of Departure from Nucleate Boiling Ratio

The DNB heat flux ratio (DNBR) as applied to this design when all flow
cell walls are heated is:

$$DNBR = \frac{q''_{DNB,\,N}}{q''_{loc}}$$
(4.4-1)

where $q''_{DNB,N}$ is the heat flux predicted by the applicable DNB
correlation; for the correlation

$$q''_{DNB,N} = \frac{q''_{DNB,\,EU}}{F}$$
(4.4-2)

and $q''_{DNB,\,EU}$ is the uniform DNB heat flux as predicted by the W-3 DNB
correlation (Tong 1967) when all flow cell walls are heated.

F is the flux shape factor to account for non-uniform axial heat flux
distributions (Tong 1967) with the "C" term modified by Tong (1972).

q''_{loc} is the actual local heat flux.

The DNBR as applied to this design when a cold wall is present is:

$$DNBR = \frac{q''_{DNB,N,CW}}{q''_{loc}}$$

(4.4-3)

where:

$$q''_{DNB,N,CW} = \frac{q''_{DNB,EU,Dh} \ x \ CWF}{F}$$

(4.4-4)

where:

$q''_{DNB,EU,Dh}$ is the uniform DNB heat flux as predicted by the W-3 cold wall DNB correlation (Tong 1972) when not all flow cell walls are heated (thimble cold wall cell).

CWF is the cold wall factor.

$$CWF \ (Tong \ 1972) \ = \ 1.0 - Ru[13.76 - 1.372e^{1.78x} - 4.732 \ \left(\frac{G}{10^6}\right)^{-0.0535}$$

$$- \ 0.0619 \ \left(\frac{P}{1000}\right)^{0.14} - 8.509Dh^{0.107}] \quad (4.4-4a)$$

and Ru = 1 - De/Dh

For the WRB-1 and WRB-2M correlations,

$$q''DNB,N = \frac{q''DNB,EU}{F}$$

where q "DNB,EU is the uniform DNB heat flux as predicted by the WRB-2M (WCAP-15025-P-A, April 1999 and D.S. Collins letter, February 2006) or the WRB-1 correlation and F is the same flux shape factor that is used with the W-3 correlation. The CWF is included in the WRB-1 and WRB-2M correlations.

4.4.2.2.3 Mixing Technology

The rate of heat exchange by mixing between flow channels is proportional to the difference in the local mean fluid enthalpy of the respective channels, the local fluid density and flow velocity. The proportionality is expressed by the dimensionless TDC which is defined as:

$$TDC = \frac{w'}{\rho \ Va}$$

(4.4-5)

where:

      w' = flow exchange rate per unit length
         (lb_m/ft-sec)
      ρ = fluid density (lb_m/ft^3)
      V = fluid velocity (ft/sec)
      a = lateral flow area between channels per unit length
         ft^2/ft)

The application of the TDC in the THINC analysis for determining the overall mixing effect or heat exchange rate is presented by Hochreiter (et al 1989). The application of TDC in the VIPRE-01 analysis is presented by Sung (et al 1999).

Various mixing tests have been performed at Columbia University by Cadek (et al 1975). These series of tests, using the "R" mixing vane grid design on 13-, 26-, and 32-inch grid spacing, were conducted in pressurized water loops at Reynolds numbers similar to that of a pressurized water reactor (PWR) core under the following single- and two-phase (subcooled boiling) flow conditions:

    Pressure   1,500 to 2,400 (psia)
    Inlet temperature   332 to 642 (°F)
    Mass velocity   1.0 to 3.5 x 10^6 ($lb_m/hr\text{-}ft^2$)
    Reynolds number   1.34 to 7.45 x 10^5
    Bulk outlet quality   -52.1 to 13.5 (percent)

The thermal diffusion coefficient is determined by comparing the THINC Code predictions with the measured subchannel exit temperatures. Data for 26-inch axial grid spacing are presented on Figure 4.4-3 where TDC is plotted versus the Reynolds number. Thermal diffusion coefficient is found to be independent of Reynolds number, mass velocity, pressure, and quality over the ranges tested. The two-phase data (local, subcooled boiling) fell within the scatter of the single phase data. The effect of two-phase flow on the value of TDC has been demonstrated by Cadek (et al 1975), Rowe and Angle (1967, 1969), and Gonzalez-Santalo and Griffith (1972). In the subcooled boiling region, the values of TDC were indistinguishable from the single-phase values. In the quality region, Rowe and Angle (1967, 1969) show that in the case with rod spacing similar to that in PWR core geometry, the value of TDC increased with quality to a point and then decreased, but never below the single-phase value. Gonzalez-Santalo and Griffith (1972) showed that the mixing TDC increased as the void fraction increased.

The data from these tests on the "R" grid showed that a design TDC value of 0.038 (for 26-inch grid spacing) can be used in determining the effect of coolant mixing in the THINC or VIPRE-01 analysis.

A mixing test program similar to the one described previously was conducted at Columbia University for the current 17 by 17 geometry and mixing vane grids on 26-inch spacing (Motley et al 1975b). The mean value of TDC obtained from these tests was 0.051, and all data were well above the current design value of 0.038.

Since the actual reactor grid spacing is approximately 20 inches, the use of TDC equal to 0.038 is conservative for this design, as the value of TDC increases as grid spacing decreases (Cadek et al 1975).

4.4.2.2.4 Hot Channel Factors

The total hot channel factors for heat flux and enthalpy rise are defined as the maximum-to-core average ratios of these quantities.

The heat flux hot channel factor considers the local maximum linear heat generation rate at a point (the hot spot), and the enthalpy rise hot channel factor involves the maximum integrated linear heat generation rate along a channel (the hot channel).

Each of the total hot channel factors is composed of a nuclear hot channel factor (Section 4.4.4.3) describing the fission power distribution and an engineering hot channel factor, which allows for variations in flow conditions and fabrication tolerances. The engineering hot channel factors are made up of subfactors which account for the influence of the variations of fuel pellet diameter, density, enrichment, and eccentricity; inlet flow distribution; flow redistribution; and flow mixing.

4.4.2.2.4.1 Engineering Heat Flux Hot Channel Factor (F_Q^E)

The engineering heat flux hot channel factor (F_Q^E) is used to evaluate the maximum linear heat generation rate in the core. This subfactor is determined by statistically combining pellet to pellet variations and regionwise deviations in enrichment, density and burnable absorber (IFBA) and has a value of 1.03 at the 95 percent probability level with 95 percent confidence. As shown by Stewart (et al 1989), no DNB penalty needs to be taken for the relatively low intensity heat flux spikes caused by variations in the above parameters as well as fuel pellet eccentricity and fuel rod diameter variations.

4.4.2.2.4.2 Engineering Enthalpy Rise Hot Channel Factor, $F_{\Delta H}^E$

The effect of variations in flow conditions and fabrication tolerances on the hot channel enthalpy rise is considered in the VIPRE-01 core thermal subchannel analysis (Section 4.4.4.5.1) under any reactor operating condition. The items included in the consideration of the engineering enthalpy rise hot channel factor are discussed as follows:

> Rod to Rod Variations in Enrichment, Density and Burnable Absorber ($F_{\Delta H,1}^E$)
>
> $F_{\Delta H,1}^E$ is similar to F_Q^E except it covers the effect of rod to rod variations. Rod to rod variations are less than pellet-to-pellet variations and $F_{\Delta H,1}^E$ will, therefore, be less than F_Q^E. The current design value of $F_{\Delta H,1}^E$ is equal to 1.02.
>
> Inlet Flow Maldistribution

The consideration of inlet flow maldistribution in core thermal performances is discussed in Section 4.4.4.2.2. A design basis of 5 percent reduction in reactor coolant flow to the hot assembly is used in the VIPRE-01 analysis.

Flow Redistribution

The flow redistribution accounts for the reduction in flow in the hot channel resulting from the high flow resistance in the channel due to the local or bulk boiling. The effect of the nonuniform power distribution is inherently considered in the VIPRE-01 analysis for every operating condition which is evaluated.

Flow Mixing

The subchannel mixing model incorporated in the VIPRE-01 Code and used in reactor design is based on experimental data (Cadek 1975) discussed in Sections 4.4.2.2.3 and 4.4.4.5.1. The mixing vanes incorporated in the spacer grid design induce additional flow mixing between the various flow channels in a fuel assembly as well as between adjacent assemblies. This mixing reduces the enthalpy rise in the hot channel, resulting from local power peaking or unfavorable mechanical tolerances.

4.4.2.2.5 Effects of Rod Bow on DNBR

The phenomenon of fuel rod bowing, as described in Skaritka (1979), must be accounted for in the DNBR safety analysis of Condition I and Condition II events for each plant application.

The safety analysis for BVPS-2 maintained sufficient margin as discussed in Section 4.4.1.1, to accommodate full and low flow DNBR penalties identified in Westinghouse (1981) and USNRC (1986) (<1.3 percent for the worst case which occurs at a burnup of 24,000 MWD/MTU).

For the upper assembly spans of the RFA, however, where additional restraint is provided with the Intermediate Flow Mixer (IFM) grids, the grid to grid spacing in DNB limiting space is approximately 10 inches compared to the 20 inches in the V5H fuel assemblies. Using the rod bow topical methods (Skaritka, 1979) and scaling with the NRC approved factor results in predicted channel closure in the 10 inch spans of less than 50 percent closure. Therefore, no rod bow DNBR penalty is required in the 10 inch spans in the RFA safety analysis.

The maximum rod bow penalties accounted for in the design safety analysis are based on an assembly average burnup of 24,000 MWD/MTU. At burnups greater than 24,000 MWD/MTU, credit is taken for the effect of $F_{\Delta H}^{N}$ burndown due to the decrease in fissionable isotopes and the buildup of fission product inventory, and no additional rod bow penalty is required (USNRC 1986).

4.4.2.2.6 Transition Core

The original Westinghouse transition core DNB methodology is given in Davidson (et al 1982) and Rahe and was approved by the NRC in Thomas.

An extension of this methodology was approved in Schueren (et al 1990). Using this methodology, transition cores are analyzed as if they were full cores of one assembly type (full V5H or full RFA), applying the applicable transition core penalties. The penalties are included in the safety analysis limit DNBRs such that sufficient margin over the design limit DNBRs exist to accommodate the transition core penalty and other applicable penalties.

4.4.2.3 Flux Tilt Considerations

Significant quadrant power tilts are not anticipated during normal operation since this phenomenon is caused by some asymmetric perturbation. A dropped or misaligned RCCA could cause changes in hot-channel factors; however, these events are analyzed separately in Chapter 15. This discussion will be confined to flux tilts caused by X-Y xenon transients, inlet temperature mismatches, enrichment variations within tolerances and so forth.

The design value of the enthalpy rise hot-channel factor $F(N,\Delta H)$ which includes an 8% uncertainty (as discussed in Section 4.3.2.2.7), is assumed to be sufficiently conservative that flux tilts up to and including the alarm point will not result in values of $F(N,\Delta H)$ greater than that assumed (alarm criteria described in the Technical Specifications and Licensing Requirements Manual). The design value of $F(Q)$ does not include a specific allowance for quadrant flux tilts.

4.4.2.4 Void Fraction Distribution

The calculated core average and the hot subchannel maximum and average void fractions are presented in Table 4.4-2 for operation at full power with overly conservative hot channel factors. The void fraction distribution in the core at various radial and axial locations is presented by Hochreiter and Chelemer (1989) based on THINC-IV predictions. The void models used in the VIPRE-01 Code are described in Section 4.4.2.7.3.

Since void formation due to subcooled boiling is an important supporting cause of interassembly flow redistribution, a sensitivity study was performed with THINC-IV using the void model by Hochreiter and Chelemer (1989).

The results of this study showed that because of the realistic crossflow model used in THINC-IV, the minimum DNBR in the hot channel is relatively insensitive to variations in this model. The range of variations considered in this sensitivity study covered the maximum uncertainty range of the data used to develop each part of the void fraction correlation.

4.4.2.5 Deleted

4.4.2.6 Core Pressure Drops and Hydraulic Loads

4.4.2.6.1 Core Pressure Drops

The analytical model and experimental data used to calculate the
pressure drops shown in Table 4.4-1 are described in Section 4.4.2.7.
The full power operation pressure drop values shown in Table 4.4-1 are
the unrecoverable pressure drops across the vessel, including the
inlet and outlet nozzles, and across the core. These pressure drops
are based on the best estimate flow for actual plant operating
conditions as described in Section 5.1.1. Section 5.1.1 also defines
and describes the thermal design flow (minimum flow) which is the
basis for reactor core thermal performance and the mechanical design
flow (maximum flow) which is used in the mechanical design of the
reactor vessel internals and fuel assemblies. Since the best estimate
flow is that flow which is most likely to exist in an operating plant,
the calculated core pressure drops in Table 4.4-1 will be greater than
pressure drops previously quoted using the thermal design flow.

Uncertainties associated with the core pressure drop values are
discussed in Section 4.4.2.9.2.

4.4.2.6.2 Hydraulic Loads

The fuel assembly holddown springs (Figure 4.2-2) are designed to keep
the fuel assemblies in contact with the lower core plate under all ANS
Condition I and II events with the exception of the turbine overspeed
transient associated with a loss of external load. The holddown
springs are designed to tolerate the possibility of an over deflection
associated with fuel assembly liftoff for this case and provide
contact between the fuel assembly and the lower core plate following
this transient. More adverse flow conditions occur during a LOCA.
These conditions are presented in Section 15.6.5.

Hydraulic loads at normal operating conditions are calculated
considering the mechanical design flow which is described in Section
5.1 and accounting for the minimum core bypass flow based on
manufacturing tolerances. Core hydraulic loads at cold plant start-up
conditions are based on the cold mechanical design flow, but are
adjusted to account for the coolant density difference. Conservative
core hydraulic loads for a pump overspeed transient, which could
possibly create flow rate 18 percent greater than the best estimate
flow, are evaluated to be approximately twice the fuel assembly
weight.

Core hydraulic loads were measured during the prototype assembly tests
described in Section 1.5. Further discussion is presented by DeMario
(1974).

4.4.2.7 Correlation and Physical Data

4.4.2.7.1 Surface Heat Transfer Coefficients

Forced convection heat transfer coefficients are obtained from the Dittus-Boelter correlation (Dittus and Boelter 1930), with the properties evaluated at bulk fluid conditions:

$$\frac{hD_e}{K} = 0.023 \left(\frac{D_e G}{\mu}\right)^{0.8} \left(\frac{C_p \mu}{K}\right)^{0.4} \qquad (4.4-6)$$

where:

h = heat transfer coefficient (Btu/hr-ft^2-°F)
D_e = equivalent diameter (ft)
K = thermal conductivity (Btu/hr-ft-°F)
G = mass velocity (lb$_m$/hr-ft^2)
μ = dynamic viscosity (lb$_m$ft-hr)
C = heat capacity (Btu/lb$_m$-°F)

This correlation has been shown to be conservative (Weisman, 1959) for rod bundle geometries with pitch to diameter ratios in the range used by PWRs.

The onset of nucleate boiling occurs when the clad wall temperature reaches the amount of superheat predicted in Thom's (et al 1955-1966) correlation. After this occurrence, the outer wall temperature is determined by:

$$\Delta T_{sat} = \left[\, 0.072 \, \exp\,(-P/1260)\right] (q")^{0.5} \qquad (4.4-7)$$

where:

ΔT = wall superheat, T_w - T_{sat} (°F)
$q"$ = wall heat flux (Btu/hr-ft^2)
P = pressure (psia)
T_w = outer clad wall temperature (°F)
T_{sat} = saturation temperature of coolant at P (°F)

4.4.2.7.2 Total Core and Vessel Pressure Drop

Unrecoverable pressure losses occur as a result of viscous drag (friction) and/or geometry changes (form) in the fluid flow path. The flow field is assumed to be incompressible, turbulent, single-

phase water. These assumptions apply to the core and vessel pressure drop calculations for the purpose of establishing the reactor coolant loops flow rate. Two-phase considerations are neglected in the vessel pressure drop evaluation because the core average void is negligible (Table 4.4-2). Two-phase flow considerations in the core thermal subchannel analyses are considered and the models are discussed in Section 4.4.4.2.3. Core and vessel pressure losses are calculated by equations of the form:

$$\Delta P_L = (K + F \frac{L}{D_e})_2 \frac{\rho V^2}{g_c (144)} \qquad (4.4-8)$$

where:

ΔP_L = unrecoverable pressure drop (lb_f/in^2)
ρ = fluid density (lb_m/ft^3)
L = length (ft)
D_e = equivalent diameter (ft)
V = fluid velocity (ft/sec)
g_c = 32.174 $(lb_m\text{-}ft/lb_f\text{-}sec^2)$
K = form loss coefficient (dimensionless)
F = friction loss coefficient (dimensionless)

Fluid density is assumed to be constant at the appropriate value for each component in the core and vessel. Because of the complex care and vessel flow geometry, precise analytical values for the form and friction loss coefficients are not available. Therefore, experimental values for these coefficients are obtained from geometrically similar models.

Values are quoted in Table 4.4-1 for unrecoverable pressure loss across the reactor vessel, including the inlet and outlet nozzles, and across the core. The results of full scale tests of core components and fuel assemblies were utilized in developing the core pressure loss characteristics. The pressure drop for the vessel was obtained by combining the core loss with correlation of 1/7th scale model hydraulic test data on a number of vessels (Hetsroni 1964, 1965) and form loss relationships (Idel'chik 1960). Moody's (1944) curves were used to obtain the single phase friction factors.

4.4.2.7.3 Void Fraction Correlation

VIPRE-01 considers two-phase flow in two steps. First, a quality model is used to compute the flowing vapor mass fraction (true quality) including the effects of subcooled boiling. Then, given the true void quality, a bulk void model is applied to compute the vapor volume fraction (void fraction).

VIPRE-01 uses a profile fit model (Sung et al 1999) for determining subcooled quality. It calculates the local vapor volumetric fraction in forced convection boiling by: 1) predicting the point of bubble departure from the heated surface and 2) postulating a relationship between the true local vapor fraction and the corresponding thermal equilibrium value.

The void fraction in the bulk boiling region is predicted by using homogeneous flow theory and assuming no slip. The void fraction in this region is therefore a function only of the thermodynamic quality.

4.4.2.8 Thermal Effects of Operational Transients

Departure from nucleate boiling core safety limits are generated as a function of reactor coolant temperature, pressure, core power, and axial power imbalance. Steady state operation within these safety limits ensures that the minimum DNBR is not less than the safety analysis limit DNBR. Figure 15.0.3-1 shows the limit lines and the resulting overtemperature ΔT trip lines (which become part of the Technical Specifications), plotted as ΔT versus T_{avg} for various pressures for DNBRs greater than or equal to the safety analysis DNBR limit. This system provides adequate protection against anticipated operational transients that are slow with respect to fluid transport delays in the RCS. In addition, for fast transients, for example, uncontrolled rod bank withdrawal at power incident, (Section 15.4.2) specific protection functions are provided as described in Section 7.2 and the use of these protection functions is described in Chapter 15. The thermal response of the fuel rod is discussed in Section 4.4.4.8.

4.4.2.9 Uncertainties in Estimates

4.4.2.9.1 Uncertainties in Fuel and Clad Temperatures

As discussed in Section 4.4.2.11, the fuel temperature is a function of crud, oxide, clad, gap, and pellet conductances. Uncertainties in the fuel temperature calculation are essentially of two types: 1) fabrication uncertainties such as variations in the pellet and clad dimensions and the pellet density; and 2) model uncertainties such as variations in the pellet densification and the gap conductance.

In addition to the above measurement uncertainty in determining the
local power, and the effect of density and enrichment variations on
the local power are considered in establishing the heat flux hot
channel factor.   These uncertainties are described in Section
4.3.2.2.1.

Reactor trip set points, as specified in the Technical Specifications,
include allowance for instrument and measurement uncertainties such as
calorimetric error, instrument drift and channel reproducibility,
temperature measurement uncertainties, noise, and heat capacity
variations.

4.4.2.9.2 Uncertainties in Pressure Drops

Core and vessel pressure drops based on the best estimate flow, as
described in Section 5.1, are quoted in Table 4.4-1.   The
uncertainties quoted are based on the uncertainties in both the test
results and the analytical extension of these values to the reactor
application.

A major use of the core and vessel pressure drops is to determine the
RCS flow rates as discussed in Section 5.1. In addition, as discussed
in Section 4.4.5.1, tests on the primary system prior to initial
criticality will be made to verify that a conservative RCS flow rate
has been used in the design and analyses of BVPS-2.

4.4.2.9.3 Uncertainties Due to Inlet Flow Maldistribution

The effects of uncertainties in the inlet flow maldistribution
criteria used in the core thermal analyses are discussed in Section
4.4.4.2.2.

4.4.2.9.4 Uncertainty in Departure from Nucleate Boiling correlation

The uncertainty in the DNB correlation (Section 4.4.2.2) can be written as a statement on the probability of not being in DNB based on the statistics of the DNB data. This is discussed in Section 4.4.2.2.2.

4.4.2.9.5   Uncertainties in Departure from Nucleate Boiling Ratio Calculations

The uncertainties in the DNBRs calculated by VIPRE-01 analysis (Section 4.4.4.5.1) due to uncertainties in the nuclear peaking factors are accounted for by applying conservatively high values of the nuclear peaking factors and including measurement error allowances in the statistical evaluation of the limit DNBR (Section 4.4.1.1) using the revised thermal design procedure (Friedland, Ray, 1989). In addition, conservative values for the engineering hot channel factors are used as discussed in Section 4.4.2.2.4.

The ability of the VIPRE-01 computer code to accurately predict flow and enthalpy distributions in rod bundles is discussed in Sections 4.4.4.5.1, 4.4.4.5.2, 4.4.4.5.3 and 4.4.4.5.4 and in (Sung et al 1999). Studies (Sung et al 1999) have been performed to determine the sensitivity of the minimum DNBR to the void fraction correlation (see also Section 4.4.2.7.3) and the inlet flow distributions. The results of these studies show that the minimum DNBR is relatively insensitive to variation in these parameters. Furthermore, the VIPRE-01 flow field model for predicting conditions in the hot channels is consistent with that used in the derivation of the DNB correlation limits including void/quality modeling, turbulent mixing and crossflow and two phase flow (Sung et al 1999).

4.4.2.9.6 Uncertainties in Flow Rates

The uncertainties associated with reactor coolant loop flow rates are discussed in Section 5.1. A thermal design flow is defined for use in core thermal performance evaluations which is less than the Best Estimate Loop Flow (by approximately 10%). In addition, another 6.5 percent of the thermal design flow is assumed to be ineffective for core heat removal capability because it bypasses the core through the various available vessel flow paths described in Section 4.4.4.2.1.

4.4.2.9.7 Uncertainties in Hydraulic Loads

As discussed in Section 4.4.2.6.2, hydraulic loads on the fuel assembly are evaluated for a pump overspeed transient which creates flow rates 18 percent greater than the best estimate flow.

4.4.2.9.8 Uncertainty in Mixing Coefficient

The value of the mixing coefficient used in THINC analyses for this
application is 0.038. VIPRE-01 uses a value equivalent to the THINC
value. The mean value of TDC obtained in the "R" grid mixing tests
described in Section 4.4.2.2.1 was 0.042 (for 26-inch grid spacing).
The value 0.038 is one standard deviation below the mean value; and
approximately 90 percent of the data gives values of TDC greater than
0.038 (Cadek et al 1975).

The results of the mixing tests done on 17 by 17 geometry, as
discussed in Section 4.4.2.2.3, had a mean value of TDC of 0.059 and
standard deviation equal to 0.007. Hence the current design value of
TDC is almost three standard deviations below the mean for 26-inch
grid spacing.

4.4.2.10 Flux Tilt Considerations

Significant quadrant power tilts are not anticipated during normal
operation since this phenomenon is caused by some asymmetric
perturbation. A dropped or misaligned rod cluster control assembly
could cause changes in hot channel factors; however, these events are
analyzed separately in Chapter 15.

Other possible causes for quadrant power tilts include X-Y xenon
transients, inlet temperature mismatches, enrichment variations within
tolerances, and so forth.

In addition to the preceding unanticipated quadrant power tilts, other
readily explainable asymmetries may be observed during calibration of
the excore detector quadrant power tilt alarm. During operation,
incore maps are taken at least once per month and, periodically,
additional maps are obtained for calibration purposes. Each of these
maps is reviewed for deviations from the expected power distributions.
Asymmetry in the core, from quadrant to quadrant, is frequently a
consequence of the design when assembly and/or component shuffling and
rotation requirements do not allow exact symmetry preservation. In
each case, the acceptability of an observed asymmetry, planned or
otherwise depends solely on meeting the required accident analyses
assumptions.

In practice, once acceptability has been established by review of the
incore maps, the quadrant power tilt alarms and related
instrumentation are adjusted to indicate zero quadrant power tilt
ratio as the final step in the calibration process. This action
ensures that the instrumentation is correctly calibrated to alarm in
the event an unexplained or unanticipated change occurs in the
quadrant to quadrant relationships between calibration intervals.
Proper functioning of the quadrant power tilt alarm is important
because no allowances are made in the design for increased hot channel

factors due to unexpected flux tilts since all likely causes are prevented by design or procedures, or are specifically analyzed. Finally in the event that unexplained flux tilts do occur, the Technical Specifications and Licensing Requirements Manual provide appropriate corrective actions to ensure continued safe operation of the reactor.

4.4.2.11 Fuel and Cladding Temperatures (Including Densification)

Consistent with the thermal-hydraulic design bases described in Section 4.4.1, the following discussion pertains mainly to fuel pellet temperature evaluation. A discussion of fuel clad integrity is presented in Section 4.2.3.1.

The thermal-hydraulic design assures that the maximum fuel temperature is below the melting point of UO_2 (Section 4.4.1.2). To preclude center melting and as a basis for overpower protection system set points, a calculated centerline fuel temperature of 4,700°F has been selected as the overpower limit. This provides sufficient margin for uncertainties in the thermal evaluations as described in Section 4.4.2.9.1. The temperature distribution within the fuel pellet is primarily a function of the local power density and the UO_2 thermal conductivity. However, the computation of radial fuel rod temperature distributions combines crud, oxide, clad gap, and pellet conductances. The factors which influence these conductances, such as gap size (or contact pressure), internal gas pressure, gas composition, pellet density, and radial power distribution within the pellet, etc, have been combined into a semiempirical thermal model (Section 4.2.3.3) with the model modifications for time dependent fuel densification given by Hellman (1975). This thermal model enables the determination of these factors and their net effects on temperature profiles. The temperature predictions have been compared to inpile fuel temperature measurements (Kjaerheim and Rolstad 1967; Kjaerheim 1969; Cohen et al 1960; Clough and Sayers 1964; Stora et al 1964; Devold 1968; and Balfour et al 1966) and melt radius data (Nelson et al 1964 and Duncan 1962) with good results.

According to Hellman (1975), fuel rod thermal evaluations (fuel centerline, average and surface temperatures) are determined throughout the fuel rod lifetime with consideration of time dependent densification. To determine the maximum fuel temperatures, various burnup rods, including the highest burnup rod are analyzed over the rod linear power range of interest.

Effect of Fuel Densification on Fuel Rod Temperatures

Fuel densification results in fuel pellet shrinkage. This affects the fuel temperatures in the following ways:

  1. Pellet radial shrinkage increased the pellet diametral gap which results in increased thermal resistance of the gap, and thus, higher fuel temperatures (see Section 4.2.3.3).

2. Pellet axial shrinkage may produce pellet to pellet gaps
    which results in local power spikes, described in Section
    4.3.2.2.5. The improved methodology described by Kersting
    (et al 1995) shows that the penalty due to this is
    negligible.

3. Pellet axial shrinkage will result in a fuel stack height
    reduction and an increased linear power generation rate
    (kW/ft) for a constant core power level. Using the methods
    described in Section 5.3 of Hellman 1973, the increase in
    linear power for the fuel rod specifications listed in Table
    4.3-1 is 0.2%.

    As described in Hellman 1973, fuel rod thermal evaluations
    (fuel centerline, average and surface temperatures) are
    determined throughout the fuel rod lifetime with
    consideration of time dependent densification. Maximum fuel
    average and surface temperatures, shown in Figure 4.4-9 as a
    function of the LHGR, are peak values attained during the
    fuel lifetime. Figure 4.4-10 presents the peak value of fuel
    centerline temperature versus linear power density which is
    attained during the fuel lifetime.

    The maximum pellet temperatures at the hot spot during full
    power steady state and at the maximum overpower trip point
    are shown in Table 4.4-1.

The principal factors which are employed in the determination of the
fuel temperature are discussed below.

4.4.2.11.1 UO_2 Thermal Conductivity

The thermal conductivity of uranium dioxide was evaluated from data
reported by Howard and Gulvin (1960); Lucks and Deem (1961); Daniel
(et al 1962); Feith (1962); Vogt (et al 1964); Nishijima (et al 1965),
Ainscough and Wheeler (1968); Godfrey (et al 1964); Stora (et al
1964); Bush (1965); Asamoto (et al 1968); Kruger (1968); and Gyllander
(1971).

At higher temperatures, thermal conductivity is best obtained by
utilizing the integral conductivity to melt, which can be determined
with more certainty. From an examination of the data, it has been
concluded that the best estimate for the value of $\int 2,800°C \, Kdt$ is 93
W/cm. This conclusion is based on the integral values reported by
Duncan (1962); Gyllander (1971); Lyons (et al 1966); Coplin (1968);
Bain (1962); and Stora (1970).

The design curve for the thermal conductivity is shown on Figure
4.4-11. The section of the curve at temperatures between 0°C and
l,300°C is in excellent agreement with the recommendation of the
International Atomic Energy Agency (1966) panel. The section of the
curve above l,300°C is derived for an integral value of 93 W/cm (Duncan
1962, Gyllander 1971, and Stora 1970).

Thermal conductivity of UO_2 at 95 percent theoretical density can be represented best by the following equation:

$$K = \frac{1}{11.8 + 0.0238T} + 8.775 \times 10^{-13} \, T^3 \qquad (4.4-9)$$

where:

    K = W/cm-°C
    T = °C

4.4.2.11.2 Radial Power Distribution in UO_2 Fuel Rods

An accurate description of the fuel rod radial power distribution as a function of burnup is needed for determining the power level for incipient fuel melting and other important performance parameters such as pellet thermal expansion, fuel swelling, and fission gas release rates.

Radial power distributions in UO_2 fuel rods are determined with the neutron transport theory code, LASER. The LASER Code has been validated by comparing the code predictions on radial burnup and isotopic distributions with measured radial microdrill data (Poncelet 1965 and Nodvick 1970). A radial power depression factor f, is determined using radial power distributions predicted by LASER. The factor f enters into the determination of the pellet centerline temperature, T_C, relative to the pellet surface temperature, T_S, through the expression:

$$\int_{T_S}^{T_C} K(T) \ dT \ = \ \frac{q' f}{4\pi} \qquad\qquad (4.4\text{-}10)$$

where:

$K(T)$ = the thermal conductivity for UO_2 with a uniform density distribution.

q' = the linear power generation rate.

4.4.2.11.3 Gap Conductance

The temperature drop across the pellet-clad gap is a function of the gap size and the thermal conductivity of the gas in the gap. The gap conductance model is selected such that when combined with the UO_2 thermal conductivity model, the calculated fuel centerline temperatures predict the inpile temperature measurements.

The temperature drop across the gap is calculated by assuming an annular gap conductance model of the following form:

$$h \ = \ \frac{K_{gas}}{\dfrac{\delta}{2} \ + \ \delta_r} \qquad\qquad (4.4\text{-}11)$$

where:

h = contact conductance (Btu/hr-ft^2-°F),

K_{gas} = thermal conductivity of the gas mixture including a correction factor (Dean 1962), for the accommodation coefficient for light gases, for example, helium (Btu/hr-ft-°F),

δ = diametral gap size (ft),

δ_r = effective gap spacing due to surface roughness (ft),

or an empirical correlation derived from thermocouple and melt radius data. The larger gap conductance value from Equations 4.4-10 and 4.4-11 is used to calculate the temperature drop across the gap for finite gaps.

For evaluations in which the pellet-clad gap is closed, a contact conductance is calculated. The contact conductance between UO_2 and Zirconium alloys has been measured and found to be dependent on the contact pressure composition of the gas at the interface and the surface roughness (Dean 1962). This information together with the pellet and clad inner surface roughness for Westinghouse fuel leads to the following correlation:

$$h = 0.6P + \frac{K_{gas}}{\delta_r} \qquad\qquad (4.4\text{-}12)$$

where:

P = contact pressure (psi)

4.4.2.11.4 Surface Heat Transfer Coefficients

The fuel rod surface heat transfer coefficients during subcooled forced convection and nucleate boiling are presented in Section 4.4.2.7.1.

4.4.2.11.5 Fuel Clad Temperatures

The outer surface of the fuel rod at the hot spot operates at a temperature of approximately 660°F for steady state operation at rated power throughout core lift due to the presence of nucleate boiling. Initially (beginning-of-life), this temperature is that of the clad metal outer surface.

During operation over the life of the core, the buildup of oxides and crud on the fuel rod surface causes the clad surface temperature to increase. Allowance is made in the fuel center melt evaluation for this temperature rise. Since the thermal-hydraulic design basis limits DNB, adequate heat transfer is provided between the fuel clad and the reactor coolant so that the core thermal output is not limited by considerations of clad temperature. Figure 4.4-12 shows the axial variations of average clad temperature for the average power rod both at beginning and end-of-life.

4.4.2.11.6 Treatment of Peaking Factors

The total heat flux hot channel factor, F_Q, is defined as the ratio of the maximum to average core heat flux. The design value for F_Q is limited as a result of certain design basis accident analyses (i.e., small-break LOCA), and is contained in Table 4.1-1.

The peak linear power resulting from overpower transients/operator errors (assuming maximum overpower of 118 percent) is 22.4 kW/ft. The centerline temperature kW/ft must be below the UO_2 melt temperature over the lifetime of the rod, including allowances for uncertainties. The fuel temperature design basis is discussed in Section 4.4.1.2 and results in a maximum allowable calculated centerline temperature of 4,700°F. The peak linear power which would result in centerline melt is less than 22.4 kw/ft. The centerline temperature at the peak linear power resulting from overpower transients/operator errors (assuming a maximum overpower of 118 percent) is below that required to produce melting.

4.4.3 Description of the Thermal and Hydraulic Design of the Reactor
Coolant System

4.4.3.1 Plant Configuration Data

Plant configuration data for the thermal hydraulic and fluid systems
external to the core are provided as appropriate in Chapters 5, 6, and
9. Implementation of the ECCS is discussed in Chapter 15. Some
specific areas of interest are as follows:

1. Total reactor coolant flow rates for the RCS and each loop
    are provided in Table 5.1-1. Flow rates employed in the
    evaluation of the core are presented throughout Section 4.4.

2. Total RCS volume including pressurizer and surge line, RCS
    liquid volume including pressurizer water at steady state
    power conditions are given in Table 5.1-1.

3. The flow path length through each volume may be calculated
    from physical data provided in the preceding referenced
    tables.

4. The height of fluid in each component of the RCS may be
    determined from the physical data presented in Section 5.4.
    The components of the RCS are water filled during power
    operation with the pressurizer being approximately 60 percent
    water filled.

5. Components of the ECCS are located to meet the criteria for
    net positive suction head (NPSH) described in Section 6.3.

6. Line lengths and sizes for the safety injection system (SIS)
    are determined so as to guarantee a total system resistance
    which will provide, as a minimum, the fluid delivery rates
    assumed in the safety analyses described in Chapter 15.

7. The parameters for components of the RCS are presented in
    Section 5.4.

8. The steady state pressure drops and temperature distributions
    through the RCS are presented in Table 5.1-1.

4.4.3.2 Operating Restrictions on Pumps

The minimum NPSH and minimum seal injection flow rate must be
established before operating the reactor coolant pumps (RCPs). With
the minimum 6 gpm labyrinth seal injection flow rate established
before each RCP operation, the operator will have to verify that the
system pressure satisfies NPSH requirements.

4.4.3.3 Power-Flow Operating Map (Boiling Water Reactor)

Not applicable to BVPS-2.

4.4.3.4 Temperature-Power Operating Map

The relationship between RCS temperature and power and the effects of
reduced core flow due to inoperative pumps is discussed in Sections
5.4.1, 15.2.5, and 15.3.4.

4.4.3.5 Load Following Characteristics

The RCS is designed on the basis of steady state operation at full
power heat load. The RCPs utilize constant speed drives as described
in Section 5.4 and the reactor power is controlled to maintain average
reactor coolant temperature at a value which is a linear function of
load, as described in Section 7.7.

4.4.3.6 Thermal and Hydraulic Characteristics Summary Table

The thermal and hydraulic characteristics are given in Tables 4.3-1,
4.4-1, and 4.4-2.

4.4.4 Evaluation

4.4.4.1 Critical Heat Flux

The critical heat flux correlation utilized in the core thermal
analysis is explained in detail in Section 4.4.2.

4.4.4.2 Core Hydraulics

4.4.4.2.1 Flow Path Considered in Core Pressure Drop and Thermal
Design

The following flow paths for core bypass flow are considered:

    1. Flow entering into the fuel assembly guide thimbles to cool
        the control rods and other core components.

    2. Flow through the spray nozzles into the upper head for head
        cooling purposes.

    3. Leakage flow from the vessel inlet nozzle directly to the
        vessel outlet nozzle through the gap between the vessel and
        the barrel.

4. Flow introduced between the baffle and the barrel for the purpose of cooling these components and which is not considered available for core cooling.

5. Flow in the gaps between the fuel assemblies on the core periphery and the adjacent baffle wall.

These flow paths are evaluated to confirm that the design value of the core bypass flow is met. The design value of core bypass flow for BVPS-2 is equal to 6.5 percent of the total vessel flow.

Of the total allowance, 4.0 percent is associated with the core and the remainder is associated with the internals (items 2 through 5). Calculations have been performed using drawing tolerance in the worst direction and accounting for uncertainties in pressure losses. Based on these calculations, the core bypass is no greater than the preceding design values quoted.

Flow model test results for the flow path through the reactor are discussed in Section 4.4.2.7.2.

4.4.4.2.2   Inlet Flow Distributions

Data from several l/7th scale hydraulic reactor model tests (Hetsroni 1964 and 1965, and Carter 1972) have been utilized in arriving at the core inlet flow maldistribution criteria to be used in the VIPRE-01 analyses (Section 4.4.4.5.1). THINC-I analyses made, using this data have indicated that a conservative design basis is to consider 5 percent reduction in the flow to the hot assembly (Shefcheck 1972). The same design basis of 5 percent reduction to the hot assembly inlet is used in VIPRE-01 analyses.

The experimental error estimated in the inlet velocity distribution has been considered as outlined by Hochreiter and Chelemer (1989) where the sensitivity of changes in inlet velocity distributions to hot channel thermal performance is shown to be small. Hochreiter and Chelemer (1989) studies made with a subchannel code show that it is adequate to use the 5 percent reduction in inlet flow to the hot assembly for a reactor coolant loop out of service based on the experimental data presented by Hetsroni (1964 and 1965).

The effect of the total flow rate on the inlet velocity distribution was studied in the experiments by Hetsroni (1964). As was expected, on the basis of the theoretical analysis, no significant variation could be found in inlet velocity distribution with reduced flow rate.

4.4.4.2.3   Empirical Friction Factor Correlations

Two empirical friction factor correlations are used in the VIPRE-01 Code (Section 4.4.4.5.1).

The friction factor for VIPRE-01 in the axial direction, parallel to the fuel rod axis, is evaluated using a correlation for a smooth tube (Sung et al 1999). The effect of two-phase flow on the friction loss is expressed in terms of the single-phase friction pressure drop and a two phase friction multiplier. The multiplier is calculated using the homogenous equilibrium flow model.

The flow in the lateral directions, normal to the fuel rod axis, views the reactor core as a large tube tank. Thus, the lateral friction factor proposed by Idel'chik (1960) is applicable. This correlation is of the form:

$$F_L \quad = \quad A \; Re_L^{-0.2} \hspace{4cm} (4.4\text{-}13)$$

where:

   A = a function of the rod pitch and diameter as given by Idel'chik (1960)

   Re_L = the lateral Reynolds number based on the rod diameter.

Extensive comparisons of VIPRE-01 to THINC-IV predictions, which are given in (Sung et al 1999), verify the applicability of the VIPRE-01 correlations in PWR design.

4.4.4.3 Influence of Power Distribution

The core power distribution which is largely established at beginning-of-life by fuel enrichment, loading pattern, and core power level is also a function of variables such as control rod worth and position, and fuel depletion throughout lifetime. Radial power distributions in various planes of the core are often illustrated for general interest, however, the core radial enthalpy rise distribution as determined by the integral of power up each channel is of greater importance for DNB analyses. These radial power distributions, characterized by $F_{\Delta H}^N$ (Section 4.3.2.2.1) as well as axial heat flux profiles are discussed in Sections 4.4.4.3.1 and 4.4.4.3.2.

4.4.4.3.1 Nuclear Enthalpy Rise Hot Channel Factor, $F_{\Delta H}^N$

Given the local linear power density q'(kW/ft) at a point x, y, z in a core with N fuel rods and height H,

$$F_{\Delta H}^N = \frac{\text{hot rod power}}{\text{average rod power}} = \frac{\text{Max} \int_o^H q'(x_o, y_o, z)\,dz}{\dfrac{1}{N} \sum_{\text{all rods}} \int_o^H q'(x, y, z)\,dz} \qquad (4.4\text{-}14)$$

The way in which $F_{\Delta H}^N$ is used in the DNB calculation is important. The location of minimum DNBR depends on the axial profile, and the value of DNBR depends on the enthalpy rise to that point. Basically, the maximum value of the rod integral is used to identify the most likely rod for minimum DNBR. An axial power profile is obtained which when normalized to the design value of $F_{\Delta H}^N$, recreates the axial heat flux along the limiting rod. The surrounding rods are assumed to have the same axial profile with rod average powers which are typical distributions found in hot assemblies. In this manner, worst case axial profiles can be combined with worst case radial distributions for reference DNB calculations.

It should be noted again that $F_{\Delta H}^N$ is an integral and is used as such in DNB calculations. Local heat fluxes are obtained by using hot channel and adjacent channel explicit power shapes which take into account variations in horizontal power shapes throughout the core.

For operation at a fraction P of full power, the design $F_{\Delta H}^N$ used is given as 1.62 for RFA and 1.456 for V5H. This analysis basis conservatively bounds the $F_{\Delta H}^N$ limits as presented in the technical specifications.

For operation at a fraction P of full power, relaxation of $F_{\Delta H}^N$ is allowed. The permitted relaxation of $F_{\Delta H}^N$ is included in the DNB protection setpoints and allows radial power shape changes with rod insertion to the insertion limits (McFarlane 1975), thus allowing greater flexibility in the nuclear design.

4.4.4.3.2 Axial Heat Flux Distributions

As discussed in Section 4.3.2.2, the axial heat flux distribution can vary as a result of rod motion, power change, or due to a spatial

xenon transient which may occur in the axial direction. Consequently, it is necessary to measure the axial power imbalance by means of the excore nuclear detectors (Section 4.3.2.2.7) and protect the core from excessive axial power imbalance. The Reactor Trip System provides automatic reduction of the trip setpoint in the Overtemperature ΔT channels on excessive axial power imbalance; that is, when an extremely large axial offset corresponds to an axial shape which could lead to a DNBR which is less than that calculated for the reference DNB design axial shape.

The reference DNB design axial shape used in this amendment is a chopped cosine shape with a peak average value of 1.55.

4.4.4.4 Core Thermal Response

A general summary of the steady state thermal-hydraulic design parameters including thermal output, flow rates, etc, is provided in Table 4.4-1 for all reactor coolant loops in operation.

As stated in Section 4.4.1, the design bases of the application are to prevent DNB and to prevent fuel melting for ANS Condition I and II events.   The protective systems described in Chapter 7 (Instrumentation and Control) are designed to meet these bases. The response of the core to ANS Condition II transients is given in Chapter 15.

4.4.4.5 Analytical Techniques

4.4.4.5.1 Core Analysis Techniques with VIPRE

The objective of reactor core thermal design is to determine the
maximum heat removal capability in all flow subchannels and to show
that the core safety limits, as presented in the Technical
Specifications, are not exceeded while compounding engineering and
nuclear effects. The thermal design takes into account local
variations in dimensions, power generation, flow redistribution, and
mixing. VIPRE-01 (VIPRE) is a three dimensional subchannel code that
has been developed to account for hydraulic and nuclear effects on the
enthalpy rise in the core and hot channels (Stewart et al 1989).
VIPRE modeling of a PWR core is based on one-pass modeling approach
(Sung, et al 1999). In the one-pass modeling, hot channels and their
adjacent channels are modeled in detail, while the rest of the core is
modeled simultaneously on a relatively coarse mesh. The behavior of
the hot assembly is determined by superimposing the power distribution
upon the inlet flow distribution while allowing for flow mixing and
flow distribution between flow channels. Local variations in fuel rod
power, fuel rod and pellet fabrication, and turbulent mixing are also
considered in determining conditions in the hot channel. Conservation
equations of mass, axial and lateral momentum, and energy are solved
for the fluid enthalpy, axial flow rate, lateral flow and pressure
drop.

4.4.4.5.2 Steady State Analysis

The VIPRE core model as approved by the U.S. Nuclear Regulatory
Commission (USNRC) (Sung et al 1999) is used with the applicable DNB
correlations to determine DNBR distributions along the hot channels of
the reactor core under all expected operating conditions. The VIPRE
code is described in detail in (Stewart et al 1989), including
discussions on code validation with experimental data. The VIPRE
modeling method is described in (Sung et al 1999), including empirical
models and correlations used. The effect of crud on the flow and
enthalpy distribution in the core is not directly accounted for in the
VIPRE evaluations. However, conservative treatment by the VIPRE
modeling method has been demonstrated to bound this effect in DNBR
calculations (Sung et al 1999).

4.4.4.5.3 Experimental Verification

Extensive experimental verification of VIPRE-01 is presented by
Stewart (et al 1989).

The VIPRE-01 analysis is based on a knowledge and understanding of the
heat transfer and hydrodynamic behavior of the reactor coolant flow
and the mechanical characteristics of the fuel elements. The use of
the VIPRE-01 analysis provides a realistic evaluation of the core
performance and is used in thermal-hydraulic analyses as described
previously.

4.4.4.5.4 Transient Analysis

VIPRE-01 is capable of transient DNB analysis. The conservative
equations in the VIPRE-01 code contain the necessary accumulation
terms for transient calculations. The input description can include
one or more of the following time dependent arrays:

        1.   Inlet flow variation
        2.   Core Heat flux variation
        3.   Core pressure variation
        4.   Inlet temperature or enthalpy variation

At the beginning of the transient, the calculation procedure is
carried out as in the steady state analysis. The time is incremented
by an amount determined either by the user or by the time step control
options in the code itself. At each new time step, the calculations
are carried out with the addition of the accumulation terms which are
evaluated using the information from the previous time step. This
procedure is continued until a preset maximum time is reached.

At time intervals selected by the user, a complete description of the
reactor coolant parameter distributions as well as DNBR is printed
out. In this manner the variation of any parameter with time can be
readily determined.

4.4.4.5.5 Fuel Temperatures

As discussed in 4.4.2.11, the fuel rod behavior is evaluated utilizing a semi-empirical thermal model which considers in addition to the thermal aspects such items as clad creep, fuel swelling, fission gas release, release of absorbed gases, cladding corrosion and elastic deflection, and helium solubility.

A detailed description of the thermal model can be found in Leech (et al 1982) and Weiner (et al 1988). A description of additional model changes is given in Foster (et al 2000).

4.4.4.6 Hydrodynamic and Flow Power Coupled Instability

Boiling flows may be susceptible to thermohydraulic instabilities (Boure, et al 1973). These instabilities are undesirable in reactors because they may cause a change in thermohydraulic conditions that may lead to a reduction in the DNB heat flux relative to that observed during a steady flow condition or to undesired forced vibrations of core components. Therefore, a thermohydraulic design criterion was developed which states that modes of operation under Condition I and II events will not lead to thermohydrodynamic instabilities.

Two specific types of flow instabilities are considered for Westinghouse PWR operation. These are the Ledinegg or flow excursion type of static instability and the density wave type of dynamic instability.

A Ledinegg instability involves a sudden change in flow rate from one steady state to another. This instability occurs (Bourne, et al 1973) when the slope of the Reactor Coolant System pressure drop-flow rate curve ($\partial\Delta P/\partial Gl$ internal) becomes algebraically smaller than the loop supply (pump head) pressure drop-flow rate curve ($\partial\Delta P/\partial Gl$ external). The criterion for stability is $\partial\Delta P/\partial Gl$ internal > $\partial\Delta P/\partial Gl$ external. The Westinghouse pump head curve has a negative slope ($\partial\Delta P/\partial Gl$ external < 0) whereas the Reactor Coolant System pressure drop-flow curve has a positive slope ($\partial\Delta P/\partial Gl$ internal > 0) over the Condition I and Condition II operational ranges. Thus, the Ledinegg instability will not occur.

The mechanism of density wave oscillations in a heated channel has been described by Lahey and Moody (1977). Briefly, an inlet flow fluctuation produces an enthalpy perturbation. This perturbs the length and the pressure drop of the single-phase region and causes quality or void perturbations in the two-phase regions which travel up the channel with the flow. The quality and length perturbations in the two-phase region create two-phase pressure drop perturbations. However, because the total pressure drop across the core is maintained by the characteristics of the fluid system external to the core, the two-phase pressure drop perturbation feeds back to the single phase region. These resulting perturbations can be either attenuated or self-sustained.

A simple method has been developed by Ishii (Saha, Ishii and Zuber, 1976) for parallel closed channel systems to evaluate whether a given condition is stable with respect to the density wave type of dynamic instability. This method has been used to assess the stability of typical Westinghouse reactor designs under Condition I and II operation. The results indicate that a large margin to density wave instability exists; for example, increases on the order of 150 to 200 percent of rated reactor power would be required for the predicted inception of this type of instability.

The application of Ishii's method to Westinghouse reactor designs is conservative because of the parallel open channel feature of Westinghouse PWR cores. For such cores, there is little resistance to lateral flow leaving the flow channels of high power density. There is also energy transfer from high power density channels to lower power density channels. This coupling with cooler channels causes an open channel configuration to be more stable than the above closed channel configuration under the same boundary conditions. Flow stability tests (Kakac et al 1974 and Taleyarkhan et al 1983) have been conducted in which the closed channel systems were shown to be less stable than when the same channels were cross-connected at several locations. The cross-connections were such that the resistance to channel-to-channel crossflow and enthalpy perturbations would be greater than that which would exist in a PWR core which has a relatively low resistance to crossflow.

Flow instabilities, which have been observed, have occurred almost exclusively in closed channel systems operating at low pressures relative to the Westinghouse PWR operating pressures. Kao, Morgan and Parker (1973) analyzed parallel closed channel stability experiments simulating a reactor core flow. These experiments were conducted at pressures up to 2200 psia. The results showed that for flow and power levels typical of power reactor conditions, no flow oscillations could be induced above 1200 psia.

Additional evidence that flow instabilities do not adversely affect thermal margin is provided by the data from the rod bundle DNB tests. Many Westinghouse rod bundles have been tested over wide ranges of operating conditions with no evidence of premature DNB or of inconsistent data which might indicate flow instabilities in the rod bundle.

In summary, it is concluded that thermohydrodynamic instabilities will not occur under Condition I and II modes of operation for Westinghouse PWR reactor designs. A large power margin, greater than doubling rated power, exists to predicted inception of such instabilities. Analysis has been performed which shows that minor plant-to-plant differences in Westinghouse reactor designs - such as fuel assembly arrays, core power to flow ratios, and fuel assembly length - will not result in gross deterioration of the above power margins.

4.4.4.7 Temperature Transient Effects Analysis

Waterlogging damage of a fuel rod could occur as a consequence of a power increase on a rod after water has entered the fuel rod through a clad defect. Water entry will continue until the fuel rod internal pressure is equal to the reactor coolant pressure. A subsequent power increase raises the temperature and, hence, could raise the pressure of the water contained within the fuel rod. The increase in hydrostatic pressure within the fuel rod then drives a portion of the water from the fuel rod through the water entry defect. Clad distortion and/or rupture can occur if the fuel rod internal pressure increase is excessive due to insufficient venting of water to the reactor coolant. This occurs when there is both a rapid increase in the temperature of the water within the fuel rod and a small defect, Zircaloy clad fuel rods which have failed due to water logging (Stephen 1970) (Western NY Nuclear Research Center 1971) indicate that very rapid power transients are required for fuel failure. Normal operational transients are limited to about 40 cal/gm-min peak rod while the Spert tests (Stephen 1970) indicate that 120 to 150 cal/gm is required to rupture the clad even with very short transients (5.5 msec. period). Release of the internal fuel rod pressure is expected to have a minimal effect on the reactor coolant system (Stephen 1970) and is not expected to result in failure of additional fuel rod (Stephen 1970). Ejection of fuel pellet fragments into the coolant stream is not expected (Stephen 1979) (Western N.Y. Nuclear Research Center 1971). A clad breech due to waterlogging is thus expected to be similar to any fuel rod failure mechanism which exposes fuel pellets to the reactor coolant stream. Waterlogging has not been identified as the mechanism for clad distortion or perforation of any Westinghouse Zirconium alloy clad fuel rods.

An excessively high fuel rod internal gas pressure could cause clad failure. One of the fuel rod design bases (Section 4.2.1.) is that the fuel rod internal gas pressure does not exceed the nominal coolant pressure even at the overpower condition. During operational transients, fuel rod clad rupture due to high internal gas pressure is precluded by meeting the above design basis.

4.4.4.8 Potentially Damaging Temperature Effects During Transients

The fuel rod experiences many operational transients (intentional maneuvers) during its residence in the core. A number of thermal effects must be considered when analyzing the fuel rod performance.

The clad can be in contact with the fuel pellet at some time in the fuel lifetime. Clad-pellet interaction occurs if the fuel pellet temperature is increased after the clad is in contact with the pellet. Clad-pellet interaction is discussed in Section 4.2.1.3.1.

Increasing the fuel temperature results in an increased fuel rod internal pressure. One of the fuel rod design bases is that the fuel rod internal pressures do not exceed the nominal coolant pressure even at the overpower condition (Section 4.2.1.1.1.).

The potential effects of operation with waterlogged fuel are discussed in Section 4.4.4.7 which concluded that waterlogging is not a concern during operational transients.

Clad flattening, as noted in Section 4.2.1.3.1, has been observed in some operating power reactors. Thermal expansion (axial) of the fuel rod stack against a flattened section of clad could cause failure of the clad. This is no longer a concern because clad flattening is precluded during the fuel residence in the core (see section 4.2.1.3.1).

There can be a differential thermal expansion between the fuel rods and the guide thimbles during a transient. Excessive bowing of the fuel rods could occur if the grid assemblies did not allow axial movement of the fuel rods relative to the grids. Thermal expansion of the fuel rods is considered in the grid design so that axial loads imposed on the fuel rods during a thermal transient will not result in excessively bowed fuel rods (see Section 4.2.1.2.2).

4.4.4.9 Energy Release During Fuel Element Burnout

As discussed, the core is protected from going through DNB over the full range of possible operating conditions. In the extremely unlikely event that DNB should occur, the clad temperature will rise due to the steam blanketing at the rod surface and the consequent degradation in heat transfer. During this time there is a potential for a chemical reaction between the cladding and the coolant. However, because of the relatively good film boiling heat transfer following DNB, the energy release resulting from this reaction is insignificant compared to the power produced by the fuel.

DNB With Physical Burnout

Westinghouse (Weisman, Wenzel, and Tong 1968) has conducted DNB tests in 25-rod bundle where physical burnout occurred with one rod. After this occurrence, the 25 rod test section was used for several days to obtain more DNB data from the other rods in the bundle. The burnout and deformation of the rod did not affect the performance of neighboring rods in the test section during the burnout or the validity of the subsequent DNB data points as predicted by the W-3 correlation. No occurrences of flow instability or other abnormal operation was observed.

DNB With Return to Nucleate Boiling

Additional DNB tests have been conducted by Westinghouse (Tong, et al. 1967) in 19 and 21 rod bundles. In these tests, DNB without physical burnout was experienced more that once on single rods in the bundles for short periods of time. Each time, a reduction in power of approximately 10 percent was sufficient to reestablish nucleate boiling on the surface of the rod. During these and subsequent tests, no adverse effects were observed on this rod or any other rod in the bundle as a consequence of operating in DNB.

4.4.4.10 Energy Release or Rupture of Waterlogged Fuel Elements

A full discussion of waterlogging including energy release is contained in Section 4.4.4.7. It is noted that the resulting energy release is not expected to affect neighboring fuel rods.

4.4.4.11 Fuel Rod Behavior Effects from Coolant Flow Blockage

Reactor coolant flow blockages can occur within the reactor coolant channels of a fuel assembly or external to the reactor core. The effects of the blockage within the assembly on fuel rod behavior are more pronounced than external blockages of the same magnitude. In both cases the flow blockages cause local reductions in reactor coolant flow. The amount of local flow reduction, where it occurs, and how far along the flow stream the reduction persists are considerations which will influence the fuel rod behavior. The effects of reactor coolant flow blockages in terms of maintaining rated core performance are determined both by analytical and experimental methods. The experimental data are usually used to augment analytical tools such as computer programs similar to the VIPRE-01 program. Inspection of the DNB correlation identified in Section 4.4.2.2 and discussed by Tong (1967) shows that the predicted DNBR is dependent upon the local values of quality and mass velocity.

The VIPRE-01 Code is capable of predicting the effects of local flow
blockages on DNBR within the fuel assembly on a subchannel basis,
regardless of where the flow blockage occurs. Sung (et al 1989)
discuss that for a fuel assembly similar to the Westinghouse design,
VIPRE-01 accurately predicts the flow distribution within the fuel
assembly when the inlet nozzle is completely blocked. Full recovery
of the flow was found to occur about 30 inches downstream of the
blockage. With the reactor operating at the nominal full power
conditions specified in Table 4.4-1, the effects of an increase in
enthalpy and decrease in mass velocity in the lower portion of the
fuel assembly would not result in the reactor reaching a minimum DNBR
below the safety limit value.

From a review of the open literature, it is concluded that flow
blockage in "open lattice cores" similar to the Westinghouse cores
cause flow perturbations which are local to the blockage. For
instance, Ohtsubo and Uruwashi (1972) show that the mean bundle
velocity is approached asymptotically about 4 inches downstream from a
flow blockage in a single flow cell. Similar results were also found
for 2 and 3 cells completely blocked. Basmer (et al 1972) tested an
open lattice fuel assembly in which 41 percent of the subchannels were
completely blocked in the center of the test bundle between spacer
grids. Their results show the stagnant zone behind the flow blockage
essentially disappears after 1.65 L/De or about 5 inches for their
test bundle. They also found that leakage flow through the blockage
tended to shorten the stagnant zone or, in essence, the complete
recovery length. Thus, local flow blockages within a fuel assembly
have little effect on subchannel enthalpy rise. The reduction in
local mass velocity is then the main parameter which affects the DNBR.
If the standard plants were operating at full power and nominal steady
state conditions as specified in Table 4.4-1, a reduction in local
mass velocity greater than 70 percent would be required to reduce the
DNBR to the safety limit. The above mass velocity effect on the DNB
correlation was based on the assumption of a fully developed flow
along the full channel length. In reality a local flow blockage is
expected to promote turbulence and thus would likely not effect DNBR
at all.

Reactor coolant flow blockages induce local crossflows as well as
promote turbulence. Fuel rod behavior is changed under the influence
of a sufficiently high crossflow component. Fuel rod vibration could
occur, caused by this crossflow component, through vortex
shedding or turbulent mechanisms. If the crossflow velocity
exceeds the limit established for fluid elastic stability, large
amplitude whirling results. The limits for a controlled
vibration mechanism are established from studies of vortex
shedding and turbulent pressure fluctuations. The crossflow

velocity required to exceed fluid elastic stability limits is dependent on the axial location of the blockage and the characterization of the crossflow (jet flow or not). These limits are greater than those for vibratory fuel rod wear. Crossflow velocity above the established limits can lead to mechanical wear of the fuel rods at the grid support locations. Fuel rod wear due to flow induced vibration is considered in the fuel rod fretting evaluation (Section 4.2).

4.4.5 Testing and Verification

4.4.5.1 Tests Prior to Initial Criticality

A reactor coolant flow test is performed following fuel loading, but prior to initial criticality. Reactor coolant loop pressure drop data are obtained in this test. This data allows determination of the reactor coolant flow rates at reactor operating conditions. This test verifies that proper reactor coolant flow rates have been used in the core thermal and hydraulic analysis. Chapter 14 describes the initial test programs.

4.4.5.2 Initial Power and Plant Operation

Core power distribution measurements are made at several core power levels (Chapter 14). These tests are used to ensure that conservative peaking factors are used in the core thermal and hydraulic analysis.

Additional demonstration of the overall conservatism of the THINC analysis was obtained by comparing THINC predictions to incore thermocouple measurements (Burke et al 1976). These measurements were performed on the Zion reactor. No further in-reactor testing is planned.

4.4.5.3 Component and Fuel Inspections

Inspections performed on the manufactured fuel are described in Section 4.2.4. Fabrication measurements critical to thermal and hydraulic analysis are obtained to verify that the engineering hot channel factors in the design analyses (Section 4.4.2.2.4) are met.

4.4.6 Instrumentation Requirements

4.4.6.1 Incore Instrumentation

Instrumentation is located in the core so that moveable neutron detectors and fixed thermocouples provide radial, axial, and azimuthal core characteristics for all core quadrants.

The incore instrumentation system is comprised of thermocouples, positioned to measure fuel assembly coolant outlet temperatures at

preselected position, and fission chamber detectors positioned in guide thimbles which run the length of selected fuel assemblies to measure the neutron flux distribution. Figure 4.4-22 shows the number and location of instrumented assemblies in the core.

The core-exit thermocouples provide a backup to the flux monitoring instrumentation for monitoring power distribution. The routine, systematic, collection of thermocouple readings by the operator provides a data base. From this data base, abnormally high or abnormally low readings, quadrant temperature tilts, or systematic departures from a prior reference map can be deduced.

The moveable incore neutron detector system would be used for more detailed mapping if the thermocouple system were to indicate an abnormality. These two complementary systems are more useful when taken together than either system alone would be. The incore instrumentation system is further discussed in Section 7.7.1.9.

The incore instrumentation is provided to obtain data from which fission power density distribution in the core, reactor coolant enthalpy distribution in the core, and fuel burnup distribution may be determined.

4.4.6.2 Overtemperature and Overpower ΔT Instrumentation

The overtemperature ΔT trip protects the core against low DNBR. The overpower ΔT trip protects against excessive power (fuel rod rating protection).

As discussed in Section 7.2.1.1.2, factors included in establishing the overtemperature ΔT and overpower ΔT trip setpoints include the reactor coolant temperature in each reactor coolant loop and, for overtemperature ΔT, the axial distribution of core power through the use of the two section excore neutron detectors.

4.4.6.3 Instrumentation to Limit Maximum Power Output

The output of the three ranges (source, intermediate, and power) of detectors, with the electronics of the nuclear instruments, are used to limit the maximum power output of the reactor within their respective ranges.

There are six radial locations containing a total of eight neutron flux detectors installed around the reactor in the neutron shield tank. Two proportional counters for the source range installed on opposite "flat" portions of the core containing the primary start-up sources at an elevation approximately one quarter of the core height. Two compensated ionization chambers for the intermediate range, located in the same instrument wells and detector assemblies as the source range detectors, are positioned at an elevation corresponding to one half of the core height. Four dual-section uncompensated ionization chamber assemblies for the power range are installed vertically at the four corners of the core and are located equidistant

from the reactor vessel at all points and, to minimize neutron flux
pattern distortions, within 1 foot of the reactor vessel. Each power
range detector provides two signals corresponding to the neutron flux
in the upper and lower sections of a core quadrant. Three ranges of
detectors are used as inputs to monitor neutron flux from a completely
shutdown condition to 120 percent of full power, with the capability
of recording overpower excursion up to 200 percent of full power.

The difference in neutron flux between the upper and lower sections of
the power range detectors are used to limit the Overtemperature ΔT
trip setpoints and to provide the operator with an indication of the
core power axial offset. In addition, the output of the power range
channels is used for:

    1. The rod speed control function,

    2. Alerting the operator to an excessive power unbalance between
        the quadrants,

    3. Protecting the core against rod ejection accidents, and

    4. Protecting the core against adverse power distributions
        resulting from dropped rods.

Details of the neutron detectors and nuclear instrumentation design
and the control and trip logic are given in Chapter 7. The
limitations on neutron detector operation and trip setpoints are given
in the Technical Specifications.

4.4.6.4 Instrumentation for Detection of Inadequate Core Cooling

Instrumentation for indication of inadequate core cooling conditions
has been provided for BVPS-2. The installed instrumentation includes
core exit thermocouples, core subcooling margin and reactor vessel
level monitoring. BVPS-2 has submitted a response to TMI Action Item
II.F.2 of NUREG-0737, "Instrumentation for Detection of Inadequate
Core Cooling," which describes in detail the characteristics of the
installed instrumentation. This system description can be found in
response to SER Open Issue No. 3, transmitted by DLC via letter
2NRC-6-037.

4.4.6.4.1 Reactor Vessel Level Instrumentation

The Reactor Vessel Level Instrumentation System (RVLIS) uses
differential pressure measuring devices to measure the vessel fluid
level or relative void content of the primary coolant. The fluid
level or void information is displayed in the main control room for
use by the operator to:

    1. Assist in detecting the presence of a gas bubble or void in
        the reactor vessel,

2.   Assist in detecting the approach of inadequate core cooling, and

3.   Indicate the formation of a void in the RCS.

4.4.6.5 Loose Parts and Monitoring System

Refer to Table 1.8-1 which describes conformance to Regulatory Guide 1.133.

4.4.6.6 Post-Accident Neutron Flux Monitoring System

The post-accident neutron flux monitoring is an excore design containing two fission chambers housed within the neutron shield tank. This system is environmentally qualified for post-accident use and provides redundant neutron indication over the range of 10^0 to 10^6 counts per second and 10^{-4} to 200 percent power.

The post-accident flux monitoring system supplies outputs to the following:

1. Plant safety monitoring system (PSMS) (Section 7.7.2.10) per Regulatory Guide 1.97

2. Alternate shutdown panel (ASP) (Section 7.4.1.3).

3. Recording device.

4.4.7 References for Section 4.4

Ainscough, J. B.; and Wheeler, M. J. 1968. Thermal Diffusivity and Thermal Conductivity of Sintered Uranium Dioxide. Proceedings of the Seventh Conference of Thermal Conductivity, p 467, National Bureau of Standards, Washington, D.C.

Asamoto, R. R.; Anselin, F. L.; and Conti, A. E. 1968. The Effect of Density on the Thermal Conductivity of Uranium Dioxide. GEAP-5493.

Bain, A. S. 1962. The Heat Rating Required to Produce Center Melting In Various UO_2 Fuels. ASTM Special Technical Publication, No. 306, pp 30-46, Philadelphia, PA.

Balfour, M. G.; Christensen, J. A.; and Ferrari, H. M. 1966. In-Pile Measurement of UO_2 Thermal Conductivity. WCAP-2923.

Basmer, P.; Kirsh, D.; and Schultheiss, G. F. 1972. Investigation of the Flow Pattern in the Recirculation Zone Downstream of Local Coolant Blockages in Pin Bundles. Atomwirtschaft, 17, No. 8, p 416-417.

Boure, J. A.; Bergles, A. E.; and Tong, L. S. 1973. Review of Two-Phase Flow Instability. Nuclear Engineering Design 25, p 165-192.

Burke, T. M.; Meyer, C. E.; and Shefcheck, J. 1976. Analysis of Data from the Zion (Unit 1) THINC Verification Test. WCAP-8454.

Bush, A. J. 1965.   Apparatus of Measuring Thermal Conductivity to 2500°C.   Westinghouse Research Laboratories Report 64-lP6-401-43, (Proprietary).

Braidwood UFSAR, USNRC Docket No. 50-456.

Cadek, F. F.; Motley, F. E.; and Dominicis, D. P. 1975.   Effect of Axial Spacing on Interchannel Thermal Mixing with the R Mixing Vane Grid. WCAP-7941-P-A (Proprietary) and WCAP-7959-A.

Cadek, F. F.   1975.   Interchannel Thermal Mixing with Mixing Vane Grids. WCAP-7667-A (Proprietary) and WCAP-7755-A.

Carter, F. D.   1972.   Inlet Orificing of Open PWR Cores.   WCAP9004 (Proprietary) and WCAP-7836.

Christensen, J. A.; Allio, R. J.; and Biancheria, A. 1965. Melting Point of Irradiated UO_2. WCAP-6065.

Clough, D. J. and Sayers, J. B. 1964.   The Measurement of the Thermal Conductivity of UO_2 Under Irradiation in the Temperature Range 150°-1600°C. AERE-R-4690, UKAEA Research Group, Harwell.

Cohen, I.; Lustman, B.; and Eichenberg, D. 1960.   Measurement of the Thermal Conductivity of Metal-Clad Uranium Oxide Rods during Irradiation. WAPD-228.

Coplin, D. H. et al 1968. The Thermal Conductivity of UO_2 by Direct In-Reactor Measurements. GEAP-5100-6.

Daniel, J. L.; Matolich, Jr. J.; and Deem, H. W. 1962. Thermal Conductivity Of UO_2. HW-69945.

Dean, R. A. 1962. Thermal Contact Conductance Between UO_2 and Zircaloy-2. CVNA-127.

Devold, I. 1968. A Study of the Temperature Distribution in UO_2 Reactor Fuel Elements, AE-318, Aktiebolaget Atomenergi, Stockholm, Sweden.

Dittus, F. W. and Boelter, L. M. K. 1930. Heat Transfer in Automobile Radiators of the Tubular Type. University of California, Berkeley, Pub. Eng., No. 13, 433.

Duncan, R. N. 1962. Rabbit Capsule Irradiation of UO_2. CVTR Project, DVNA-142.

Feith, A. D. 1962. Thermal Conductivity Of UO_2 by a Radial Heat Flow Method. TID-21668.

Godfrey, T. G.; Fulkerson, W.; Killied, T. G.; Moore, J. P.; and McElroy, D. L. 1964. Thermal Conductivity of Uranium Dioxide and Armco Iron by an Improved Radial Heat Flow Technique. ORNL-3556.

Gonzalez-Santalo, J. M. and Griffith, P. (1972). Two-phase Glow Mixing in Rod Bundle Subchannels. ASME Paper 72-WA/NE-19.

Griffith, P.; Clark, J. A.; and Rohsenow, W. M. (1958). Void Volumes in Subcooled Boiling Systems. ASME Paper No. 58-HT-19.

Gyllander, J. A. 1971. In-Pile Determination of the Thermal Conductivity UO_2 in the Range 500-2500°C. AE-411.

Hellman, J. M. (Ed) 1973. Fuel Densification Experimental Results and Model for Reactor Application. WCAP-8218-P-A (Proprietary) and WCAP-8219-A.

Hetsroni, G. 1964. Hydraulic Tests of the San Onofre Reactor Model. WCAP-3269-8.

Hetsroni, G. 1965. Studies of the Connecticut-Yankee Hydraulic Model. NYO-3250-2.

Hill, K. W. Motley, F. E.; and Cadek, F. F. 1973. Effect of Local Heat Flux Spikes on DNB in Non-Uniform Heated Rod Bundles. WCAP-8174 (Proprietary) and WCAP-8202.

Hill, K. W.; Motley, F. E.; Cadek, F. F.; and Wenzel, A. H. 1975. Effect of 17 x 17 Fuel Assembly Geometry on DNB. WCAP-8296-P-A (Proprietary) and WCAP-8297-A.

Hochreiter, L. E. and Chelemer, H. 1989. Application of the THINC IV Program to PWR Design. WCAP-8054-P-A (Proprietary) and WCAP-8195.

Hochreiter, L. E.; Chelemer, H.; and Chu, P. T. 1989. THINC-IV: An Improved Program for Thermal and Hydraulic Analysis of Rod Bundle Cores. WCAP-7956-A.

Howard, V. C. and Gulvin, T. G. 1960. Thermal Conductivity Determinations of Uranium Dioxide by a Radial Flow Method. UKAEA IG-Report 51.

Idel'chik, I. E. 1960. Handbook of Hydraulic Resistance, AEC-TR-6630.

International Atomic Energy Agency 1966. Thermal Conductivity of Uranium Dioxide. Report of the Panel held in Vienna, April, 1965. IAEA Technical Reports Series, No. 59, Vienna, The Agency.

Kakac, S.; Veziroglu, T. N.; Akyuzlu, K.; and Berkol, O. 1974. Sustained and Transient Boiling Flow Instabilities in a Cross-Connected Four-Parallel-Channel Upflow System. Proceedings of 5th International Heat Transfer Conference, Tokyo, Japan.

Kao, H. S.; Morgan, C. D.; and Parker, W. B. 1973. Prediction of Flow Oscillation in Reactor Core Channel. Tranactions of the ANS, Vol. 16, pp 212-213.

Kersting, P. J. (et al) March 1995. Assessment of Clad Flattening and Densification Power Spike Factor Elimination in Westinghouse Nuclear Fuel. WCAP-13589-A.

Kjaerheim, G. and Rolstad, E. 1967. In Pile Determination of UO Thermal Conductivity, Density Effects and Gap Conductance. HPR-80.

Kjaerheim, G. 1969. In-Pile Measurements of Center Flue Temperatures and Thermal Conductivity Determination of Oxide Fuels. Paper IFA-175 presented at the European Atomic Energy Society Symposium on Performance Experience of Water-Cooled Power Reactor Fuel, Stockholm, Sweden.

Kruger, O. L. 1968. Heat Transfer Properties of Uranium and Plutonium Dioxide. Paper 11-N-68F presented at the Fall meeting of Nuclear Division of the American Ceramic Society, Pittsburgh, PA.

Lahey, R. T. and Moody, F. J. 1977. The Thermal Hydraulics of a Boiling Water Reactor. American Nuclear Society.

Leech, W. J. (et al) October 1982. Revised PAD Code Thermal Safety Model. WCAP-8720, Addendum 2.

Lucks, C. F. and Deem, H. W. 1961. Thermal Conductivity and Electrical Conductivity of UO. In Progress Reports Relating to Civilian Applications, BMI-1448 (Rev.) for June, 1960; BMI-1489 (Rev.) for December, 1960, and BMI-1518 (Rev.) for May, 1961.

Lyons, M. F. et al. 1966. UO_2 Power and Pellet Thermal Conductivity During Irradiation. GEAP-5100-1.

McFarlane, A. F. 1975. Power Peaking Factors. WCAP-7912-P-A (Proprietary) and WCAP-7912-A.

Moody, L. F. 1944. Friction Factors for Pipe Flow. Transaction of the American Society of Mechanical Engineers, 66, 671-684.

Morita, T. et al. 1974. Power Distribution Control and Load Following Procedures, WCAP-8385 (Proprietary) and WCAP-8403.

Motley, F. E. and Cadek, F. F. 1972. Application of Modified Spacer Factor to L Grid Typical and Cold Wall Cell DNB. WCAP-7988 (Proprietary) and WCAP-8030-A.

Motley, F. E.; Wenzel, A. H.; and Cadek, F. F. 1975a. Critical Heat Flux Testing of 17 x 17 Fuel Assembly Geometry with 22-Inch Grid Spacing. WCAP-8536 (Proprietary) and WCAP-8537.

Motley, F. E.; Wenzel, A. H.; and Cadek, F. F. 1975b. The Effect of 17 x 17 Fuel Assembly Geometry on Interchannel Thermal Mixing. WCAP-8298-P-A (Proprietary) and WCAP-8299-A.

Motley, F. E. and Cadek, F. F. 1975c. DNB Test Results for New Mixing Vane Grids. WCAP-7695-P-A (Proprietary) and WCAP-7958-A.

Nelson, R. C.; Coplin, D. H.; Lyons, M. F.; and Weidenbaum, B. 1964. Fission Gas Release from UO_2 Fuel Rods with Gross Central Melting. GEAP-4572.

Nishijima, T.; Dawada, T.; and Ishihata, A. 1965. Thermal Conductivity of Sintered UO_2 and Al_2O_3 at High Temperatures. Journal of the American Ceramic Society. 48, 31 34.

Nodvick, R. J. 1970. Saxton Core II Fuel Performance Evaluation, Part II, and Evaluation of Mass Spectrometric and Radiochemical Materials Analyses of Irradiated Saxton Plutonium Fuel. WCAP-3385-56.

Ohtsubo, A. and Uruwashi, S. 1972. Stagnant Fluid Due to Local Flow Blockage. Journal Nuclear Science Technology, 9, No. 7, p 433-434.

Poncelet, C. G.   1965.   Burnup Physics of Heterogeneous Reactor Lattices.   WCAP-6069.

Rowe, D. S. and Angle, C. W. 1967.   Crossflow Mixing Between Parallel Flow Channels During Boiling, Part II Measurements of Flow and Enthalpy in Two Parallel Channels. BNWL-371, Part 2.

Rowe, D. S. and Angle, C. W. 1969.   Crossflow Mixing Between Parallel Flow Channels During Boiling, Part III Effect of Spacers on Mixing Between Two Channels. BNWL-371, Part 3.

Saha P.; Ishii, M.; and Zuber, N. 1976.   An Experimental Investigation of the Thermally Induced Flow Oscillations in Two-Phase Systems. Journal of Heat Transfer, pp 616-662.

Shefcheck, J. 1972.   Applications of the THINC Program to PWR Design, WCAP-7359-L (Proprietary) and WCAP-7838.

Skaritka, J. (Ed.) 1979.   Fuel Rod Bow Evaluation.   WCAP-8691, Revision 1 (Proprietary) and WCAP-8692, Revision 1 (Non-proprietary).

South Texas Project-1 UFSAR, USNRC Docket No. 50-498.

Stora, J. P.; Debernardy, Desigoyer, B.; Delmas, R.; Deschamps, P.; Ringot, C.; and Lavaud, B. 1964.   Thermal Conductivity of Sintered Uranium Oxide under In-Pile Conditions, EURAEC-1095.

Stora, J. P. 1970.   In-Reactor Measurements of the Integrated Thermal Conductivity of UO_2 - Effect of Porosity. Trans. ANS, 13, pp 137-138.

Taleyarkhan, R.; Podowski, M.; Lahey, Jr., R. T.; An Analysis of Density - Wave Oscillations in Ventilated Channels.   NUREG/CR-2972, March 1983.

Thom, J. R. S.; Walker, W. M.; Fallon, T. A.; and Reising, G. F. S. 1965-66.   Boiling in Sub-cooled Water During Flowup Heated Tubes or Annuli, Proceedings of the Institute for Mechanical Engineers, 180, Pt. C, 226-46.

Tong, L. S. 1967.   Prediction of Departure from Nucleate Boiling for an Axially Non-Uniform Heat Flux Distribution.   Journal Nuclear Energy, 21, pp 241-248.

Tong, L. S.   1972.   Boiling Crisis and Critical Heat Flux.   USAEC Critical Review Series, TID-25887.

Virgil C. Summer UFSAR, USNRC Docket No. 50-395.

Vogt, J.; Grandell, L.; and Runfors, U. 1964.   Determination of the Thermal Conductivity of Unirradiated Uranium Dioxide.   AB Atomenergi Report RMB-527, 1964, Quoted by IAEA Technical Report Series No. 59, Thermal Conductivity of Uranium Dioxide.

Weisman, J. 1959. Heat Transfer to Water Flowing Parallel to Tube Bundles, Nuclear Science Engineers, 6, 78-79.

USNRC 1978. Personal communication between C. Elcheldiner, Westinghouse and J. F. Stoltz, USNRC. Subject: Staff Evaluations of WCAP-7956, WCAP-8054 (Proprietary) WCAP-8567, and WCAP-8762, Letter dated April 19, 1978.

Westinghouse 1981. Letter, E.P. Rahe, Jr. (Westinghouse) to J.R. Miller (USNRC), NS-EPR-2515, dated, October 9, 1981, entitled: Partial Response to Request Number 1 for Additional Information on WCAP-8691, Revision 1, and letter, E.P. Rahe, Jr. (Westinghouse) to J.R. Miller (USNRC), NS-EPR-2572, dated March 16, 1982, entitled: Remaining Response to Request Number 1 for Additional Information on WCAP-8691, Revision 1.

USNRC 1986.   letter, C.H. Berlinger (USNRC) to E.P. Rahe, Jr. (Westinghouse), dated June 18, 1986, entitled: Request for Reduction in Fuel Assembly Burnup Limit for Calculation of Maximum Rod Bow Penalty.

D. H. Risher, Jr., "An evaluation of the Rod Ejection Accident in Westinghouse Pressurized Water Reactors Using Spatial Kinetics Methods," WCAP-7588, Revision 1, Westinghouse Electric Corporation (December, 1971).

D. H. Coplin, et al., "The Thermal Conductivity of UO_2 by Direct In-reactor Measurement," GEAP5100-6, General Electric Corporation (March, 1968).

A. M. Ross and R. L. Stoute, "Heat Transfer Coefficient Between UO_2, and Zircaloy-2," AECL-1552, Atomic Energy of Canada, Ltd. (June, 1962).

L. S. Tong, Boiling Heat Transfer and Two-Phase Flow, John Wiley & Sons, New York (1965).

L. S. Tong, "Critical Heat Fluxes on Rod Bundles," in "Two-Phase Flow and Heat Transfer in Rod Bundles," 31-41, American Society of Mechanical Engineers, New York (1969).

F. E. Motley, K. W. Hill, F. F. Cadek, J. Shefcheck, "New Westinghouse Correlation WRB-1 for Predicting Critical Heat Flux in Rod Bundles with Mixing Vane Grids," WCAP-8762-P-A, Westinghouse Electric Corporation (July 1984).

R. A. Weiner (et al), "Improved Fuel Performance Models for Westinghouse Fuel Rod Design and Safety Evaluations," WCAP-11873-A, August 1988.

J. Weisman, A. J. Wenzel, L S. Tong, D. Fitzsimmons, W. Thome, and J. Batch, "Experimental Determination of the Departure for Nucleate Boiling in Large Rod Bundles at High Pressures," <u>Chemical Engineering Program Symposium Ser. 64</u>, No. 82, 114-125 (1968).

L. A. Stephen, "The Effects of Cladding Material and Heat Treatment on the Response of Waterlogged UO_2 Fuel Rods to Power Bursts," IN-ITR-111, Aeoject Nuclear, Idaho National Engineering Laboratory (January, 1970).

Western New York Nuclear Research Center Correspondence with the AEC on (February 11 and August 27, 1971), Docket 50-57.

L. S. Tong, et al., "Critical Heat Flux (DNB) in Square and Triangular Array Rod Bundles," presented at the Japan Society of Mechanical Engineers Semi-International Symposium held at Tokyo, Japan, 25-34 (September 4-8, 1967).

A. J. Friedland, and S. Ray, "Revised Thermal Design Procedure," WCAP-11397 (Proprietary), (February 1987) and Letter, A. C. Thadani (USNRC) to W. J. Johnson (Westinghouse), "Acceptance for Referencing of Licensing Topical Report WCAP-11397, Revised Thermal Design Procedure," (January 1989).

D. B. Owen, "Factors for One-Sided Tolerance Limits and for Variable Sampling Plant," SCR-607, (March 1963).

A. J. Friedland, and S. Ray, "Improved THINC-IV Modeling for PWR Core Design," WCAP-12330-P-A (September 1991).

Schueren, P. McAtee, K. R., "Extension of Methodology for Calculating Transition Core DNBR Penalties," WCAP-11837-P-A, January 1990.

Kitchen, T. J., "Generic Safety Evaluation for 17 x 17 Standard Robust Fuel Assembly (17 x 17 STD RFA)," SECL-98-056, Rev. 0, September 30, 1998.

Liparulo, N. J. (Westinghouse) letter to Lyons, J. E. (NRC), "Transmittal of Response to NRC Request for Information on Wolf Creek Fuel Design Modifications," NSD-NRC-97-5189, June 30, 1997.

Liparulo, N. J., (Westinghouse) letter to Jones, R. C. (NRC), "Transmittal of Presentation Material from NRC/Westinghouse Meeting on April 15, 1996," NSD-NRC-96-4964, April 22, 1996.

Davidson, S. L., (Editor), "Westinghouse Fuel Criteria Evaluation Process," WCAP-12488-A, October 1994.

Smith, L. D., et. al., "Modified WRB-2 Correlation, WRB-2M, for Predicting Critical Heat Flux in 17 x 17 Rod Bundles with Modified LPD Mixing Vane Grids, "WCAP-15025-P-A, April 1999.

Davidson, S. L., (Editor), "Reference Core Report - VANTAGE 5 Fuel Assembly," WCAP-10444-P-A, September 1985, "VANTAGE 5H Fuel Assembly," WCAP-10444-P-A, Addendum 2-A, April 1998.

Sepp, H. A., (Westinghouse) letter to T. E. Collins (NRC), "Fuel Criteria Evaluation Process Notice for 17 x 17 Robust Fuel Assembly with IFM Grid Design," October 13, 1998.

T. P. Williams, J. R. Reagan, and C. R. Tuley, "Westinghouse Revised Thermal Design Procedure Instrumentation Uncertainty Methodology for Duquesne Light Company for Beaver Valey Unit 2," WCAP-15265, Revision 3, May 2001.

S. D. Hollingsworth and D. C. Wood, "Reactor Core Response to Excessive Secondary Steam Releases," WCAP-9226-P-A, Revision 1, February 1998.

Kitchen, T. J., "Generic - Implementation of Robust Fuel Assembly-2 (RFA-2) Design Changes," EVAL-01-066, August 31, 2001.

Kitchen, T. J., "Beaver Valley Power Station Units 1 and 2 EVAL-03-61 - RFA/RFA-2 Robust Fuel Assembly and IFM Implementation," LTR-ESI-03-35, April 24, 2003.

S. L. Davidson, J. A. Iorii, (Ed), "Reference Core Report - 17x17 Optimized Fuel Assembly," WCAP-9500-A, May 1982.

J. P. Foster and S. Sidener, "Westinghouse Improved Performance Analysis and Design Model (PAD4.0)," WCAP-15063-P-A, Revision 1, July 2000.

E. P. Rahe (Westinghouse) letter to Miller (NRC) dated March 19, 1982, NS-EPR-2573, WCAP-9500 and WCAPs 9401/9402, "NRC SER Mixed Core Compatibility Items."

Sepp, H. A. (Westinghouse) letter to T. E. Collins (NRC), "Notification of FCEP Application for WRB-1 and WRB-2 Applicability to the 17x17 Modified LPD Grid Design for Robust Fuel Assembly Application," NSD-NRC-98-5722, March 25, 1998.

Stewart, C. W., et al, "VIPRE-01: A Thermal-Hydraulic Code for Reactor Core," Volume 1-3 (Revision 3, August 1989), Volume 4 (April 1987), NP-2511-CCM-A, Electric Power Research Institute.

Sung, Y. X., et al, "VIPRE-01 Modeling and Qualification for Pressurized Water Reactor Non-LOCA Thermal-Hydraulic Safety Analysis," WCAP-14565-P-A and WCAP-15306-NP-A, October 1999.

C. O. Thomas (NRC) letter to Rahe (Westinghouse), "Supplemental Acceptance No. 2 for Referencing Topical Report, WCAP-9500," January 1983.

Letter from D. S. Collins (NRC) to J. A. Gresham (W), entitled "Modified WRB-2 correlation WRB-2M for predicting Critical Heat Flux in 17 x 17 Rod Bundles with Modified LPD Mixing Vane Grids," February 2, 2006.

Tables for Section 4.4

TABLE 4.4-1

THERMAL AND HYDRAULIC PARAMETERS

Design Parameters	Design Value
Reactor core heat output (MWt)	See Table 4.1-1
Reactor core heat output (10^6Btu/hr)	See Table 4.1-1
Heat generated in fuel (%)	See Table 4.1-1
System pressure, nominal (psia)	See Table 4.1-1
Minimum DNBR at nominal design conditions	
Typical flow channel	2.83(RFA/RFA-2) 2.56(V5H)
Thimble (cold wall) flow channel	2.76(RFA/RFA-2) 2.24(V5H)
Minimum DNBR for design transients, typical/thimble	See Table 4.1-1
DNB correlation	WRB-2M(RFA/RFA-2) WRB-1(V5H)
Coolant Flow	
Total thermal flow rate (10^6 lbm/hr)	See Table 4.1-1
Effective flow rate for heat transfer (10^6 lbm/hr)	See Table 4.1-1
Effective flow area for heat transfer (ft^2)	See Table 4.1-1
Average velocity along fuel rods (ft/sec)	See Table 4.1-1
Average mass velocity (10^6 lbm/hr-ft^2)	See Table 4.1-1
Coolant Temperatures	
Nominal inlet (°F)	See Table 4.1-1
Average rise in vessel (°F)	See Table 4.1-1
Average rise in core (°F)	See Table 4.1-1

TABLE 4.4-1 (Cont)

Design Parameters	Design Value
Average in core (°F)	See Table 4.1-1
Average in vessel (°F)	See Table 4.1-1
Heat Transfer	
Active heat transfer, surface area (ft^2)	See Table 4.1-1
Average heat flux (Btu/hr-ft^2)	See Table 4.1-1
Maximum heat flux for normal operation (Btu/hr-ft^2)	See Table 4.1-1
Average linear power (kW/ft)	See Table 4.1-1
Peak linear power for normal operation (kW/ft)	See Table 4.1-1
Peak linear power resulting from overpower transients/operator errors, assuming a maximum overpower of 118% (kW/ft) [Note 1]	See Table 4.1-1
Peak linear power which would result in centerline melt (kW/ft) [Note 2]	22.4
Fuel Central Temperature	
Peak at linear power for prevention of centerline melt (°F)	See Table 4.1-1
Pressure drop [Note 3]	
Across core (psi)	22.3±2.2(RFA/RFA-2) 20.25±2.0(V5H)
Across vessel, including nozzle (psi)	43.25±4.3(RFA/RFA-2) 41.23±4.1(V5H)

NOTES:

1. See Section 4.3.2.2.6.
2. See Section 4.4.2.11.6.
3. Based on best estimate reactor coolant flow rate as discussed in Section 5.1.

TABLE 4.4-2

VOID FRACTIONS AT NOMINAL REACTOR CONDITIONS
WITH DESIGN HOT CHANNEL FACTORS

	Average (%)	Maximum (%)
Core	0.0	-
Hot Subchannel	0.7	3.6

TABLE 4.4-3

Deleted
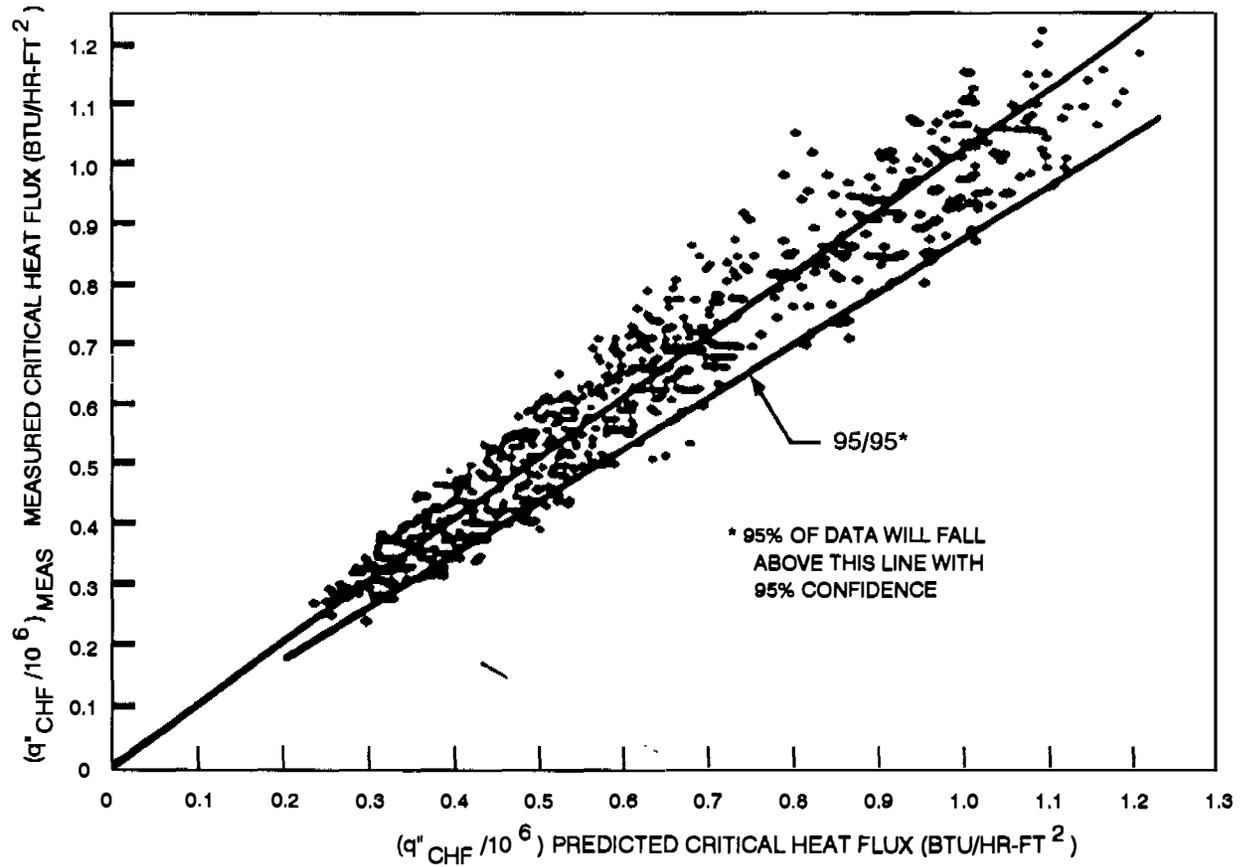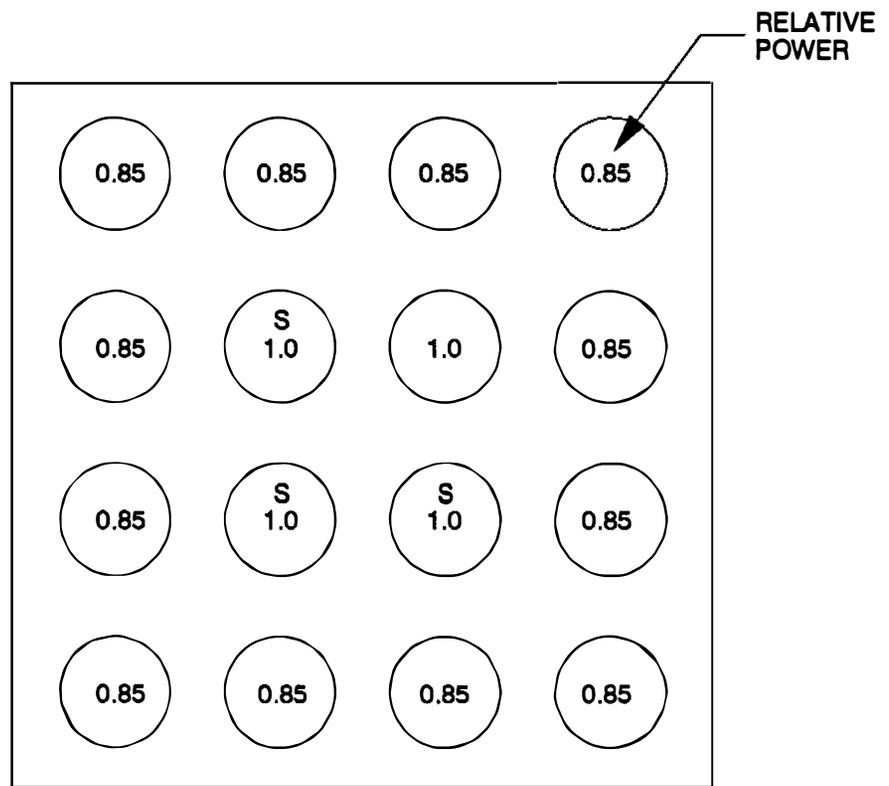
FIGURE 4.4-1
MEASURED VERSUS PREDICTED CRITICAL
HEAT FLUX - WRB-1 CORRELATION
BEAVER VALLEY POWER STATION-UNIT 2
FINAL SAFETY ANALYSIS REPORT

RELATIVE POWER

0.85	0.85	0.85	0.85
0.85	S 1.0	1.0	0.85
0.85	S 1.0	S 1.0	0.85
0.85	0.85	0.85	0.85

"S" - SPIKED ROD LOCATIONS

FIGURE 4.4-1A
TEST SECTION CROSS-SECTION FOR
DNB SPIKE TEST
BEAVER VALLEY POWER STATION-UNIT 2
FINAL SAFETY ANALYSIS REPORT

SPIKE HEAT FLUX/LOCAL HEAT FLUX = 1.2
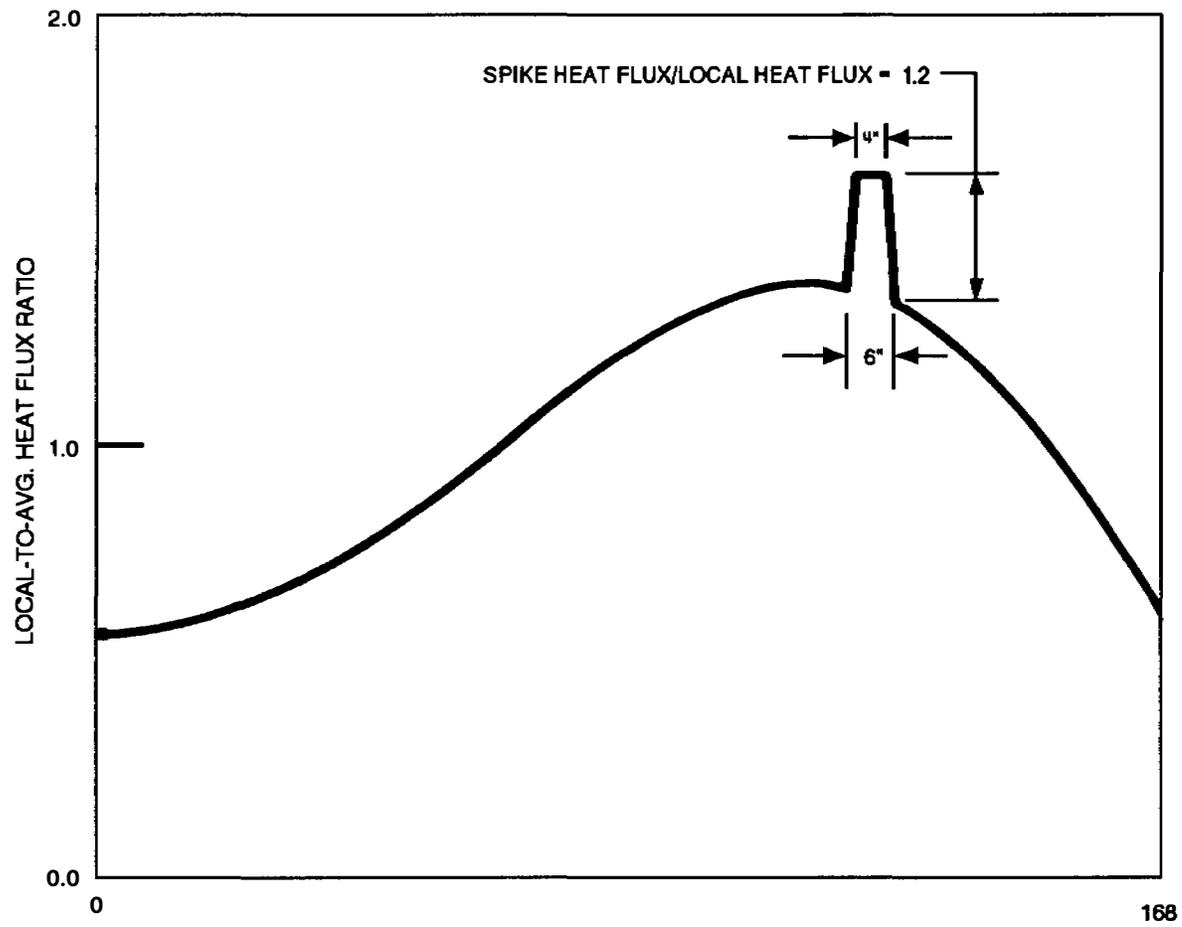
FIGURE 4.4-2

AXIAL HEAT FLUX PROFILE WITH 20%

SPIKE FOR 168 INCH RODS

BEAVER VALLEY POWER STATION-UNIT 2

FINAL SAFETY ANALYSIS REPORT
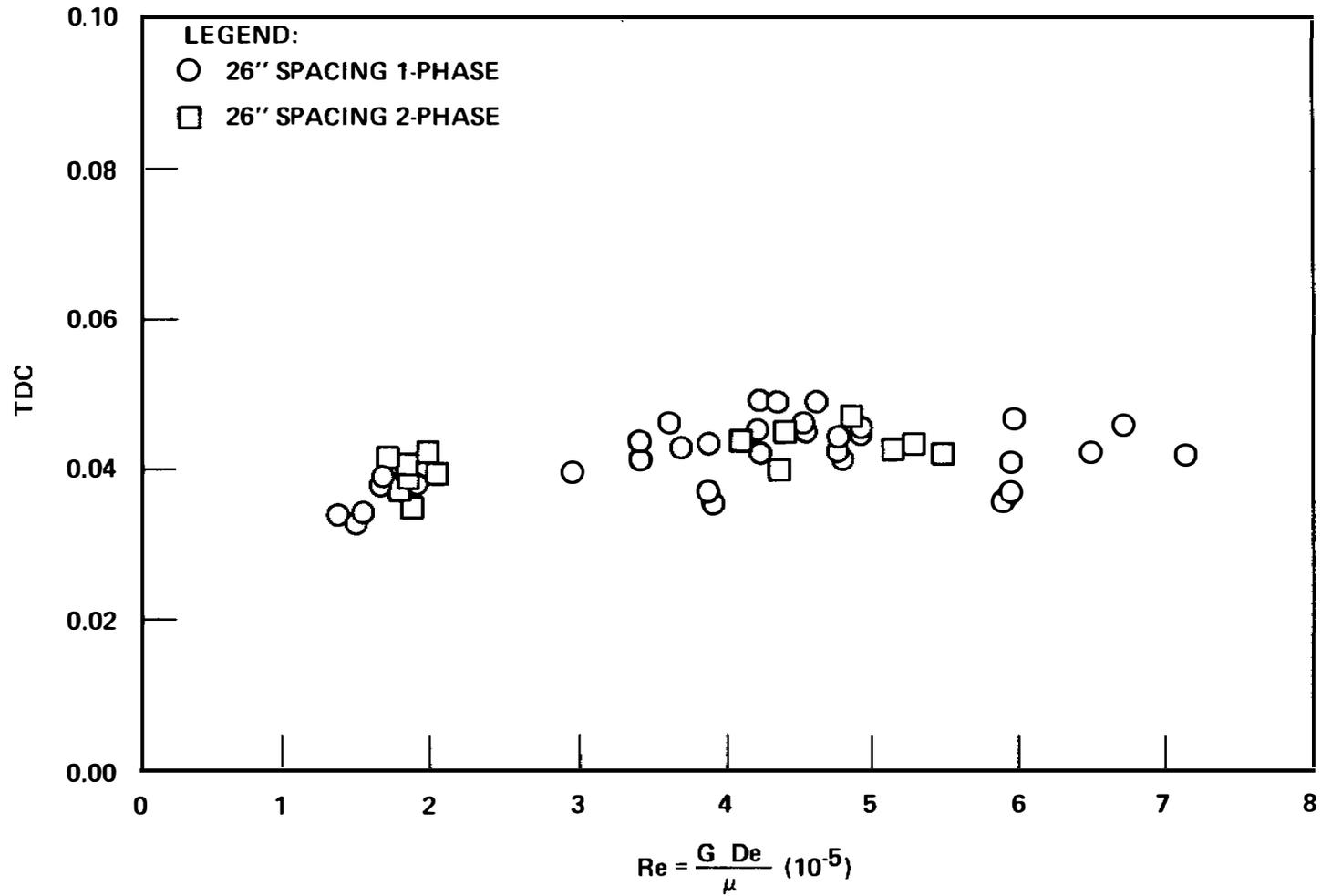
FIGURE 4.4-3
TDC vs. REYNOLDS NUMBER FOR
26 INCH GRID SPACING
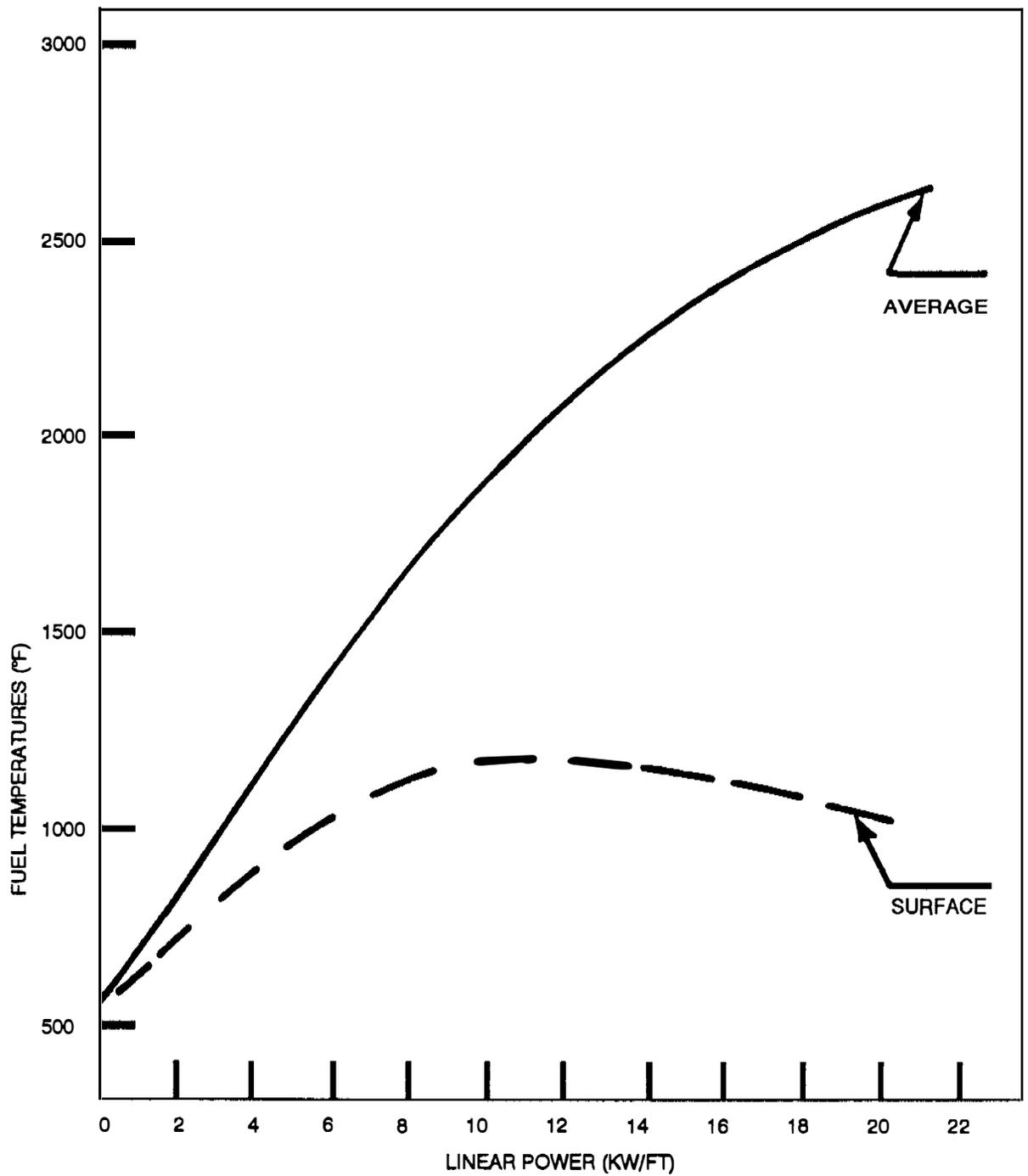BEAVER VALLEY POWER STATION−UNIT 2
FINAL SAFETY ANALYSIS REPORT

FIGURE 4.4-9
PEAK FUEL AVERAGE AND SURFACE
TEMPERATURES DURING FUEL ROD
LIFETIME VS LINEAR POWER
BEAVER VALLEY POWER STATION-UNIT 2
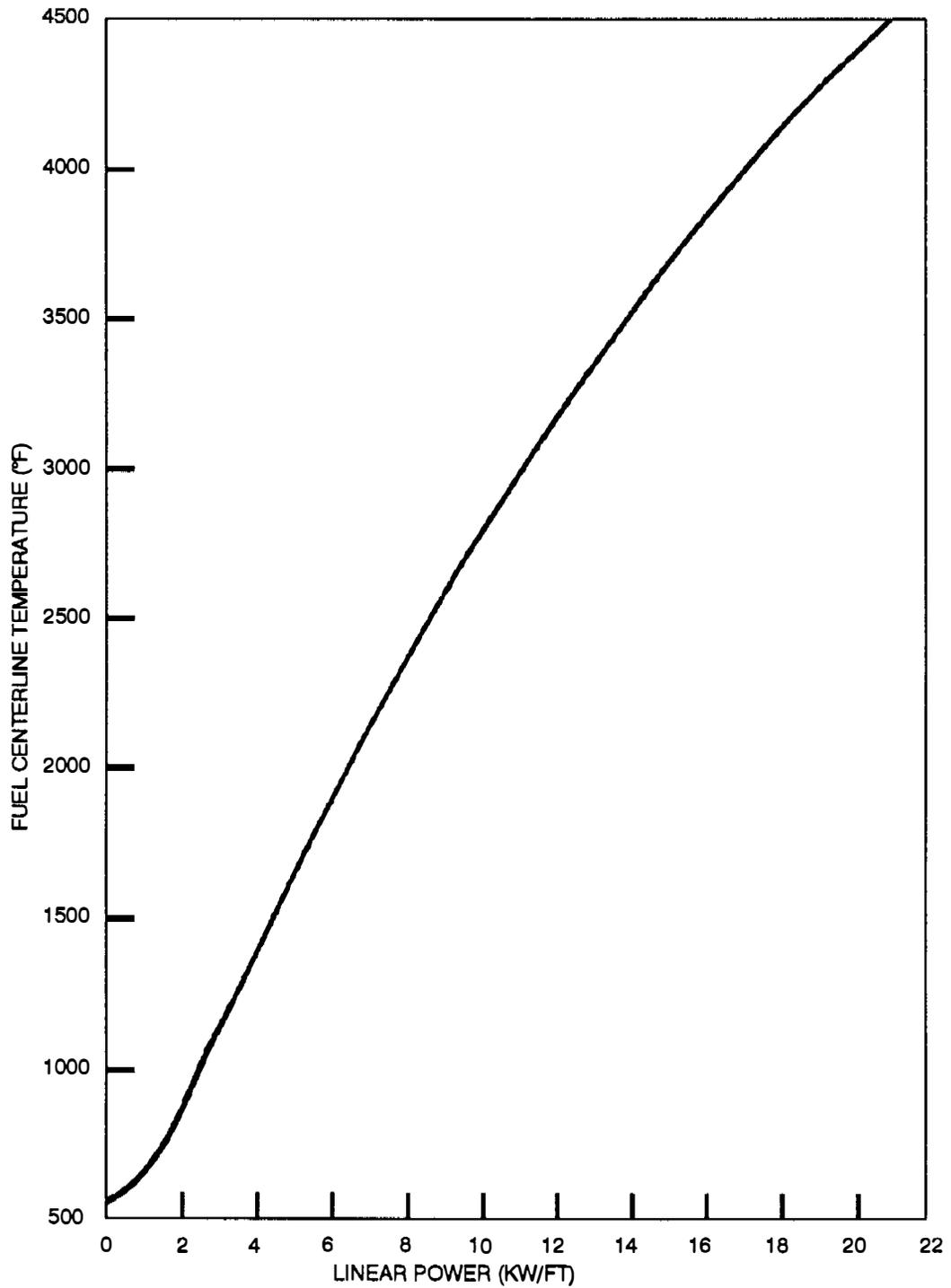FINAL SAFETY ANALYSIS REPORT

FIGURE 4.4-10
PEAK FUEL CENTERLINE
TEMPERATURE DURING FUEL ROD
LIFETIME VS LINEAR POWER
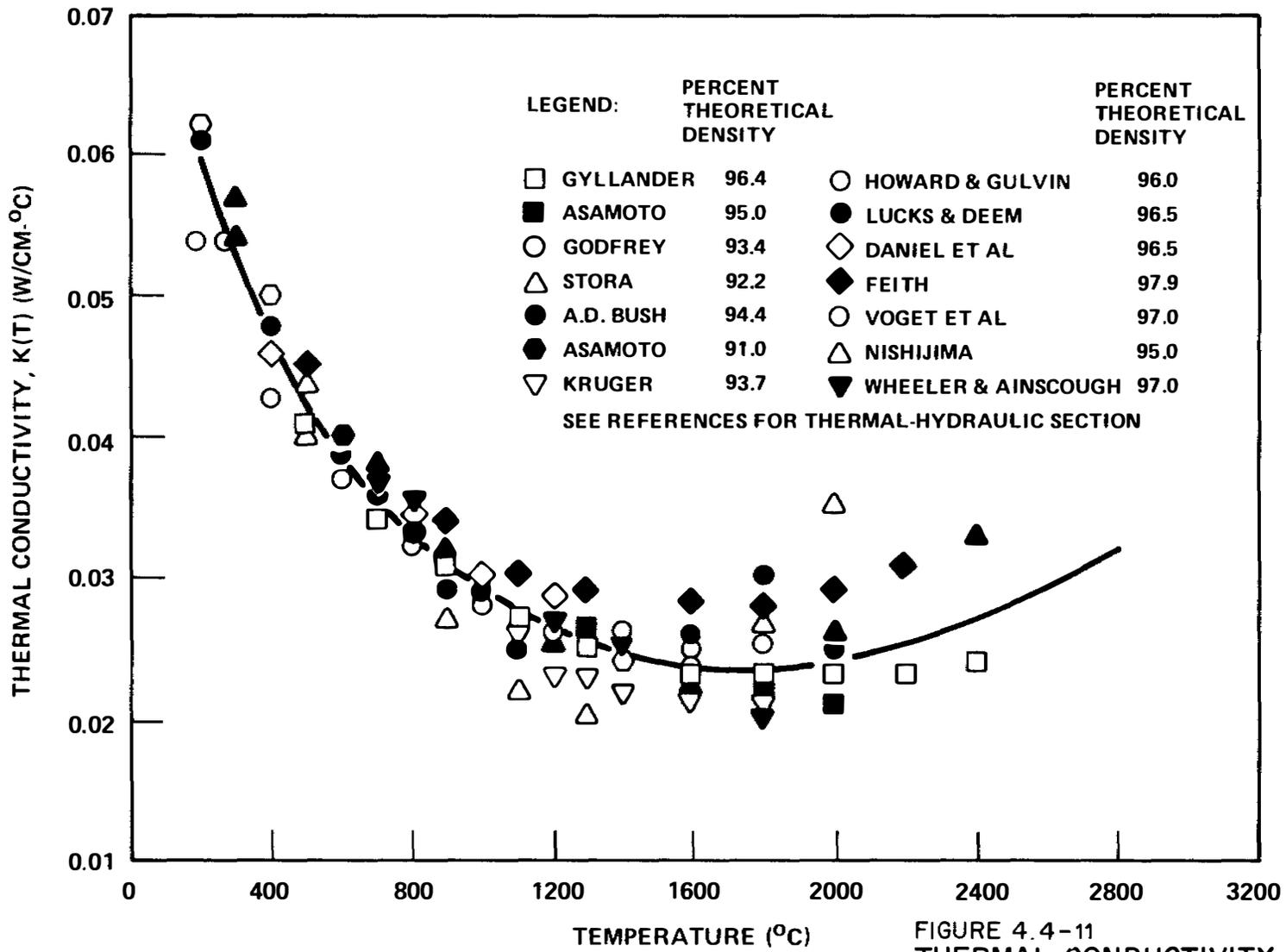BEAVER VALLEY POWER STATION-UNIT 2
FINAL SAFETY ANALYSIS REPORT

FIGURE 4.4-11
THERMAL CONDUCTIVITY OF UO²
(DATA CORRECTED TO 95%
THEORETICAL DENSITY)
BEAVER VALLEY POWER STATION-UNIT 2
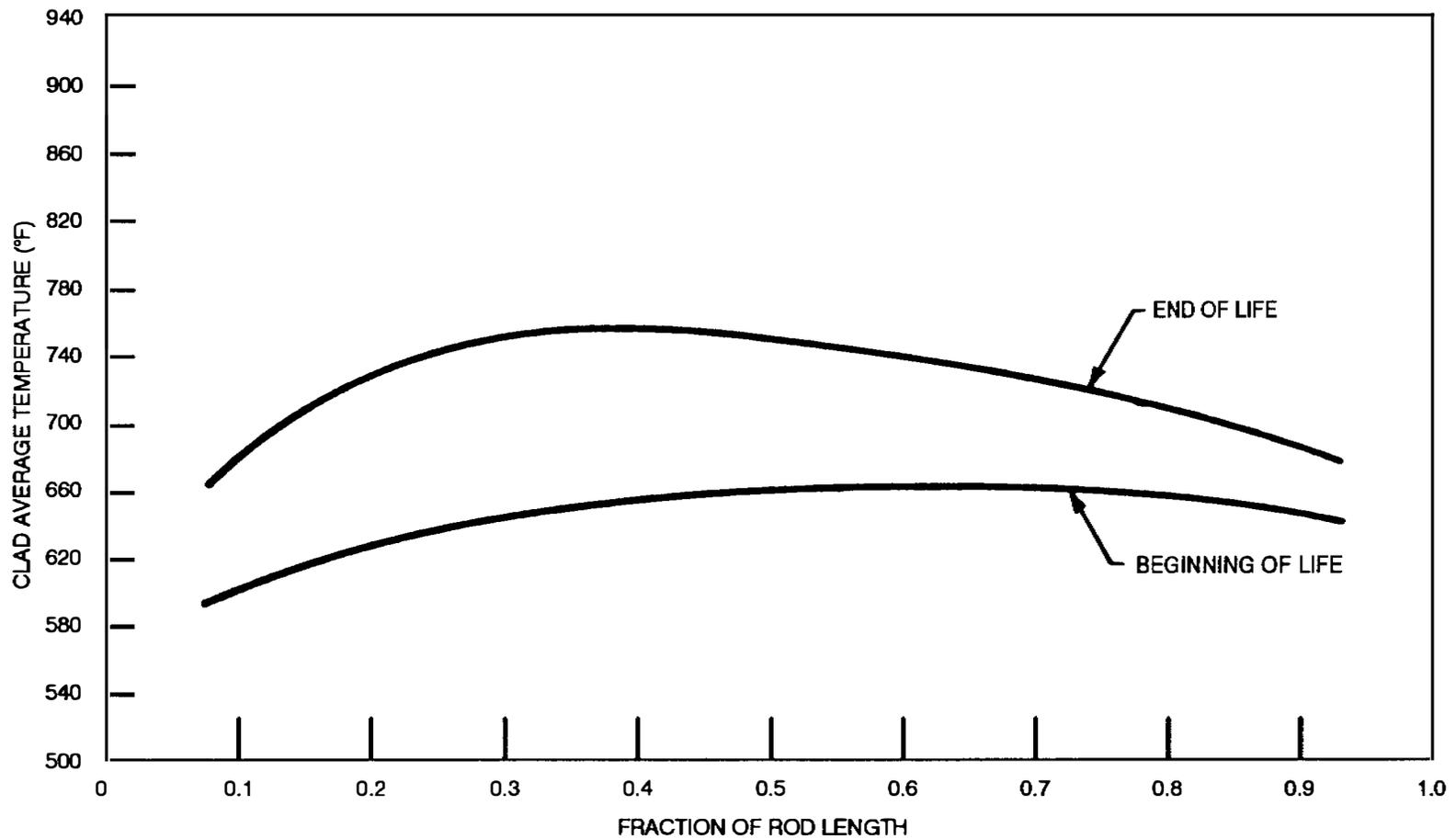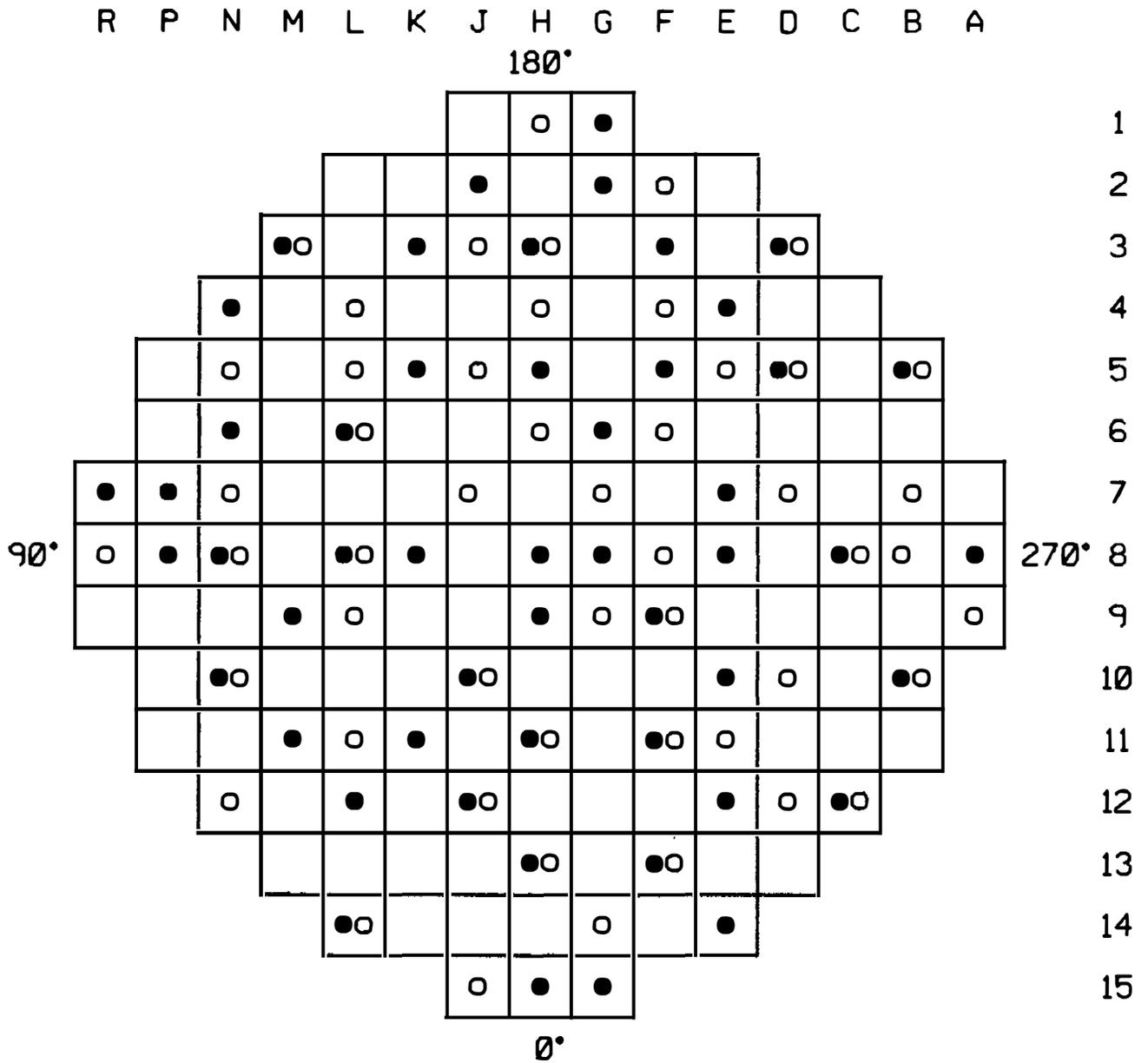FINAL SAFETY ANALYSIS REPORT

FIGURE 4.4-12
AXIAL VARIATION OF AVERAGE CLAD
TEMPERATURE FOR ROD OPERATING AT
5.43 KW/FT
BEAVER VALLEY POWER STATION-UNIT 2
FINAL SAFETY ANALYSIS REPORT

FIGURE 4.4-22
DISTRIBUTION OF INCORE
INSTRUMENTATION
BEAVER VALLEY POWER STATION-UNIT 2
UPDATED FINAL SAFETY ANALYSIS REPORT

4.5 REACTOR MATERIALS

This section provides a discussion of the materials employed in the control rod drive system and for the reactor internals.

A more detailed evaluation of the reactor materials and reactivity control systems indicating the degree of conformance with the recommendations of the applicable Regulatory Guides is presented in this final safety analysis report (FSAR) as follows:

1. Control Rod Drive Mechanism and Reactor Internals: Chapter 3.

2. Control Rod Drive Mechanism Testing: Chapters 3, 14, and 16.

3. Control Rod Drive Mechanism and Reactor Internals Materials: Chapter 5.

4. Safety Injection System: Chapter 6.

5. Instrumentation for Reactor Control and Protection: Chapter 7.

6. Failure of the Control Rod Drive Mechanism Cooling System and Chemical and Volume Control System: Chapter 9.

4.5.1 Control Rod Drive System Structural Materials

4.5.1.1 Materials Specifications

All parts exposed to reactor coolant are made of metals which resist the corrosive action of the water. Three types of metals are used exclusively: stainless steels, nickel-chromium-iron, and cobalt based alloys. In the case of stainless steels, only austenitic and martensitic stainless steels are used. For pressure boundary parts, martensitic stainless steels are not used in the heat treated conditions which cause susceptibility to stress corrosion in the Westinghouse pressurized water reactor (PWR) water chemistry.

1. Pressure Boundary

    All pressure retaining materials comply with Section III of the ASME Boiler and Pressure Vessel Code and are fabricated from austenitic (300 series) stainless steel.

2. Coil Stack Assembly

    The coil housings require a magnetic material. Both low carbon cast steel and ductile iron have been successfully tested for this application. On the basis of performance, ductile iron was selected for the control rod drive

mechanism (CRDM). The finished housings are zinc plated or flame sprayed to provide corrosion resistance.

Coils are wound on bobbins of glass reinforced silicon thermoset molding material, with double glass insulated copper wire. Coils are then vacuum impregnated with silicon resin. A wrapping of mica sheet is secured to the coil outside diameter. The result is a well insulated coil capable of sustained operation at 200°C.

3.   Latch Assembly

Magnetic pole pieces are fabricated from type 410 stainless steel or equivalent. All nonmagnetic parts, except link pins and springs, are fabricated from type 304 stainless steel or equivalent. Haynes 25 or equivalent is used to fabricate link pins. Springs are made from nickel-chromium-iron alloy (Inconel-X750) or equivalent. Latch arm tips are clad with Stellite-6 or similar hardened material to provide improved wearability. Hard chrome plate and Stellite-6 or other wear resistant materials are used selectively for bearing and wear surfaces.

4.   Drive Rod Assembly

The drive rod assembly utilizes a type 410 stainless steel or equivalent, drive rod and disconnect rod assembly. The coupling is machined from type 403 stainless steel or equivalent. Other parts are type 304 stainless steel or equivalent with the exception of the springs, which are nickel-chromium-iron alloy (Inconel-X750) or equivalent, and the locking button, which is Haynes 25 or equivalent; and the belleville washers which are Inconel-718 or equivalent. Several small parts (screws and pins) are Inconel-600 or equivalent.

Material specifications for Class 1 components of the CRDM are as follows: (Equivalent materials may have been substituted.)

CRDM, upper head	SB-166 or SB-167 and SA-182 Grade F304
Latch housing	SA-182, Grade F304 or SA-351 Grade CF8
Rod travel housing	SA-182, Grade F304 or SA-336 Class F8
Cap	SA-479, Type 304
Welding materials	Stainless Steel Weld Metal Analysis A-8

4.5.1.2 Austenitic Stainless Steel Components

1. All austenitic stainless steel materials used in the fabrication of CRDM components are processed, inspected, and tested to avoid sensitization and prevent intergranular stress corrosion cracking.

    The rules covering these controls are stipulated in Westinghouse process specifications. As applicable, these process specifications supplement the equipment specifications and purchase order requirements of every individual austenitic stainless steel component regardless of the ASME Code Classification.

    Westinghouse practice is that austenitic stainless steel materials of product forms with simple shapes need not be corrosion tested provided that the solution heat treatment is followed by water quenching. Simple shapes are defined as all plates, sheets, bars, pipe and tubes, as well as forgings, fittings, and other shaped products which do not have inaccessible cavities or chambers that would preclude rapid cooling when water quenched. When testing is required, the tests are performed in accordance with ASTM A 262, Practice A or E, as amended by Westinghouse Process Specification 84201 MW.

    If, during the course of fabrication, the steel is inadvertently exposed to the sensitization temperature range (800 to 1,500°F), the material may be tested in accordance with ASTM A 262, as amended by Westinghouse Process Specification 84201 MW to verify that it is not susceptible to intergranular attack, except that testing is not required for:

    a. Cast metal or weld metal with a ferrite content of 5 percent or more.

    b. Material with a carbon content of 0.03 percent or less that is subjected to temperatures in the range of 800 to 1,500°F for less than 1 hour.

    c. Material exposed to special processing provided the processing is properly controlled to develop a uniform product and provided that adequate documentation exists of service experience and/or test data to demonstrate that the processing will not result in increased susceptibility to intergranular stress corrosion.

        If it is not verified that such material is not susceptible to intergranular attack, the material will be resolution annealed and water quenched or rejected.

2.   The welding of austenitic stainless steel is controlled to mitigate the occurrence of micro fissuring or hot cracking in the weld.

Available data indicates that a minimum delta ferrite level expressed in ferrite number (FN), above which the weld metals commonly used by Westinghouse will not be prone to hot cracking, lies somewhere between 0 FN and 3 FN. The undiluted weld deposits of the starting welding materials are required to contain a minimum of 5 FN.

4.5.1.3 Other Materials

The CRDMs are cleaned prior to delivery in accordance with the guidance of ANSI 45.2.1. Westinghouse personnel conduct surveillance to ensure that manufacturers and installers adhere to appropriate requirements.

Haynes 25 is used in small quantities to fabricate link pins. The material is ordered in the solution treated and cold worked condition. Stress corrosion cracking has not been observed in this application over the last 15 years.

The CRDM springs are made from nickel-chromium-iron alloy (Inconel-750) ordered to MIL-S-23192 or MIL N-24114 Class A No. 1 temper drawn wire. Operating experience has shown that springs made of this material are not subject to stress-corrosion cracking.

4.5.1.4 Cleaning and Cleanliness Control

The CRDMs are cleaned prior to delivery in accordance with the guidance of ANSI 45.2.1. Measures are taken, as appropriate, to apply packaging requirements to procurement orders; to review supplier packaging procedures; to apply proper cleaning requirements, marking, and identification; to provide protection to equipment from physical or weather damage; to apply special handling precautions; and to define storage requirements. The present Westinghouse Water Reactor Division's Quality Assurance Program is described in Westinghouse topical report WCAP-8370, Revision 9A (Westinghouse 1979).

4.5.2 Reactor Internals Materials

4.5.2.1 Materials Specifications

All the major material for the reactor internals is type 304 stainless steel or equivalent. Parts not fabricated from type 304 stainless steel include bolts and dowel pins which are fabricated from type 316 stainless steel or equivalent and radial support key bolts and clevis insert bolts which are fabricated from Inconel-X750 or equivalent. Clevis inserts are made from Inconel-600 or equivalent. These materials are listed in Table 5.2-2 and 5.2-4. An optional hard chrome plating may be applied to the outside diameter of the rod control cluster assembly rodlets. There are no other materials used in the reactor internals or core

support structures which are not included in the ASME Code, Section III, Appendix I.

4.5.2.2 Controls on Welding

The discussions provided in Section 5.2.3 are applicable to the welding of reactor internals and core support components. The core support component weld inspection requirements are in accordance with ASME Section III, NG-5000.

4.5.2.3   Nondestructive Examination of Wrought Seamless Tubular Products and Fittings

The nondestructive examination of wrought seamless tubular products and fittings is in accordance with Section III of the ASME Code.

4.5.2.4   Fabrication and Processing of Austenitic Stainless Steel Components

Conformance of reactor internals and core support structures with Regulatory Guide 1.44 is discussed in Sections 1.8 and 5.2.3.

Conformance of reactor internals and core support structures with Regulatory Guide 1.31 is discussed in Sections 1.8 and 5.2.3.

Conformance of reactor internals with Regulatory Guide 1.34 is discussed in Section 1.8.

Conformance of reactor internals and core support structures with Regulatory Guide 1.71 is discussed in Section 1.8.

4.5.2.5 Contamination Protection and Cleaning of Austenitic Stainless Steel

The discussions provided in Sections 1.8 and 5.2.3 are applicable to the reactor internals and core support structures and verify conformance with ANSI 45 specifications and Regulatory Guide 1.37.

4.5.3 Reference for Section 4.5

Westinghouse Electric Corporation 1979. Westinghouse Water Reactor Division's Quality Assurance Plan. WCAP-8370, Revision 9A.

4.6   FUNCTIONAL DESIGN OF REACTIVITY CONTROL SYSTEMS

4.6.1   Information for Control Rod Drive System

The control rod drive system (CRDS) is described in Section 3.9N.4.1. Figures 3.9N-3 and 3.9N-4 provide the details of the control rod drive mechanisms (CRDMs), and Figure 4.2-8 provides the layout of the CRDS. No hydraulic system is associated with its functioning. The instrumentation and controls for the reactor trip system (RTS) are described in Section 7.2 and the reactor control system is described in Section 7.7.

4.6.2   Evaluation of the Control Rod Drive System

The CRDS has been analyzed in detail in a failure mode and effects analysis (FMEA) by Shopsky (1977). This FMEA and the analyses presented in Chapter 15, demonstrate that the CRDS performs its intended safety function, a reactor trip, by putting the reactor in a subcritical condition when a safety system setting is approached, with any assumed credible failure of a single active component. The essential elements of the CRDS (those required to ensure reactor trip) are isolated from nonessential portions of the CRDS as described in Section 7.2.

Despite the extremely low probability of a common mode failure impairing the ability of the RTS to perform its safety function, analyses have been performed in accordance with the requirements of WASH-1270. These analyses documented by Westinghouse (1974) and Gangloff and Loftus (1971) have demonstrated that the acceptable safety criterion would not be exceeded even if the CRDS was rendered incapable of functioning during a reactor transient for which its function would normally be expected.

The design of the CRDM is such that failure of the CRDM cooling system will, in the worst case, result in an individual control rod trip or a full reactor trip. Section 9.4.7.4 discusses the control rod drive mechanism ventilation system.

4.6.3   Testing and Verification of the Control Rod Drive System

The CRDS is extensively tested prior to its operation. These tests may be subdivided into five categories: 1) prototype tests of components, 2) prototype CRDS tests, 3) production tests of components following manufacture and prior to installation, 4) onsite preoperational and initial startup tests, and 5) periodic inservice tests. These tests, which are described in Sections 3.9N.4.4, 4.2, 14.2, and 16.2, are conducted to verify the operability of the CRDS when called upon to function.

4.6.4 Information for Combined Performance of Reactivity Systems

As indicated in Chapter 15, the only postulated events which assume credit for reactivity control systems other than a reactor trip to render the plant subcritical are the steam line break (SLB), feedwater line break, and loss-of-coolant accident (LOCA). The reactivity control systems for which credit is taken in these accidents are the RTS and the safety injection system (SIS). Additional information on the CRDS is presented in Section 3.9N.4 and on the SIS in Section 6.3. Note that no credit is taken for the boration capabilities of the chemical and volume control system (CVCS) in the analysis of transients presented in Chapter 15. Information on the capabilities of the CVCS is provided in Section 9.3.4. The adverse boron dilution possibilities due to the operation of the CVCS have been presumed as an initial condition to evaluate transients and appropriate Technical Specifications have been prepared to ensure the correct operation or remedial action.

4.6.5 Evaluation of Combined Performance

The evaluation of the SLB, feedwater line break, and the LOCA which presume the combined actuation of the RTS to the CRDS and the SIS are presented in Sections 15.1.5, 15.2.8 and 15.6.5. Reactor trip signals and safety injection signals for these events are generated from functionally diverse sensors and actuate diverse means of reactivity control, that is, control rod insertion and injection of soluble poison.

Nondiverse, but redundant types of equipment, are only utilized in the processing of the incoming sensor signals into appropriate logic which initiates the protective action. This equipment is described in detail in Sections 7.2 and 7.3. In particular, note that protection from equipment failures is provided by redundant equipment and periodic testing. Effects of failures of this equipment have been extensively investigated as reported by Eggleston, Rawlins and Petrow (1976). The FMEA verifies that any single failure will not have a deleterious effect upon the engineered safety features actuation system. Adequacy of the emergency core cooling system and SIS performance under faulted conditions is verified in Section 6.3.

4.6.6 References for Section 4.6

Eggleston, F. T.; Rawlins, D. H.; and Petrow, J. R. 1976. Failure Mode and Effects Analysis (FMEA) of the Engineering Safeguard Features Actuation System. WCAP-8584 (Proprietary) and WCAP-8760 (Non-Proprietary).

Gangloff, W. C. and Loftus, W. D. 1971. An Evaluation of Solid State Logic Reactor Protection in Anticipated Transients. WCAP-7706-L (Proprietary) and WCAP-7706 (Non-Proprietary).

Shopsky, W. E. 1977. Failure Mode and Effects Analysis (FMEA) of the Solid State Full Length Rod Control System. WCAP-8976.

Westinghouse 1974. Westinghouse Anticipated Transients Without Trip Analysis. WCAP-8330.